Aus dem Biomedizinischen Centrum
der Ludwig-Maximilians-Universität München
Lehrstuhl Physiologische Chemie
Vorstand: Prof. Andreas Ladurner

Elucidating the molecular mechanism of Isw1a and Isw1b chromatin remodeler recruitment

Dissertation
zum Erwerb des Doktorgrades der Naturwissenschaften
an der Medizinischen Fakultät der
Ludwig-Maximilians-Universität zu München

vorgelegt von
Lena Susanne Bergmann

aus
Lichtenfels

2021

Mit Genehmigung der Medizinischen Fakultät
der Universität München

Betreuerin:	Prof. Dr. Michaela Smolle
Zweitgutachter:	Prof. Dr. Peter B. Becker
Dekan:	Prof. Dr. med. Thomas Gudermann
Tag der mündlichen Prüfung:	16.02.2022

Eidesstattliche Versicherung

Hiermit erkläre ich, Lena Bergmann, an Eides statt, dass die vorliegende Dissertation mit dem Titel

Elucidating the molecular mechanism of Isw1a and Isw1b chromatin remodeler recruitment

selbstständig verfasst, mich außer der angegebenen keiner weiteren Hilfsmittel bedient und alle Erkenntnisse, die aus dem Schrifttum ganz oder annähernd übernommen worden sind, als solche kenntlich gemacht und nach ihrer Herkunft unter Bezeichnung der Fundstelle einzeln nachgewiesen habe.
Ich erkläre des Weiteren, die hier vorgelegte Dissertation nicht in gleicher oder in ähnlicher Form bei einer anderen Stelle zur Erlangung eines akademischen Grades eingereicht wurde.

San Francisco, 01.03.2022
Ort, Datum

Bergmann
Unterschrift
(Lena Bergmann)

Acknowledgements

First, I would like to thank my supervisor Michaela for the opportunity to work as a PhD student in her lab. Being a pharmacist and foreign in the field, I appreciate the trust she put in me. We discussed experiments and outcomes on a daily basis until I was confident enough to work on my own. Thank you Michaela for chats in between, for the great project, an open door, that you gave me the freedom to choose my experiments and for your scientific support.

Next, I would like to thank my TAC, Peter and Felix for your scientific input, break-through ideas and advice in how to become a complete PhD student. Both of you invited me to come to you and seek advice whenever I needed it.

Besides my TAC, I appreciate the input from the Remodeler Club. I found having other people to supervise your experiments to be super helpful - especially when you are so into something that you cannot see the obvious.

Philipp Voight, we never met or talked, but I hope you know you saved my PhD when sending us your peptide-ligated octamers. The same holds true for Till Bartke (and his PhD student), who supplied me with a bunch of different octamers that allowed me to pipet my second project in record time.

In general, I would like to thank the people from the Becker department for constant invitations for coffee and chats, particularly Irina and Elisa.

I may not forget Elizabeth, whose door was open too, providing advice in difficult times and always giving her best to comfort each PhD student. Thank you for introducing me into the IRTG. You are such a great coordinator.

I was also lucky to be part of the Ladurner Department and I thank all of you for welcoming me so warmly. There are a couple of people to which I would like to express my special gratitude.

Ameirika, Andreia and Ling Ling. We, the Smolle group, all sit in the same boat and before Corona, we used to sit together, laugh, watch Youtube Videos, sing Britney together, share (or steal) snacks and cheer each other up when experiments did not work.

Special thanks go out to Moritz, my lunch and party partner. With whom I could dance and drink for hours with, and who would still make sure I get home safely. Before Corona, we started our first drinks Friday after Journal Club, and we never knew what the evening would bring. With you I gained not just a nice working colleague but also a reliable friend.

Charlotte, you also became more of a friend than just a colleague, and I will never forget our summer 2018 when we explored all the crazy cold waters ranging from Munich to Greece. This was one of my best summers, and you were a big part of it.

Gunnar and Thomas, without both of you I would not have survived my first weeks. Thank you for introducing me into the world of protein purification. No matter how often I came to your desk or how stupid my questions were, you never made me feel like I was not welcomed. You always readily helped me with ÄKTA problems and interpreting all the peaks when I was supposed to see only one.

Anton, who smiles at me in the morning and who was always happy to chat. With the door always open, I felt that I could come around with any question, and you always immediately did your best to solve any problem I had.

Caterina, who invited me for collaboration and a paper. This publication is my very first and this happy thought will always be connected with you.

Special thanks go out to Julia. I was incredibly lucky to not just get any technician, but to work with you. Your understanding for the matter was outstanding, your work clean and quick. Thank you, Julia, for cloning every (!) construct I demanded, for pouring my gels, all the PCRs and Midi-preps you did for me. For constant buffer supply for the group and always an open ear. Your work was great! Whenever I asked you for a favor, the question was not if, but when you should do it. Whenever I was

stuck on an experiment that didn't work, you always helped me out. You were always there to discuss and share findings. I cannot explain how much I appreciate your help. Without you, I would not even have been half through the PhD by now. Thank you!!

Besides my work colleagues, there are some people I want to express my gratitude to as well.

Einar, whenever I was sad at home, you poured me an Aperol Spritz to cheer me up. Whenever I was delighted and happy that an experiment went well, you poured me an Aperol Spritz to celebrate with me. You always listened to my presentations and had such clever questions. With you I could always discuss my findings and sometimes you were more excited than me. Your words were always positive and motivating. You were always there to give me love and support without requesting anything back. We both made it through our PhDs together and I look forward to a happy life with you. I thank you so much.

My family; Peter, Christine, and Johanna, for their unconditional love. You have no clue what I am doing here. Nevertheless, you enabled the life I have now. Thank you for all your trust and support (and money). My Dad for immediate help when I seek it. My Mom especially for daily calls on my way home. Thank you for your immense food supply whenever I went home to make sure I eat well. Thank you for always having my back. Thank you for believing in me, and that I could do this PhD.

Preface

The results in this work were all generated by myself, if not stated otherwise. Therefore, I would like to thank Jian Li for generating the crystal structure of the Ioc4 PWWP domain. All proteins used in this study were purified by myself. I designed all constructs while Julia Schluckebier performed all cloning for all constructs under my supervision. Umut Günsel gifted purified 6xHis-MBP. Circular dichroism measurements were performed with help from Brigitte Nuscher under the supervision of Frits Kamp. The northern blots and ChIP-chip data were performed and analyzed by Michaela Smolle. All *in vitro* assays were performed and analyzed by me. The nucleosomes were generated and gifted from different research groups. H3K36me0- and H3K36me3-containing octamers were kindly gifted by Philipp Voigt. The laboratory of Till Bartke generated and kindly gifted H3K4me0-, H3K4me3-, H3K4me3-H2A.Z-, H3K9,14ac-, H3K4me3 - H3K9,14,18,23,27ac-, H4K5,8,12ac-, H2A.Z- containing octamers, that were all reconstituted by myself. Julia Schluckebier helped with PCR amplification of the widom 601 sequence as well as nucleosome reconstitutions.

Publications evolved during this PhD:

H3K36 methylation and DNA-binding are critical for Ioc4 recruitment and Isw1b remodeller function. under review in *NAR* (2021). (uploaded in BioRxiv)
Li, Jian*; **Bergmann, Lena***; Webb, Kimberly M.; Gogol, Madelaine M.; Voigt, Philipp; Liu, Yingfang; Liang, Huanhuan; Smolle, Michaela M.

Contribution to other manuscripts:

Further, for this publication I separated digested Fab antibodies from a pool of undigested IgGs.

Features of MOG required for recognition by patients with MOG-antibody-associated disorders. *Brain* (2021).
Macrini, Caterina; Gerhards, Ramona; Winklmeier, Stephan; **Bergmann, Lena**; Mader, Simone; Spadaro, Melania; Vural, Atay; Smolle, Michaela; Hohlfeld, Reinhard; Kümpfel, Tania; Lichtenthaler, Stefan; Franquelim, Henri; Jenne, Dieter; Meinl, Edgar.

* These authors contributed equally to this work

TABLE OF CONTENTS

Summary

Each cell in our body compromises around 2 m of DNA in its nucleus, which encompasses just a few micrometer in diameter. To efficiently store it, DNA is packaged in chromatin. Its repeating unit is called a nucleosome and consists of 147 base pairs DNA wrapped around a histone octamer. Histone octamers consist of one histone H3/H4 tetramer and two histone H2A/H2B dimers.

During transcription, nucleosomes represent a considerable barrier for RNA polymerase II, which can only successfully transcribe genes when the underlying DNA sequence is made accessible. Several regulatory mechanisms are involved in this process. Due, it is possible to exchange canonical histones with histone variants. Posttranslational modifications on canonical histones and histone variants can silence or activate gene transcription. Histone chaperones, histone modifying enzymes and chromatin remodelers add another layer of complexity to transcriptional regulation. Through ATP hydrolysis, remodeler complexes generate the energy they need for nucleosome movement. This regulatory machinery can be summarized under the term 'epigenetics'. This branch of biology compromises changes that do not alter the DNA sequence, yet alters gene expression levels. Being conserved from yeast to humans, examining the role of chromatin remodelers in yeast is also relevant for the functions of human homologs.

In my thesis I focused on the molecular recruitment mechanisms of two such yeast chromatin remodelers, named Isw1a and Isw1b. They consist of Isw1, Ioc3 and Isw1, Ioc2, Ioc4, respectively. They share the catalytic ATPase subunit Isw1.

Particularly, I found that the PWWP domain of Ioc4 in Isw1b is responsible for recruiting the Isw1b complex onto chromatin. The PWWP domain specifically recognizes trimethylated lysine 36 on histone H3 (H3K36me3), which is found at mid to 3'-ends of genes. Our collaboration partner Jian Li solved the crystal structure of the $Ioc4_{PWWP}$ domain. Besides the conserved β-barrel and the α-helix bundle, he noticed a long, unique insertion motif. Using electrophoretic mobility shift assays I demonstrated that the presence of an intact PWWP domain is crucial for full Isw1b functions. Mutations inside the PWWP domain shed light on the molecular mechanisms governing remodeler functions. Therefore, DNA-binding is a prerequisite for the PWWP to stably interact with nucleosomes. Histone-binding

ability seems to be an adjuvant, but not crucial. However, lack of the insertion motif resulted in reduced histone-binding ability, yet left other functions unchanged. Isw1b remodeling activity was monitored by sliding assays. The Isw1b complex needs a functional, DNA-binding PWWP domain to fully remodel mononucleosomes. Using northern blots, we showed that the presence of an intact PWWP domain prevents the rise of cryptic transcripts.

Besides Isw1b, I studied the molecular mechanisms underlying Isw1a recruitment. Unlike Isw1b, Isw1a gets recruited to the ends of genes. Acting in the promoter region it can easily impact whether transcription takes place or not. Precisely, the complex is recruited to the +1 nucleosome, the first nucleosome in a gene, as well as to the terminal nucleosome. The +1 nucleosome contains acetylation, methylation and the histone variant H2A.Z to ensure a sophisticated mechanism of transcription regulation. I tested whether any of these histone marks specifically interact with Isw1a. I found that Isw1a preferentially binds to and mobilizes H2A.Z-containing nucleosomes *in vitro*.

Since the Ioc subunits determine substrate specificity, I hypothesized that H2A.Z recognition derives from specific contacts with Ioc3 rather than Isw1. It was further suggested that the acidic patch on H2A.Z serves as a recruitment platform for potential direct interaction partners. To find the H2A.Z-recognition site I inspected the published crystal structure of Ioc3. I observed that both N- and C-termini were not present. Thus no information about their roles is known, yet they contained many basic residues. To evaluate the functions of the Ioc3 termini, I deleted its N-terminus and/or C-terminus. In electrophoretic mobility shift assays I detected that the Ioc3 N-terminus promotes interaction with H2A.Z, while the C-terminus controls nucleosome attachment of Isw1a over all. However, the lack of the Ioc3 C-terminus did not interfere with Isw1a sliding ability. Notably, the missing Ioc3 N-terminus increased the differences between canonical and H2A.Z-containing nucleosomes in sliding assays. This result suggests a second H2A.Z recognition motif, since the missing N-terminus resulted in loss of H2A.Z-recognition in binding assays. This also suggests that sliding activity is uncoupled from binding.

In summary, my work gives new insights into the molecular mechanisms of Isw1a and Isw1b chromatin remodeler recruitment in yeast *in vitro*.

Zusammenfassung

Jede Zelle unseres Körpers beinhaltet 2 m an DNS in ihrem Zellkern, der nur ein paar Mikrometer Durchmesser misst. Um DNS effizient zu verstauen, ist sie in Chromatin verpackt. Seine sich wiederholende Einheit heißt Nukleosom und besteht aus 147 Basenpaaren DNS, die um ein Histonoktamer gewickelt sind. Ein Histonoktamer besteht aus einem H3/H4 Histontetramer und zwei H2A/H2B Histondimeren. Während der Transkription repräsentieren die Nukleosome die ultimative Barriere für die RNA Polymerase II, die nur erfolgreich transkribieren kann, wenn die darunter liegende DNA Sequenz frei zugänglich ist. Verschiedene Regulationsmechanismen steuern diesen Prozess. So ist es möglich, kanonische Histone durch Histonvarianten auszutauschen. Posttranslationale Modifikationen am kanonischen Histon oder Histonvarianten können ebenfalls die Gentranskription ausschalten oder aktivieren. Histon-Chaperone, Histon-modifizierende Enzyme und Chromatin-Remodeler fügen eine weitere komplexe Schicht im Zusammenspiel der Regulation von Transkription hinzu. Durch ATP Hydrolyse generieren Remodeler Komplexe die Energie, die sie benötigen um Nukleosome zu bewegen. Dieses Regularium kann unter dem Begriff der Epigenetik zusammen gefasst werden. Dieser Teilbereich der Biologie umfasst Veränderungen, die nicht die DNS Sequenz betreffen, sondern lediglich Expressionslevel. Da sie von der Hefe bis zum Menschen konserviert sind, erlaubt die Untersuchung der Chromatin-Remodeler in Hefe Rückschlüsse auf menschliche Homologe.

In meiner Doktorarbeit war es mein besonderes Interesse, den molekularen Mechanismus von zwei solchen Hefe-Remodelern, nämlich Isw1a und Isw1b, und ihrer Rekrutierung an Chromatin zu untersuchen. Sie bestehen aus Isw1 und Ioc3, beziehungsweise aus Isw1, Ioc2 und Ioc4. Sie teilen sich die Isw1 Untereinheit, welche in beiden Komplexen jeweils die ATPase darstellt.

Im Speziellen habe ich herausgefunden, dass die PWWP Domäne von Ioc4 im Isw1b Komplex dafür verantwortlich ist, den Isw1b Komplex an seine richtige Stelle im Chromatin zu rekrutieren. Die PWWP Domäne erkennt im speziellen das an Histon H3 trimethylierte Lysin 36 (H3K36me3), welches im mittleren bis hinteren Teil von Genen zu finden ist. Unser Kooperationspartner Jian Li hat die

Kristallstruktur der $Ioc4_{PWWP}$ Domäne gelöst. Neben den konservierten β-Faltblatt und α-Helix Strukturen, hat er ein langes, einzigartiges Insertionsmotif gefunden. Mit Hilfe von elektrophoretischen Analysen war es mir möglich zu zeigen, dass die Existenz einer intakten PWWP Domäne ausschlaggebend für die vollen Funktionen von Isw1b ist. Mutationen innerhalb der PWWP Domäne haben den molekularen Mechanismus weiter aufklären können. So ist die Bindung an DNA eine Voraussetzung, damit PWWP stabil mit Nukleosomen interagieren kann. Die Bindung an Histone ist hilfreich, jedoch nicht ausschlaggebend. Ohne das Insertionsmotif war die Fähigkeit der PWWP Domäne Histone zu binden verringert, allerdings waren andere Funktionen unbeeinträchtigt. Die Fähigkeit von Isw1b Nukleosome zu bewegen, wurde in analysiert. Auch hier benötigt der Isw1b Komplex eine funktionale, DNA-bindende PWWP Domäne um Mononukleosome vollständig zu bewegen. Mittels Northern Blots konnten wir zeigen, dass die Anwesenheit einer intakten PWWP Domäne das Entstehen von kryptischen Transkripten weitestgehend verhindert.

Neben Isw1b habe ich auch den molekularen Mechanismus zur Rekrutierung von Isw1a untersucht. Anders als Isw1b wird Isw1a an den Anfang und das Ende von Genen rekrutiert. Da es in der Promoterregion agiert, kann Isw1a einfach beeinflussen, ob Transkription statt findet oder nicht. Genauer gesagt wird der Komplex an das +1 Nukleosom gebunden, welches das erste Nukleosom in einem Gen darstellt, sowie an das letzte Nukleosom. Im +1 Nukleosom finden wir Acetylierungen, Methylierungen ebenso wie die Histonvariante H2A.Z um einen ausgeklügelten Mechanismus zur Regulation von Transkription zu ermöglichen. Ich habe getestet, ob eine dieser Histonmodifikationen beziehungsweise -varianten spezifisch mit Isw1a interagiert. Dabei habe ich herausgefunden, dass Isw1a bevorzugt an Nukleosome mit H2A.Z bindet beziehungsweise mobilisiert.

Da die Ioc Untereinheiten über die Substrat-Spezifität entscheiden, stellte ich die Hypothese auf, dass der Effekt von Ioc3 und nicht von Isw1 kommen muss. Weiterhin wurde bereits konstatiert, dass der positiv geladene Teil von H2A.Z als Rekrutierungsplattform für mögliche, direkte Interaktoren fungieren muss. Um die H2A.Z-Erkennungsstelle in Ioc3 näher zu charakterisieren, habe ich die zuvor veröffentlichte Kristallstruktur inspiziert. Dabei ist mir aufgefallen, dass der N-Terminus und der C-terminus von Ioc3 nicht Teil der Struktur sind. Allerdings

enthalten sie viele negativ geladene Aminosäuren. Um die Funktionen der Ioc3 Termini zu untersuchen, habe ich in Ioc3 den N-Terminus und/oder den C-Terminus entfernt. In elektrophoretischen Bindeversuchen habe ich entdeckt, dass der N-Terminus von Ioc3 einen ursächlichen Beitrag zur Erkennung von H2A.Z leistet während der C-Terminus die Binding von Isw1a an Nukleosomen allgemein fördert. Der fehlende C-Terminus hatte jedoch keinerlei Auswirkungen auf die Fähigkeit von Isw1a Nukleosome zu mobilisieren. Dieses Ergebnis eröffnet die Möglichkeit, dass es ein zweites H2A.Z-Erkennungsmotif geben muss, da in Bindeversuchen ein Fehlen des N-Terminus keine spezifische H2A.Z-Erkennung mehr ergab. Weiterhin deutet es darauf hin, dass die Fähigkeiten Nukleosome zu binden und sie zu bewegen voneinander gekoppelt sein müssen.

Zusammenfassend bringt meine Arbeit neueste *in vitro* Erkenntnisse bezüglich des molekularen Mechanismus der Remodeler Isw1a und Isw1b und ihrer Rekrutierung an Chromatin in Hefe.

1. Introduction

1.1 Chromatin organization, epigenetics and transcription

DNA is organized in chromatin

Deoxyribonucleic acid (DNA) is the fundamental molecule carrying all genetic information needed for living beings. Its two strands are held together by hydrogen bonds. Pairing of Thymine (T) with Adenine (A) establishes two hydrogen bonds, while the pairing of Guanine (G) and Cytosine (C) forms three hydrogen bonds between the base pairs (bp) generating a double helix with a minor and a major groove and a 10 bp periodicity. The double helices measure in total ca. 2 m of total DNA that each eukaryotic cell needs to package inside its small nucleus (Figure 1.1A)[1,2].

In 1997, Karolin Luger and colleagues solved the crystal structure of a nucleosome core particle (Figure 1.1B)[3]. It is composed of 147 base pairs of DNA wrapped 1.7 times around a histone octamer. A canonical histone octamer consists of a histone H3/H4 tetramer, sandwiched on either side by two histone H2A/H2B dimers. The DNA major groove faces towards the histone octamer core. Base pair 73 marks the nucleosome dyad, which is the pseudo-symmetrical axis in a nucleosome core particle. This position is the theoretical super-helical turn 0 (SHL 0). They count from -7 to +7, depending on their locations towards the dyad (Figure 1.1B)[3–5]. Besides the core histones H2A, H2B, H3 and H4, a linker histone exits, called histone H1. Histone H1 binds to the linker DNA that connects nucleosomes[6]. Each histone protein contains N- and/or C-terminal, unstructured histone tails, protruding from the core[3]. Thus, DNA is organized in chromatin. Linker DNA connects each nucleosome with the next one, forming a beads-on-a-string-like primary structure[7]. In general, nucleosome stability can be explained by the negatively charged phosphate backbone of the DNA that packs against the positively charged surface of the histone octamer. The primary ‘beads on a string’ chromatin structure can be condensed even further forming 30 nm fibers. The existence of this secondary fiber structure is still controversial. Nevertheless two competing models exist that depict its structure, called solenoid or zigzag (Figure 1.1A). Their structural differences derive from either a rigid (zigzag model) or free, variable linker DNA (solenoid model)[8,9]. Tertiary

structure can be achieved by condensing the fibers into chromosomes (Figure 1.1A)[10–13]. Condensation of chromatin as well as incorporation of the linker histone H1 is often associated with the formation of heterochromatin[14]. This transcriptionally inactive chromatin is widespread in higher eukaryotes, e.g. the fly genome compromises ca. 30% of heterochromatin with gene-poor and repetitive DNA sequences[15]. In yeast only the HMR mating type locus and telomeres are packed as heterochromatin, thus ca. 85% of the genome is expressed and packaged as euchromatin[16–18]. Nevertheless, organization of higher-order chromatin structure remains poorly understood.

Besides the formation of heterochromatin and euchromatin, phase separation within a cell nucleus can affect chromatin architecture and accessibility, thus transcription and activity as well[19–23]. During liquid-liquid phase separation, droplets inside the cytoplasm form compartments without forming a membrane enclosure, thus its components can still be exchanged with their surroundings[24]. A fixed stoichiometry is lacking in such assemblies. This phenomena was also observed in yeast upon stress induction, marked by the accumulation of the stress granule marker Pab1[25].

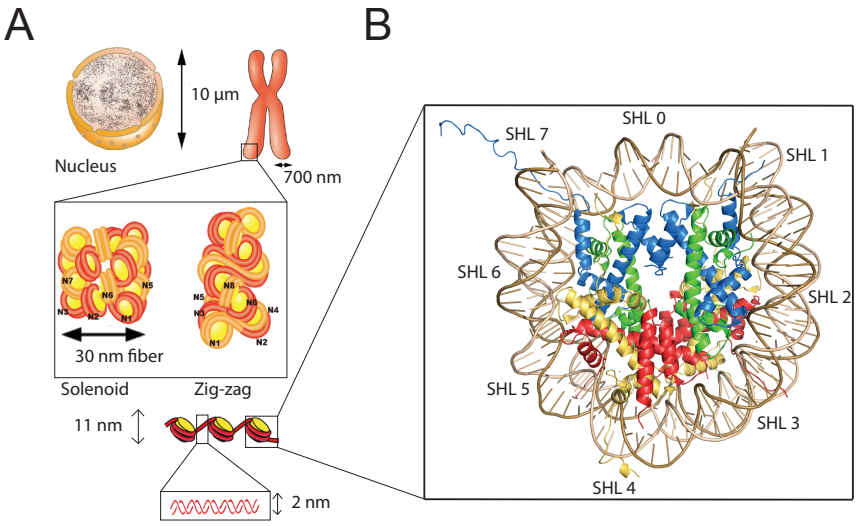

Figure 1.1 Packaging of DNA inside the cell nucleus. (A) DNA is packed as nucleosomes, forming the primary beads on a string chromatin structure. Further condensation leads to the 30 nm fiber *in vitro* that can get packed as a chromosome and is stored inside the cell nucleus. Adapted and printed with permission from Maeshima *et al.* following the Creative Commons Attribution 4.0 International License[13]. **(B)** Crystal structure of a nucleosome core particle at 2.8 Å. 146 bp of dsDNA (light and dark brown) wrapped around a histone octamer consisting of H2A (yellow), H2B (red), H3 (blue) and H4 (green). SHL 0 to 7 is indicated. Adapted from Luger *et al.* using the accession code 1AOI in the Protein Data Bank[3].

Chromatin structure can regulate transcription initiation

Nucleosomes represent a barrier for RNA Polymerase II, which can only transcribe when open access to DNA is ensured. DNA is usually openly accessible in nucleosome depleted regions (NDRs), sometimes also referred to as nucleosome free regions (NFRs). They encompass enhancers, origins of replication and most importantly promoters. Promoters usually span 150 – 200 bp[26,27]. In yeast, a well-positioned -1 and +1 nucleosome upstream and downstream the transcription start site (TSS), respectively, marks the NDR (Figure 1.2)[28,29]. The subsequent nucleosomes get aligned by the position of the +1 nucleosome, which leads to highly positioned arrays and a high nucleosomal occupancy (peak height/trough depth)[28,30,31]. Nevertheless, those arrays can be mainly found over housekeeping or constitutively active genes and can be described as genes with canonical promoters. In these genes the average linker length between two positioned nucleosomes is 18 bp, leading to a 165 bp repeat length for the budding yeast *Saccharomyces cerevisiae*[32,33]. Silent or inducible genes contain promoters which are called non-canonical[34–36]. These are characterized by a small NDR that can even be filled with nucleosomes as it was observed in the *PHO5* or several *GAL* promoters[37].

Besides the canonical promoter, promoter-like elements exist that can possibly lie within intergenic or intragenic regions, open reading frames or on the antisense strand. In properly organized chromatin they are hidden inside a nucleosome. When exposed, RNA Polymerase II can use this site for the production of cryptic transcripts or noncoding RNAs, that can be sense or antisense[38–40]. These transcripts are usually not translated into proteins, since they become rapidly degraded by the exosome. If translation is possible, it can lead to the formation of false and shortened proteins[40,41]. In wild type cells expression levels of noncoding RNAs are generally low, but existent[42]. It was further observed that ncRNAs can have important functions for gene expression, too. For instance, the noncoding, 3' antisense RNA of the *PHO5* gene results in histone eviction at its promoter and is therefore a transcription activating ncRNA[43].

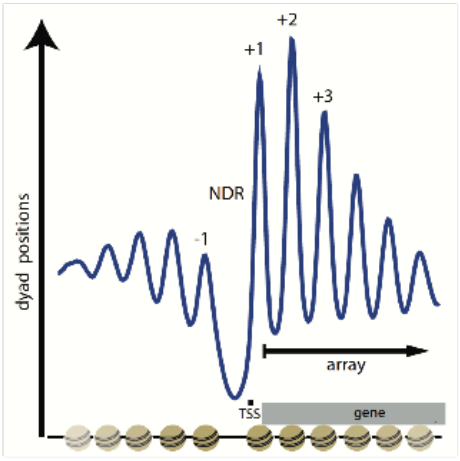

Figure 1.2 Schematic representation of a nucleosomal array. In yeast, the NDR correlates with promoters that allow transcription initiation and the production of canonical mRNAs. The TSS gets flanked by a well-positioned -1 and +1 nucleosome in wild type settings. Proper chromatin organization efficiently hides cryptic promoter sites and keeps cryptic transcription at low levels. Adapted and printed with permission from Lieleg *et al.*[28].

Epigenetic tools modulate transcription

Regulation of DNA accessibility goes beyond the classical understanding of biology, where a gene leads to a function. Epigenetics was once described by Conrad Waddington as "the branch of biology which studies the causal interactions between genes as their products which bring the phenotype into being"[44,45]. Currently, the understanding is defined by "the study of changes in gene function that are mitotically and/or meiotically heritable and that do not entail a change in DNA sequence"[45]. Indeed, DNA methylation, posttranslational histone modifications and the exchange of histone variants can have profound impact on DNA accessibility yet do not alter the underlying DNA sequence and are not necessarily heritable[46,47].

While humans count almost 20 different histone variants, the model organism *S. cerevisiae*, which was used in this work, encompasses merely two different histone variants. Htz1 (H2A.Z) and Cse4 (CENP-A) are the only representatives[48]. Cse4 is a centromeric histone H3 variant and leads to the formation of centromeric chromatin[49,50]. A detailed analysis of the structure and functions of H2A.Z (Htz1) can be found in section 1.2.2. The extensive possibilities of posttranslational histone modifications (PTMs) can control the transcription machinery even further. Those small, chemical modifications occur on many amino acids located in the histone tails, but also globular histone modifications are possible[51]. The wide range of resulting signaling pathways are not fully understood, a small insight is given in section 1.2,

focusing on the PTMs that were relevant for this study. To add another layer of transcription regulation, crosstalk between all the above-mentioned epigenetic marks is possible (Figure 1.2).

Since DNA accessibility is a key prerequisite for RNA Polymerase II functions, it must be modulated carefully[52]. Nucleosomes represent a physical barrier for RNA Polymerase II. Histone chaperones, chromatin remodelers and histone modifying enzymes all modulate DNA accessibility. Functions of chromatin remodelers will be especially examined in this work. Therefore, deeper insight is given in section 1.3.

1.2 Posttranslational modifications of histones

As discussed in the section before, epigenetics or chromatin biology explain altered chromatin structure, so that transcriptional repression or activation is taking place, despite the underlying DNA code is unchanged. For the purpose of better understanding the outcome of the experiments performed, I will only explain the histone variant H2A.Z and selected posttranslational histone modifications in more detail.

1.2.1 The versatile role of PTMs

Posttranslational histone modifications represent one complex layer of gene regulation in epigenetic contexts. Directly by altering chromatin moieties, or indirectly by recruiting factors, PTMs can facilitate or impede RNA Polymerase II accessibility on chromatin. They can serve as a recruitment platform for chromatin related proteins that are then referred to as "reader" proteins. Whereas phosphorylation, methylation, acetylation and ubiquitylation are among the most abundant and well studied PTMs, a plethora of further possible modifications include SUMOylation, formylation, glycosylation, ADP-ribosylation, butyrylation, deamination, propionylation and crotonylation[53]. Usually, writers and erasers posttranslationally modify the histone tails, but also the histone fold domain can undergo substantial modifications. The concerted action of such "reader", "writer" and "eraser" proteins thus allow fine-tuning of transcription. In terms of relevance for this study, a special emphasis will be on histone methylation and acetylation.

Methylation takes place as mono- (me1) or dimethylation (me2) on lysines or arginines, whereas trimethylation (me3) occurs only on lysines. This does not alter the positive charge of the nitrogen. Methylation can be, but does not have to be symmetrical, considering each histone modification existing twice per nucleosome[54,55]. Given those possibilities, methylation creates the most diverse patterns among PTMs. In yeast, H3K4, H3K36, H3K79 and H4K20 are common methylation sites. Writer proteins such as methyltransferases (KMTs) catalyze the transfer of methyl groups from S-adenosyl-L-methionine (SAM)[56]. Being methylated,

it can recruit reader proteins that contain domains, specialized for methylation recognition, e.g. PWWP domains or PHD fingers[57].

The KTM Set2 mediates mono-, di- and trimethylation of H3K36 at mid to 3'-ends of genes in budding yeast, acting as a writer[58–61]. The transcription elongation factor Spt6 is required for regulating Set2 activity. Recognizing the highly phosphorylated C-terminal domain (CTD) through a SH2 domain[62,63], Spt6 directly binds to Rpb1, the largest subunit of RNA Polymerase II[64–66]. This allows Set2 to associate with the elongating form of RNA Polymerase II through a putative WW domain[67,68]. Methylated H3K36 is crucial for recruiting the deacetylase Rpd3S onto RNA Polymerase II, since only methylation activates its activity[69], ensuring that histones residing in coding regions remain in a hypoacetylated state[58,70–72]. Therefore, H3K36me3 represses intragenic transcription and is a mark of actively transcribed genes[58,73]. While Set2 methylates H3K36 over gene bodies, Set1 methylates H3K4 at the 5'-ends of genes in yeast. Demethylation of that specific mark is carried out by Jhd2[74]. Both the H3K4me3 and H3K36me3 methylation marks are enriched over actively transcribed genes, yet are found at distinct locations[75]. Set1 is one out of seven proteins forming the COMPASS complex[76–78]. It is recruited to the 5'-ends of genes by binding the Ser5-phosphorylated CTD through its N-terminal domain[77,79–82]. Notably, COMPASS activity relies on the prior H2B ubiquitylation[83,84].

Acetylated histones have a stronger and cumulative effect on chromatin landscape per se. Through charge neutralization, acetylation generates a more open chromatin structure. Using acetyl-CoA, histone acetyl transferases (HATs) acetylate lysines, including numerous lysine residues on histones H3 and H4 and thus act as writers. Specific acetylation readers such as bromodomains can be recruited[85–88]. Vice versa, histone deacetylases (HDACs) remove this mark by splitting off acetate, thereby repressing transcription[89]. HATs can be distinguished in two groups[53,90]. Type A HATs only acetylate histones packed in nucleosomes and are therefore found in the nucleus. Such a HAT is Gcn5 in yeast, which is part of the 19 subunit SAGA complex[91–97]. Acting within SAGA, Gcn5 acetylates H3K9, H3K14, H3K18 and H3K23[94]. H3K9ac and H3K14ac can be found at the TSS[98]. On the other hand, type B HATS can only acetylate free, soluble histones and are thus located in the cytoplasm. Few type B HATs have been identified, e.g. Rtt109, which is responsible for H3K56ac[99–101]. Notably, substrate specificity can differ for *in vitro* and *in vivo* settings. Therefore, *in vitro* activity of Rtt109 is greatly enhanced when complexed

with Asf1[102]. H4 acetylation can be performed by the SAS and the NuA4 complexes[103,104]. Increasing H4 acetylation, especially H4K16ac, destabilizes nucleosomes and is connected to DNA repair[105–108]. The resulting "loose" chromatin structure allows facilitated passage of RNA Polymerase II, thus enhances transcription, however, also cryptic transcription.

1.2.2 The conflicting role of histone H2A.Z

The canonical histone octamer consists of a H3/H4 tetramer, associated on either side by a H2A/H2B dimer. Histone variants are known for all histones except H4 in higher eukaryotes. In yeast, only histone H2A and H3 can be replaced by Htz1 and Cse4, respectively[53,109].

The histone variant H2A.Z is one of numerous histone variants for H2A in mammals. In budding yeast, the homolog to H2A.Z is Htz1. First described in 1980 in mouse L1210 cells[110], it became obvious that H2A.Z is essential for viability in metazoans, however, not in *S. cerevisiae*, where its deletion leads to a mere growth defect[111,112]. Overexpression of Htz1 in yeast leads to abnormalities in budding, indicating that a fine-tuned Htz1 expression is required[113,114]. The two yeast histone chaperones Chz1 and Nap1 shuttle Htz1 from the cytoplasm into the nucleus[115–118]. The 14-subunit SWR1 complex catalyzes the ATP-dependent deposition of Htz1 in yeast, displacing H2A-H2B dimers in a stepwise reaction[119–121]. Both variants (human H2A.Z and yeast Htz1) share a ca. 69 % identity, marking its conservation (Figure 1.3A). Yeast canonical H2A and Htz1 share only ca. 61 % sequence identity (Figure 1.3B). Both, the lack of H2A.Z and overexpression of H2A.Z lead to dramatic outcomes since the latter one associates with a poor prognosis in human breast cancer progression[122,123]. A properly organized deposition of H2A.Z is therefore required.

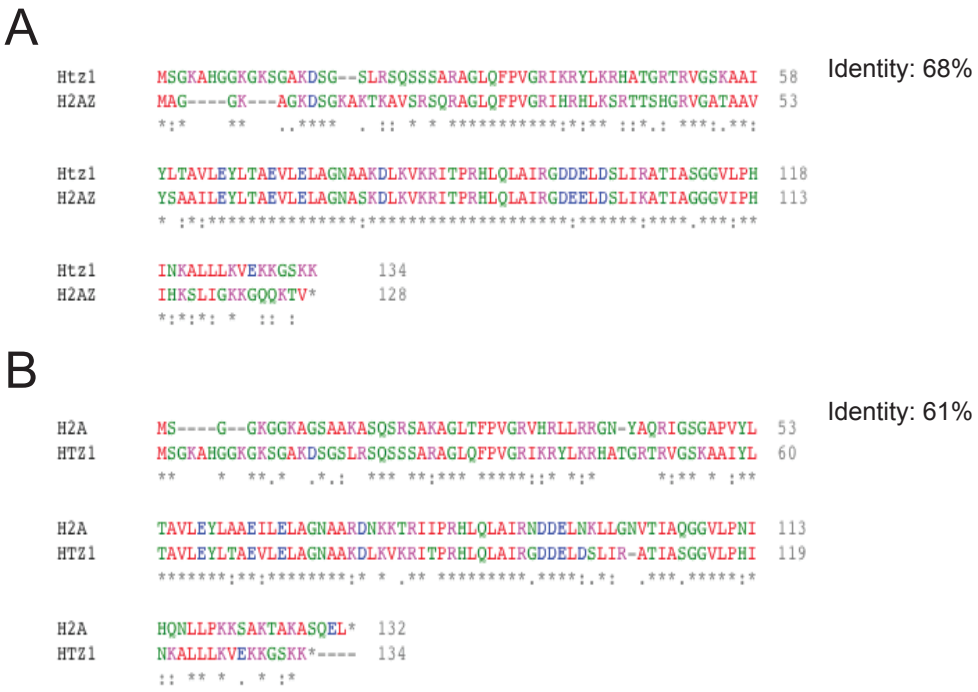

Figure 1.3 Sequence alignments of Htz1 with H2A and human H2A.Z. (A) Color-coded sequence alignment of yeast Htz1 with human H2A.Z. Sequence identity is 68 %. The star (*) marks identical amino acids, the double points (:) and the point (.) mark similar amino acids. **(B)** Color-coded sequence alignment of yeast Htz1 with yeast H2A. Sequence identity is 61 %. The star (*) marks identical amino acids, the double points (:) and the point (.) mark similar amino acids.

A consensus about the precise role of H2A.Z does not yet fully exist. The conflicting role of H2A.Z can be already detected at a structural level. The crystal structure containing H2A.Z is in principle similar to the canonical structure, however, suggesting different stability outcomes (Figure 1.4A). The incorporation of H2A.Z may lead to a subtle destabilization between the H2A.Z-H2B dimer and the H3/H4 tetramer inside the nucleosome, indicating that the whole H2A.Z-NCP is in general more destabilized. Compared to the canonical NCP structure, an extended acidic patch belonging to H2A.Z, protruding the core, can serve as an interaction platform for recruitment factors. A further, significant difference is the orientation of the L1 loop at the homotypic H2A-H2A' and H2A.Z-H2A.Z' contact points, being antiparallel in H2A- and parallel in H2A.Z-NCPs (Figure 1.4B), respectively. This element is responsible for holding the DNA gyres together suggesting a more stable H2A.Z-NCP than H2A-NCP and implying the incorporation of only H2A or H2A.Z due to steric reasons[124]. Meanwhile, the crystal structure of so-called heterotypic (H2A.Z and H2A inside the same octamer) nucleosomes suggest this being the most

stable alternative rather than the homotypic nucleosomes and indeed rejecting the hypothesis of a steric clash between the different L1 loops[125]. In terms of NCP stability, research outcomes are still controversial. Abbott and colleagues report a destabilizing effect coming from the incorporation of H2A.Z[126]. Supporting the other possibility is a further study revealing that H2A.Z-NCPs are less prone do DNA dissociation in rising salt environments, thus connecting H2A.Z with nucleosome stabilization[127]. A last, remarkable differences observed in the initial crystal structure by Suto *et al.* was the discovery of a bound metal ion displayed at the nucleosomal surface[124]. It can potentially alter nucleosomal moieties, creating a new recruitment surface – possibly PHD finger-domain containing proteins[124].

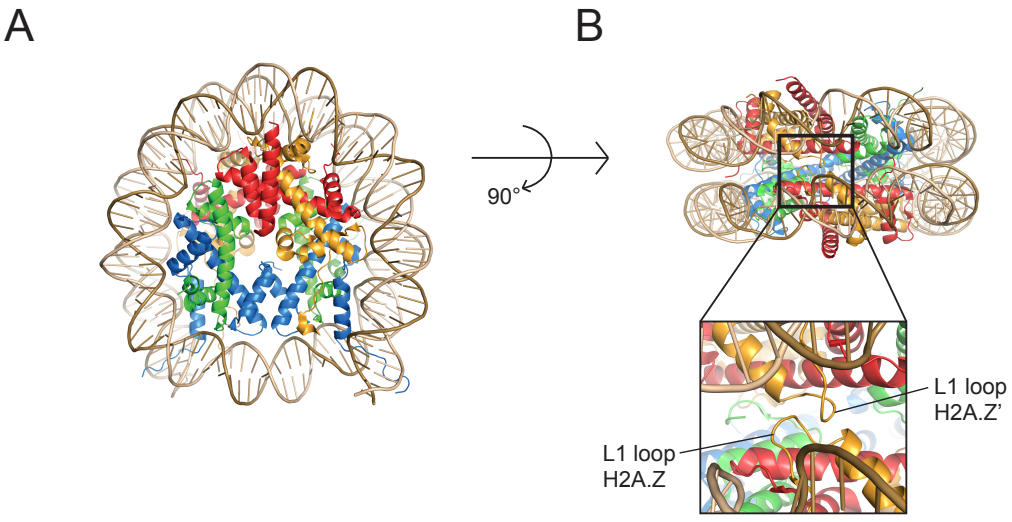

Figure 1.4 Crystal structure of H2A.Z-NCP. (A) Crystal structure of H2A.Z-NCP at 2.6 Å. The DNA double helix is wrapped around a histone octamer. H2A.Z is in orange, H2B is in red, H3 is in blue, H4 is in green. DNA double helix is in brown. **(B)** 90° rotation of the H2A.Z-NCP crystal structure. Boxed area was zoomed in below to point out the parallel orientation of the L1 loops of H2A.Z and H2A.Z'. Adapted from Suto *et al.*, using the accession code 1F66 for the structure from the Protein Data Bank[124].

Posttranslational modifications of H2A.Z add an additional layer of complexity and regulation. All studies and experimental outcomes regarding stabilization or destabilization of H2A.Z-containing nucleosomes are likely to be true for their own experimental setups. In fact, acetylated H2A.Z seems to play key role, whether the resulting NCP is stabilized or destabilized[128]. In yeast, Htz1 gets acetylated by the NuA4 complex on K14[129] but also K3ac, K8ac and K10ac are possible[130]. Interestingly, NuA4 shares four subunits with SWR1[68,120,131].

Regarding location, H2A.Z can be especially found at the +1 and the -1 nucleosome, flanking the transcription start site (TSS)[132]. Despite being close, its presence at the -1 nucleosome is connected to gene activity while its presence at the +1 nucleosome is thought to represent a barrier for RNA Polymerase II[133]. Gu *et al.* found up to 15 % Htz1 signals in yeast at the 3'-ends of genes for the purpose of marking the start of antisense transcripts there (5'-end of antisense transcripts)[134]. In line with this is the finding of Bagchi *et al.*, when H2A.Z is incorporated at the -1 nucleosomes it is considered to be a +1 nucleosome during antisense transcription and marking bidirectional transcription[135]. Taken together, H2A.Z localization marks the start of transcription at any given location and directionality.

Notably, H3K4me3, can be found in combination with H2A.Z-containing nucleosomes – a sign of active chromatin[136]. Predominantly found at actively transcribed genes, H2A.Z can also mark enhancers, here likely together with H3K27ac[137]. The spatial distribution of H2A.Z together with its distinct structural moieties may facilitate the formation of a compacted chromatin fiber[127,138], however, euchromatic regions encompassing H2A.Z were observed to be less stable[139,140].

On a functional level, H2A.Z has a conflicting role, too. While most studies correlate H2A.Z with transcription activation and open chromatin, some report a negative impact on the transcription machinery. More precisely, in *S. cerevisiae* the *PHO5* and *GAL1* promoters containing histone Htz1 become activated[48]. The HMR locus and telomeres, however, are silenced when histone Htz1 is present[141]. This controversial scientific debate just underlines the highly dynamic nature of H2A.Z.

1.3 Chromatin remodelers in yeast

Chromatin naturally hinders all processes that require DNA access such as transcription, DNA damage repair and replication. Besides histone variants and PTMs, histone chaperones and chromatin remodelers are further options to modulate chromatin organization.

1.3.1 ATP-dependent chromatin remodelers

Chromatin remodelers are mostly large, multi-subunit complexes that use the energy won from ATP hydrolysis to slide, evict, exchange, assemble or space nucleosomes[26,142]. Based on the structural similarity of their ATPases, four major families were classified in *S. cerevisiae*: SWI/SNF, CHD, INO80 and ISWI. They belong to the superfamily II (SF2) helicase/translocase like proteins[143,144]. All families with the exception of Chd1 contain more than one remodeler as well as further subunits that lead to increased functional diversity[145].

The SWI/SNF family was the first one to be discovered. Its name derives from *swi*tch defective/*s*ucrose *n*on-*f*ermenting. The abbreviation points towards its *in vivo* function, since it was identified as a regulator of the sucrose fermentation pathway and further regulates yeast mating type *swi*tching[146–148]. In yeast, they form two separate complexes, SWI/SNF (with its ATPase Swi2/Snf2) and RSC (with its ATPase Sth1)[143]. The split ATPase (Figure 1.5) of the Swi2/Snf2 subunit is stimulated by DNA and mechanistically translocates it[149,150].

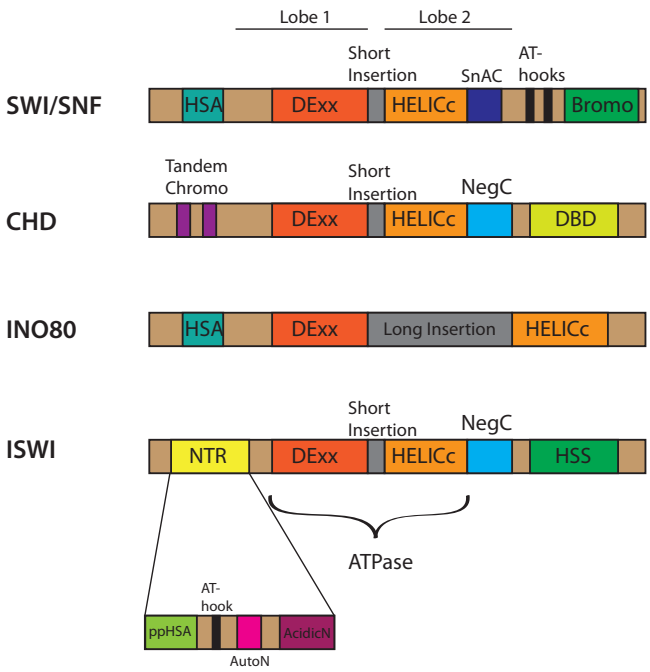

Figure 1.5 Overview of the four major chromatin remodeler families in yeast. SWI/SNF, CHD, INO80 and ISWI form the major families in yeast. Their ATPases are highly conserved, yet INO80 displays a split ATPase, indicated by the long insertion. All others just have a short insertion (gray). ISWI is intrinsically regulated by AutoN and NegC. CHD harbors a tandem chromodomain. Adapted and modified from Workman *et al.*[53] and Ludwigsen *et al.*[151].

Chd1 is the only representative of the CHD (*C*hromodomain, *h*elicase, *DNA-bind*ing) family in yeast and also the only monomeric remodeler. However, the CHD family is highly conserved from yeast to humans[143,152]. It has two characteristic, N-terminal chromodomains (Figure 1.5). Chd1 is involved in nucleosome positioning. Deletion of the chromatin remodeler together with Isw1 correlates with growth defects and a decreased lifespan in yeast[153–157]. Additionally, Chd1 ensures recycling of existing nucleosomes over gene bodies. This results in less incorporation of H3K56ac over ORFs. Thus, keeping cryptic transcription at minimal levels, since intragenic transcription initiation is mostly prevented[158,159].

The INO80 (*ino*sitol requiring *80*) family has two main ATPases, Ino80 and Swr1 that lend their names to the respective complexes. Swr1 can restructure the nucleosome by exchanging the canonical H2A/H2B dimer into Htz1/H2B dimers using the energy generated during ATP hydrolysis[120,160]. Among the 14 subunits, not all are unique to Swr1, since e.g. Arp4 or Act1 are within the group forming the Ino80 chromatin remodeling complex. INO80 is involved in DNA damage repair[161,162],

slides and spaces nucleosomes and positions the +1 and -1 nucleosome flanking the TSS[163–165]. It preferentially exchanges H2A.Z-H2B dimers back into their canonical versions[165]. The redundant subunits are auxiliary but not exclusively necessary for histone exchange, albeit *arp1*Δ reduces replacement activity by 28 %[119]. Although not specifically recruited to H2A.Z containing sites, Ino80 displays increased sliding ability *in vitro* when using H2A.Z-containing nucleosomes. In contrast, there is some data showing that activities of Chd1, Rsc, Swi/Snf and Isw1 were decreased in Htz1-containing nucleosomes in *S. cerevisiae*[166].

The ISWI (*I*mitation *swi*tch) family shares two ATPase homologs: Isw1 and Isw2[157]. They contain a C-terminal HAND-SANT-SLIDE domain (HSS) that mediates histone H3 (SANT) and DNA (SLIDE) interactions[167,168]. Activity of the catalytic subunit is intrinsically regulated by the AutoN and NegC regions[169]. The AutoN motif is embedded in the N-terminal region (NTR) (Figure 1.5)[151]. Isw2 can form a complex with Itc1[157]. Isw1 and Isw2 complexes were discovered in 1999 by the Wu Lab, it was first suggested that Isw1 forms a four component complex[157]. Later on, Vary *et al.* revealed that Isw1 forms two separate complexes[170]. Together with Ioc3 it forms the Isw1a complex, while it associates with Ioc2 and Ioc4 to form the Isw1b complex[170]. Isw1 monomer seems to exist independently as well. It interacts with Rrp6, which is part of the nuclear exosome that degradates unmatured RNAs. Together they act as quality control factors for proper nuclear mRNA surveillance[171–175]. Further, Isw1 associates with the rDNA locus, keeping it in a heterochromatin state[176]. In *S. cerevisiae*, the CHD and ISWI families have overlapping functions, hence when functions and impact on chromatin are to be studied, double or triple deletions in combination with *chd1*Δ or *isw2*Δ are commonly used[157,177,178]. A separate analysis of the functions of Isw1a and Isw1b complex will be introduced in section 1.3.3.

1.3.2 A conserved mechanism of DNA translocation to achieve chromatin remodeling

Chd1, Snf2, Ino80^{core} and Isw1 complexes differ substantially in their structures and auxiliary subunits. Evolutionary conservation hinted, and recently published crystal structures or cryogenic electron microscopy (cryo-EM) structures further suggested a fundamentally common, ATP-dependent DNA translocation during the nucleosome sliding process[144,165,179–181].

The ATPase of Chd1 binds at SHL +2 according to its crystal structure, although the double chromodomain contacts DNA at SHL +1, explaining the mutually exclusive presence of linker histone H1 and Chd1 at the same sites. While lobe 1 of the ATPase interacts with histone H3, lobe 2 recognizes the histone H4 tail[182–185]. Notably, Chd1 binds to nucleosomal DNA by swinging its double chromodomain at around 15°[186]. Extranucleosomal DNA is only weakly recognized. At the beginning of the reaction the ATPase is only partially closed. Upon ATP hydrolysis, the ATPase is fully closing, translocating 1 bp DNA per sliding reaction. The detached DNA is moved in a 5' to 3' direction towards the histone octamer dyad. During this process, Chd1 manages to stay attached to the histones.

The cryo-EM structure of Isw1 also reveals a conserved mechanism of DNA distortion. Being bound at SHL +2, hydrolysis of ATP leads to a conformational change. Lobe 2 of the ATPase rotates about 148°, creating a lobe 1 - lobe 2 cleft that serves as a new DNA-binding site (Figure 1.6). Thereby, the inhibitory AutoN region does not touch the nucleosome and thus enables remodeling activity. When bound to ADP, Isw1 creates a 1 bp bulge, translocating DNA from the entry[187]. Surprisingly, the AutoN region seems to have a dual role in Isw1 activity regulation. In the absence of a nucleosome it intrinsically inhibits ATPase activity, by mimicking the basic patch of the H4 tail[169,188,189]. Once activated it supports nucleosome sliding by interacting with lobe 1 of the ATPase. The NegC region couples of ATP hydrolysis to translocation[169]. However, it is melted in the activated state[187]. Orientation of the HSS domain could not be observed in the cryo-EM structure.

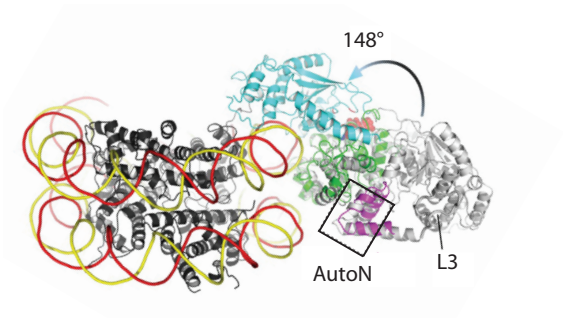

Figure 1.6 Cryo-EM structure of Isw1 bound to a nucleosome. Upon ATP hydrolysis lobe 2 of the ATPase (cyan) rotates 148° towards the nucleosome, opening a new DNA-binding site for proper attachment. The inhibitory AutoN region does not get in touch with the nucleosome end thus enables remodeling activity. Adapted and printed with permission from Yan *et al.*[187].

The current knowledge of all four families displays a conserved mechanism of DNA translocation to achieve chromatin remodeling. Small differences make each complex unique, the addition of further subunits is likely to change the mechanism even further to fine-tune nucleosome sliding. The following section will especially examine the structure and discrepancies between Isw1a and Isw1b complex.

1.3.3 Isw1 chromatin remodelers

1.3.3.1 Structure and functions of the Isw1a complex

The Isw1a complex consists of Isw1 and Ioc3[170]. Complex formation of Isw1a is regulated by SUMOylation. Multiple sites become SUMOylated within the Isw1 C-terminusand inside the HSS domain, promoting Ioc3 interaction. Without SUMOylation complex formation decreases up to 50 %[190]. The crystal structure of Ioc3 complexed with the Isw1 HSS domain reveals that the HSS-binding domain in Ioc3 interacts with the SLIDE domain of Isw1 (Figure 1.7)[167,168]. The SLIDE domain also associates with the Ioc3 core (Figure 1.7). Ioc3 compromises a HLB domain and a CLB N-coil and CLB C-coil that mediate all potential DNA contacts. Moreover, the Ioc3 HLB domain is responsible for dinucleosome recognition by Isw1a[191]. The Ioc3-HSS crystal structure was obtained using a truncated version of Ioc3 (aa 138-747 out of 1-787), leaving the structure of the N- and C-termini unknown[167].

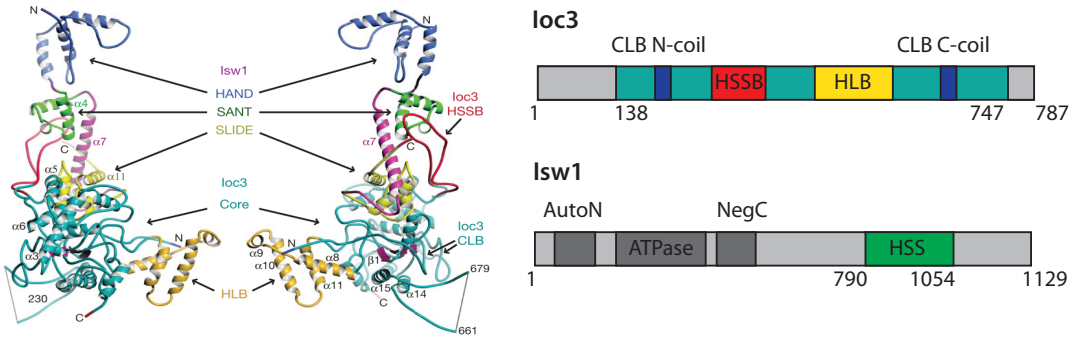

Figure 1.7 Crystal structure of Ioc3-HSS. In the crystal structure (left) the Ioc3 core is colored in cyan and compromises the CLB N- and C-coil. The HLB domain and the HSSB domain are colored in yellow and red, respectively. The Isw1 HAND-SANT-SLIDE domain is colored in violet, green and light yellow. In the simplified schematic representation (right) only colored parts could be observed the crystal structure. Adapted and printed with permission from Yamada *et al.*[167].

Our lab and others have shown that Ioc3 is recruited to the ends of genes, more precisely to the +1 nucleosome and the terminal nucleosome[158,192]. Ioc3 enrichment is also taking place at ncRNA and tRNA genes[193]. Currently, it is unclear what factors recruit Ioc3/Isw1a to those specific sites and whether recruitment is direct or indirect. In the absence of the two histone chaperones Chz1 and Nap1, Ioc3 and Isw1 were

detected to interact with Htz1 in mass spectrometry experiments[115]. Yamada *et al.* propose that the whole complex binds to the -2 and -1 nucleosomes, allowing for the repositioning of the -1 and +1 nucleosomes. A possible sequence specificity by Ioc3 was suggested to regulate Isw1a orientation[167].

In vivo, Isw1a has been shown to repress initiation and transcription of *MET16* by shifting its -1 nucleosome, masking the TATA box[168,194,195]. Using northern blots, we see elevated levels of cryptic transcription for *ioc3*Δ*chd1*Δ compared to wild type. Our unpublished data further indicate higher levels of histone turnover over transcription start sites in an *ioc3*Δ mutant, illustrated by the increased incorporation of H3K56ac.

Isw1a possess also a functional antagonism to the acetyltransferases Sas3 and Gcn5. While a *gcn5*Δ *sas3* yeast strain displayed a growth defect, additional deletion of *IOC3* rescued the phenotype. Further, deletion of these two enzymes decreased RNA polymerase II occupancy over active genes. However, additional Isw1a inactivation was able to restore RNA polymerase II occupancy, pointing towards a suppressive role for the remodeler complex[196].

In vitro, Isw1a slides end-positioned nucleosomes towards a centered position. However, it fails to move a nucleosome closer than 15 bp from a DNA end[177,197]. The specificity for end-positioned nucleosomes is not just an *in vitro* artifact, but rather due to the Ioc3 HLB domain. Isw1a$_{\Delta HLB}$ changes its substrate specificity towards middle-positioned nucleosomes. In general, Isw1a exhibited better remodeling activity when dinucleosomes instead of mononucleosomes were used as a substrate[191].

Together with the barrier factors Abf1 or Reb1, Isw1a was demonstrated to form correctly spaced arrays in yeast by positioning the +1 nucleosome[164]. This *in vitro* finding might be relevant for *in vivo* situations, where Isw1a regulates gene expression by toggling the +1 nucleosome.

1.3.3.2 Functions of the Isw1b complex

The ATPase Isw1 also forms a stable complex with Ioc2 and Ioc4 called Isw1b. Complex formation is dependent on all three proteins. Deletion of one subunit disrupts the whole Isw1b complex[170]. While Ioc3 connects only with the SLIDE domain of Isw1 to form Isw1a, Ioc4 and Ioc2 require both, the SANT and the SLIDE domains to form a stable complex, as well as the Isw1 C-terminus. The exact interaction sites in Ioc4 and Ioc2 are unknown. Moreover, the Isw1 N-terminus seems to play a crucial role in Isw1b complex formation[168].

The only known domain in Ioc4 is the PWWP domain. For further information about PWWP-domain containing proteins see chapter 1.4. Ioc2 has a putative PHD-like domain and harbors a sequence that shares homology to the human androgen receptor (Figure 1.8)[170]. The importance of those two domains and the whole Ioc2 subunit for the Isw1b complex remain largely unknown.

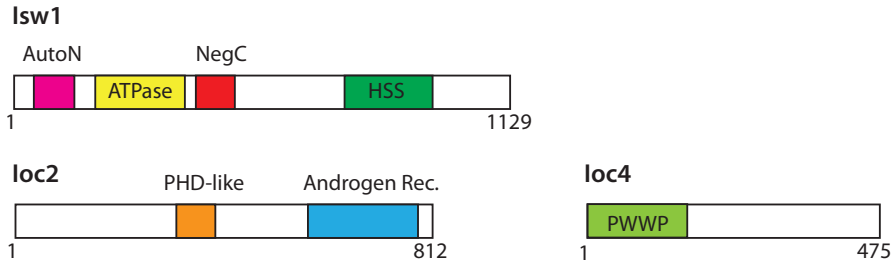

Figure 1.8 Domain diagrams of Isw1, Ioc2 and Ioc4 that form the Isw1b complex.

In vitro functions of Isw1b are similar to *in vitro* Isw1a function, yet there are differences. Both complexes can slide nucleosomes. While Isw1a prefers middle-positioned nucleosomes as a substrate, Isw1b prefers end-positioned nucleosomes[170,177]. A recent study states that *in vitro* remodeling activity of Isw1b is around 20 times faster than of Isw1a for mononucleosomes[191]. This is in contradiction with older studies, where sliding activity for mononucleosomes seems to be similar for both Isw1a and Isw1b[170,198]. Isw1b in general recognizes mononucleosomes and dinucleosomes equally well. The Ioc3-HLB domain is responsible for preferring binding to dinucleosomes in Isw1a. Hence, sliding activity is enhanced for dinucleosomes when using Isw1a as a remodeler. This is not the case for Isw1b, nevertheless it resolves close-packed dinucleosomes[191,199,200]. Further, both complexes can space nucleosomes, yet spacing activity of Isw1a is greater than that of

Isw1b[164,170]. Nucleosome recognition takes place in an ATP-independent manner[170]. Suggesting that Isw1b is less sensitive to DNA than Isw1a, Isw1b has the ability to disrupt nucleosomes and 'unravel' DNA from nucleosomes[199].

In vivo, Isw1b differs from Isw1a functions. In microarray analyses, Vary and colleagues found distinct transcriptional repression profiles for *ioc2*Δ and *ioc3*Δ, indicating that Isw1a and Isw1b act on different loci in the genome[170]. In wild type settings, mid to 3'-ends of genes become H3K36 trimethylated by Set2[58,201]. H3K36me3 is a mark for actively transcribed genes and recruits Isw1b through the $Ioc4_{PWWP}$ domain[158,202]. During transcription, RNA polymerase II needs access to free DNA, therefore, histones are ejected and/or disassembled[203–206]. Being recruited to ORFs, Isw1b together with Chd1 prevent trans-histone exchange by recycling K36 methylated histones[158]. New, soluble and highly acetylated histones do not get incorporated, so that the chromatin structure remains in a hypoacetylated state and cryptic promoter-like elements stay hidden[158,207,208]. The chromatin remodelers prevent the rise of cryptic transcription that occurs with increased levels of histone acetylation over ORFs (Figure 1.9).

Specifically, aromatic cage mutations in the PWWP domain resulted in reduced chromatin association of Isw1b[202]. The question whether other binding sites in Ioc2 or Ioc4 contribute to chromatin associations is yet unanswered. It was further suggested, that Isw1 recognizes H3K4me3 *in vivo*[209], yet the question whether Isw1b also recognizes H3K4me3 was clearly rejected[202].

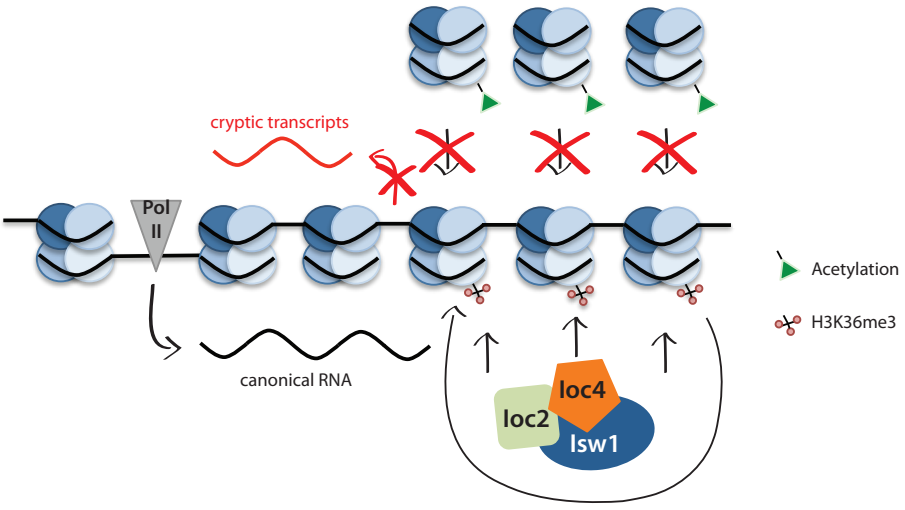

Figure 1.9 Current model of Isw1b functions. Isw1b is recruited to H3K36me3-containing nucleosomes, which are located at mid to 3'-ends of genes. There, the complex prevents the incorporation of acetylated histones and thereby inhibits the rise of cryptic transcription (red).

1.4 PWWP-domain containing proteins

PWWP-domain containing proteins were first described in 1998. The team around Johan T. den Dunnen identified the 84 amino acid long domain in the Wolf Hirschhorn syndrome candidate 1 protein (WHSC1)[210]. Its inactivation leads to Wolf-Hirschhorn syndrome[210]. So far, more than 20 PWWP-domain containing proteins have been identified in humans. PWWP domains implement into the Royal superfamily of chromatin readers, which includes Chromo, malignant brain tumor (MBT) and Tudor domains. Evolutionary sharing a structurally common ancestor characterized by three β-strands, their tasks are all among reading histone modifications[211].

The name "PWWP" derives from the embedded motif (proline – tryptophan – tryptophan – proline). The P-W-W-P motif is mostly conserved, but was only accidentally chosen[210,212]. The first proline and the adjacent tryptophan are often exchanged into serine and/or alanine, leading to e.g. S-A-W-P (Ioc4)[202] or S-W-W-P (Dnmt3a)[213], but also P-H-W-P (HDGF)[214] motifs exist. The last two amino acids (W-P) are conserved more often. Exceptions exist (P-S-Y-P motif), however they are rare. Further the composition of the P-W-W-P motif allows conclusions about protein moieties. Having a proline as the first amino acids may produce a protein, which is more stable, less dynamic and less prone to aggregation compared to alanine[215].

The consensus of length and composition of its amino acid sequence in a 'regular' PWWP domain has changed over time. Most PWWP domain span 70-100 amino acids while some are much longer (178 amino acids in Ioc4). The discrepancy was revealed by comparing the published crystal structures (see for example Figures 1.10A and 1.11A). The regular PWWP domain has an N-terminal β–barrel, consisting of five β–strands packed against each other and is the most conserved part (Figure 1.10A)[216,217]. The P-W-W-P motif can be found in the β1-β2 arch, which represents the most conserved interface of the β-strands[218–220]. Least conserved is, however, the β2-β3 loop. Some PWWP domains exhibit an insertion motif between β2 and β3, which can vary in length and structure (BRPF1 in Figure 1.11A, HDGF, HDGF2, Pdp1 and Ioc4)[216,218,219,221–224]. Evolved by intron/exon sliding, the amount of α-helices and the existence of an optional insertion motif explain the variety in domain

length[212]. A striking variety can be observed in the C-terminus, consisting of one to six α-helices (Figure 1.10A). Only one α-helix is virtually identical in all PWWP domains and always packs against the β–barrel[221].

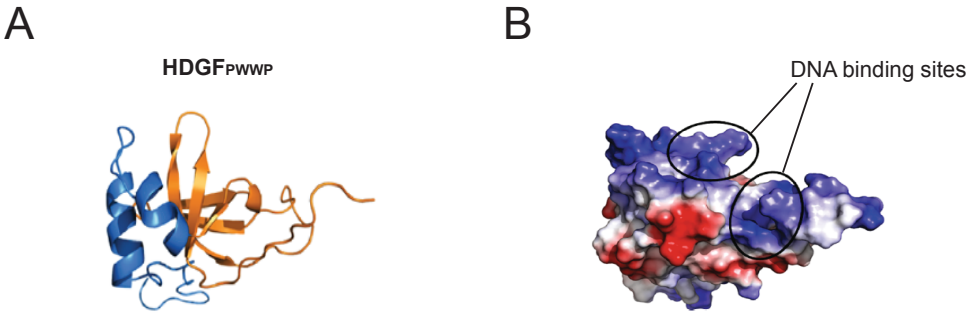

Figure 1.10 structure of the HDGF$_{PWWP}$ domain. (A) A C-terminal α-helix bundle (blue) packs against the well-conserved β–barrel (orange). **(B)** Electrostatic surface of the HDGF$_{PWWP}$ domain shows acidic (red) and basic (blue) patches. Marked elements mediate DNA-binding. Adapted and printed with permission from Rona *et al.*[225].

The crystal structures provide more instructive features. Having first suggested that PWWP domains mediate protein-protein interactions only[210], they are now well known DNA- and histone-binding domains[215,216,231,219,222,225–230]. Through a basic patch on the surface, dsDNA-binding can be mediated (Figure 1.10B). The interaction gets established through electrostatic interactions with the negatively charged phosphate backbone rather than sequence specific interactions with DNA bases. Only HDGF shows a preference for binding to the SMYD1 promoter containing a GC-rich element[226,232]. Further, DNMT3a does not seem to preferentially bind to AT-rich DNA sequences[213,216,233]. A recent publication suggests that the HRP3$_{PWWP}$ domain recognizes the minor groove of dsDNA[230]. DNA-binding occurs in the nM to μM ranges. Not all PWWP domains were examined well enough to clearly identify sequence specific binding preferences. Whether PWWP domains have significant affinities to ssDNA, dsRNA or ssRNA remains largely unknown[227,234,235].

The second predominant activity is the recognition of trimethylated lysines. Most of the PWWP domains have been shown to interact with trimethylated lysine 36 at histone H3 (H3K36me3)[228]. Only Pdp1 and HDGF2 prefer H4K20me and HDGF preferentially recognizes H3K79me3[219,223,236,237]. Overlays of PWWP crystal structures show that lysine recognition is well conserved. The aromatic cage lies within the β–barrel, precisely inside the β2 - β3 loop[219,223], generating a hydrophobic cavity to mediate contacts to the positively charged nitrogen via cation – π

interactions (Figure 1.11A)[238]. The K_d values for histone peptide binding are much lower compared to DNA-binding and range from µM to mM concentrations[234,235]. In 2020, Wang *et al.* published the crystal structure of the $LEDGF_{PWWP}$ domain bound to a nucleosome[239]. The specific binding site of the PWWP domain correlates with the protruding H3 tail, which harbors K36 methylation. The orientation of the PWWP domain allows simultaneous binding to H3K36me3 as well as to the adjacent DNA sites (Figure 1.11B)[239].

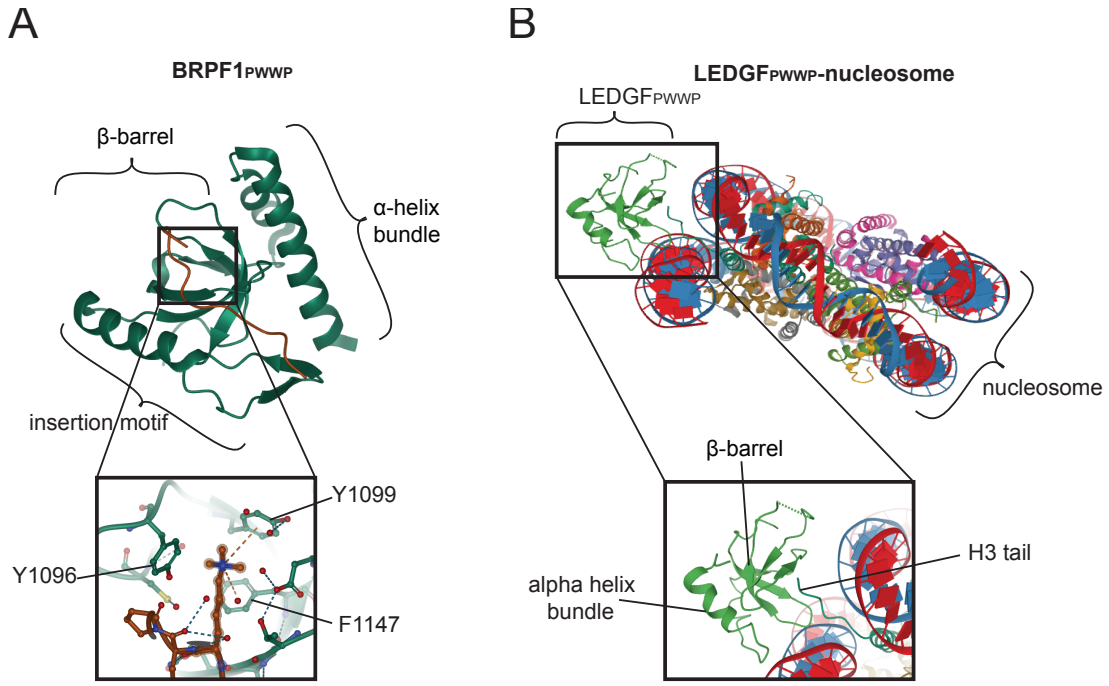

Figure 1.11 PWWP domains recognize methylated lysines. (A) $BRPF1_{PWWP}$ consist of a β barrel and a α-helix bundle. A long insertion motif between β2 and β3 can be observed, that is mostly folded. Zooming into the β–barrel, the aromatic cage can be seen (residues indicated) that bind to the positively charged amino group (blue) from Lys36 on histone H3. Adapted from Vezzoli *et al.* and analyzed in the Protein Data Bank using the accession code 2X4W[218]. **(B)** $LEDGF_{PWWP}$ bound to a nucleosome. The PWWP domain binds the nucleosome, where the H3 tail protrudes the core (zoom). This position enables DNA-binding and H3K36me3 recognition. Adapted from Wang *et al.* and analyzed using the accession code 6S01 in the Protein Data Bank[239].

The concerted action of DNA and histone-binding is not fully understood. Though association with DNA does not preclude binding to other substrates. Undisputedly, DNA-binding and histone recognition guide PWWP domains to their preferred targets. The PWWP domain is usually embedded at the N-terminus of their respective proteins. These fulfill a plethora of different functions that vary from development

(HDGF), transcriptional coactivation and lentiviral integration, which is crucial for HIV integration (PSIP1/LEDGF)[224,227,240]. Clinical outcomes for humans vary among schizophrenia and bipolar affective disorder (BRPF1) to tumorigenesis (HDGF) and colorectal cancer (MSH6)[241–245].

1.5 Objectives

In my PhD project I gained experience in the purification and quality control of recombinant and endogenous proteins. I established different purification strategies to achieve highly purified proteins to be used in *in vitro* assays. I focused on the purification of native complexes from wild type and mutant Isw1a and Isw1b chromatin remodelers, as well as overexpression and purification of recombinant wild type and mutant Ioc4, PWWP, Ioc3 and Isw1.

Highly purified proteins allowed me to conduct a number of *in vitro* assays to further understand the molecular recruitment mechanisms of Isw1a and Isw1b. Up to now, little is know about Isw1a recruitment. Our lab and others found that Isw1a is recruited to +1 nucleosomes. Since Isw1a and Isw1b share the same Isw1 subunit, we hypothesized that crucial features, that localizes Isw1a to the 5'-ends of genes must derive from the Ioc3 subunit. I therefore aimed to understand what attracts the complex. I further wanted to dissect what part in Ioc3 is responsible for doing so. The published crystal structure of Ioc3-HSS provides information about DNA interactions, however, leaves the question of a direct interaction partner to be elusive. By introducing truncations in Ioc3 I aimed to elucidate functional sites in Ioc3.

Knowledge of Isw1b recruitment is more advanced, since it is commonly accepted that the Ioc4$_{PWWP}$ domain recruits Isw1b to mid to 3'-ends of genes *in vivo*. This location includes Set2-mediated H3K36me3. The PWWP domain is a known methyl lysine reader and coordinates binding through its aromatic cage. It is not understood, though, whether auxiliary binding sites Ioc4 or Isw1b contribute to chromatin association. Further, I wanted to give special emphasis on the PWWP domain and evaluate its binding abilities with different substrates. Point mutants allowed me to analyze the importance of its DNA-binding ability. Our collaboration partner Jian Li obtained the crystal structure of Ioc4$_{PWWP}$ where we noticed a large insertion motif. Insertion motifs exist, however, few PWWP domains compromise one and no PWWP domain displays an insertion motif of this size. Thus, I planned to evaluate the contribution of such motif for PWWP, Ioc4 and lastly Isw1b.

2. Results

2.1 Refining purification and quality control of proteins

2.1.1 Purification of recombinant proteins

Biochemical *in vitro* studies often require large amounts of highly purified proteins. Often endogenous protein levels in yeast do not result in sufficient protein yields. Instead, recombinant proteins can be overexpressed and purified from *Escherichia coli (E. coli)*. However, this procedure may affect folding and stability of the proteins. Highly purified and stable proteins are essential to avoid false negative outcomes during experiments owing to protein misfolding, or false positive outcomes due to protein contaminations. To ensure that the biochemical *in vitro* experiments in this study were conducted with high quality proteins, several state-of-the-art techniques such as nanoDSF were applied. I also ensured optimized storage conditions for all proteins. General purification protocols can be found in Materials and Methods section 4.3.

2.1.1.1 Purification and quality control of wild type and mutant PWWP domain constructs

The wild type and one mutant ($PWWP_{2KE}$) domain were purified via a N-terminal 6xHis-tag (Figure 2.1.1). $PWWP_{2KE}$ was generated by mutating Lys149 and Lys150 both into glutamic acid.

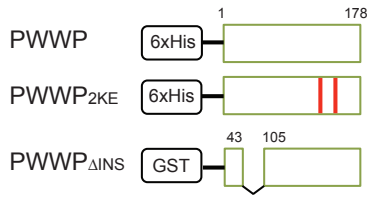

Figure 2.1.1 Diagram of the wild type and mutant PWWP domains.

After initial affinity chromatography the dialyzed proteins (6xHis-PWWP and 6xHis-$PWWP_{2KE}$) were subjected to anion exchange chromatography to separate the proteins from possible contaminations. The chromatograms for both the PWWP domain and $PWWP_{2KE}$ clearly show the separation from minor contaminations (Figure 2.1.2A). $PWWP_{\Delta INS}$ was purified through an N-terminal GST-tag (Figure 2.1.1), which was cleaved during the purification process. This truncation mutant was generated by deleting aa 43-105. $PWWP_{\Delta INS}$ did not undergo anion exchange chromatography, since after the GST-cleavage, no contaminations were visible in an SDS-PAGE gel (Figure 2.1.2B).

A

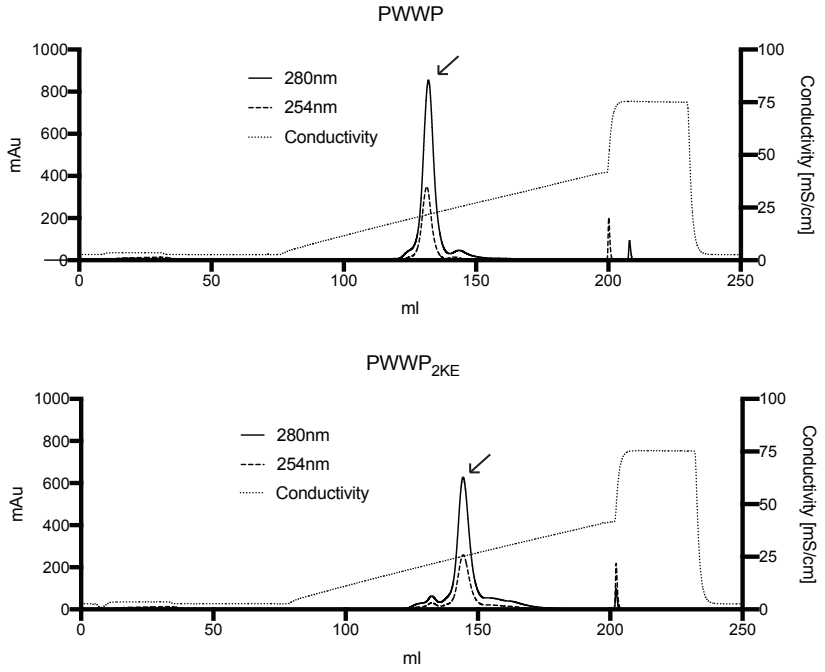

B

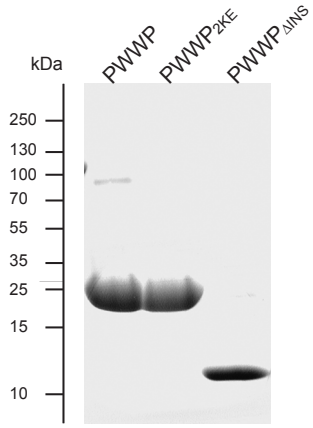

C

Protein	Mass	Concentration	A_{260}/A_{280}
PWWP	27 kDa	1.63 mg/ml	0.55
$PWWP_{2KE}$	27 kDa	1.05 mg/ml	0.54
$PWWP_{\Delta INS}$	13 kDa	0.63 mg/ml	0.57

Figure 2.1.2 Elution chromatograms for PWWP and $PWWP_{2KE}$ using anion exchange. **(A)** Protein eluates were applied to anion exchange chromatography. Purified proteins were eluted using a 10 mM – 1 M NaCl gradient. The arrow (←) indicates the peak of interest. **(B)** SDS-PAGE gel of PWWP, $PWWP_{2KE}$ and $PWWP_{\Delta INS}$ demonstrating a highly purified protein preparation. **(C)** Overview of final yields for each recombinant protein. Mass and concentration were calculated considering the tags. Note that $PWWP_{\Delta INS}$ is without tag.

Notably, a sharp and high peak indicates the detection of 6xHis-PWWP and 6xHis-$PWWP_{2KE}$, respectively (Figure 2.1.2A). Relevant elution fractions were pooled, concentrated and run on a SDS-PAGE gel (Figure 2.1.2B). Spectrophotometry was applied to measure the concentration of protein in each sample. The absorbance of proteins peaks at A = 280 nm, the absorbance of DNA at peaks 254 nm. Therefore an A_{254nm}/A_{280nm} ratio of 0.5 is desirable, since it indicates no contamination by DNA. The final concentrations and A_{254nm}/A_{280nm} ratios of each protein is shown in Figure 2.1.2C.

Protein stability is typically addressed by thermal unfolding experiments. Here, a Thermal Shift Assay (TSA) was performed to screen for optimal buffer conditions (Figure 2.1.3) and stabilizing additives (Figure 2.1.4). Optimal buffer conditions are characterized by increased melting temperatures (T_m), while destabilizing buffer conditions lower the T_m. Proteins were especially stable in phosphate buffer at pH 7.0. Also, the addition of 0.5 M - 1 M NaCl as well as 10 % (v/v) glycerol helped stabilize all PWWP domain constructs.

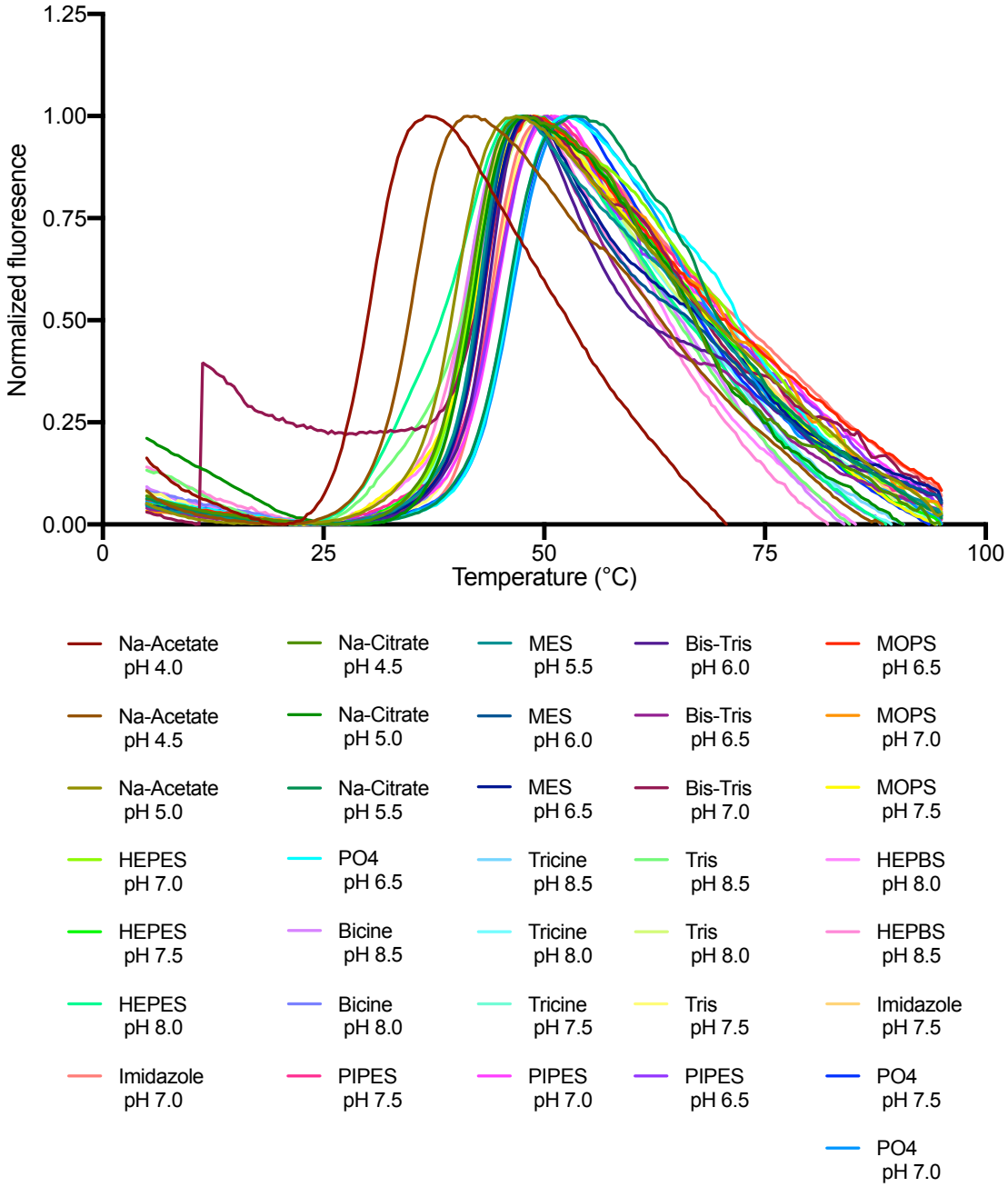

Figure 2.1.3 TSA screens for optimal buffer conditions for the wild type PWWP domain. Stability test for purified PWWP with several, color coded buffers reveal different melting curves. TSAs for buffer additive screen for $PWWP_{2KE}$ and $PWWP_{\Delta INS}$ can be found in Supplementary Figures 5.1 and 5.3, respectively.

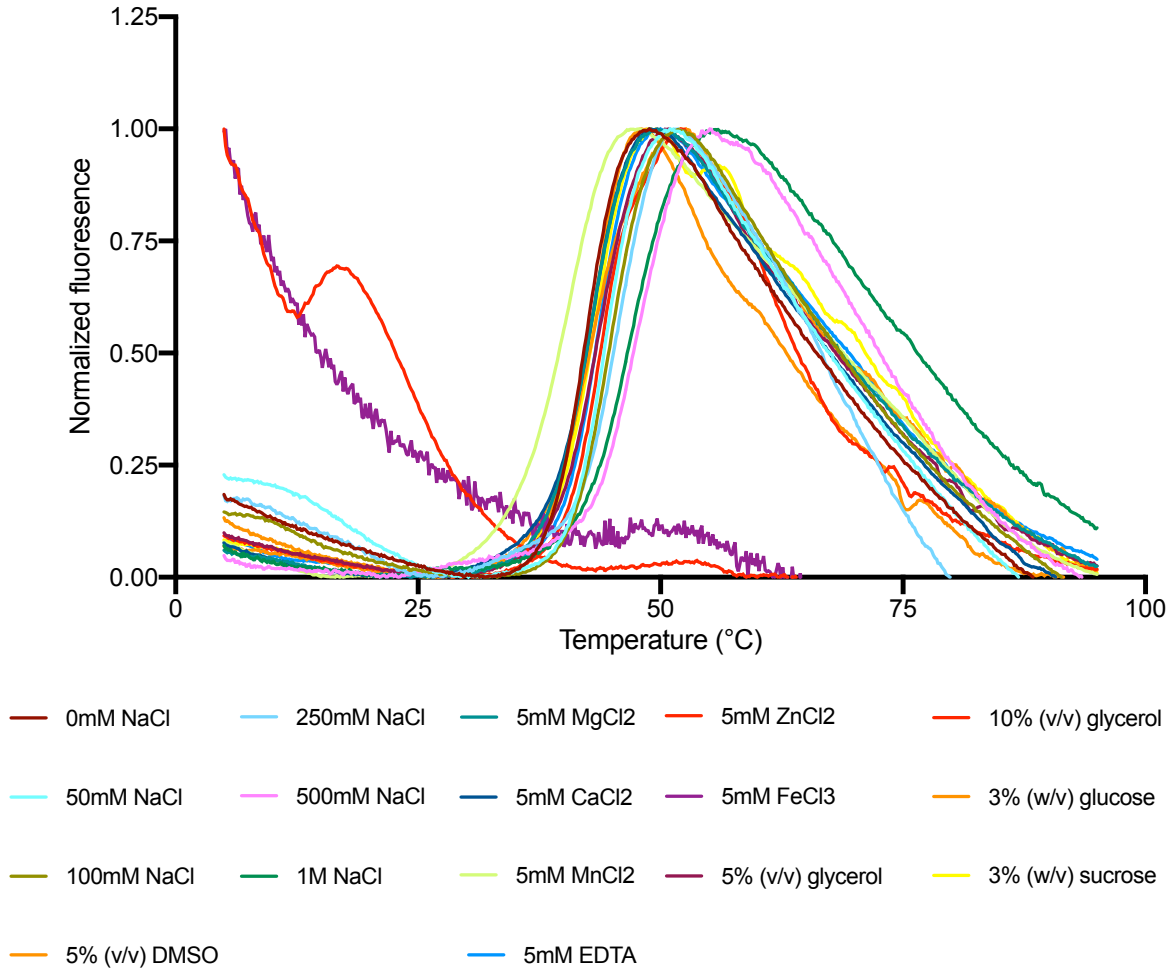

Figure 2.1.4 TSA screens for optimal buffer additives for the wild type PWWP domain. Stability tests with PWWP show that high salt concentrations (500 mM and 1 M) are suitable buffer additives, whereas $ZnCl_2$ and $FeCl_3$ result in protein aggregation. TSAs for buffer additive screen for $PWWP_{2KE}$ and $PWWP_{\Delta INS}$ can be found in Supplementary Figures 5.2 and 5.4, respectively.

Based on the TSA results, all PWWP constructs were dialyzed against a buffer containing 50 mM PO_4^{3-} pH 7.0, 500 mM NaCl and 10 % (v/v) glycerol.

Circular dichroism spectroscopy (CD) gave further insights into protein folding. The principle of CD is that circularly polarized light absorbs differently when meeting secondary protein structures, revealing important characteristics about optically active molecules. Measuring the far UV range (190 nm - 240 nm), α-helices, β-sheets and random coils display characteristic CD spectra (Figure 2.1.5A). Alpha-helices exhibit a double minimum at 208 nm and 222 nm and a stronger maximum at 191 nm. Analog, β-sheets have a minimum at 215 nm and a maximal absorption peak

at 198 nm. Random coils, i.e. unfolded parts display minima and maxima directly opposing those observed from α-helices and β-sheets[246,247].

6xHis-PWWP dips at around 205 nm and peaks towards 191 nm, displaying the presence of α-helices. The rising slope towards 222 nm indicates for the existence of β-sheets. As expected the point mutant $PWWP_{2KE}$ exhibits almost the same CD spectrum as wild type PWWP. The truncation mutant $PWWP_{\Delta INS}$ reveals a slightly different spectrum. The typical dip at 208 nm, indicating for α-helices, is slightly shifted towards 215 nm, suggesting a higher proportion of β-sheets within the structure. Supporting the evidence for β-sheets is a steep slope, peaking in a maximum between 190 nm - 200 nm, overlapping with the maxima peak for α-helices. The presence of such is also visible at a distinct minimum at 208 nm[246]. This is in agreement with observations from the crystal structure obtained for the wild type PWWP domain (see Figure 2.2.2A). To summarize, the CD spectra for all three proteins suggest that they are folded (Figure 2.1.5B).

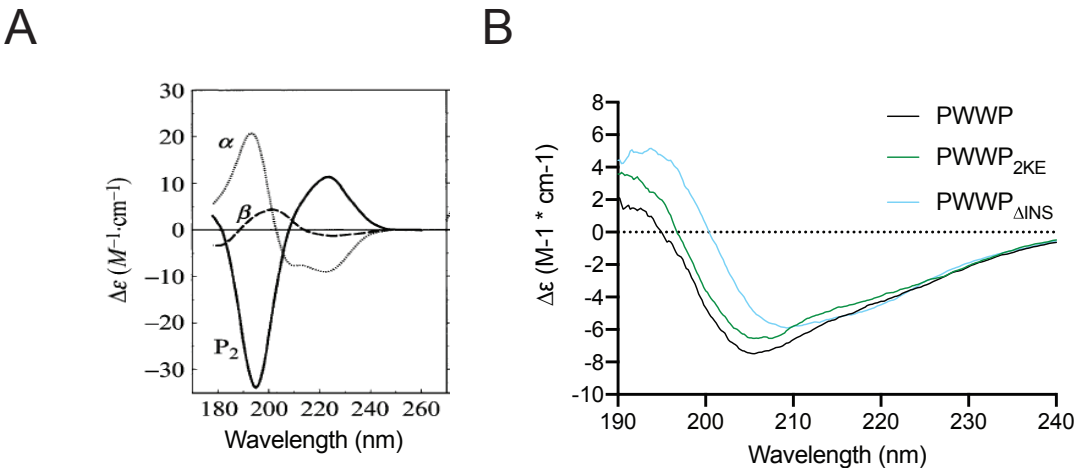

Figure 2.1.5 Circular dichroism of PWWP, $PWWP_{2KE}$ and $PWWP_{\Delta INS}$ showes folding of all three constructs. (A) Exemplary CD spectra showing perfect minima and maxima for α-helices, β-sheets and unstructured proteins (P_2). Figure adapted and printed with permission from Sreerama *et al.*[246]. **(B)** CD spectra for PWWP, $PWWP_{2KE}$ and $PWWP_{\Delta INS}$ revealing the presence of α-helices and β-sheets.

Finally, I used nanoDSF to determine more accurate melting temperatures and to investigate protein aggregation. nanoDSF is a technique which measures the autofluorescence of proteins determined by the number of exposed tryptophanes in a temperature gradient. During the unfolding process hidden tryptophanes become exposed or vice versa, and the change in autofluorescence is measured. The

instrument measures the $F_{350/330}$ ratio. While the intrinsic fluorescence of tryptophane is at 350 nm in water, a change in emission towards 330 nm takes place when thermal unfolding starts. This reveals the melting point in the first derivative of its function. Uniform curves and a well-shaped first derivative are quality control factors for highly purified and folded proteins. Secondly, by measuring the sample scattering, this provides information about protein aggregation. Figure 2.1.6A clearly shows that all three proteins are folded and not aggregated. Additionally the melting temperatures of PWWP and $PWWP_{2KE}$ are very similar (Figure 2.1.6B).

A

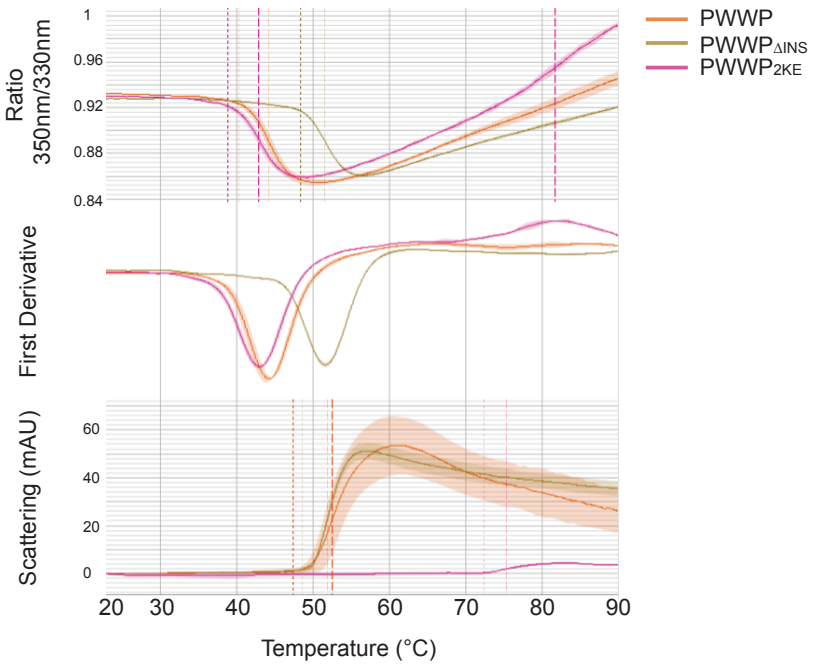

B

Protein	T_m
PWWP	44.21°C
$PWWP_{2KE}$	42.96°C
$PWWP_{\Delta INS}$	51.58°C

Figure 2.1.6 NanoDSF spectra of wild type and mutant PWWP. (A) NanoDSF reveals that PWWP, $PWWP_{2KE}$ and $PWWP_{\Delta INS}$ are folded. Calculating their first derivative corresponds to the melting temperature (T_m). Scattering curves exclude protein aggregation. **(B)** Melting temperatures extracted from the first derivative data in (A).

2.1.1.2 Purification and quality control of wild type and mutant Ioc4 constructs

Wild type and mutant Ioc4 constructs were tagged using an N-terminal 6xHis-MBP-tag (Figure 2.1.7). $Ioc4_{2KE}$ was generated by mutating Lys149 and Lys150 into glutamic acid. The two truncation mutants $Ioc4_{\Delta INS}$ and $Ioc4_{\Delta PWWP}$ were generated by deleting aa 43-105 and 1-178, respectively. To achieve reliable data concerning future binding ability in downstream applications, highly purified and stable protein was produced.

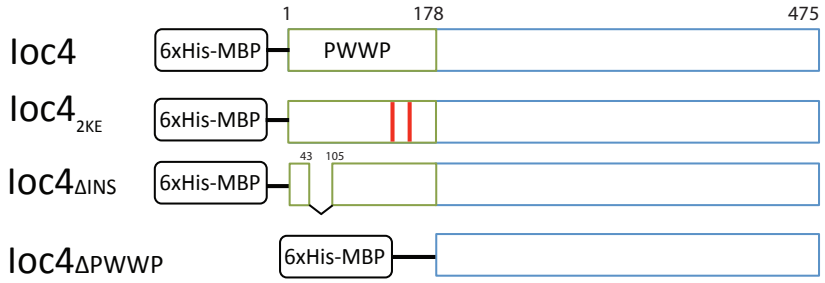

Figure 2.1.7 Diagram of the wild type and mutant Ioc4.

Initially purified by Ni-NTA chromatography, all proteins revealed high levels of DNA contamination based on absorbance measurements (data not shown). Therefore, all Ioc4 constructs were further purified by heparin chromatography (Figure 2.1.8A). Heparin mimics the backbone of DNA and is therefore often used for the purification of DNA-binding proteins. Relevant peak fractions were pooled and concentrated (Figure 2.1.8B).

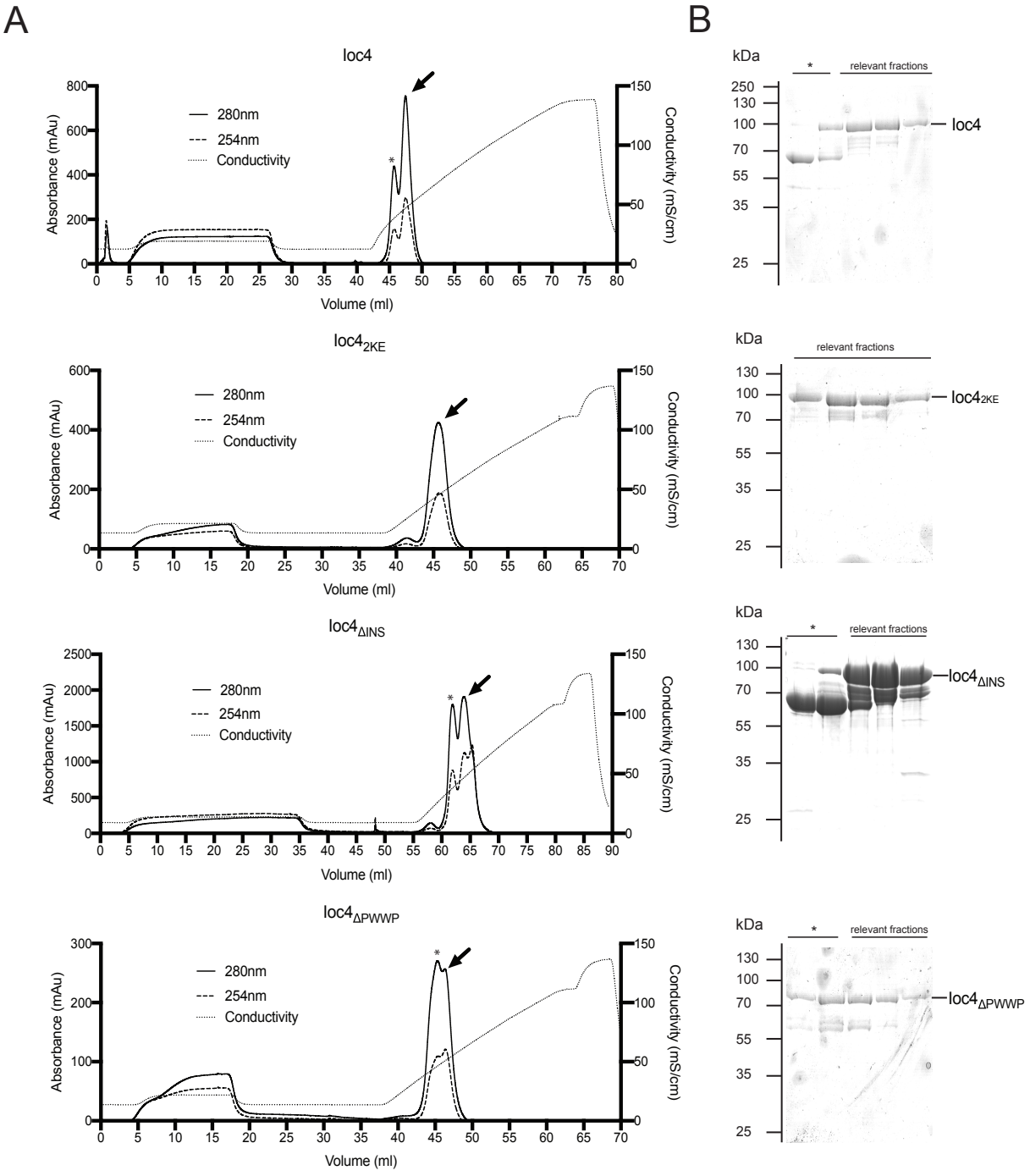

Figure 2.1.8 Chromatograms for wild type and mutant Ioc4 using heparin chromatography. **(A)** All proteins were loaded individually on a HiTrap Heparin column. Arrows (←) indicate the peaks of interest. Stars (*) indicate contaminations. **(B)** SDS-PAGE gels of the observed peaks. Stars (*) indicate the peaks containing contaminations. Fractions marked as 'relevant' derive from the peak of interest (←) and were further processed.

Heparin columns only clear proteins from DNA but not necessarily from other proteins and neither do they reveal aggregates. Size exclusion chromatography was used as a final polishing step. Relevant fractions were pooled, concentrated and

loaded on a size exclusion chromatography column (Figure 2.1.9A). This step separated proteins by size. Aggregated protein eluted in the void volume of 8 ml. Only nonaggregated protein was collected. SDS-PAGE gels of peak fractions revealed aggregation (Figure 2.1.9B, marked as *1) or contaminations (marked as *2 and *3 or x).

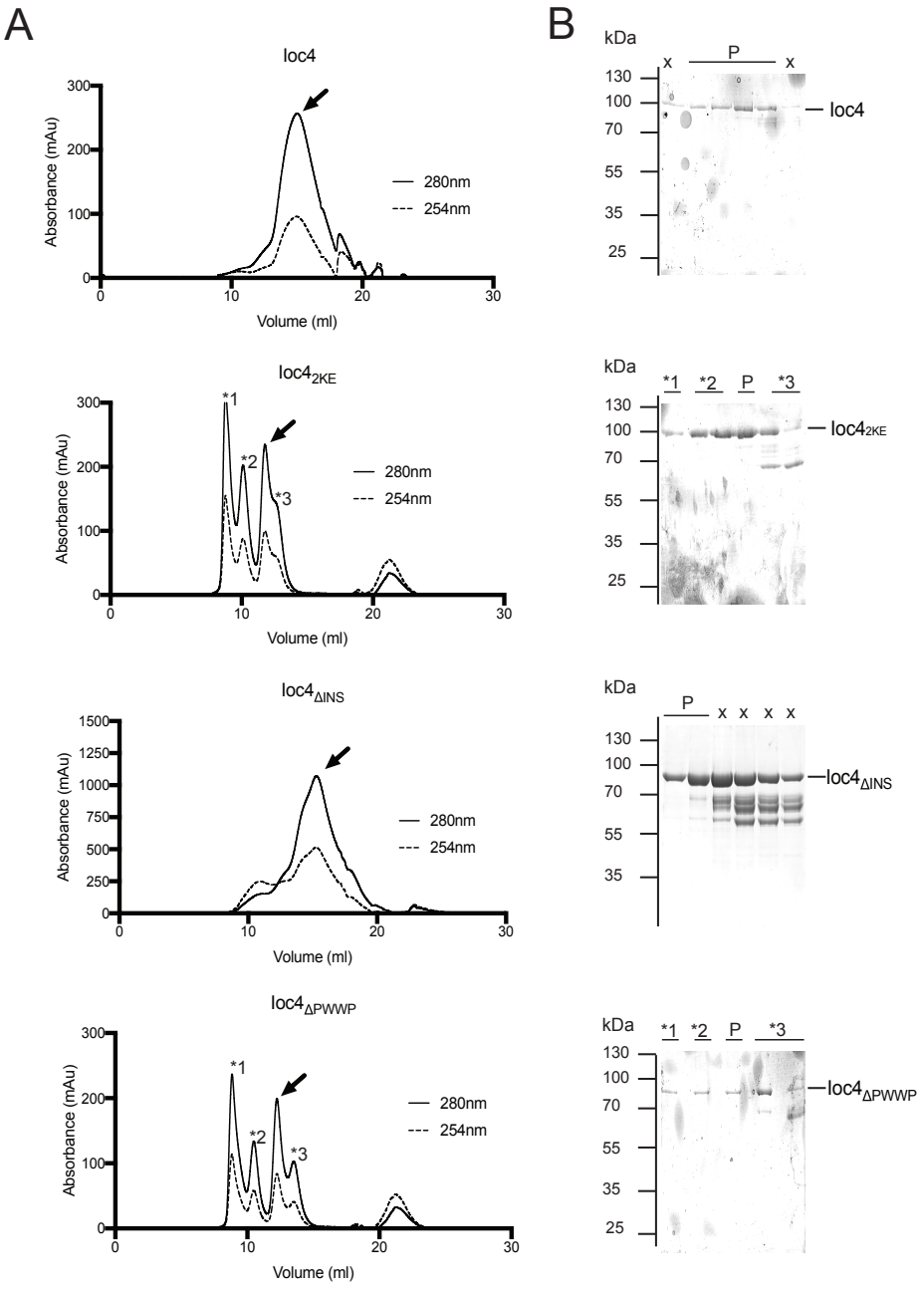

Figure 2.1.9 Size exclusion chromatograms for wild type and mutant Ioc4. (A) Individual proteins were loaded onto a Superdex200 Increase 10/300 GL column for size separation. Arrows (←) indicate the peaks of interest. Stars (*) indicate contaminations. **(B)** SDS-PAGE gels of the observed peaks. Stars (*) indicate the peaks containing contaminations. The adjacent numbers correlate with the numbers next to peaks in (A). Fractions marked as 'P' derive from the peak of interest (←) and were collected and concentrated. Fractions marked

with ‘x’ still contain the protein of interest, however, due to high amounts of additional contaminations, were discarded.

After pooling and concentrating relevant fractions, a SDS-PAGE gel and absorbance measurements confirm the purity (Figure 2.10A). The final concentrations and A_{254nm}/A_{280nm} ratios of each protein can be monitored in Figure 2.1.10B.

A

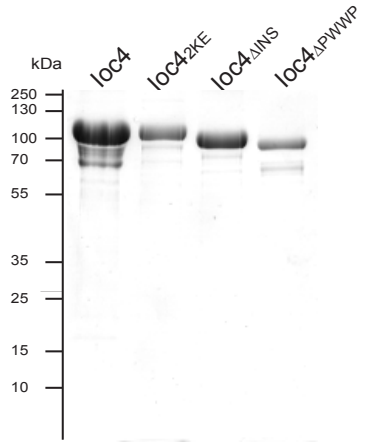

B

Protein	Mass*	Concentration*	A_{260}/A_{280}
Ioc4	116 kDa	0.41 mg/ml	0.48
$Ioc4_{2KE}$	116 kDa	0.8 mg/ml	0.65
$Ioc4_{\Delta INS}$	104 kDa	0.88 mg/ml	0.47
$Ioc4_{\Delta PWWP}$	89 kDa	0.69 mg/ml	0.69

Figure 2.1.10 Final yields of wild type and mutant Ioc4. (A) SDS-PAGE gel of Ioc4, $Ioc4_{2KE}$, $Ioc4_{\Delta INS}$ and $Ioc4_{\Delta PWWP}$ demonstrating a high quality protein preparation. **(B)** Overview of final yields for each recombinant protein. The star (*) indicated that mass and concentration were calculated considering the tags.

The protein yields were too low for CD spectroscopy and TSA measurements. However, nanoDSF measurements could be performed (Figure 2.1.11A, B). To exclude the possibility that the N-terminal 6xHis-MBP tag affects measurements, the purified tag was used as a control (kind gift from Umut Günsel) (Supplementary Figure 5.5A, B). NanoDSF shows that all four proteins are folded and not aggregated.

A

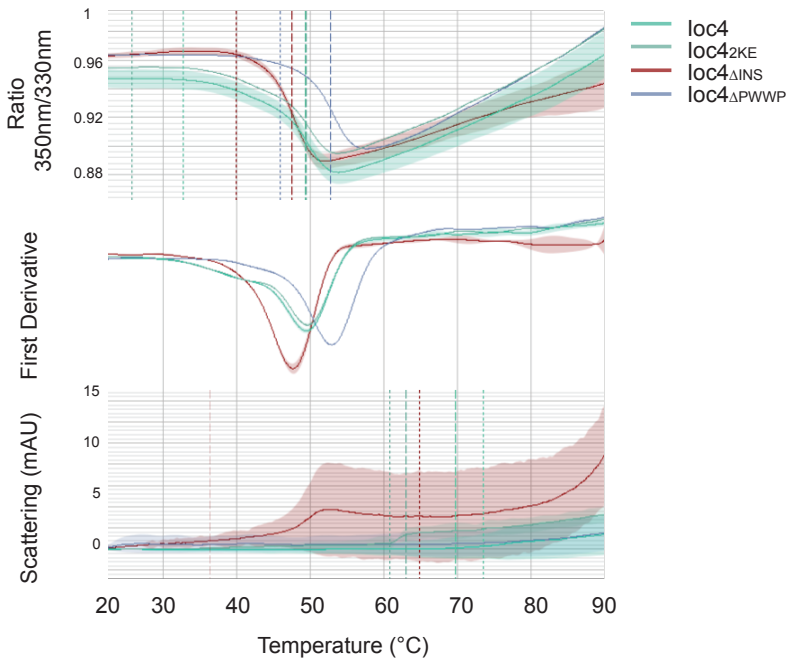

B

Protein	T_m
Ioc4	49.37°C
Ioc4$_{2KE}$	49.51°C
Ioc4$_{\Delta INS}$	47.54°C
Ioc4$_{\Delta PWWP}$	52.83°C

Figure 2.1.11 NanoDSF spectra of wild type and mutant Ioc4. **(A)** NanoDSF reveals that Ioc4, Ioc4$_{2KE}$, Ioc4$_{\Delta INS}$ and Ioc4$_{\Delta PWWP}$ are folded. Calculating their first derivative corresponds to the melting temperature (T_m). Scattering curves exclude protein aggregation. **(B)** Extracted T_m from the first derivative in **(A)**.

2.1.1.3 Purification and quality control of Isw1

Isw1 is part of both the Isw1a and Isw1b complexes. Performing reliable assays is crucial for data interpretation, therefore highly purified protein essential. After the initial affinity chromatography 6xHis-MBP-Isw1 showed high DNA contamination according to spectrophotometry measurements (data not shown). Hence further purification by heparin chromatography was necessary (Figure 2.1.12).

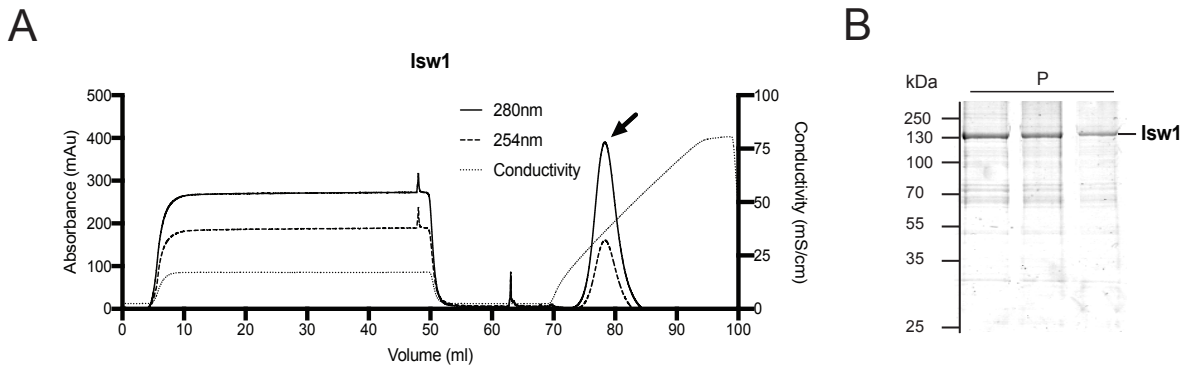

Figure 2.1.12 Chromatogram for Isw1 using heparin chromatography. Isw1 was loaded onto a HiTrap Heparin column. The arrow (←) indicates the peak of interest. **(A)** Isw1 was loaded on a HiTrap Heparin column. The arrow (←) indicates the peak of interest. **(B)** SDS-PAGE gels of the observed peak. Fractions marked as 'P' derive from the peak of interest (←) and were collected and concentrated.

After pooling and concentrating relevant fractions, a SDS-PAGE gel confirms the purity of the recombinant protein (Figure 2.1.13A). NanoDSF measurements were performed and indicate that Isw1 is not aggregated (Figure 2.1.13B). The final concentration of 6xHis-MBP-Isw1 is 22.5 µM. The melting temperature of 6xHis-MBP-Isw1 is 48.57 °C.

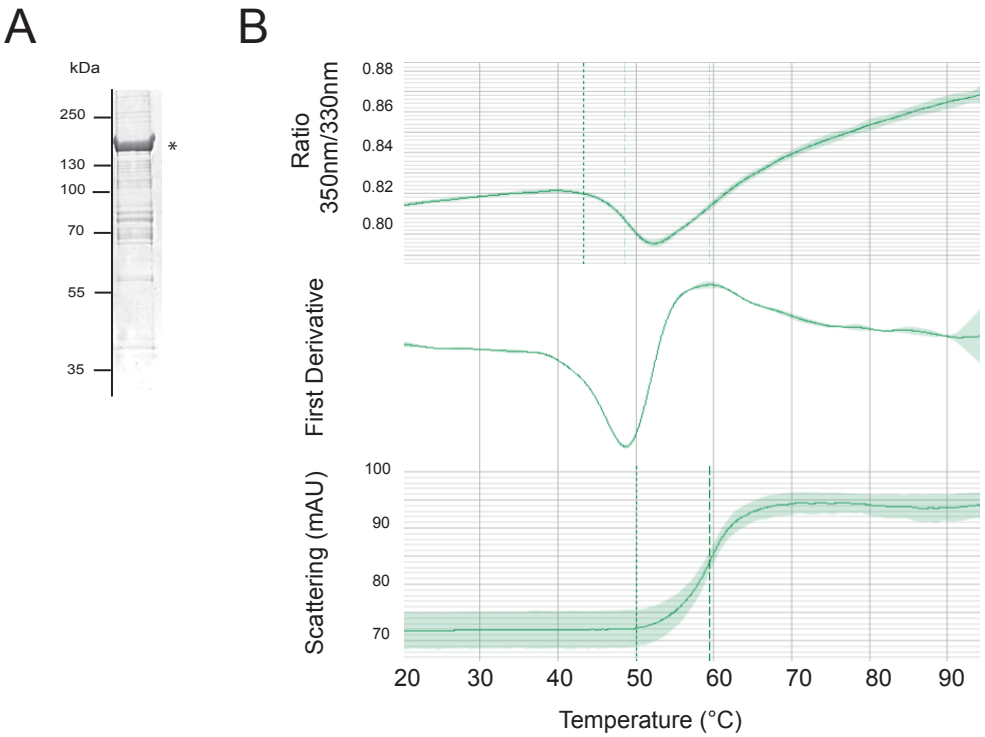

Figure 2.1.13 Final Isw1 protein preparation. **(A)** SDS-PAGE gel of purified, recombinant Isw1 (*). **(B)** NanoDSF of Isw1 did not detect any aggregation in the scattering plot.

2.1.1.4 Purification and quality control of Ioc3

Ioc3 was purified as a MBP-Ioc3-13xHis construct as described in Materials and Methods section 4.3. After the initial affinity chromatography, the protein was further purified by SEC to remove protein aggregates (Figure 2.1.14A). The initial ‘shoulder’ in the chromatogram at the void volume of 8 ml indicated aggregates. Therefore, the main peak was subject to SDS-PAGE (Figure 2.1.14B)

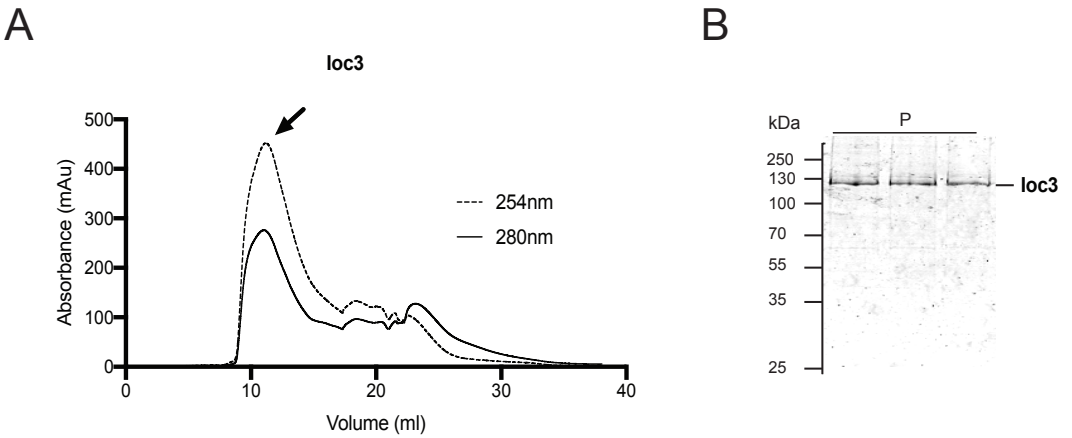

Figure 2.1.14 Chromatogram for Ioc3 SEC. (A) Ioc3 was loaded on a Superdex200 Increase 10/300 GL column for size separation. The arrow (←) indicates the peak of interest at 11 ml elution volume. The peak-'shoulder' beforehand was discarded, since it contained aggregates. **(B)** The main peak, starting at 11 ml elution volume, was subjected to SDS-PAGE. Peak fraction is marked with 'P'.

As observed in the chromatogram, MBP-Ioc3-13xHis elutes with a high $A_{254/280}$ ratio, indicating a high amount of bound DNA. Hence, relevant fractions were pooled and subjected to heparin chromatography (Figure 2.1.15). Elution fractions were pooled, concentrated and run on a SDS-PAGE gel (Figure 2.1.16A).

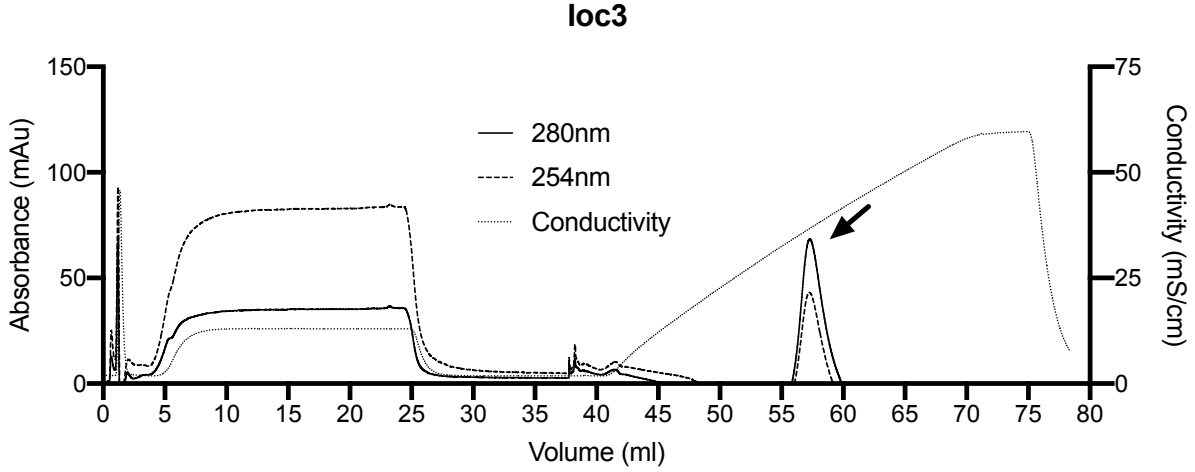

Figure 2.1.15 Chromatogram for Ioc3 using heparin chromatography. Ioc3 was loaded on a HiTrap Heparin column. The arrow (←) indicates the peak of interest.

Purification was challenging, requiring many improvement steps since Ioc3 was prone to aggregation and instability. A number of different constructs and purification protocols were evaluated. Thus, it is very important to monitor protein stability and aggregation by nanoDSF. The sharp peak in the first derivative and the rise in scattering indicate that Ioc3 is folded and not aggregated (Figure 2.1.16B). The final concentration of MBP-Ioc3-13xHis was 4.5 µM. The melting temperature of MBP-Ioc3-13xHis is 52.69 °C.

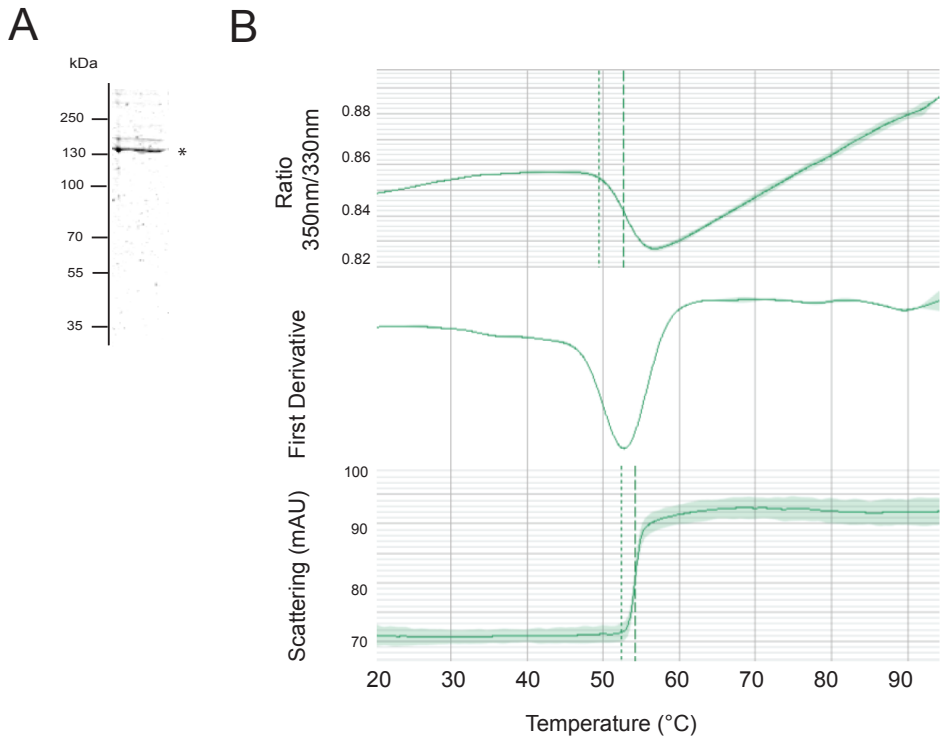

Figure 2.1.16 Final Ioc3 protein preparation. (A) SDS-PAGE gel of purified, recombinant Ioc3 (*). **(B)** NanoDSF of Ioc3 did not detect any aggregation in the scattering plot.

2.1.2 Purification of native complexes

Recombinant protein purification may lead to high protein yields when purified as single proteins. Purifying protein complexes that consist of two or more subunits, are often purified from their natural host. Endogenous protein complex purifications from yeast might lead to lower yields. The purified complexes were analyzed using silver stains due to its sensitivity. The tandem affinity purification protocol starting from yeast overnight cultures can be found in Materials and Methods section 4.4.

2.1.2.1 Purification of wild type and mutant Isw1b chromatin remodelers

After the initial affinity chromatography (section 4.4), the purified wild type and mutant Isw1b remodeler complexes were examined by silver stain, which shows few contamination bands (Figure 2.1.17C). Native Isw1b complex forms stable interactions between Isw1, Ioc2 and Ioc4. The mutants contain changes in the Ioc4 subunit only (Figure 2.1.17A). Thus, $Isw1b_{2KE}$ consists of Isw1, Ioc2 and $Ioc4_{2KE}$. $Isw1b_{\Delta INS}$ consists of Isw1, Ioc2 and $Ioc4_{\Delta INS}$ and $Isw1b_{\Delta PWWP}$ consists of Isw1, Ioc2 and $Ioc4_{\Delta PWWP}$. The calculated sizes are shown in Figure 2.1.17E. All mutants formed stable complexes, since the Ioc4 subunits were tagged and used for co-purification. None of the mutations interfere with complex formation, since in each purification, stoichiometric amounts of Ioc2 and Isw1 can be found. The two, marked bands (***) in Figure 2.1.17C are contaminants. They were sent for analysis to mass spectrometry and were revealed to be TEV protease used for tag cleavage in the purification protocol. To monitor protein degradation, a western blot against the CBP-tag was performed and revealed the high stability of all four complexes due to the single Ioc4 band in the gel (Figure 2.1.17D).

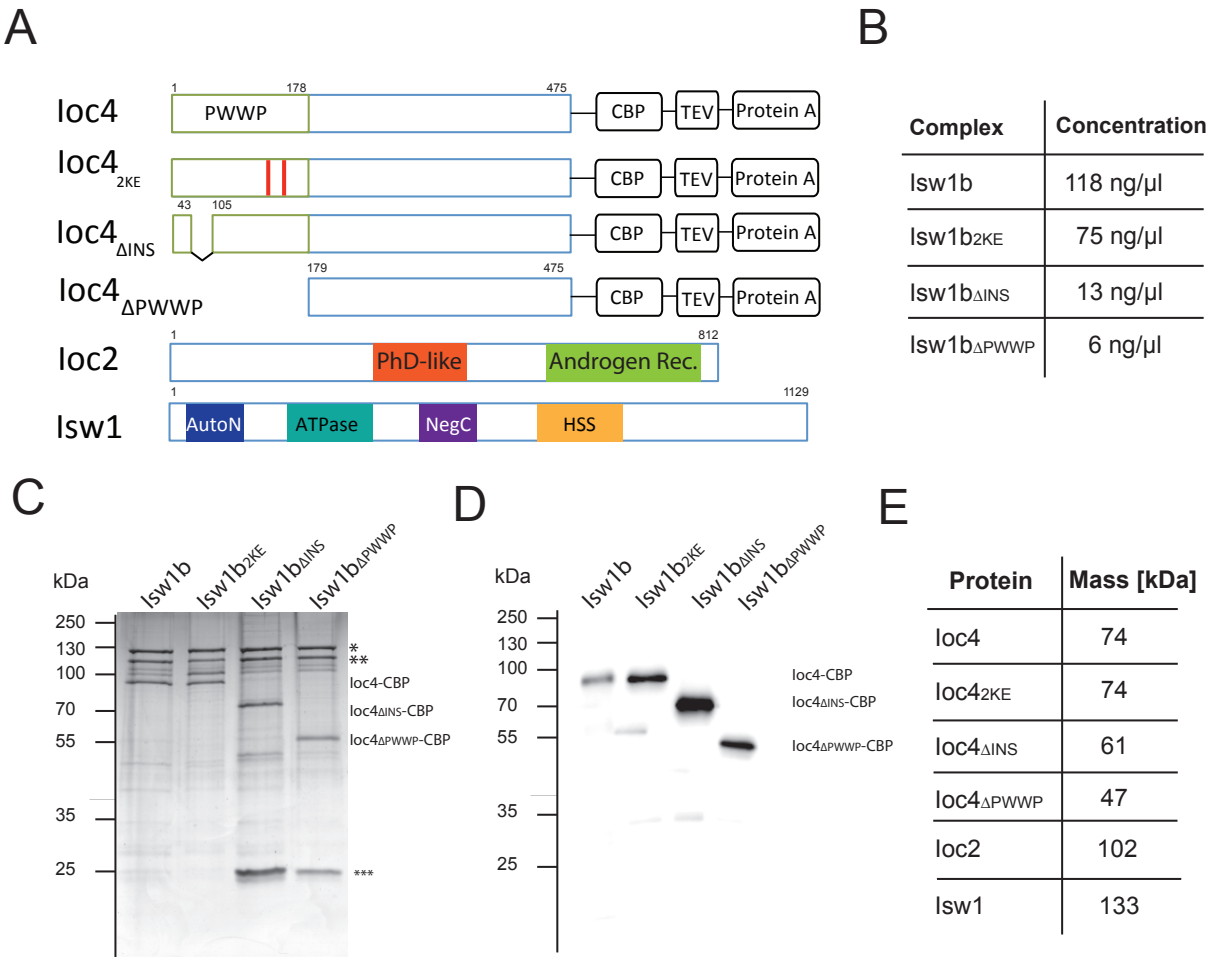

Figure 2.1.17 Wild type and mutant Isw1b protein complex purification. (A) Diagram of wild type and mutant Ioc4 subunit and wild type Ioc2 and Isw1 used for purification of Isw1b complexes. Ioc4 runs larger than expected and has already been observed previously[170]. **(B)** Concentration overview after TAP-purified wild type and mutant Isw1b complex purifications from 12 l of yeast cultures. **(C)** Silver stain of wild type and mutant Isw1b complexes. The star (*) indicates Isw1. The double stars (**) indicate Ioc2. The triple stars (***) indicate the TEV protease, confirmed by mass spectrometry. **(D)** Western blot against CBP. **(E)** Overview of protein sizes for each component forming wild type or mutant Isw1b. Masses are calculated without the attached CBP-tag on wild type and mutant Ioc4 constructs.

2.1.2.2 Purification of wild type and mutant Isw1a chromatin remodelers

Wild type Isw1a and all truncation mutants underwent the same purification protocol as the wild type and mutant Isw1b complexes (see section 4.4). Protein A was cleaved by TEV after the first purification step, leaving each construct with a CBP-tag. Wild type Isw1a consists of Isw1 and Ioc3. All mutants carry truncations in the Ioc3 N-terminus, C-terminus or both, resulting in a number of different mutant complexes (Figure 2.1.18).

A

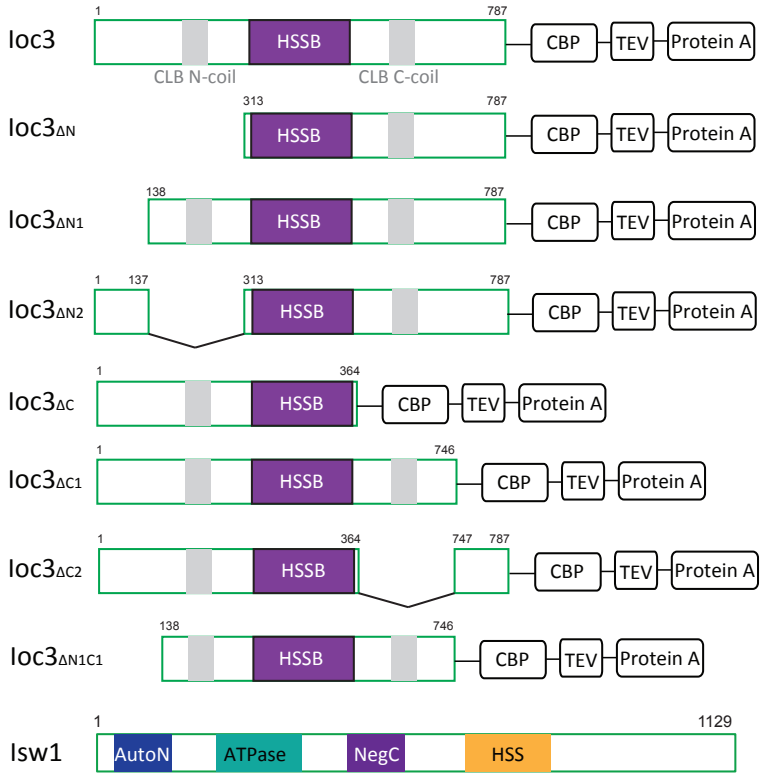

B

Protein	Mass* [kDa]
Ioc3	91
Ioc3ΔN	56
Ioc3ΔN1	76
Ioc3ΔN2	71
Ioc3ΔN1C1	71
Ioc3ΔC	41
Ioc3ΔC1	86
Ioc3ΔC2	46
Isw1	133

Figure 2.1.18 Wild type and mutant Isw1a protein complex overview. (A) Simplified diagrams of wild type and mutant Ioc3 used to purify Isw1a complexes. The HSSB domain was found to be the crucial part for a stable Isw1a complex formation, since Ioc3 interacts with Isw1 through its HSSB domain[167]. Thus, each construct harbors an intact Ioc3-HSSB domain. The CLB N- and C-coil mediate DNA contacts and are crucial as well. **(B)** Overview of protein masses for each wild type or mutant subunits. Mass (*) is calculated without the 5 kDa CBP-tag on wild type and mutant Ioc3 constructs.

To test, whether any of the mutants affect the stability of the Isw1a remodeler, I performed a silver stain following complex purification via the Ioc3 subunit. It revealed that only Isw1a$_{\Delta N1}$, Isw1a$_{\Delta C1}$ and a combination of both, Isw1a$_{\Delta N1C1}$ were

stable. All other mutants were unstable (Figure 2.1.19A, B). The large truncations in Ioc3 presumably led to a rapid degradation since the silver stain does not even reveal the purification of the respective Ioc3-CBP constructs. The concentrations of all stably purified complexes can be see in Figure 2.1.19C. All *in vitro* experiments were subsequently conducted with wild type Isw1a, Isw1a$_{\Delta N1}$ and Isw1a$_{\Delta C1}$ and a combination of both, Isw1a$_{\Delta N1C1}$.

A

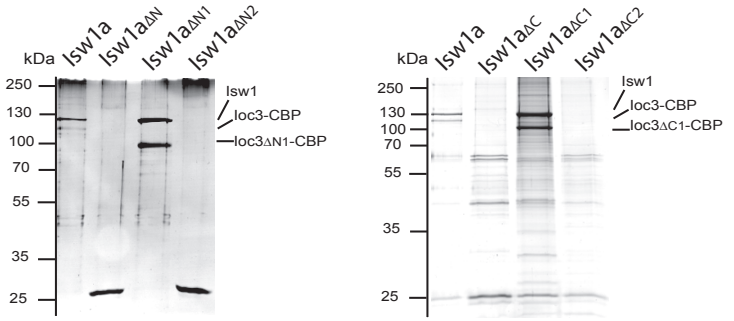

B

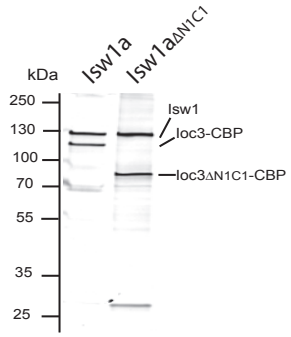

C

Complex	Concentration
Isw1a	626 ng/µl
Isw1a$_{\Delta N}$	NA
Isw1a$_{\Delta N1}$	315 ng/µl
Isw1a$_{\Delta N2}$	NA
Isw1a$_{\Delta C}$	NA
Isw1a$_{\Delta C1}$	48 ng/µl
Isw1a$_{\Delta C2}$	NA
Isw1a$_{\Delta N1C1}$	66 ng/µl

Figure 2.1.19 Wild type and mutant Isw1a protein complex purification. (A) Silver stains of wild type and mutant Isw1a complexes. **(B)** Silver stain of wild type Isw1a and Isw1a$_{\Delta N1C1}$. **(C)** Concentration overview after TAP-purified wild type and mutant Isw1a complexes. 'NA' indicates that no stable complex could be obtained.

2.2 The pivotal role of the PWWP domain in Isw1b function and recruitment

2.2.1 The Ioc4 PWWP domain is necessary to mediate the Isw1b complex correctly onto chromatin

Isw1b localization correlates with H3K36me3 distribution on average genes

Previous studies provide first insights into the mechanisms of chromatin remodeling and remodeler recruitment, our lab having focused on the Isw1b complex in particular. In order to further analyze the impact of the PWWP domain on Ioc4 and the Isw1b complex, Michaela Smolle performed ChIP-on-chip to examine Ioc4 localization genome-wide. Assuming that Ioc4 predominantly forms stable interactions with Ioc2 and Isw1, its localization correlates with Isw1b localization. The results obtained show that the Isw1b complex gets recruited to the mid to 3'-ends of genes (Figure 2.2.1A). This correlates with the distribution of trimethylated K36 on histone H3 (H3K36me3) along actively transcribed genes. We hypothesized that selective Isw1b recruitment is attributable to the PWWP domain, since PWWP domains commonly are methyl lysine readers. Mostly, they preferentially recognize H3K36me3 (see chapter 1.4). To obtain more information about the role of the Ioc4 PWWP domain, we generated a yeast strain lacking the $Ioc4_{PWWP}$ domain (Figure 2.2.1B). Consequently, ChIP-on-chip of $Ioc4_{\Delta PWWP}$ revealed that it gets randomly recruited along gene bodies (Figure 2.2.1A). On the other hand, wild type Ioc4 was genome-wide analyzed in a *set2*Δ mutant, abrogating H3K36 methylation in yeast. As expected, Ioc4, and by implication Isw1b, randomly localized along gene bodies in the absence of H3K36me3, suggesting a pivotal role of the $Ioc4_{PWWP}$ interaction with H3K36me3. However, the *in vitro* functions of the whole PWWP domain, full-length Ioc4, and its impact on Isw1b function were unknown.

A

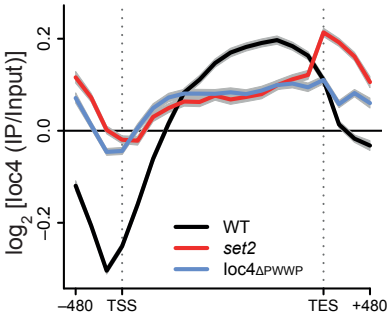

B

```
Ioc4        1         10        20        30        40        50        60

  1 MSEAIFQPTD IVLAKVKGFS AWPAMIIPNE LIPDNILKTK PVSVHKGKSG SDKKANEDID
 61 ADMESEARDR EQSEEEEDIE DFGESEANPE KFIIYTPVLK FRKNDTLKST YCVKFFCDDS
121 YIWVKPMDMK ILTSEDCRKW LSGKQRKNKK LIPAYEMAMR GKNGIDIWEF VEYGSYGKPD
181 EEEYVEEEEE ENEPEKKAIR PTRSSSRQRQ KRASETEKSE GGNSNKRKRV TRSTRQQAID
241 ASEEEEEEEE EKVQEAVRKR PQRTKTKKVV VSKTKPNPKT KAKKEKPKPP KPIKYHFEDD
301 EDWSIVGLGP QDLSIEKTMD PIAKKLSQKK NLEKHVEIKL DLEDKLAGIN KLLCDVLCSA
361 INQAVSIKDD FEIILDELQI ALDTRGSRNE FITIFQSNNS LLLNFRILFN LRKRELNKWD
421 LWDRFQDIFK HIYSYQFIPD TEDWQLEQNM EIEEMDREKP SFSEDVKEEE SKVGA*
```

Figure 2.2.1 Ioc4 localizes to mid to 3'-ends of genes. (A) ChIP-on-chip analysis of Ioc4 localization in wild type (black), *set2*Δ background (red) and Ioc4$_{\Delta PWWP}$ (blue) is shown as an average gene analysis performed by Michaela Smolle. Transcription start (TSS) and Transcription end sites (TES) are indicated. **(B)** Amino acid sequence of Ioc4. Green residues indicate the PWWP domain that were truncated for Ioc4$_{\Delta PWWP}$. Residues F19, W22 and F115 form the aromatic cage are shown in pink[202]. K149 and K150 are marked in blue.

Ioc4 achieves full DNA-binding ability through its PWWP domain

Our collaboration partner Jian Li successfully crystallized the Ioc4$_{PWWP}$ domain. (Figure 2.2.2A). Unless mentioned otherwise, "PWWP" refers to Ioc4$_{PWWP}$. An N-terminal β-barrel consisting of five β–strands forms the core of the structure. The C-terminal α-helix bundle consists of three α-helices. Both, the β-barrel and the α-helix bundle are common features of PWWP-domain containing proteins (see chapter 1.4). Between β2 and β3, an insertion motif can be observed (Figure 2.2.2A). The aromatic cage of PWWP domains specifically recognizes methylated lysines and is highly conserved. Maltby *et al.* tested the residues responsible for H3K36me3 recognition in the Ioc4$_{PWWP}$ domain[202]. An overlay with the aromatic cage of BRPF1$_{PWWP}$ confirms the high degree of structural conservation and orientation of the residues (Figure 2.2.2B).

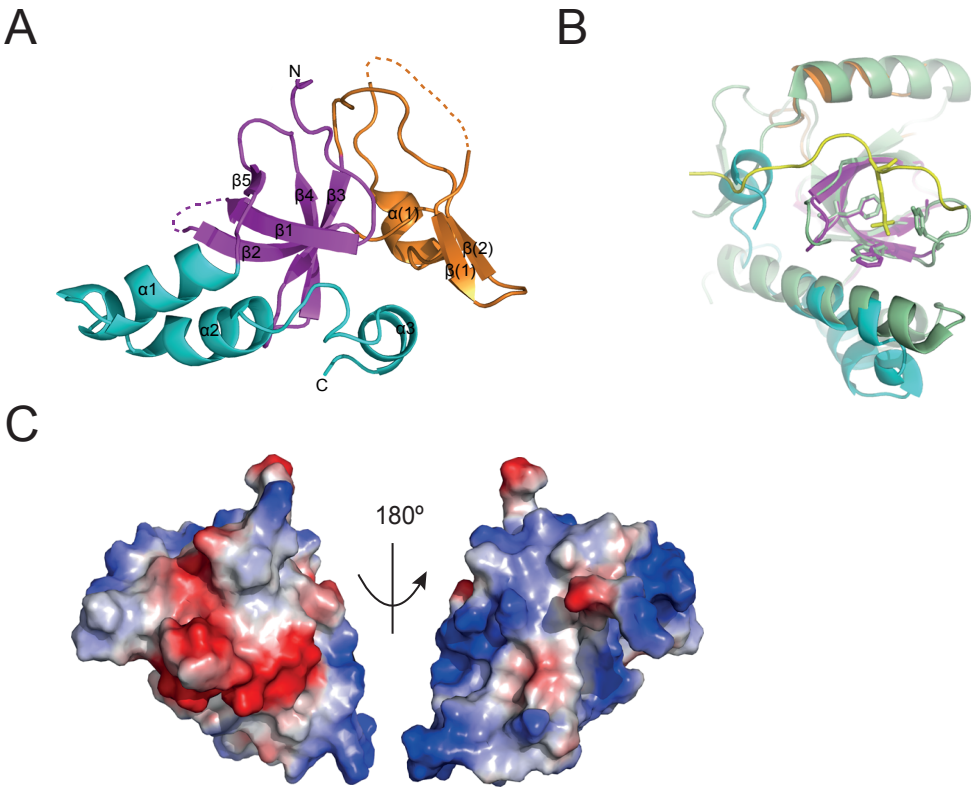

Figure 2.2.2 The Ioc4$_{PWWP}$ crystal structure reveals acidic and basic patches. (A) Crystal structure of the Ioc4$_{PWWP}$ domain. An N-terminal beta-barrel containing five β–strands (purple) is interrupted between β2 and β3 by a long, partially unstructured insertion motif (orange), before three α-helices (cyan) form the C-terminal end. **(B)** Overlay of the aromatic cage of the PWWP domains of Ioc4 and BRPF1 determine a high degree of structural conservation. **(C)** Electrostatic surface of the Ioc4$_{PWWP}$ domain. Basic patches (blue) and acidic patches (red) are indicated. The crystal structure was obtained and the figures generated by Jian Li.

Inspecting its electrostatic surface two basic patches stand out. We hypothesized that these patches may bind the negatively charged DNA (Figure 2.2.2C). Electrophoretic mobility shift assays (EMSAs) were carried out to assess binding abilities of Ioc4 and its PWWP domain to DNA *in vitro*. I found that Ioc4 binds DNA with high affinity (Figure 2.2.3B). The purified PWWP was also found to bind DNA, albeit at lower affinities (Figure 2.2.3B, C). Ioc4 lacking its PWWP domain (Ioc4$_{\Delta PWWP}$) was generated (Figure 2.2.3A) and showed decreased DNA-binding affinity (Figure 2.2.3D). Notably, the Ioc4$_{\Delta PWWP}$ construct retained residual DNA-binding ability (Figure 2.2.3B, C), suggesting auxiliary DNA-binding motifs outside the PWWP domain.

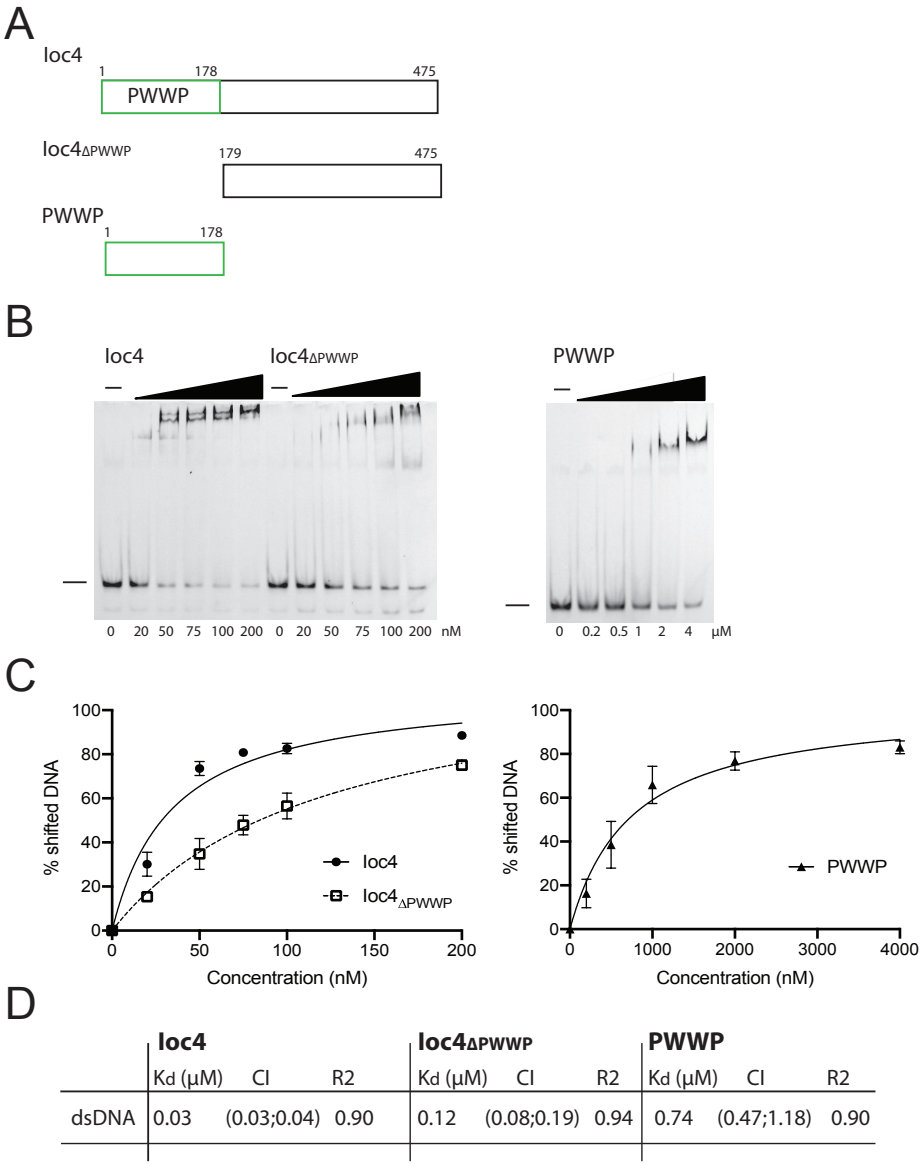

	Ioc4			Ioc4ΔPWWP			PWWP		
	Kd (µM)	CI	R2	Kd (µM)	CI	R2	Kd (µM)	CI	R2
dsDNA	0.03	(0.03;0.04)	0.90	0.12	(0.08;0.19)	0.94	0.74	(0.47;1.18)	0.90

Figure 2.2.3 The PWWP domain contributes to DNA-binding for Ioc4. (A) Diagram of Ioc4, Ioc4$_{\Delta PWWP}$ and PWWP. For simplicity tags used for purification are not shown. For more details, see result section 2.1 and Supplementary Figure 5.5. **(B)** Electrophoretic mobility shift assays (EMSA) demonstrate ability of Ioc4, Ioc4$_{\Delta PWWP}$ and PWWP to Cy5-labeled DNA (30 bp). DNA concentration was kept constant at 1 nM, whereas increasing protein concentrations are indicated below each gel. Ioc4 and PWWP can stably interact with dsDNA. Ioc4$_{\Delta PWWP}$ displays unstable binding behavior to dsDNA. **(C)** DNA-binding affinities in comparison for all proteins are plotted. All free DNA bands from **(B)** were quantified using Image Quant TL and normalized to the lanes with no protein (lane 1 or lane 7). EMSAs were quantitated and plotted as mean ± SEM. The number of replicates is at least three for all independent experiments. **(D)** Table showing calculated K_d, 90 % CI and R^2 for Ioc4, Ioc4$_{\Delta PWWP}$ and PWWP for dsDNA.

The protein-DNA interactions beyond the PWWP domain can be explained by examining the amino acid sequence of Ioc4$_{\Delta PWWP}$, encoding a series of positively

charged residues such as lysines and arginines (Figure 2.2.1C). Indeed, such positively charged arginine and lysine residues form basic patches in Ioc4$_{PWWP}$. Thus, the residual DNA-binding ability could derive nonspecifically from those residues. Most PWWP domains have been found to bind DNA nonspecifically, leading to the hypothesis that DNA-binding comes from electrostatic interaction with the negatively charged backbone of the DNA. Most PWWP domains investigated to far interact by such means in sequence-independent manners. To assess this possibility for the Ioc4$_{PWWP}$ domain, EMSAs with double-stranded (ds) DNA and RNA and single-stranded (ss) DNA and RNA were conducted. The PWWP domain was able to also bind to dsDNA with higher affinities when compared to dsRNA (Figure 2.2.4A). Additionally, the construct bound to DNA:RNA hybrid molecules with similar affinities as for dsDNA (Figure 2.2.4A). Further, PWWP binds both ssRNA and ssDNA, although the domain showed slightly higher affinity towards ssRNA (Figure 2.2.4B). The PWWP domain of HDGF specifically recognizes the SMYD promoter, nevertheless most PWWP domains are unable to distinguish between AT-rich or GC-rich sequences (see chapter 1.4). Like the majority of PWWP domains, the Ioc4$_{PWWP}$ domain did not distinguish between AT-rich dsRNA sequences and GC-rich dsRNA sequences (Figure 2.2.4C). Our findings are thereby in agreement with the literature, suggesting that most PWWP domains bind nucleic acids though electrostatic interactions with the sugar-phosphate backbone, rather than by sequence specific bases.

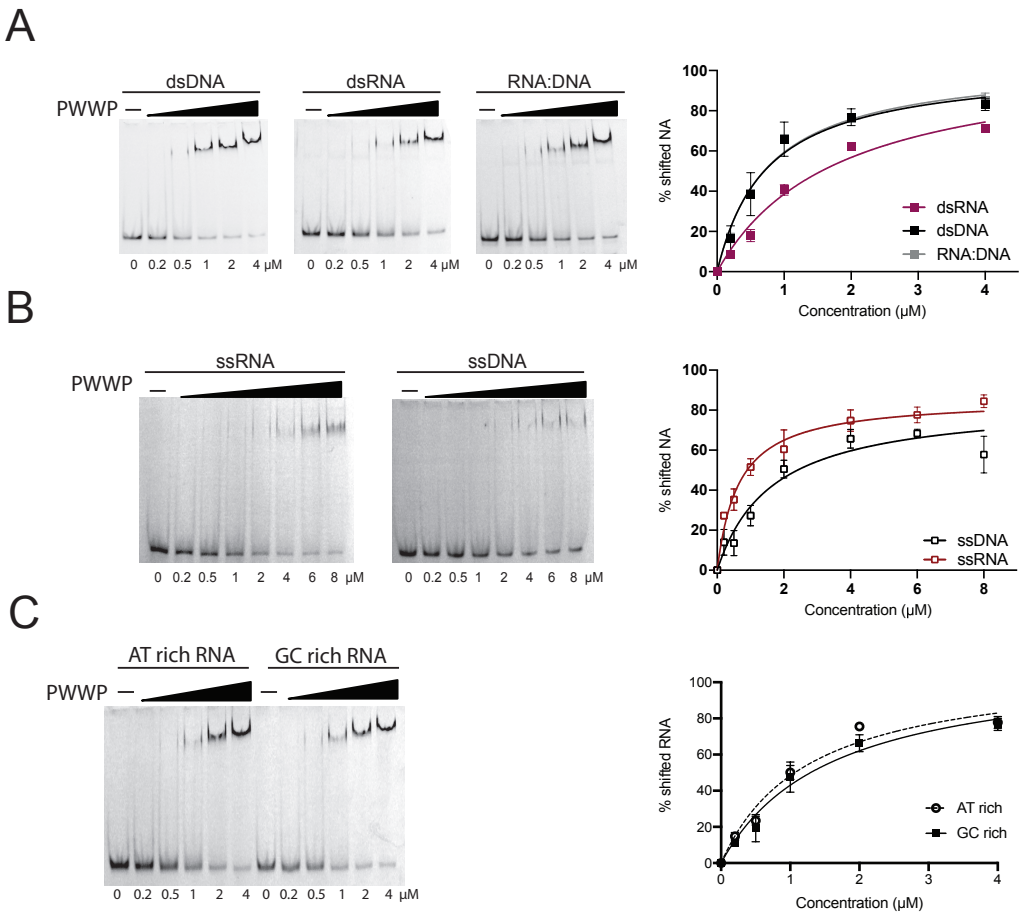

Figure 2.2.4 PWWP can bind to nucleic acids. (A) Representative EMSA and quantitation of PWWP binding to dsDNA, dsRNA and a DNA:RNA hybrid displaying lower affinity to dsRNA. **(B)** Representative EMSA and quantitation of PWWP binding to ssDNA, ssRNA displaying higher affinity to ssDNA. **(C)** Representative EMSA and quantitation of PWWP binding to AT-rich RNA and GC-rich RNA sequences. No preference could be detected. EMSAs were quantitated and plotted as mean ± SEM. The number of replicates is at least three for all independent experiments.

To evaluate nucleic acids binding ability in full-length Ioc4, the same assays were conducted and led to a similar outcome. Since Ioc4 was purified with a 6xHis-MBP tag, I wanted to rule out that the tag could mediate DNA-binding and performed control EMSAs with the tag alone. It was unable to bind DNA (Supplementary Figure 5.5). Secondly, I found that also full-length Ioc4 has a higher affinity to dsDNA and dsRNA than to ssDNA and ssRNA, respectively (Figure 2.2.5A, B). The affinity differences between dsDNA, dsRNA and a DNA:RNA hybrid molecule were small (Figure 2.2.5A). Similar to the PWWP domain, Ioc4 had no sequence preference when testing an AT-rich and a GC-rich RNA sequence (Figure 2.2.5C). The overall affinity to nucleic acids is much higher for Ioc4 than for the PWWP domain alone.

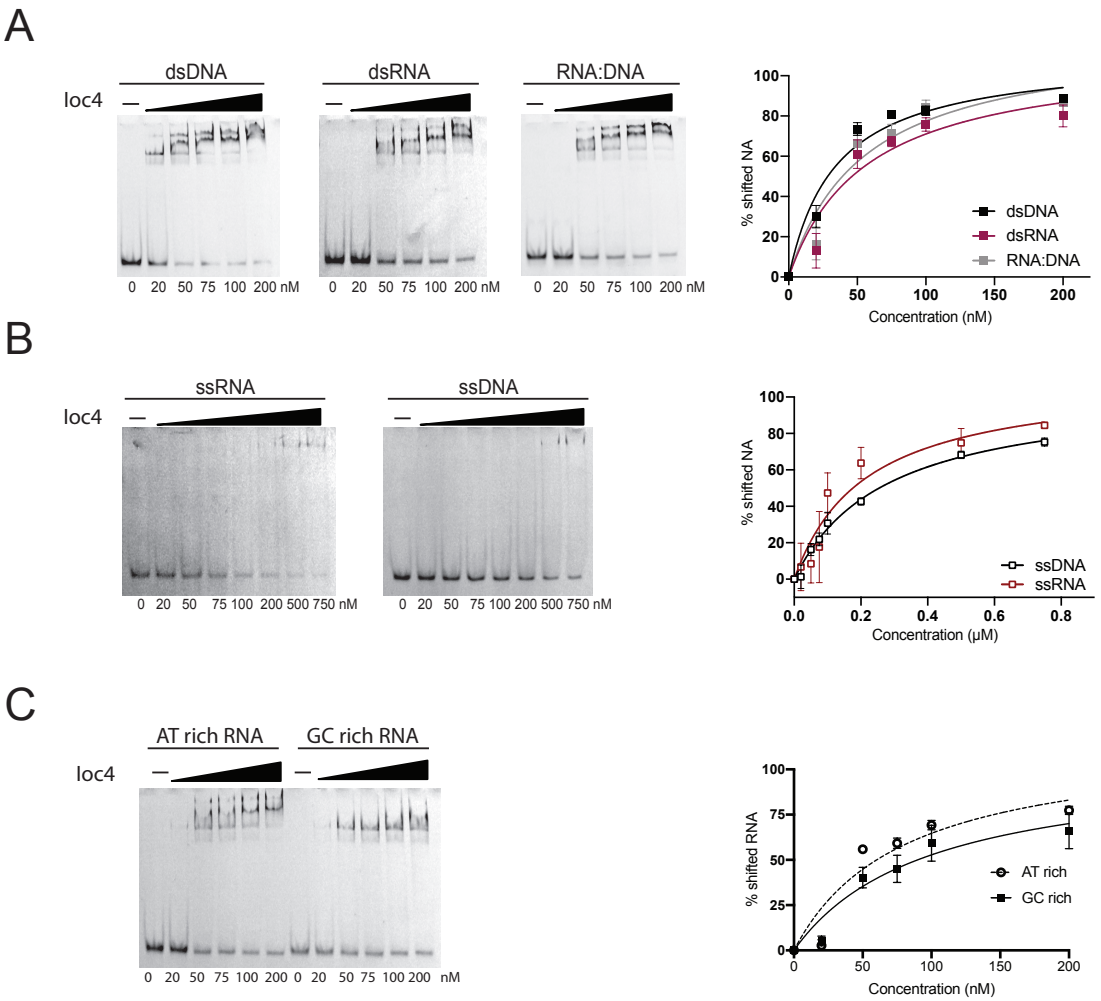

Figure 2.2.5 Ioc4 can bind to nucleic acids. (A) Representative EMSA and quantitation of Ioc4 binding to dsDNA, dsRNA and a DNA:RNA hybrid displaying similar affinities to double-stranded nucleic acids. **(B)** Representative EMSA and quantitation of Ioc4 binding to ssRNA, dsRNA displaying equal affinity to both substrates, yet Ioc4 is unable to establish stable interactions with ssRNA **(C)** Representative EMSA and quantitation of Ioc4 binding to AT-rich RNA and GC-rich RNA sequence. No preference could be detected. EMSAs were quantitated and plotted as mean ± SEM. The number of replicates is at least three for all independent experiments.

The PWWP domain contributes to histone-binding of Ioc4

The PWWP crystal structure reveals an acidic patch of unknown relevance (Figure 2.2.2A). Histones are very positively charged proteins, allowing them to form tight interactions with negatively charged DNA. Accordingly, I hypothesized that the negatively charged residues aspartic acid and glutamic acid in the PWWP domain contribute to histone-binding. Indeed, the PWWP domain binds histones evidenced by pull down assays (Figure 2.2.6C). Full-length Ioc4 binds to histone octamers as well

(Figure 2.2.6A). Direct comparisons of the constructs suggest that full-length Ioc4 possesses a higher affinity to histones than the PWWP domain alone (Figure 2.2.6D). Suggesting that the PWWP domain contributes to histone-binding, Ioc4 and Ioc4$_{\Delta PWWP}$ were compared directly (Figure 2.2.6B). I could, however, not demonstrate differing binding behaviors between the two constructs, possibly due to pull down assays not being sensitive enough to pick up smaller differences. Examining the sequence of Ioc4$_{\Delta PWWP}$, many aspartic acids and glutamic acids could be identified (Figure 2.2.1 B). Although Ioc4$_{\Delta PWWP}$ has impaired DNA- and nucleosome-binding ability, histone-binding ability is retained (Figure 2.2.6B). Conclusively, the PWWP domain appears not exclusively responsible for, but contributes to, binding of Ioc4 to histone octamers.

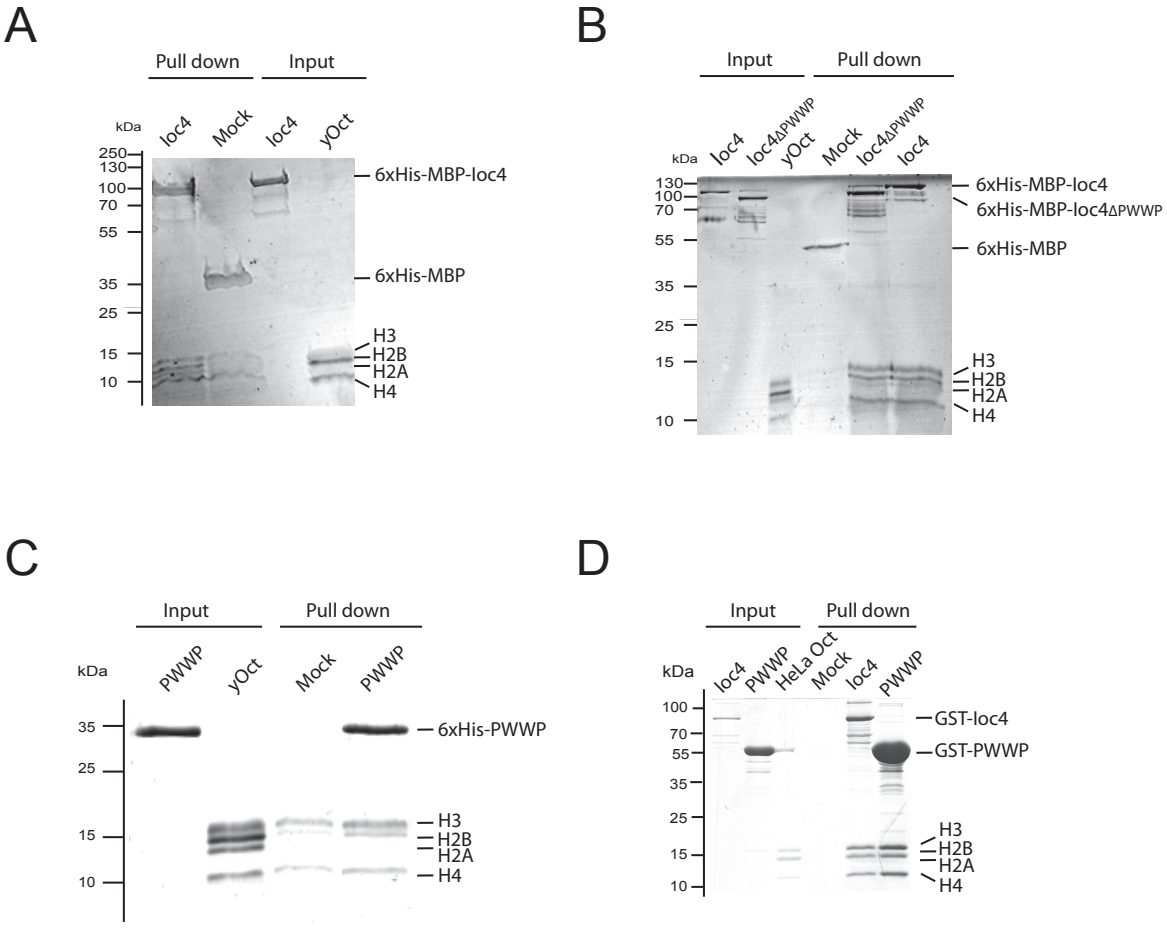

Figure 2.2.6 Ioc4, Ioc4$_{\Delta PWWP}$ and the PWWP alone can bind histones. (A) Pull down assay of Ioc4 with yeast octamers. **(B)** Pull down assay of Ioc4, Ioc4$_{\Delta PWWP}$ with yeast octamers. Both proteins bind histone octamers equally well. **(C)** Pull down assay of PWWP with yeast octamers. **(A-C)** Input of recombinant proteins and yeast octamers is 20 % of amount loaded for the pull down. **(D)** Pull down assay of Ioc4 and PWWP with HeLa octamers. Input of recombinant proteins and octamers is 10 % of amount loaded for the pull down. The number of replicates is at least three for all independent experiments.

The Ioc4$_{PWWP}$ domain is solely responsible for H3K36me3 recognition

Having demonstrated that Ioc4 binds DNA and histones, I set out to investigate Ioc4 nucleosome-binding. Strikingly, PWWP alone could bind wild type nucleosomes. Its affinity to nucleosome core particles (NCPs) and mononucleosomes with linker DNA appear comparable (Figure 2.2.7A). Considering the DNA- and histone-binding ability of full-length Ioc4, it is not surprising that Ioc4 also binds wild type nucleosomes with elevated affinity (Figure 2.2.7B). To exclude the possibility that additional sites outside the PWWP domain mediate nucleosome-binding, I assessed nucleosome-binding of the Ioc4$_{\Delta PWWP}$ construct. This truncation mutant exhibited reduced nucleosome-binding (Figure 2.2.7B), supporting the notion that nucleosome-binding is predominantly mediated by the PWWP domain.

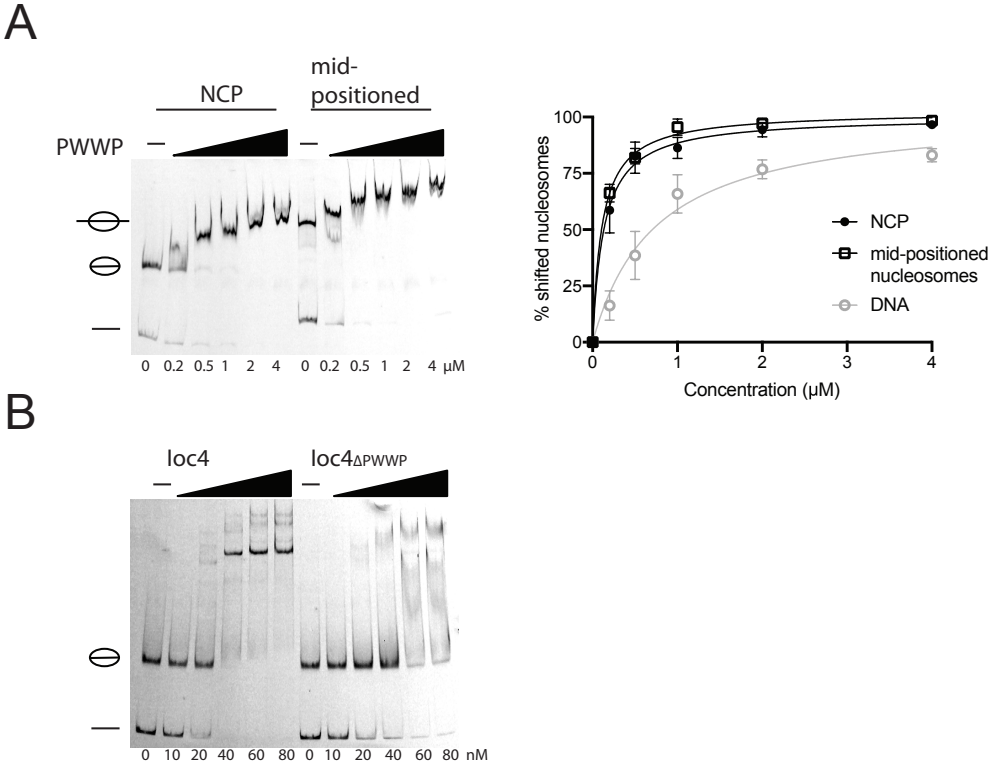

Figure 2.2.7 The PWWP domain is necessary for stable NCP binding. (A) EMSA of PWWP binding to NCP (0-N-0) or mid-positioned nucleosomes (34-N-34) displays equality for both substrates. EMSAs were quantitated and plotted as mean ± SEM. The number of replicates is at least three for all independent experiments. As a comparison, affinity to DNA is plotted. Data for DNA affinities were taken from 2.2.4A. **(B)** EMSA of Ioc4 and Ioc4$_{\Delta PWWP}$ with wild type NCP displays weaker binding ability and unstable interaction of Ioc4$_{\Delta PWWP}$ to NCPs. The number of replicates is at least three for the experiment.

Next, H3K36me3 binding was investigated. The H3K36me0 and H3K36me3 histone octamers used in this study were prepared using a chemical ligation strategy (a kind

gift by Philipp Voigt). Unlike the alkylation method used for producing H3K36C methyl-lysine analogues, the chemical ligation strategy employs a tailless histone H3 ($H3_{T45C}$), onto which methylated histone tail peptides are ligated. Hence, the $H3_{T45C}$ K36me3 harbors a real lysine residue at position 36 instead of a chemically modified cysteine. The resulting trimethylated cysteine is chemically very comparable to trimethylated lysines, but works less well when monitoring weaker binding behaviors of proteins. $H3_{T45C}$K36me3 and $H3_{T45C}$K36me0 ensure that proteins can bind to nucleosomes in the most native-like way possible. For simplicity, $H3_{T45C}$ K36me3 and $H3_{T45C}$K36me0 are from here on referred to as H3K36me3 and H3K36me0, respectively. To better distinguish between the substrates and to investigate smaller binding differences in affinities, a second approach was established besides conventional EMSAs. In so-called competitive EMSAs (cEMSA), nucleosomes are separately reconstituted with different fluorescently labeled DNAs and brought together in one reaction. Here, H3K36me0 was reconstituted with IRD700-labeled DNA, which appears red and H3K36me3 was reconstituted with IRD800-labeled DNA, which appears green. Both differently labeled mononucleosomes were incubated with increasing amounts of protein (Figure 2.2.8). The tested protein must 'choose' between those two substrates, competing for binding. In case of preferential binding, one nucleosome, i.e. one color gets shifted first, whereas the other remains for longer as a free nucleosome. This system better mimics an *in vivo*-like situation, where different modification states are present simultaneously.

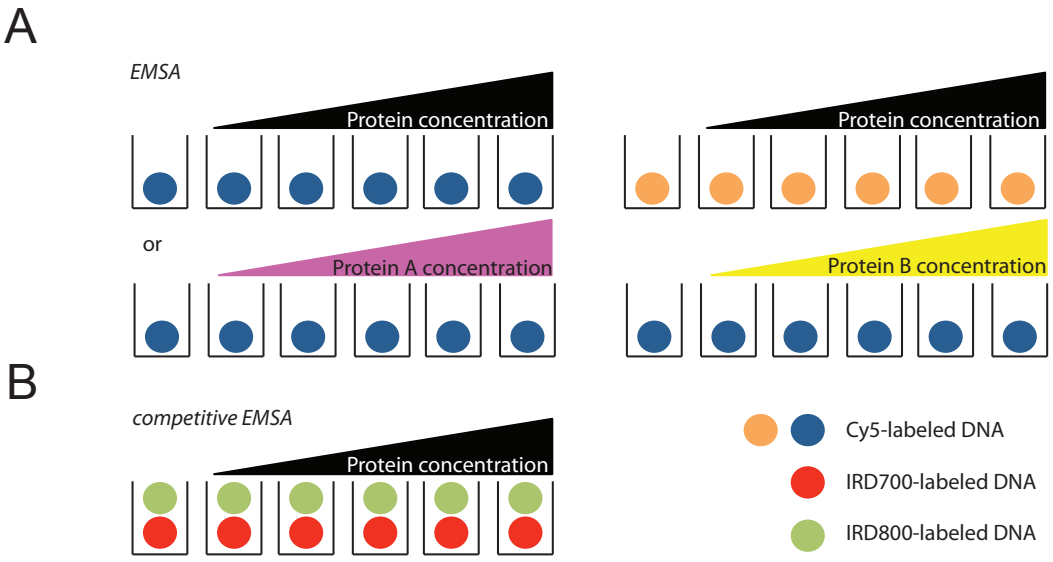

Figure 2.2.8 Principles of EMSA and competitive EMSA. (A) Regular EMSAs can be carried out using either the same protein and two different substrates next to each other or vice versa. **(B)** The advantage of competitive EMSAs is that two different substrates (e.g.

differently labeled nucleosomes) can be combined in one reaction into which protein is titrated. This set-up mimics an *in vivo*-like situation. Small differences can be displayed, since the preferred substrate will be preferentially bound, leaving the other unbound.

The PWWP domain is a H3K36me3 reader, since it preferentially binds H3K36me in a regular EMSA setting (Figure 2.2.9A, D). The preference becomes more obvious when applying cEMSAs (Figure 2.2.10A). Full-length Ioc4 displays only a small, but reproducible preference for H3K36me3 (Figure 2.2.9B, D), in agreement with previously published data[158]

A

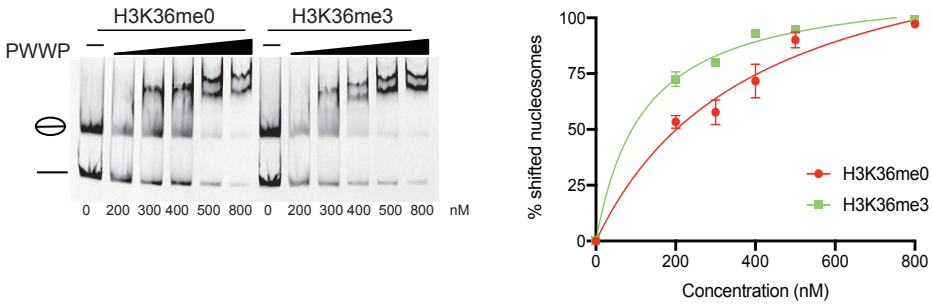

B

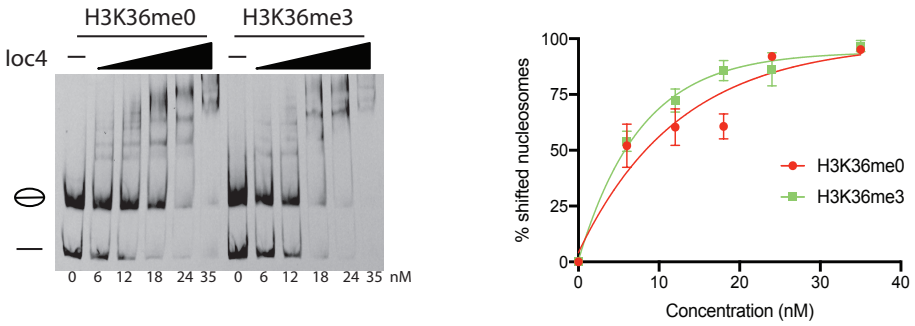

C

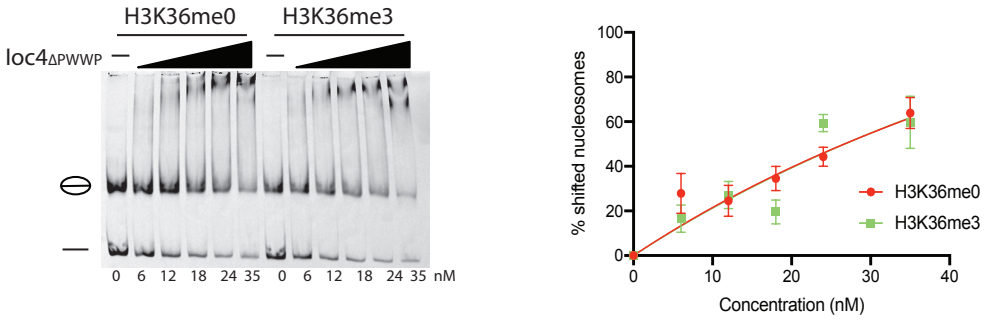

D

	Ioc4			PWWP		
	K_d (nM)	CI	R2	K_d (µM)	CI	R2
H3K36me0	10.8	(5.0;22.5)	0.88	0.4	(0.25;0.61)	0.95
H3K36me3	6.7	(4.5;9.7)	0.96	0.12	(0.09;0.15)	0.99

Figure 2.2.9 Ioc4 needs the PWWP domain to distinguish between H3K36me0- and H3K36me3-containing nucleosomes. (A) The purified PWWP domain preferentially binds H3K36me3 in EMSA settings. **(B)** Ioc4 preferentially binds H3K36me3 in EMSA settings. **(C)** $Ioc4_{\Delta PWWP}$ bind nucleosomes with reduced affinity and cannot distinguish between H3K36me0 and H3K36me3. **(D)** Table showing calculated K_d, 90 % CI and R^2 of Ioc4 and PWWP for H3K36me0- and H3K36me3-containing nucleosomes. EMSAs were quantitated and plotted as mean ± SEM. The number of replicates is at least three for all independent experiments.

Notably, Ioc4 lacking its PWWP domain was unable to distinguish between H3K36me0- and H3K36me3-containing nucleosomes. Further, nucleosome association was diminished compared to full-length Ioc4 (Figure 2.2.9C). Using cEMSAs shows further that the previously demonstrated preference could be increased when Ioc4 was provided both options (Figure 2.2.10B). The small preference can be explained that although PWWP is a strong H3K36me3 interactor, previous EMSAs with Ioc4$_{\Delta PWWP}$ reveal residual DNA-, histone- and nucleosome-binding capacity (Figures 2.2.3B, 2.2.6B and 2.2.7B). Small affinities towards H3K36me3 are thereby masked by auxiliary interaction sites.

Nonetheless, the Isw1b complex still distinguished between H3K36me0 and H3K36me3 (Figure 2.2.10C). To point out the specificity for the Isw1b complex, the same binding experiment was conducted with purified Isw1a complex. Isw1a shares the catalytic Isw1 subunit with Isw1b, but contains Ioc3 as an associated subunit instead of Ioc4 and Ioc2. I found that Isw1a binds H3K36me0- and H3K36me3-containing nucleosomes equally well (Supplementary Figure 5.6).

These comprehensive binding assays demonstrate that the Ioc4$_{PWWP}$ domain is solely responsible for H3K36me3 recognition. In conclusion, the Ioc4$_{PWWP}$ domain guides Isw1b through a combination of binding to DNA, histones and H3K36me3 correctly onto chromatin, providing new insights in the multivalent binding abilities of the Ioc4$_{PWWP}$ domain.

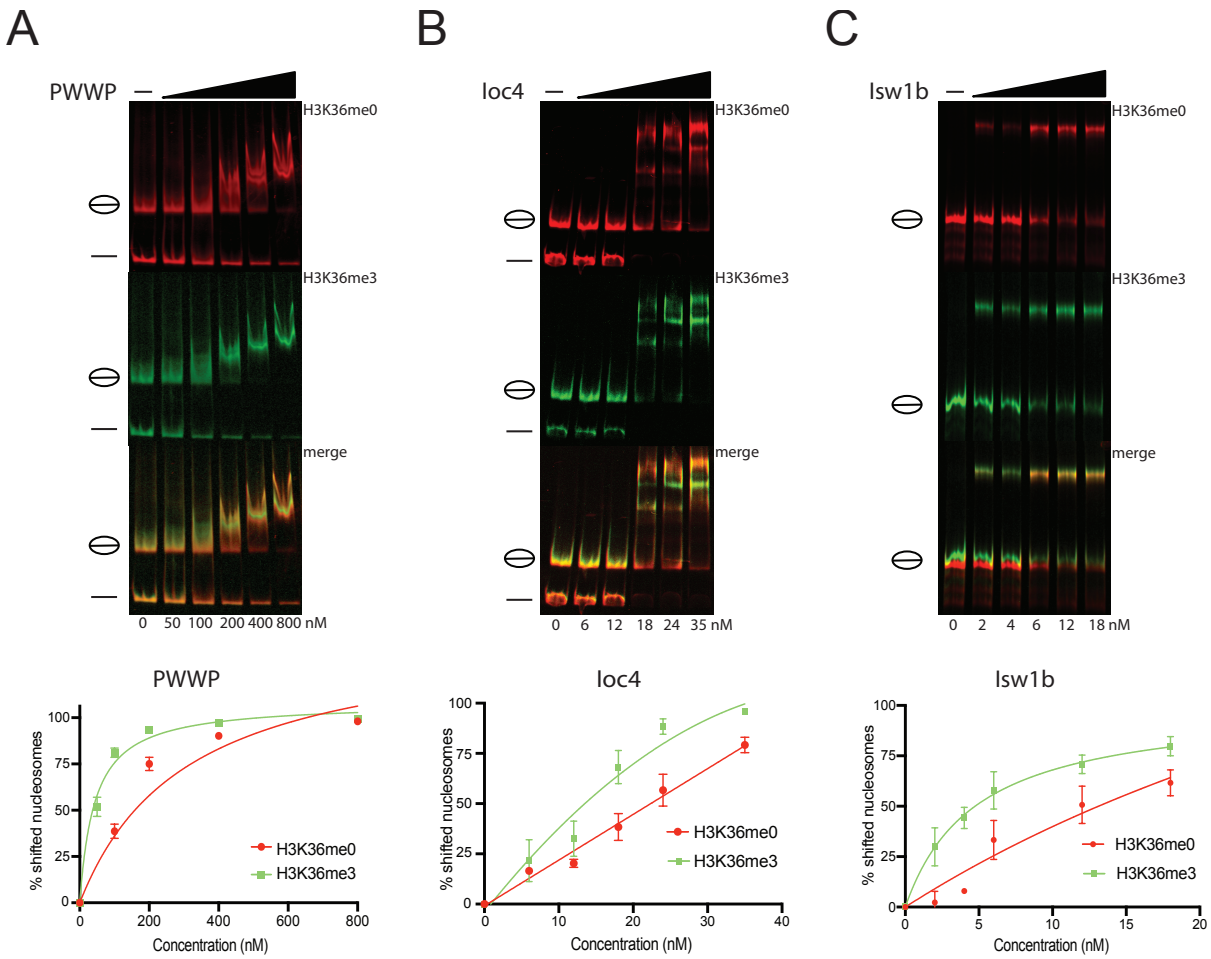

Figure 2.2.10 Distinction between H3K36me0- and H3K36me3-containing nucleosomes gets increased in cEMSAs. (A-C) Competitive EMSAs of **(A)** PWWP, **(B)** Ioc4 and **(C)** Isw1b reveal preferential binding for H3K36me3-containing nucleosomes. H3K36me0-containing octamers were reconstituted with IRD700-labeled DNA and appears red. H3K36me3-containing octamers were reconstituted with IRD800-labeled DNA and appears green. The overlay of both colors appears yellow. Competitive EMSAs were quantitated and plotted as mean ± SEM. The number of replicates is at least three for all independent experiments.

2.2.2 DNA-binding of the Ioc4$_{PWWP}$ domain is a prerequisite for correct Isw1b localization on chromatin

Having demonstrated the DNA-binding ability of the Ioc4$_{PWWP}$ domain, I wanted to evaluate its importance for the Isw1b complex. Wondering whether a DNA-binding deficient mutant could still mediate Ioc4 and/or Isw1b onto chromatin, two point mutations were introduced in one of the basic patches of the PWWP domain. Having tested several combinations of lysines and arginines, Lys149 (K149) and Lys150 (K150) were both mutated into glutamic acid (E) resulting in a charge reversal (Figure 2.2.11 and 2.2.1)

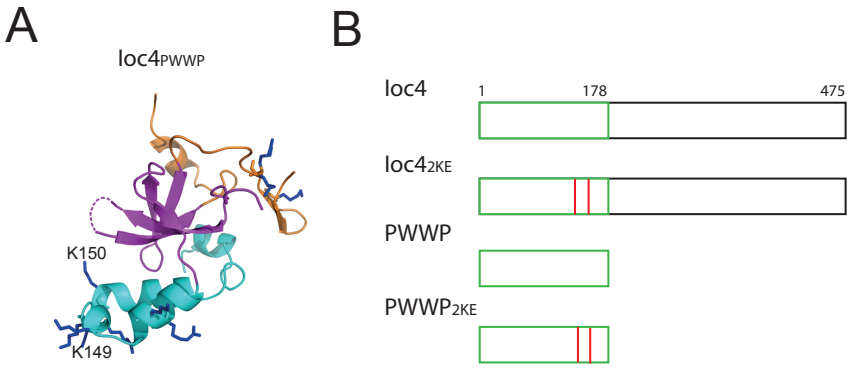

Figure 2.2.11 Overview of implemented point mutations. (A) Crystal structure of the PWWP domain. Residues K149 and K150 are indicated and were mutated into Glu. Crystal structure was obtained and figure generated by Jian Li. **(B)** Diagram of Ioc4, Ioc4$_{2KE}$, PWWP and PWWP$_{2KE}$. The schematic positions of the point mutations are marked in red.

I hypothesised that the PWWP domain mediates DNA-binding through electrostatic interactions between basic residues, and the negatively charged sugar-phosphate backbone of the DNA. Supporting this hypothesis, the PWWP$_{2KE}$ mutant was unable to bind DNA (Figure 2.2.12A). Further, PWWP$_{2KE}$ was nucleosome-binding deficient. This proves the role of PWWP acting as a DNA-binding domain. Further, the two lysines 149 and 150 seem to a key role in mediating protein-DNA contacts.

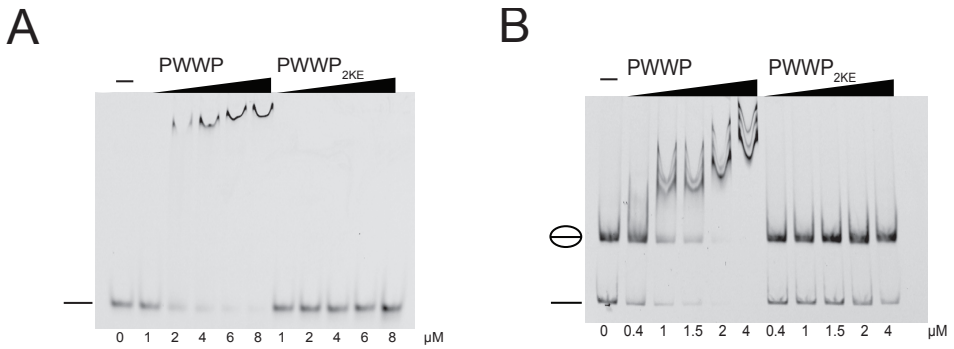

Figure 2.2.12 $PWWP_{2KE}$ is DNA- and nucleosome-binding deficient. (A) PWWP binds to DNA, whereas $PWWP_{2KE}$ is DNA-binding deficient in EMSAs. **(B)** PWWP can bind nucleosomes, whereas $PWWP_{2KE}$ is nucleosome-binding deficient. Nucleosomes and free DNA, that was not reconstituted into nucleosomes are indicated. The number of replicates is at least three for all independent experiments.

Full-length Ioc4 owes its DNA-binding ability mainly to its PWWP domain, but other positively charged residues weakly contribute to DNA-binding. Nevertheless, introducing the two point mutations at the same sites in full-length Ioc4 (Figure 2.2.11B), $Ioc4_{2KE}$ resulted in reduced affinity towards DNA (Figure 2.2.13A). To assess the hypothesis that the two point mutations also prevent Ioc4 to stably bind nucleosomes, EMSAs were carried out testing $Ioc4_{2KE}$ together with wild type nucleosomes. Notably, $Ioc4_{2KE}$ shows fewer stable interactions with nucleosomes than wild type Ioc4 (Figure 2.2.13B). The two point mutations do not affect protein folding (see chapter 2.1). If this were the case, I would not observe DNA and nucleosome recognition. Accordingly, I consider the aromatic cage, annotated as the H3K36me3 recognition module[202], unaffected. Therefore, $Ioc4_{2KE}$ should be able to distinguish between H3K36me0 and H3K36me3. However, I could not validate this by EMSA (Figure 2.2.13C). I speculate that without stable protein-DNA contacts, the aromatic cage in $Ioc4_{PWWP}$ does not get in close proximity of the nucleosome, allowing formation of a H3K36me3 interaction. Cation – π forces, formed between the positively charged trimethylated lysine and the benzol rings of F19, W22 and F115 can be masked by the adjacent electrostatic repulsion of the two introduced glutamic acids.

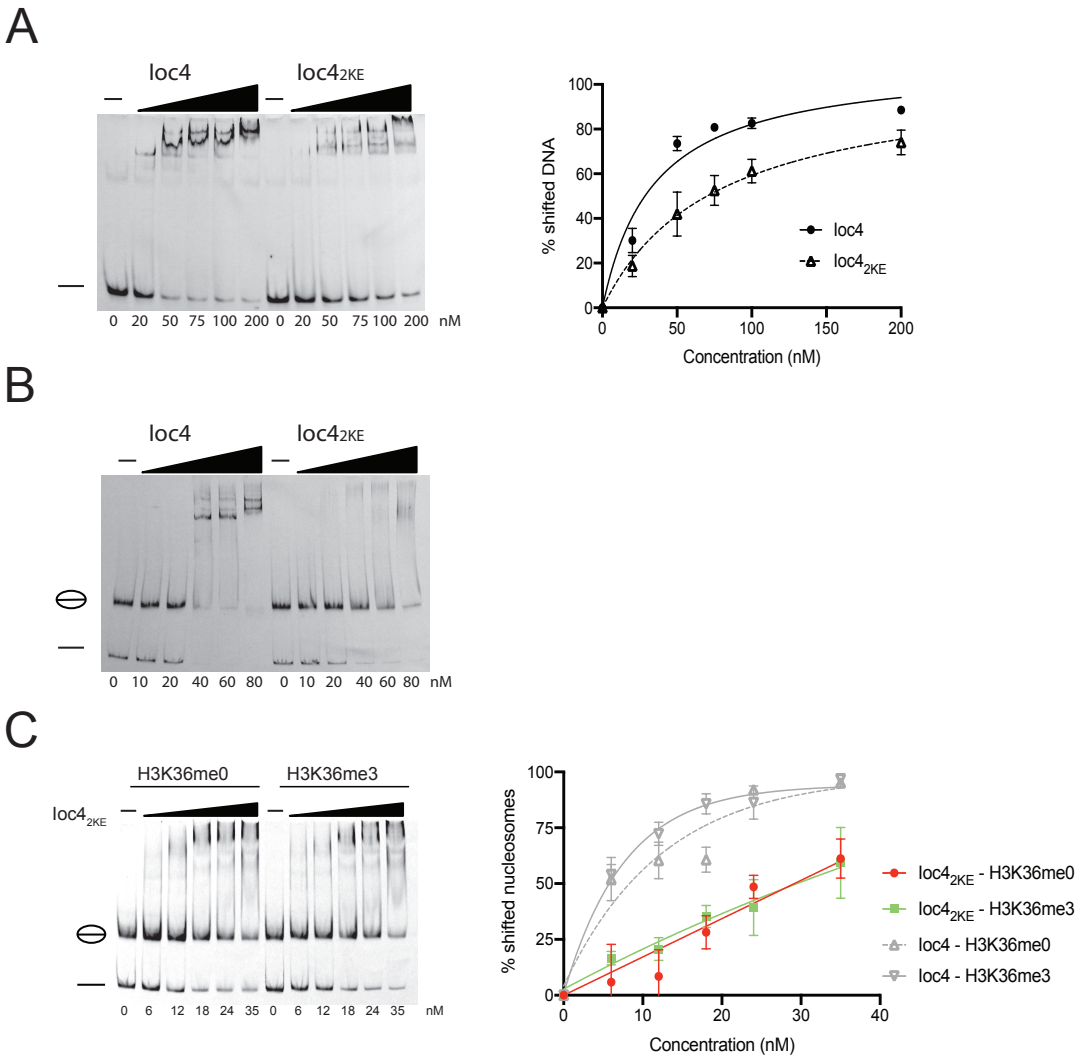

Figure 2.2.13 Ioc4$_{2KE}$ displays reduced binding abilities than Ioc4. **(A)** EMSA of Ioc4$_{2KE}$ displays reduced affinity to DNA compared to Ioc4. **(B)** EMSA of Ioc4$_{2KE}$ displays reduced affinity to NCP compared to Ioc4. **(C)** EMSA of Ioc4$_{2KE}$ displays reduced affinity to NCP and no distinction between H3K36me0- and H3K36me3-containing nucleosomes. EMSAs were quantitated and plotted as mean ± SEM. The number of replicates is at least three for all independent experiments.

Remarkably, the DNA-binding deficient PWWP$_{2KE}$ mutant can bind to histone octamers (Figure 2.2.14A) pointing out that histone-binding is independent from DNA-binding. Further, Ioc4$_{2KE}$ still associates with histone octamers, with similar affinities as Ioc4 (Figure 2.2.14B). However, I find that in both, the PWWP$_{2KE}$ and Ioc4$_{2KE}$ mutant, histone-binding ability alone cannot rescue nucleosome-binding when DNA-binding is interrupted, possibly due to repulsion between the introduced glutamic acids and the DNA sugar-phosphate backbone.

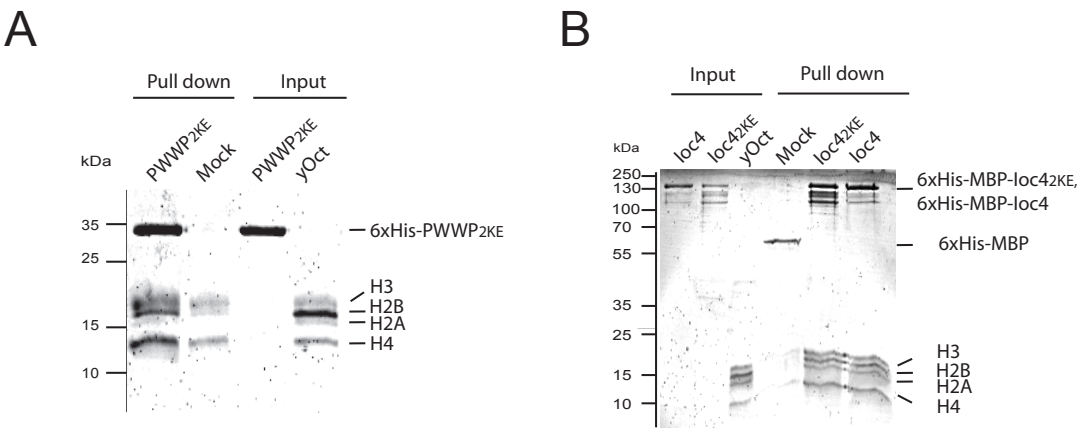

Figure 2.2.14 $PWWP_{2KE}$ and $Ioc4_{2KE}$ can both bind to histone octamers. (A) $PWWP_{2KE}$ binds to histone octamers. Mock includes histone octamers and beads, but no protein. **(B)** $Ioc4_{2KE}$ binds to histone octamers with similar affinities than Ioc4. Mock includes histone octamers, 6xHis-MBP and beads, but no protein. The number of replicates is at least three for all independent experiments.

Analyzing the localization of $Ioc4_{2KE}$ in a ChIP-on-chip experiment allowed us to obtain more information about the effects of a DNA-binding impaired mutant *in vivo* (Figure 2.2.15A). $Ioc4_{2KE}$, and by implication $Isw1b_{2KE}$, randomly localized on gene bodies on a genome-wide analysis, in a similar manner as $Ioc4_{\Delta PWWP}$ or Ioc4 in a *set2*Δ mutant (Figure 2.2.1A). The results are striking, since Isw1b consists of not just Ioc4, but also of Ioc2 and Isw1, the latter known to interact with nucleosomes through its HSS domain. Therefore, residual chromatin association is expected, however, specific recruitment is not observed. Wang *et al.* published the cryo-EM structure of the $LEDGF_{PWWP}$ domain attached to a nucleosome[239] (see chapter 1.4 and Figure 1.10B). Modeling the $Ioc4_{PWWP}$ domain accordingly onto a nucleosome, it becomes clear that the basic patch harbouring K149 and K150, is in close proximity to nucleosomal DNA to mediate its binding (Figure 2.2.15B). Introducing a charge reversal, the negative charge of glutamic acid prevents a fully stable protein-DNA contact at that specific location. Therefore, chromatin association of $Isw1b_{2KE}$ is impaired, presumably since the adjacent aromatic cage of the $Ioc4_{PWWP}$ domain cannot recognize Lys36 of the protruding histone H3 tail.

The PWWP domain of Ioc4 thus gets an extraordinary role assigned for Isw1b: DNA-binding of the $Ioc4_{PWWP}$ domain is an absolute prerequisite for correct Isw1b localization on chromatin.

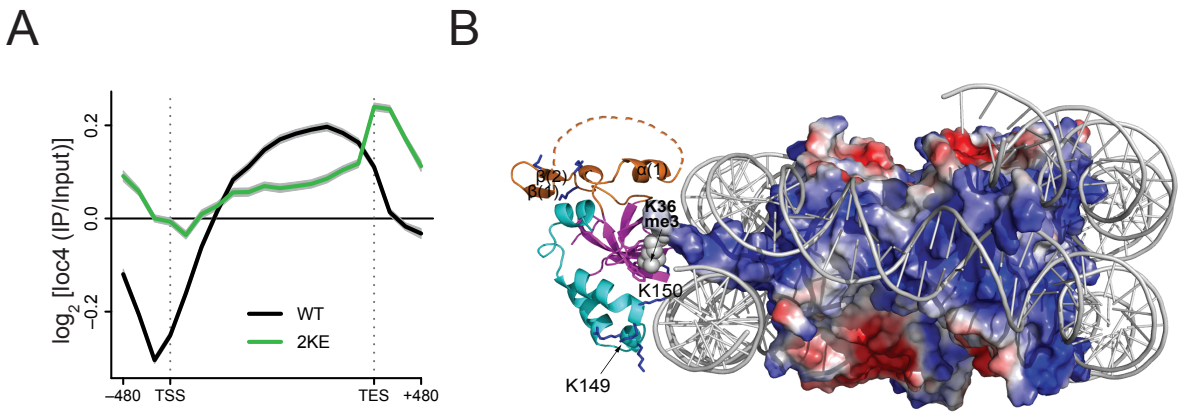

Figure 2.2.15 Ioc4$_{2KE}$ leads to mislocalization of Isw1b$_{2KE}$ on ORFs *in vivo*. (A) ChIP-on-chip analysis of Ioc4$_{2KE}$ (green) and Ioc4 (black) is shown as an average gene analysis performed by Michaela Smolle. Transcription start (TSS) and Transcription end sites (TES) are indicated. **(B)** Homology model based on the LEDGF$_{PWWP}$ domain[239] bound to a nucleosome (see chapter 1.4). Residues K149 and K150 are indicated. The protruding H3K36me3 histone tail is indicated. Model and figure generated by Jian Li.

2.2.3 The unique insertion motif enhances Ioc4$_{PWWP}$ binding to DNA and nucleosomes

Solving the crystal structure of the Ioc4 PWWP domain reveals an insertion (aa 27-110) between β–strands β2 and β3 (Figure 2.2.16A, C). Since all previously crystallized PWWP domain-containing proteins harbor either no or comparatively short insertions at this location (see chapter 1.4), this unusually long insertion motif peaked our interest. I generated a PWWP$_{\Delta INS}$ truncation mutant to explore the function of the insertion motif (Figure 2.2.16B). I also tested its impact in the context of full-length Ioc4 and the Isw1b complex. To minimize potential misfolding the truncation spans aa 43-105 only, yet disrupting the majority of the insertion motif.

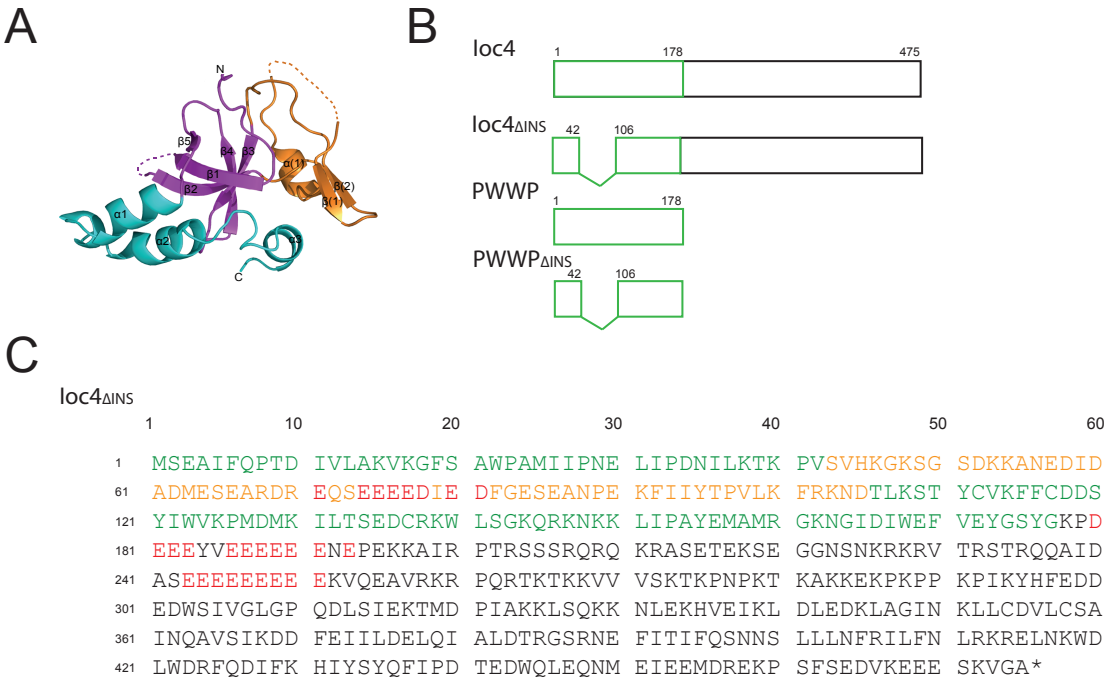

Figure 2.2.16 The insertion motif is unique to the Ioc4$_{PWWP}$ domain. (A) Crystal structure of the PWWP domain. An N-terminal β-barrel containing of five β–strands (purple) is interrupted between β2 and β3 to form a long insertion (orange), before three α-helices (cyan) form the C-terminal end. Crystal structure was obtained and figure generated by Jian Li. **(B)** Diagram of Ioc4, Ioc4$_{\Delta INS}$, PWWP and PWWP$_{\Delta INS}$. Tags are not shown. For more details see section 2.1. **(C)** Amino acid sequence of Ioc4$_{\Delta INS}$. Green residues indicate the PWWP domain, orange residues indicate the insertion motif that was truncated for Ioc4$_{\Delta INS}$ and PWWP$_{\Delta INS}$. Red residues indicate stretches of acidic residues.

Initially, I assessed DNA-binding ability with $PWWP_{\Delta INS}$. Lysines and arginines inside the insertion motif made us speculate that the insertion motif may stabilize DNA-binding. Compared to PWWP, $PWWP_{\Delta INS}$ showed reduced DNA-binding, yet it was not as binding deficient as the $PWWP_{2KE}$ mutant (Figure 2.2.17A and 2.2.12A). The smeary DNA bands indicate a small, residual affinity to DNA, but highlighting the failure to form a stable complex. Further, nucleosome-binding was assessed. Similar to the DNA EMSAs, nucleosome EMSAs displayed the same smeary band of the initial substrate (Figure 2.2.17B). Nucleosome-binding seems to be impaired, as well. These experiments point towards a crucial role of the insertion motif to stabilize DNA-binding of the PWWP domain.

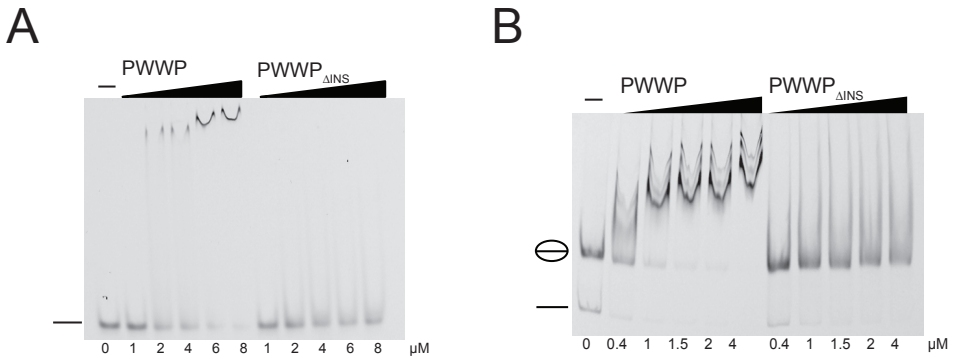

Figure 2.2.17 The insertion motif promotes DNA and nucleosome-binding for PWWP. (A) EMSA of $PWWP_{\Delta INS}$ displays reduced affinity to DNA compared to PWWP. **(B)** EMSA of $PWWP_{\Delta INS}$ displays reduced affinity to NCP compared to PWWP. The number of replicates is at least three for all independent experiments.

Next, the function of the insertion motif in the context of full-length Ioc4 was investigated. In contrast to $PWWP_{\Delta INS}$, $Ioc4_{\Delta INS}$ showed no diminished DNA-binding (Figure 2.2.18A) when compared to wild type Ioc4. This indicates that the insertion motif plays a minor role regarding DNA-binding. Next, nucleosome-binding was tested. In EMSAs, no difference in binding affinity to nucleosomes between wild type Ioc4 and $Ioc4_{\Delta INS}$ could be observed, although I did notice a slightly different binding pattern in the shifted bands (Figure 2.2.18B). Without the insertion motif, multiple binding events take place, which indicates that the insertion motif causes steric hindrance.

Truncation of the insertion motif in Ioc4 is not thought to interfere with the formation of the aromatic cage, which is located inside the β–barrel (Figure 2.2.1B and 2.2.2A). Nonetheless, I set out to test this by assessing its interaction with

H3K36me3-containing nucleosomes. Ioc4$_{\Delta INS}$ can differentiate between H3K36me0 and H3K36me3 in a similar manner as Ioc4 in cEMSAs (Figure 2.2.18C). This can be explained by the fact, that although Ioc4$_{\Delta INS}$ misses a smaller domain, no charge reversal was introduced unlike in Ioc4$_{2KE}$. The aromatic cage still has the possibility to come into close proximity to its target.

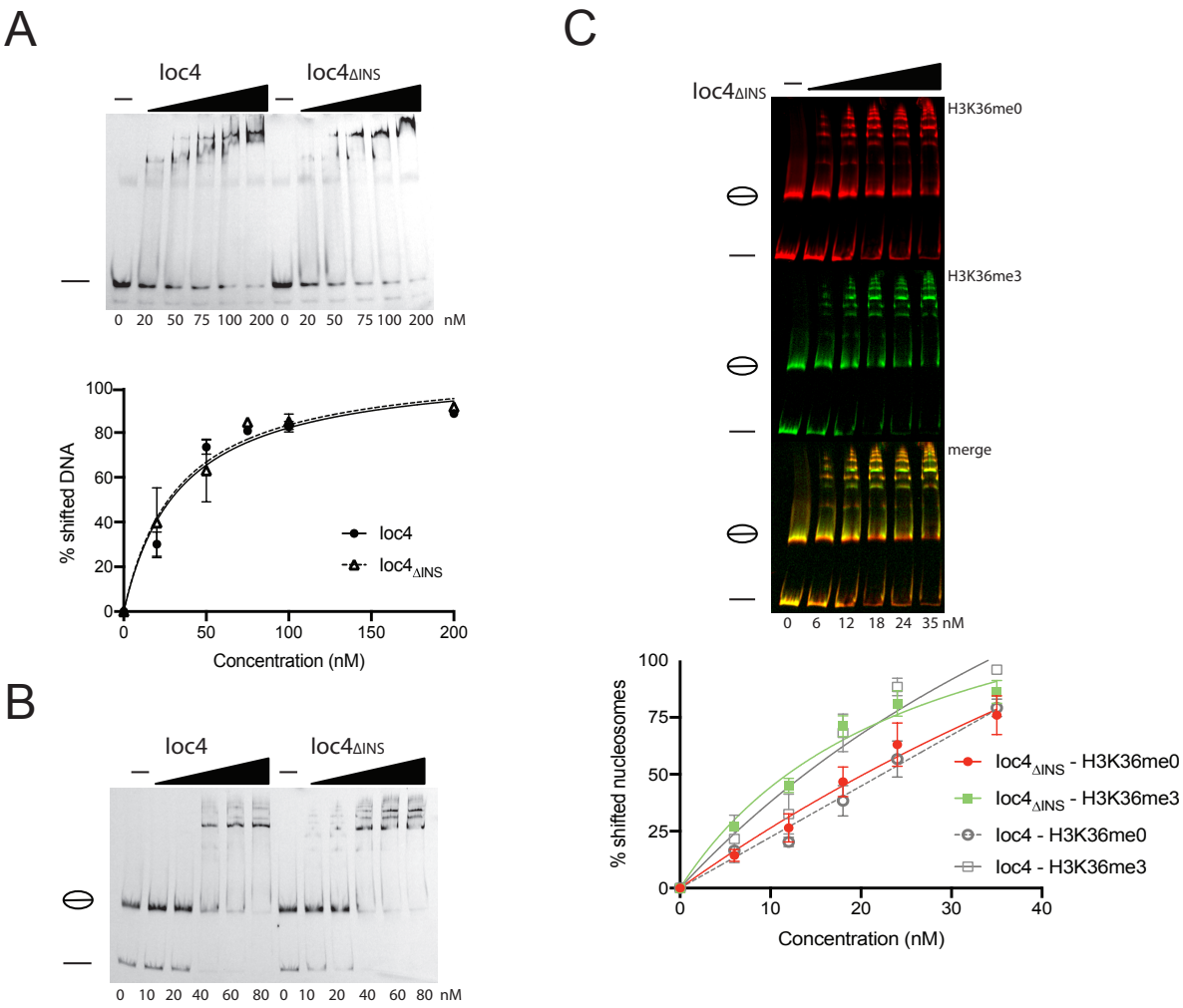

Figure 2.2.18 Lack of the insertion motif has no impact on full-length Ioc4. (A) EMSA with Ioc4 and Ioc4$_{\Delta INS}$ show no difference between the two in affinity for dsDNA. **(B)** EMSA with Ioc4 and Ioc4$_{\Delta INS}$ shows no difference in affinity for NCP. Nevertheless, Ioc4$_{\Delta INS}$ exhibits a different binding pattern, where multiple protein molecules might bind single nucleosomes. **(C)** Competitive EMSA of Ioc4$_{\Delta INS}$ shows that the protein can differentiate between H3K36me0- and H3K36me3-containing nucleosomes. Data for Ioc4 was taken from Figure 2.2.10 and plotted in grey. EMSAs were quantitated and plotted as mean ± SEM. The number of replicates is at least three for all independent experiments.

Seeing that the insertion motif has only impact on the PWWP domain and not on full-length Ioc4, histone-binding ability was examined in pull down assays. Inside the insertion motif we found a stretch of acidic residues that can potentially mediate

PWWP-histone contacts. In general, full-length Ioc4 can bind octamers and dimers. The PWWP domain displays reduced histone-binding affinity compared to Ioc4 and a slight preference for binding to histone H3/H4 tetramers (Figure 2.2.19A). This outcome becomes more obvious when testing histone-binding ability of Ioc4 and PWWP when using specifically histone H3/H4 tetramers (Figure 2.2.19C) and histone H2A/H2B dimers (Figure 2.2.19C). Investigating the contribution of the insertion motif, we tested $PWWP_{\Delta INS}$ together with recombinant octamers (Figure 2.2.19D). $PWWP_{\Delta INS}$ does not bind histone octamers, leading us to speculate that the acidic residues inside the insertion motif are important for histone-binding. Elucidating the function of the insertion motif even further, $PWWP_{\Delta INS}$ loses the binding ability to histone H3/H4 tetramers (Figure 2.2.19A, D, E last lanes). This leads us to conclude that the main function of the insertion motif is not DNA, but rather histone-binding. This idea is supported by our findings that the purified insertion motif alone is able to bind histone H3/H4 tetramers in pull down assays (Figure 2.2.19C). Introducing the truncation in full-length Ioc4, generating $Ioc4_{\Delta INS}$, made me speculate whether the severe impact on the PWWP domain can still be noticed in full-length Ioc4. Unsurprisingly, deletion of the insertion motif had no impact on the histone-binding ability of the $Ioc4_{\Delta INS}$ construct (Figure 2.2.19B). This outcome can be explained by the many, residual negatively charged amino acids in $Ioc4_{\Delta INS}$ (Figure 2.2.16C) that may mediate protein-histone contacts.

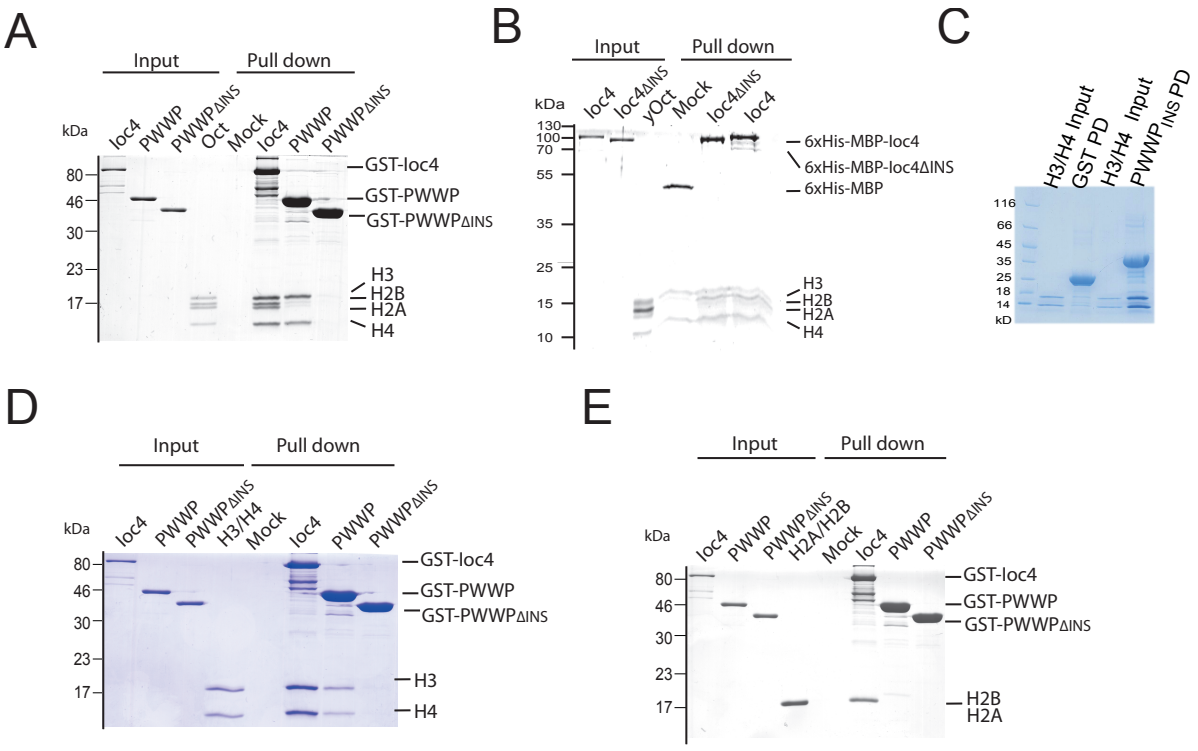

Figure 2.2.19 The insertion motif contributes to histone-binding. A representative gel showing **(A)** Pull down assay of Ioc4, PWWP and $PWWP_{\Delta INS}$ with recombinant histone octamers. **(B)** Pull down assay of Ioc4 and $Ioc4_{\Delta INS}$ with yeast octamers**. (C)** Pull down assay of histone H3/H4 tetramers with the insertion motif only ($PWWP_{INS}$). **(D)** Pull down assay of Ioc4, PWWP and $PWWP_{\Delta INS}$ with histone H3/H4 tetramers. **(E)** Pull down with Ioc4, PWWP and $PWWP_{\Delta INS}$ with histone H2A/H2B dimers. **(A, D, E)** and **(C)** were performed by Michaela Smolle and Jian Li, respectively. The number of replicates is at least three for all independent experiments.

To investigate the importance of the insertion motif in vivo, we performed a genome-wide analysis of $Ioc4_{\Delta INS}$ localization using ChIP-on-chip experiments (Figure 2.2.20A). $Ioc4_{\Delta INS}$ gets recruited to mid to 3'-ends of genes, in line with the distribution of H3K36me3 over actively transcribed genes. Distribution overlaps almost exactly with the distribution of wild type Ioc4 along gene bodies. The lacking insertion motif, however, has no impact on $Ioc4_{\Delta INS}$, and by implication $Isw1b_{\Delta INS}$, localization. Looking at the homology model, the insertion motif is located towards DNA as well, possibly mediating stabilizing contacts (Figure 2.2.20B). $PWWP_{\Delta INS}$ implemented just a deletion and not a charge reversal (as in $PWWP_{2KE}$). The smeary bands of the DNA and nucleosome EMSAs explain residual, but no full DNA-binding ability. While the PWWP core, consisting of the β–barrel and the α-helix bundle, is evolutionary conserved, the existence and extent of the insertion motif is highly

variable. Thus the insertion motif may play a crucial role for the PWWP domain alone, yet its importance gets lost in Ioc4 or Isw1b settings, where many other auxiliary sites mediate DNA and histone-binding.

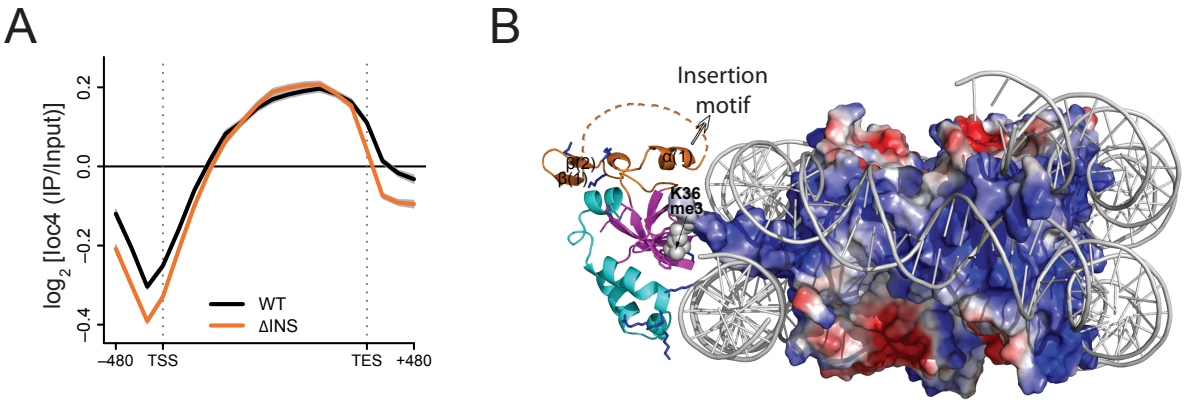

Figure 2.2.20 Ioc4$_{\Delta INS}$ does not impact localization of Isw1b$_{\Delta INS}$ on ORFs *in vivo*. (A) ChIP-on-chip analysis of Ioc4$_{\Delta INS}$ (orange) and Ioc4 (black) is shown as an average gene analysis performed by Michaela Smolle. Transcription start (TSS) and Transcription end sites (TES) are indicated. **(B)** Homology model based on the LEDGF$_{PWWP}$ domain[239] bound to a nucleosome (see chapter 1.4). The insertion motif is indicated (orange). Model and figure generated by Jian Li.

Taken together, correct localization of the Isw1b complex depends on DNA-binding and H3K36me3 recognition, but not on the Ioc4 PWWP insertion motif. Histone-binding does not seem to be crucial in this process. In conclusion, the unique Ioc4$_{PWWP}$ domain insertion motif appears predominantly a histone-binding motif that also enhances PWWP binding to DNA and nucleosomes. The enhancing effect is lost in full-length Ioc4 or Isw1b, when other compensatory DNA-binding sites are available.

2.2.4 The Ioc4 PWWP domain ensures effective Isw1b remodeling activity

The previous results obtained indicate an important role for the $Ioc4_{PWWP}$ domain for Isw1b function. PWWP guides Isw1b in a DNA- and H3K36me3-dependent manner onto chromatin. Ioc4, and by implication Isw1b, gets specifically recruited to those sites to maintain proper chromatin organization. *In vitro,* remodeling activity can be monitored in nucleosome sliding assays. I purified endogenous, wild type Isw1b from yeast (see chapter 2.1). Isw1b slides mid-positioned nucleosomes towards an end-position in a time dependent manner [177]. To analyse the impact of specifically $Ioc4_{PWWP}$, a truncation mutant complex was generated, consisting of Isw1, Ioc2 and $Ioc4_{\Delta PWWP}$ ($Isw1b_{\Delta PWWP}$). Compared to wild type Isw1b, $Isw1b_{\Delta PWWP}$ exhibited reduced sliding ability (Figure 2.2.21A, B) for canonical nucleosomes, consistent with $Ioc4_{\Delta PWWP}$ exhibiting reduced nucleosome affinity. Residual nucleosome-binding and sliding activity could be due to Ioc2 and Isw1. The function of Ioc2 is still unknown while Isw1 is known to interact with both DNA and histones via its HSS domain. In order to evaluate the impact of DNA-binding on sliding activity, $Isw1b_{2KE}$, bearing the same point mutations in $Ioc4_{2KE}$ and $PWWP_{2KE}$, was generated. Previous experiments identified an intact basic patch inside the PWWP domain to be crucial for optimal nucleosome recognition (see sections 2.2.1 and 2.2.2). Consistently, $Isw1b_{2KE}$ also exhibited diminished sliding capacities (Figure 2.2.21A, B). Lastly, the impact of the insertion motif in the PWWP domain was tested in Isw1b complex settings regarding sliding ability. No difference between wild type Isw1b and $Isw1b_{\Delta INS}$ could be detected, supporting the notion that the insertion motif, mainly mediating histone-binding, is redundant for Isw1b remodeler functions. Interestingly, in binding assays $Ioc4_{\Delta INS}$ but not $PWWP_{\Delta INS}$ behaved like wild type Ioc4 and PWWP, respectively, suggesting that the missing insertion motif has no consequence on Isw1b remodeler function. The same trend was apparent when H3K36me3-containing nucleosomes were used as a substrate (Figure 2.2.21C). While Isw1b efficiently slides trimethylated nucleosomes, $Isw1b_{2KE}$ and especially $Isw1b_{\Delta PWWP}$ exhibited reduced activity. Again, $Isw1b_{\Delta INS}$ showed no difference in sliding activity compared to wild type Isw1b.

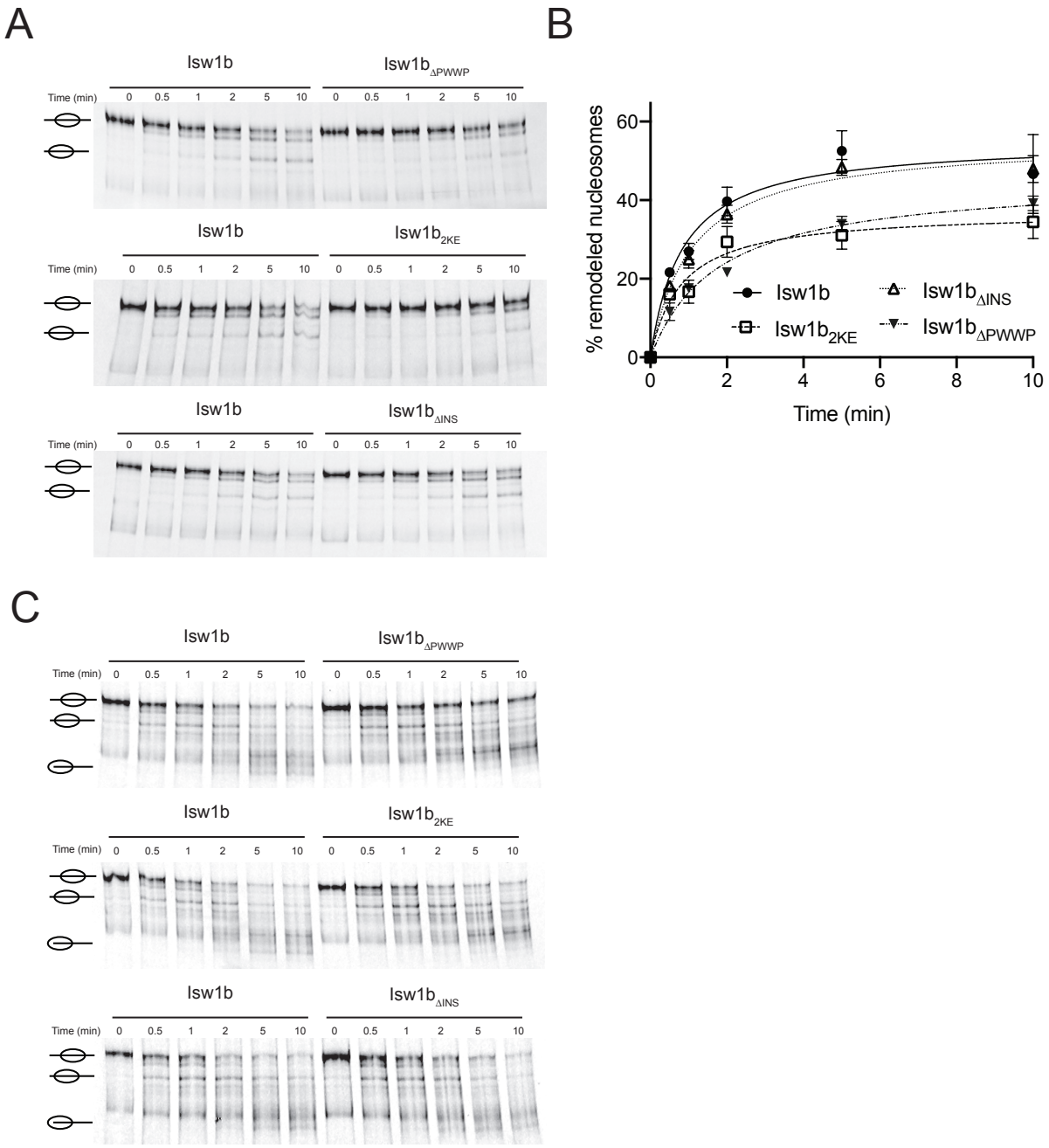

Figure 2.2.21 Isw1b needs a DNA-binding PWWP domain to effectively remodel nucleosomes. (A) Sliding assays with wild type nucleosomes. Isw1b$_{\Delta PWWP}$ (upper panel), Isw1b$_{2KE}$ (middle panel) and Isw1b$_{\Delta INS}$ (lower panel) were compared to Isw1b remodeling in a time-dependent manner. Isw1b$_{2KE}$ and Isw1b$_{\Delta PWWP}$ display reduced sliding ability, whereas Isw1b$_{\Delta INS}$ shows no difference compared to wild type Isw1b. **(B)** Quantitation of the remodeled nucleosomes. **(C)** Sliding assays with H3K36me3-containing nucleosomes. Isw1b$_{\Delta PWWP}$ (upper panel), Isw1b$_{2KE}$ (middle panel) and Isw1b$_{\Delta INS}$ (lower panel) were compared to Isw1b remodeling in a time-dependent manner. Isw1b$_{2KE}$ and Isw1b$_{\Delta PWWP}$ display reduced sliding ability, whereas Isw1b$_{\Delta INS}$ shows no difference compared to wild type Isw1b. Sliding assays were quantitated and plotted as mean ± SEM. The number of replicates is at least three for all independent experiments.

The *in vitro* sliding assays provide a contributional overview of Isw1b functions, leaving the open question whether those observations correlate with *in vivo* findings. Isw1b prevents trans-histone exchange and thereby keeps cryptic promoter-like sites hidden in nucleosomes. This makes them unreachable for RNA Polymerase II and thus suppresses cryptic transcription [158,208]. Cryptic transcripts can be visualized in northern blots. As expected, the rise of cryptic transcripts could be detected in the same mutants that displayed impaired remodelling activity *in vitro* (Figure 2.2.22). The amount of cryptic transcripts was evaluated in a *chd1*Δ background, since Isw1 and Chd1 remodelers have overlapping functions[157,177,178]. Here, we found the deletion of *IOC4* exhibits the strongest phenotype in a *chd1*Δ background since the Isw1b complex cannot form at all. Isw1 does not associate with Ioc2 in the absence of Ioc4 and vice versa[170]. $IOC4_{\Delta PWWP}$ leads to the second strongest phenotype, followed by $IOC4_{2KE}$. $IOC4_{\Delta INS}$ displayed no cryptic transcription compared to wild type yeast. Those findings are in agreement with all previously conducted *in vitro* binding and sliding experiments. Our findings support the hypothesis of a strong role for the PWWP domain since *in vitro* outcomes correlate with *in vivo* results. In conclusion the $Ioc4_{PWWP}$ domain is a multivalent binding domain, which correctly recruits the Isw1b complex through a combination of DNA, histone-binding and H3K36me3 recognition onto chromatin and thereby targets Isw1b remodeler function to correct genomic locations.

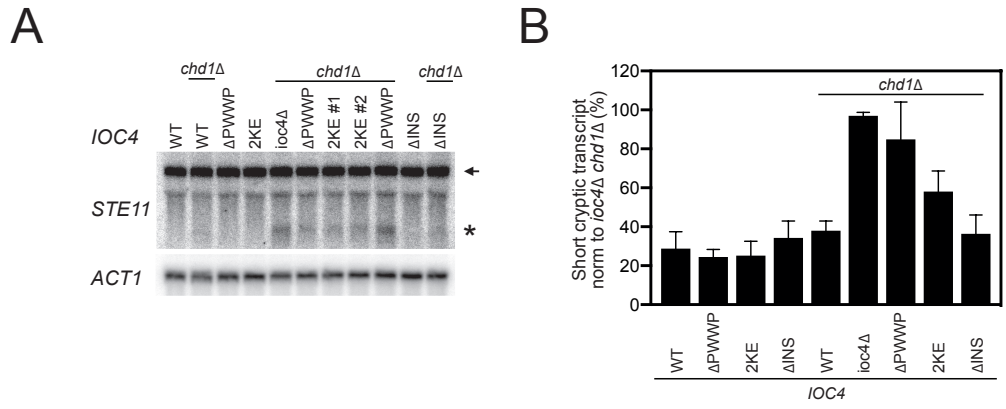

Figure 2.2.22 Northern blots detect the rise of cryptic transcripts in *STE11*. (A) Northern blot showing the rise of cryptic transcripts in a *chd1*Δ background. Full-length transcripts (←) and cryptic transcripts (*) are indicated. **(B)** Quantitation of the intensity of cryptic transcript normalized to *ACT1*. Northern blots were performed and analysed by Michaela Smolle.

2.3 Elucidating the recruitment mechanism of Isw1a to target sites

2.3.1 Unraveling preferred targets of Isw1a *in vitro*

The previous chapter shed light on recruitment of Isw1b onto chromatin. While both, Isw1b and Isw1a remodeler complexes share the same associated ATPase subunit, the attached Ioc subunits are unique. This results in distinct *in vivo* and *in vitro* functions of the individual complexes. In this chapter I will discuss the mechanism on how Isw1a gets recruited specifically to the ends of genes. It is agreed upon that Ioc3 occupancy over ORFs is over the ends of genes. Assuming stable interactions with Isw1, the whole Isw1a chromatin remodeler complex can be found in the vicinity of the +1 and the terminal nucleosomes[158,192]. Some of the posttranslational modifications (PTMs) especially found at 5'-ends of genes include acetylation, H3K4me3 and the histone variant H2A.Z. While acetylation leads to a more open chromatin structure, the impact of methylation and H2A.Z is context dependent (see chapter 1.2).

2.3.1.1 Isw1a does not get recruited by H3K4 methylation

In order to evaluate whether histone methylation or acetylation play a role in Isw1a recruitment, EMSAs were conducted to examine binding affinities between unmodified and modified nucleosomes. H3 methylation/acetylation and H4 acetylation were achieved by purifying tailless $H3_{T32C}$ and $H4_{I29C}$ histones, respectively. Using a native chemical ligation strategy, methylated/acetylated peptides that contained a C-terminal benzyl thioester, were added in a separate reaction. Modified octamers were reconstituted onto 215 bp of DNA, containing the 601 positioning sequence forming an end-positioned nucleosome. Using *in vitro* binding experiments, Isw1a showed no distinct preference for H3K4me0- or H3K4me3-containing nucleosomes (Figure 2.3.1A). Competitive EMSAs are better suited to

investigate smaller differences in affinity. However, the Isw1a remodeler complex still does not distinguish between H3K4me0- and H3K4me3-containing nucleosomes (Figure 2.3.1B). This robust outcome excludes histone methylation at lysine 4 as a recruitment target for the Isw1a complex, although they co-localize.

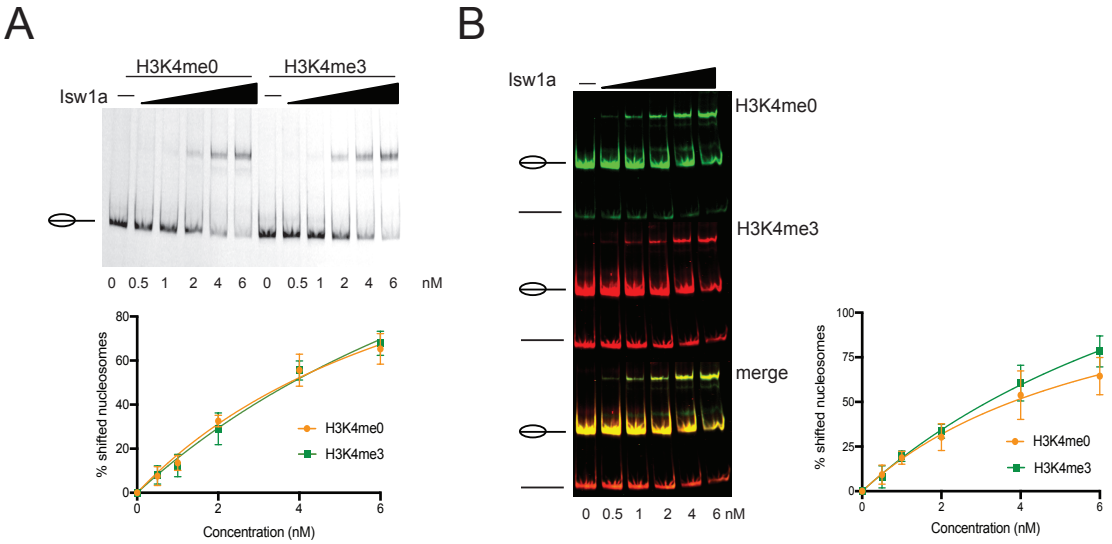

Figure 2.3.1 Isw1a does not preferentially bind to H3K4me3-containing nucleosomes. **(A)** EMSA and quantification of Isw1a binding to either H3K4me0- or H3K4me3-containing nucleosomes. **(B)** Competitive EMSA of Isw1a binding to H3K4me0- (green) and H3K4me3-constaining nucleosomes (red). EMSAs and cEMSAs were quantitated and plotted as mean ± SEM. The number of replicates is at least three for all independent experiments.

2.3.1.2 Isw1a does not get recruited by histone H3 or H4 acetylation

Highly acetylated histones get incorporated at the 5'-ends of genes, too. Thus, they seem promising candidates for Isw1a recruitment. Several combinations of histone H3 and H4 acetylation were analyzed. In detail, H3K9,14ac and H4K5,8,12ac and also a methylation-acetylation combination (H3K4me3-K9,14,18,23,27ac) were tested in binding assays. Additionally, a combination of both, histone H3 and H4 acetylation (H3K4,9,14,18-H4K5,8,12,16ac = poly-acetylated nucleosomes) was tested.

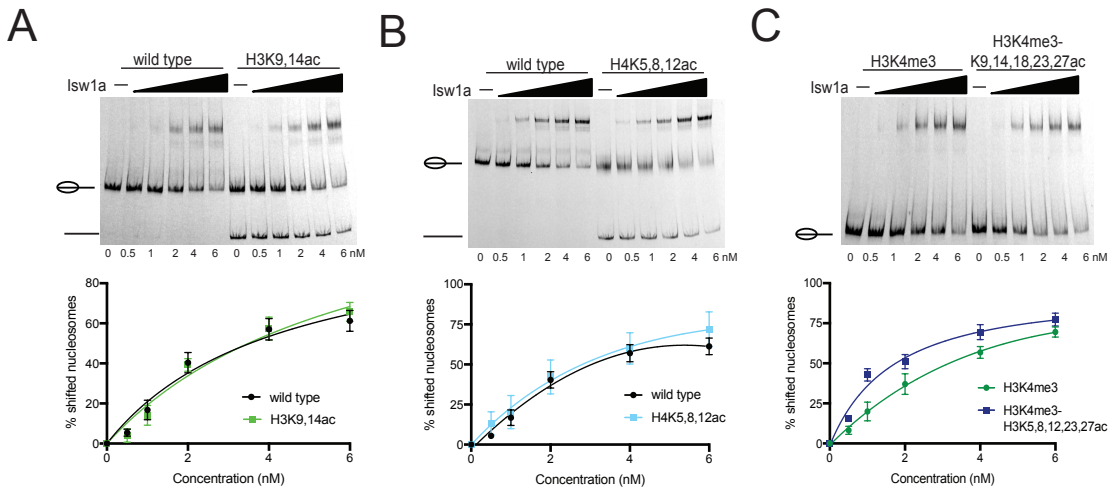

Figure 2.3.2 Isw1a is not recruited by histone acetylation. (A) EMSA of Isw1a with wild type and acetylated H3K9,14-containing nucleosomes. **(B)** EMSA of Isw1a with wild type and acetylated H4K5,8,12-containing nucleosomes. **(C)** EMSA of Isw1a with H3K4me3 and H3K4me3-K9,14,18,23,27ac-containing nucleosomes. EMSAs were quantitated and plotted as mean ± SEM. The number of replicates is at least three for all independent experiments.

Evidently, neither H3K9,14ac-, nor H4K5,8,12ac-containing nucleosomes significantly recruit Isw1a compared to unacetylated, wild type nucleosomes, *in vitro* (Figure 2.3.2A, B). Only the methylation-acetylation combination (H3K4me3-K9,14,18,23,27ac) displayed a small difference (Figure2.3.2C). Using cEMSAs, it is obvious that Isw1a has no preference for binding H3K9,14ac-containing nucleosomes (Figure 2.3.3A). Nevertheless, the preference for H4K5,8,12ac-containing nucleosomes could be increased for the last two endpoints (Figure 2.3.3B). Since all other concentrations clearly overlap and the results obtained by regular EMSAs show no preference, too, I conclude that H4K5,8,12ac-containing nucleosomes do not preferentially recruit Isw1a. Regarding the methylation-acetylation combination (H3K4me3-K9,14,18,23,27ac), the cEMSAs clarified the outcome here, as well. Having observed a slight preference in regular EMSAs towards H3K4me3-K9,14,18,23,27ac-containing nucleosomes, cEMSAs indicate no preferential binding by Isw1a (Figure 2.3.3C). Preferential binding takes place, when observing a preference in regular EMSAs that can be increased in competitive settings.

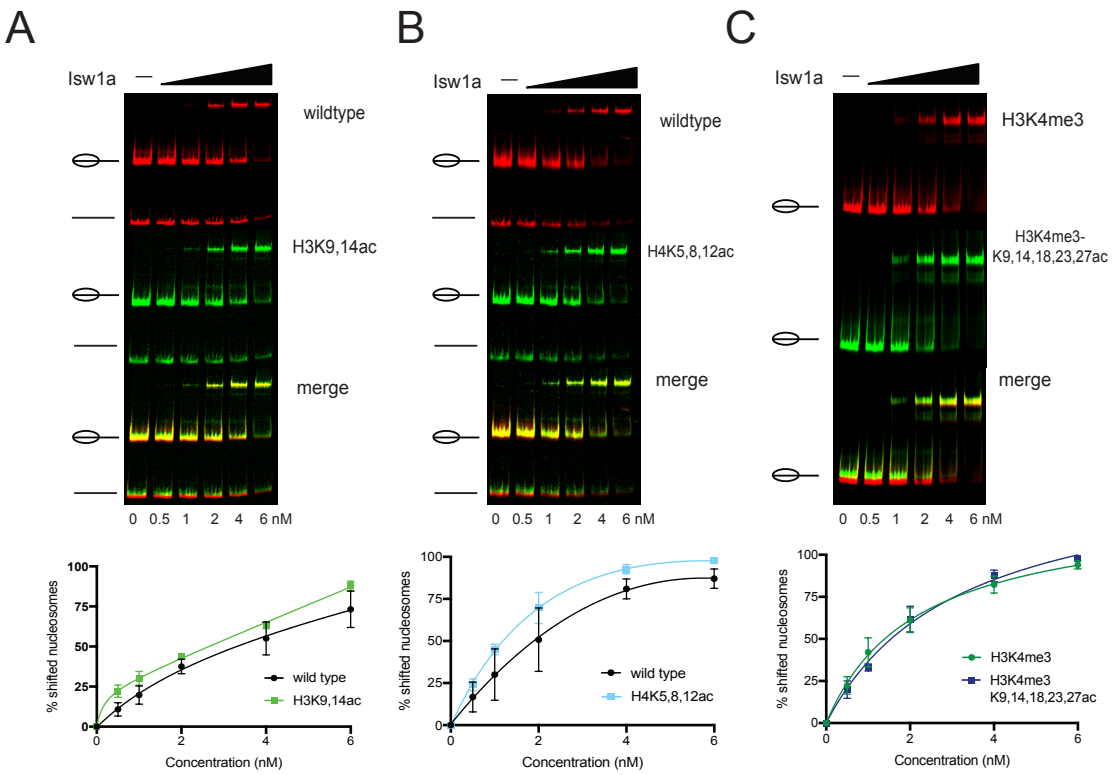

Figure 2.3.3 Isw1a does not get recruited by histone methylation or acetylation in cEMSAs. (A) Competitive EMSA of Isw1a with wild type and acetylated H3K9,14-containing nucleosomes. **(B)** Competitive EMSA of Isw1a with wild type and acetylated H4K5,8,12-containing nucleosomes. **(C)** Competitive EMSA of Isw1a with H3K4me3 and H3K4me3-K9,14,18,23,27ac-containing nucleosomes. Competitive EMSAs were quantitated and plotted as mean ± SEM. The number of replicates is at least three for all independent experiments.

The reconstitution of the poly-acetylated nucleosomes was very inefficient, leading to a low yield of reconstitution and poor positioning, resulting in comparatively undefined bands after electrophoresis (Lane 7 in Figure 2.3.4). The high degree of acetylation naturally leads to loose mononucleosomes. Even strong positioning sequences such as the 601 sequence face problems in providing sufficient DNA-histones contacts to achieve a cleanly positioned mononucleosome. Therefore, interpretation of these binding assays is somewhat challenging. The EMSA experiments support the hypothesis that a high degree of acetylation cannot preferentially recruit Isw1a *in vitro* (Figure 2.3.4). This is in line with the outcome of the EMSAs with fewer acetylation. In conclusion H3K4 trimethylation or histone H3 or H4 acetylation cannot recruit Isw1a to the ends of genes.

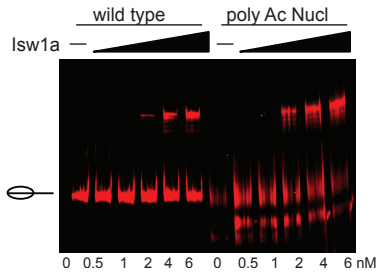

Figure 2.3.4 Isw1a has no preference for highly acetylated nucleosomes EMSA of Isw1a with wild type and poly-acetylated nucleosomes did not show a preference. The number of replicates is three.

2.3.1.3 Isw1a is a novel histone H2A.Z interactor

Not just PTMs surround promoter areas. Also the histone variant H2A.Z (Htz1 in yeast) flanks the transcription start site. It is incorporated instead of the canonical histone H2A variant. Therefore, histone H2A.Z is a promising candidate for Isw1a recruitment, since they co-localize in the genome.

Indeed, *in vitro* binding assays confirm a preference for H2A.Z-containing mononucleosomes (Figure 2.3.5A). To depict a more *in vivo* – like situation, cEMSA experiments were carried out to confirm these results (Figure 2.3.5B). While H2A.Z-containing nucleosomes get shifted first (green), wild type nucleosomes are partially left as free nucleosomes (red). In these experiments the human histone H2A.Z variant was used, since it forms more stable and better positioned, reconstituted mononucleosomes.

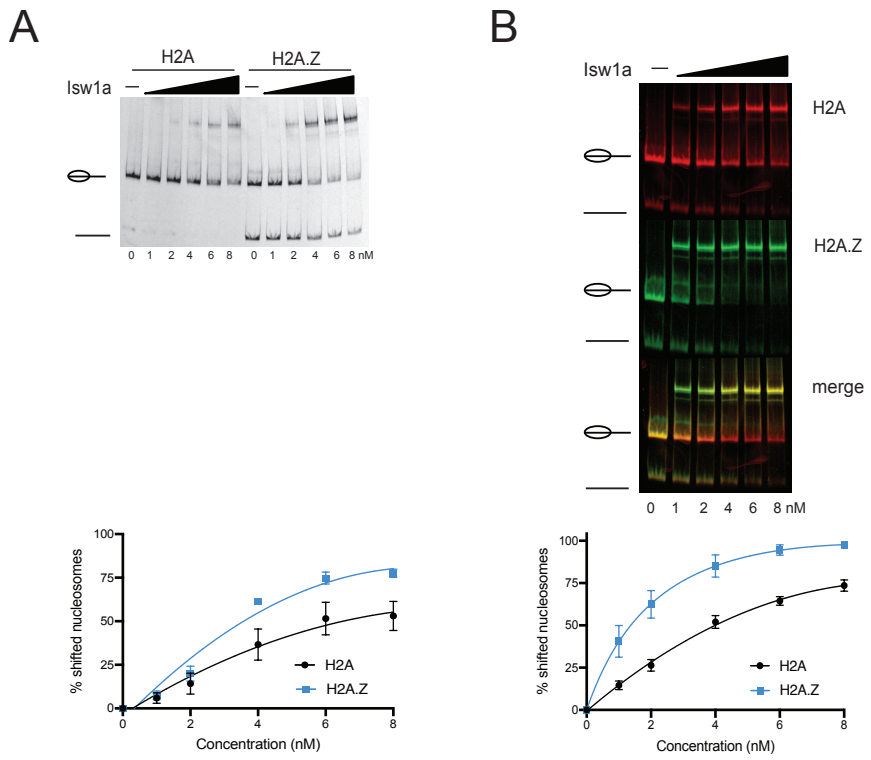

Figure 2.3.5 Isw1a preferentially binds to H2A.Z-containing nucleosomes. (A) Isw1a preferentially binds to H2A.Z-containing nucleosomes compared to wild type nucleosomes when assessed by EMSA. **(B)** Isw1a preferentially binds to H2A.Z-containing nucleosomes compared to wild type nucleosomes in cEMSAs. EMSAs and cEMSAs were quantitated and plotted as mean ± SEM. The number of replicates is at least three for all independent experiments.

H2A.Z-containing nucleosomes lead to a rather tightly packed nucleosome according to the crystal structure[124]. In fact, human H2A.Z and yeast Htz1 share a ca. 77% similarity (Figure 2.3.6B). To verify that the preference for Htz1 is true, two control experiments were conducted. Yeast Htz1-containing nucleosomes were reconstituted and Isw1a binding was evaluated. Notably, reconstitution led to two main, rather fuzzy bands, indicating the inability to establish the intended DNA-histone contacts. However, Isw1a shows a preference for Htz1-containing nucleosomes in comparison to wild type nucleosomes (Figure 2.3.6A). To further validate the outcome, a dye switch was performed to confirm that the preference does not come from a stronger or weaker signal produced by the IRD800 (green) or IRD700 (red) dye, respectively. The experiment shows that both dyes work equally well (Supplementary Figure 5.7).

To check whether Isw1a also preferentially interacts with histone Htz1 *in vivo*, co-immunoprecipitation experiments (Co-IPs) were performed. However, under the conditions tested, no stable interaction could be detected with either H3 (Figure

2.3.6C) or Htz1 (Figure 2.3.6D). Further, proteomics experiments performed on TAP-purified Ioc3 did not identify histone Htz1 as a significantly enriched interactor (data not shown). This is not surprising since Isw1a interaction with Htz1 was only observed in an additional *nap1Δchz1* deletion background[115]. Currently, the Smolle Lab is investigating the role of histone Htz1 in the recruitment of Isw1a *in vivo* using CUT&RUN.

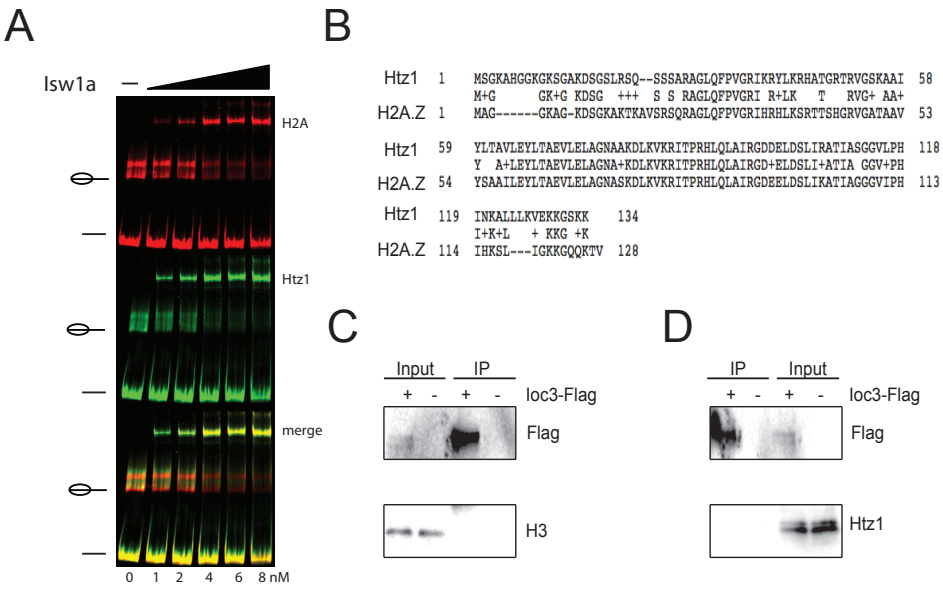

Figure 2.3.6 Isw1a preferentially binds to Htz1 *in vitro*. (A) Isw1a preferentially binds to Htz1-containing nucleosomes compared to wild type H2A nucleosomes in cEMSAs. The number of replicates is at least three for all independent experiments. **(B)** Sequence alignment (Protein Blast) of yeast Htz1 and human H2A.Z. Similarity of the amino acid sequence is 77%. **(C)** Co-IP of Flag-tagged Ioc3 compared to an untagged wild type control. No histone H3 can be detected by Western blot. **(D)** Co-IP of Flag-tagged Ioc3 compared to an untagged wild type control. No Htz1 can be detected by western blot.

Having shown that the Isw1a complex displays a preference for H2A.Z-containing nucleosomes, the next aim was to discover which subunit is responsible for this effect. Recombinant Isw1 and Ioc3 were purified from *E. coli* (see section 2.1). Neither Isw1 nor Ioc3 were able to establish stable interactions with either DNA or nucleosomes (Figure 2.3.7). This is in agreement with the findings of the Tsukiyama Lab[170] . Using pull down experiments they showed that Isw1 monomer is not capable of forming stable interactions with DNA or nucleosome. My data leads to the same conclusion. Ioc3 displays some affinity towards DNA and nucleosome, but is not able to form

stable complexes as evidenced by smears. Only in complex they achieve full functionality.

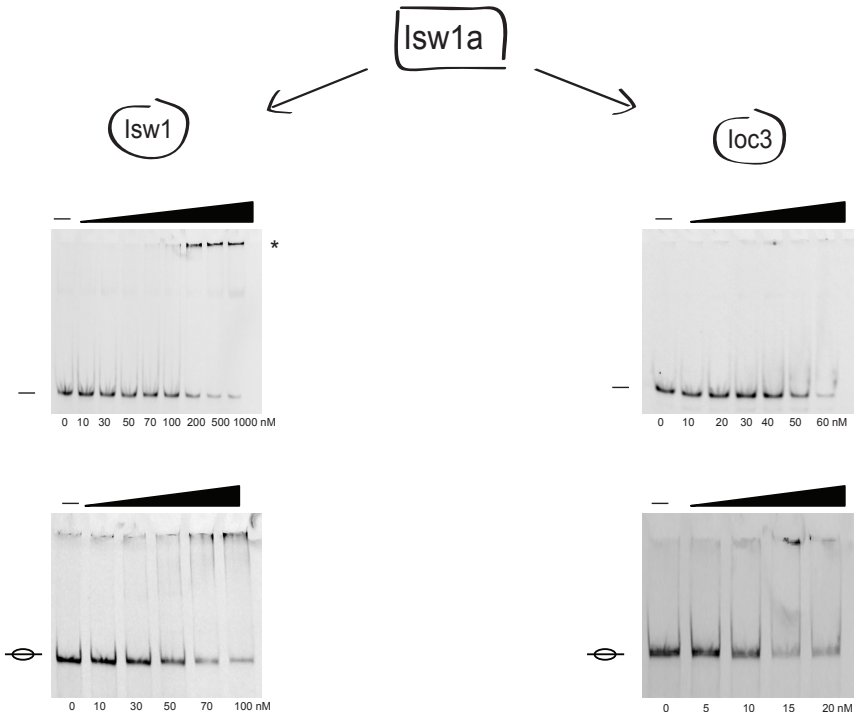

Figure 2.3.7 Recombinant Isw1 and Ioc3 do neither bind DNA nor nucleosomes. The two Isw1a subunits Isw1 and Ioc3 do both neither form stable interactions with DNA (upper panels) nor with mid-positioned nucleosomes (34-N-34, lower panels). The star (*) indicates precipitation in the well.

In contrast, both, Isw1 and Ioc3 can weakly bind to histone octamers in pull down assays. This also indicates that both proteins are functional per se (Figure 2.3.8A). More specifically, Ioc3 alone displays a small preference for Htz1-containing octamers (Figure 2.3.8B). Pull down assays with Isw1 and Htz1-containing octamers were not possible, owing to the fact that the mock control of Isw1 was not completely free of histones (see Figure 2.3.8A lane 3). Therefore, comparison of pull down efficiencies between canonical octamers and Htz1-containing octamers would not be meaningful.

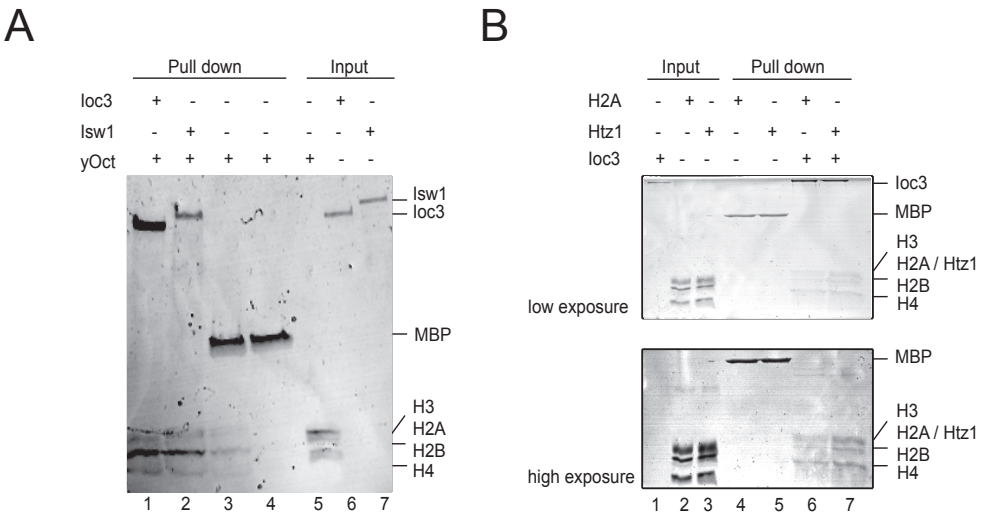

Figure 2.3.8 Isw1 and Ioc3 can bind histone octamers. (A) Pull Down assay with recombinant Ioc3 and Isw1 show weak binding to wild type octamers. 6xHis-MBP was added to mock pull downs. Note that Ioc3 was pulled down using amylose sepharose (lane 1), leaving no residual octamers binding to the beads (lane 4). Isw1 was pulled down using Ni-NTA beads (lane 2), leaving a small amount of octamers binding in the mock pull down (lane 3). **(B)** Ioc3 shows a slight preference for Htz1-containing octamers (lane 7) compared to canonical H2A-containing octamers (lane 6). 6xHis-MBP was added to mock pull downs. The upper panel shows a low exposure of the gel. The lower panel shows a high exposure of the same gel, focusing on the lower part of the gel. 20% were loaded for the input, 80% were loaded for the pull down and the mock.

To investigate whether Histone H2A.Z and H3K4me3 might result in combinatorial effects regarding the association with Isw1a, I tested H2A.Z-H3K4me3-containing octamers that were reconstituted into stable nucleosomes. In direct comparison with H2A.Z-containing nucleosomes, however, H2A.Z-H3K4me3-containing nucleosomes did not increase affinity for Isw1a (Figure 2.3.9). Histone H2A.Z seems to be primarily responsible for Isw1a binding *in vitro*.

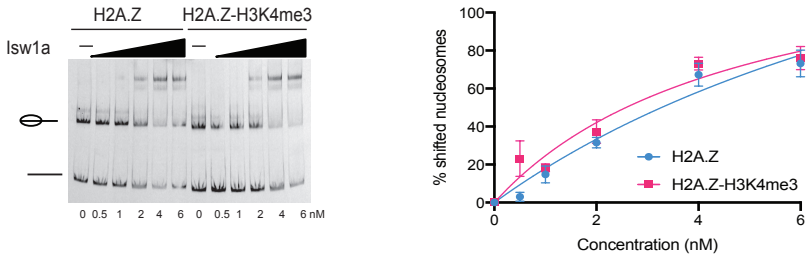

Figure 2.3.9 H2A.Z-H3K4me3-containing nucleosome does not increase specificity for Isw1a. EMSA shows similar binding affinities for Isw1a to H2A.Z- and H2A.Z-H3K4me3-containing nucleosomes. Quantification of the free nucleosome bands indicates no preferential binding. EMSAs were quantitated and plotted as mean ± SEM. The number of replicates is at least three for all independent experiments.

To summarize, Isw1a is a novel histone H2A.Z interactor. *In vitro* binding assays confirm preferential binding of Isw1a to H2A.Z/Htz1. Both, Isw1 and Ioc3 subunits bind to histone octamers. Yet, Ioc3 is seemingly responsible for Htz1 recognition. Additional PTMs such as H3K4me3 could not increase affinity for H2A.Z-containing nucleosomes.

2.3.1.4 The histone variant H2A.Z increases sliding activity of Isw1a *in vitro*

In principle, PTMs or histone variants can recruit chromatin remodelers. However, this provides no information about remodeling activity. PTMs such as H3K4me or histone acetylation do not promote Isw1a binding to nucleosomes *in vitro*, while the histone variant H2A.Z has a sizeable effect. Therefore, I wanted to investigate the roles of these PTMs and histone variant on Isw1a remodeling activity. By precisely measuring the remodeling of end-positioned mononucleosomes in a time dependent manner, the remodeling activity of Isw1a can be evaluated. Furthermore, it is possible that a histone modification may not be involved in remodeler recruitment, yet still plays a role for ATPase activation. Given this possibility, remodeling activity of Isw1a was tested using acetylated nucleosomes. These were reconstituted with Cy5-, IRD700- or IRD800-labeled 215 bp DNA harboring the widom 601 positioning sequence to produce end-positioned nucleosomes (0-N-68). In binding assays, no elevated affinity for acetylation was observed. In sliding assays, no increased activity was seen, as well, irrespective of whether histone H3 (Figure 2.3.10A) or H4 was acetylated (Figure 2.3.10B). Competitive sliding assays further validate these findings (Figure 2.3.10C, D).

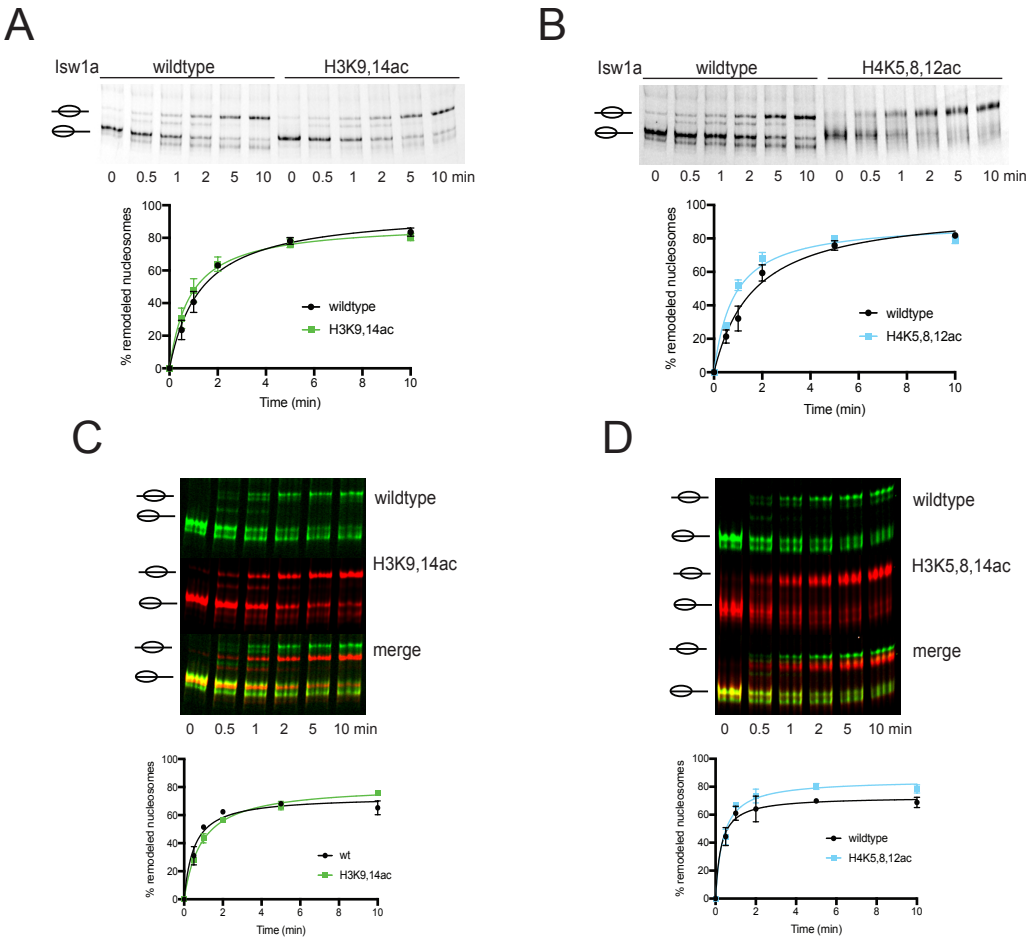

Figure 2.3.10 Acetylated nucleosomes do not increase Isw1a sliding activity. (A) Sliding assay of wild type and H3K9,14ac-containing nucleosomes. No differences for either substrate could be observed. **(B)** Sliding assay of wild type and H4K5,8,12ac-containing nucleosomes. No differences for either substrate could be observed. **(C)** Competitive sliding assay of Isw1a between wild type and H3K9,14ac-containing nucleosomes. **(D)** Competitive sliding assay of Isw1a between wild type and H4K5,8,14ac-containing nucleosomes. Sliding assays and competitive sliding assays were quantitated and plotted as mean ± SEM. The number of replicates is at least three for all independent experiments.

Having shown that acetylation does not impact Isw1a remodeling activity, I wanted to investigate whether H4K4me3 does so. Notably, H3K4me3-containing nucleosomes could not preferentially recruit Isw1a in *in vitro* EMSA experiments (see Figure 2.3.1). This histone modification could also not enhance sliding activity in regular sliding assays (Figure 2.3.11A) nor in a competitive system (Figure 2.3.11C). Incorporation of H3K4me3 and acetylation in the same mononucleosome (H3K4me3-K9,14,18,23,27ac) also had no effect on remodeling activity (Figure 2.3.11B, D). Taken together, the outcome of all binding and sliding assays suggest that neither H3K4me3 nor acetylation have any effect on Isw1a recruitment and activity.

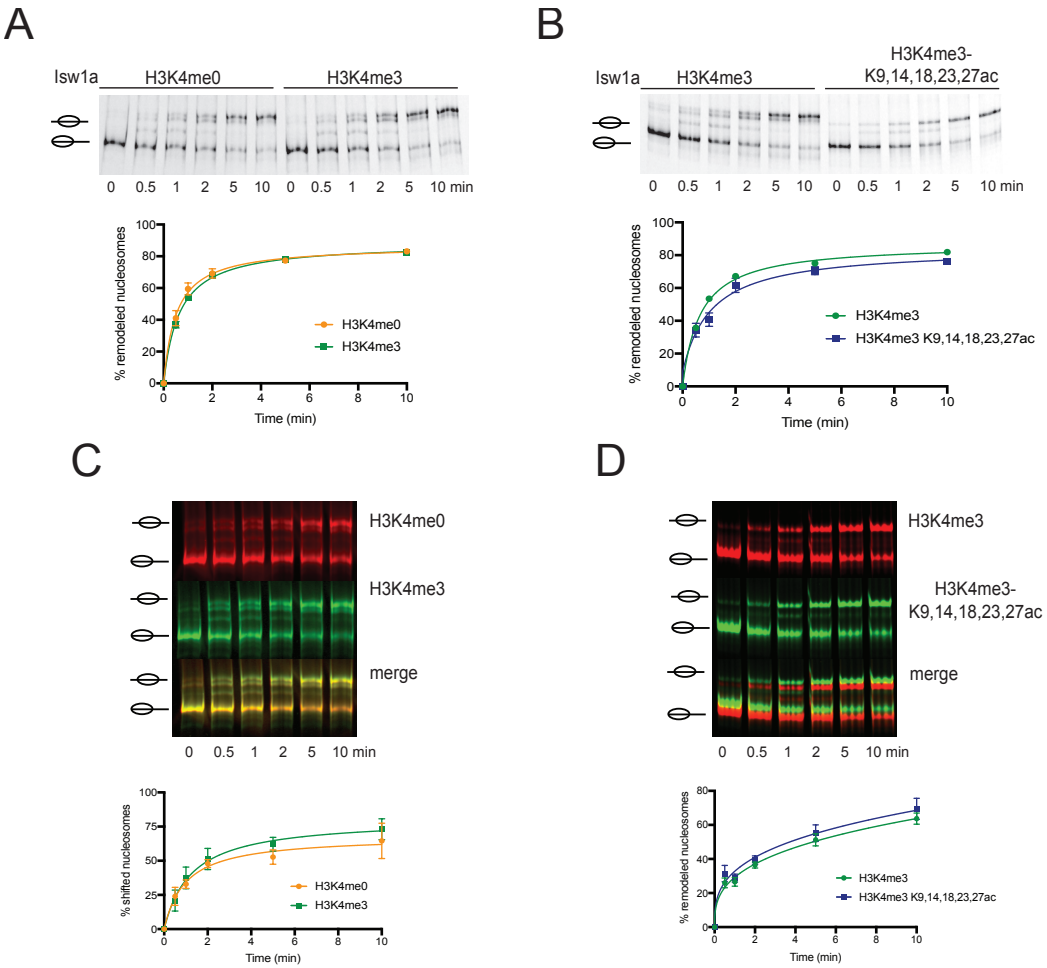

Figure 2.3.11 Methylated nucleosomes do not increase Isw1a sliding activity. **(A)** Sliding assay of wild type and H3K4me3-containing nucleosomes. No differences for either substrate could be observed. **(B)** Sliding assay of H3K4me3- and H3K4me3-K9,14,18,23,27ac-containing nucleosomes. No differences for either substrate could be observed. **(C)** Competitive sliding assay of Isw1a between H3K4me0- and H3K4me3-containing nucleosomes. **(D)** Competitive sliding assay of Isw1a between H3K4me3- and H3K4me3-K9,14,18,23,27ac-containing nucleosomes. Sliding assays and competitive sliding assays were quantitated and plotted as mean ± SEM. The number of replicates is at least three for all independent experiments.

However, the histone H2A.Z variant did have an effect on Isw1a binding affinity (see section 2.3.2). Unsurprisingly, Isw1a also displayed increased remodeling activity for H2A.Z-containing nucleosomes (Figure 2.3.12A). Combination of histone H2A.Z with H3K4me3 did not result in a combinatorial effect, and no further increase in sliding activity could be observed (Figure 2.3.12C). This is in agreement with previous binding assays. Additional competitive sliding assays underline the different remodeling activities for canonical H2A and H2A.Z-containing nucleosomes (Figure 2.3.12B). This suggests that Isw1a is not just recruited by histone H2A.Z, but also its

activity is increased. However, the ATPase Isw1 is not unique to Isw1a but it is also present in Isw1b. Only the associated Ioc subunits differ. To confirm the effects of histone H2A.Z on Isw1a activity specifically, sliding assay with Isw1b and H2A.Z-containing nucleosomes were conducted. These showed no difference for H2A- versus H2A.Z-containing substrates (Supplementary Figure 5.8A). These experiments allow two conclusions: (i) H2A.Z-mediated, enhanced sliding activity is Isw1a specific and (ii) the subunit predominantly responsible for this effect is Ioc3. If Isw1 were the reason for preferential H2A.Z binding or activity, then Isw1b would be expected to behave similarly. Pull down experiments (see Figure 2.3.9) confirm this finding. Summarizing, the histone variant H2A.Z, but not H3K4me3 or acetylation increase sliding activity of Isw1a *in vitro*.

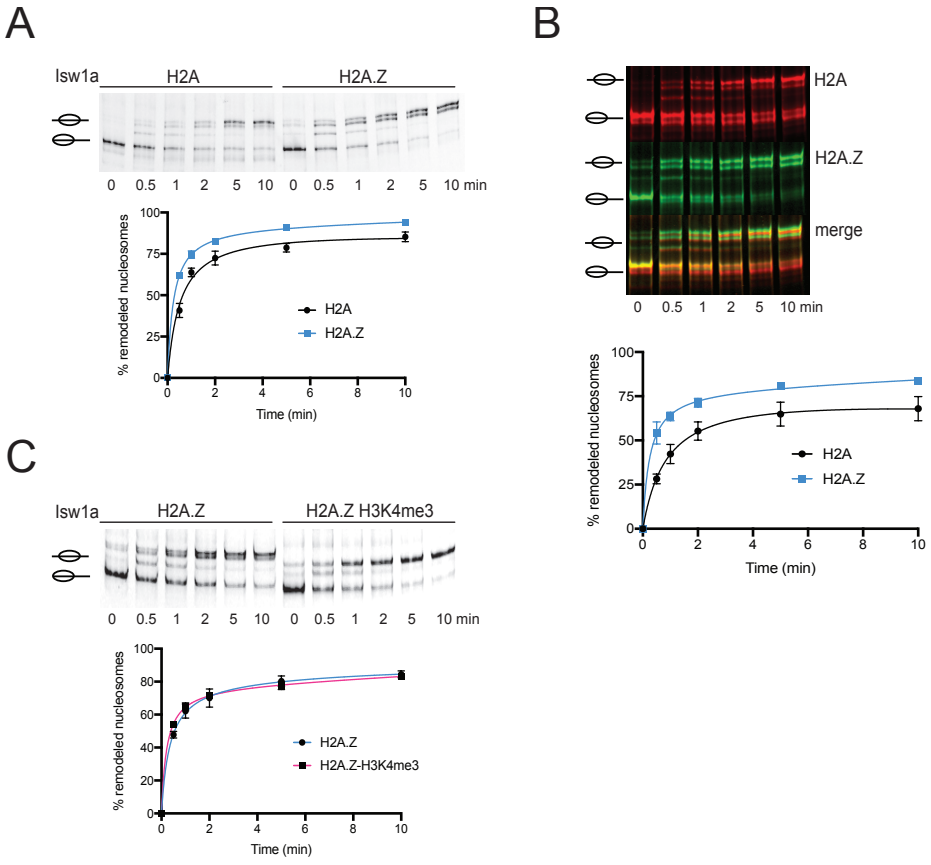

Figure 2.3.12 H2A.Z-containing nucleosomes increase Isw1a sliding activity. **(A)** Isw1a preferentially slides H2A.Z-containing nucleosomes. **(B)** Competitive sliding assay of Isw1a directly compares remodeling activity between canonical and H2A.Z-containing nucleosomes. **(C)** Sliding assay of H2A.Z- and H2A.Z-H3K4me3-containing nucleosomes. No differences for either substrate could be observed hence methylation does not increase sliding activity.

2.3.2 The Ioc3 termini control functions of Isw1a *in vitro*

To investigate which part of Ioc3 is responsible for H2A.Z-mediated nucleosome-binding, several Ioc3 truncation mutants were designed. As described in section 2.1.2.2, only three mutants formed stable complexes following purification of endogenous Isw1a from yeast. Design of the constructs was based on the published crystal structure of Ioc3-HSS[167]. Regarding Ioc3, the structure only contains amino acids 138-747. The N- (aa 1-137) and C-terminus (aa 748-787) are missing, presumably because these parts are largely flexible. Thus, there are no details about their structure or function. Both termini raised particular interest since the crystal structure leaves open questions regarding nucleosome and histone contacts. DNA contacts observed through the CLB N-coil and CLB C-coil that remain in both C- and N-terminal truncations, so as the HLB domain.

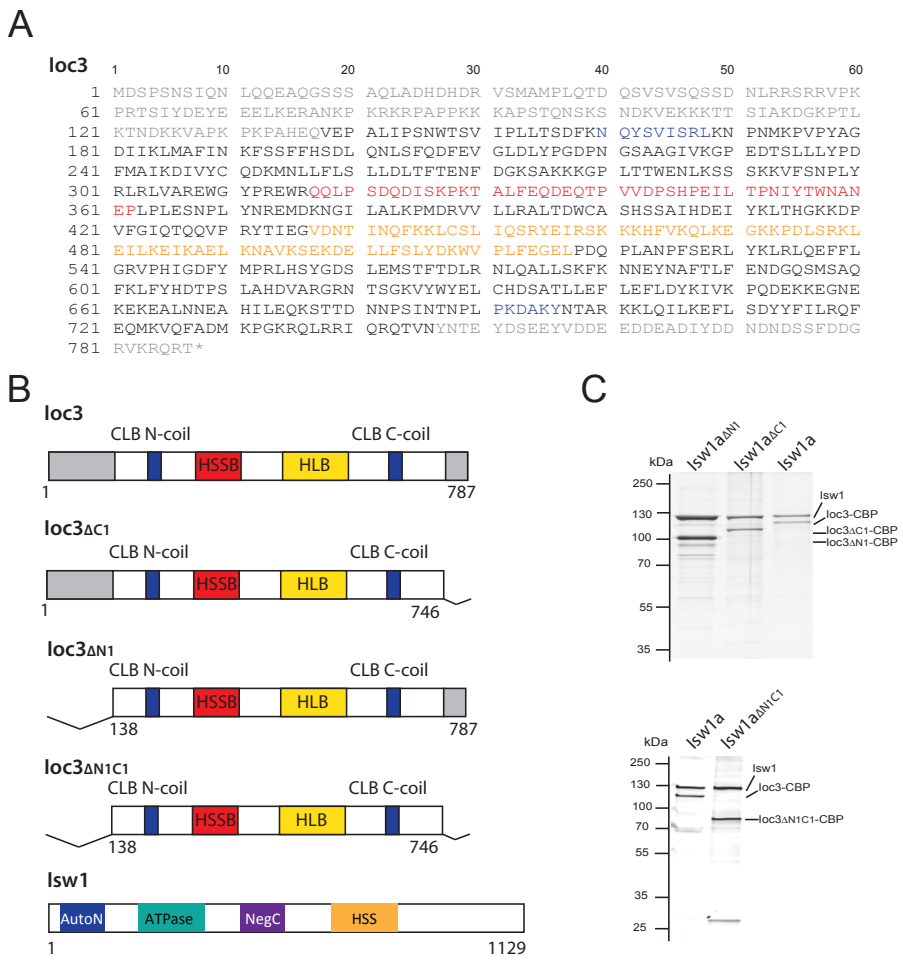

Figure 2.3.13 Schematic representation of wild type and mutant Isw1a complexes. (A) Amino acid sequence of full-length Ioc3. Parts that were not crystallized are in grey. The N- and C-terminal coils are in blue. The HSSB and HLB domain are shown in red and yellow,

respectively. **(B)** Schematic representation of the wild type and mutant Ioc3 subunit that form together with the Isw1 subunit wild type and mutant Isw1a complexes, respectively.
(C) Silver stain of purified wild type and mutant Isw1a complexes.

2.3.2.1 The Ioc3 C-terminus mediates nucleosome-binding

First, the function of the missing C-terminus was analyzed. The C-terminal truncation is rather small and amounts to ca. 5 kDa. However, it does not affect the interaction of $Ioc3_{\Delta C1}$ with Isw1 to form the $Isw1a_{\Delta C1}$ complex. Also, the HLB domain remains unaffected. Inspecting the amino acid sequence of the truncated C-terminus reveals an extensive acidic patch (Figure 2.3.13A). I speculate that it may be involved in the interaction between $Isw1a_{\Delta C1}$ with H2A.Z. Surprisingly, in comparison to Isw1a, $Isw1a_{\Delta C1}$ is nucleosome-binding deficient (Figure 2.3.14A). Further hypothesizing that the C-terminus is only capable of binding the preferred H2A.Z target, the experiment was repeated using H2A.Z-containing nucleosomes (Figure 2.3.14B). $Isw1a_{\Delta C1}$ was also H2A.Z-nucleosome-binding-deficient, concluding that the C-terminus is not responsible for H2A.Z binding, but rather for recognizing nucleosomes in general.

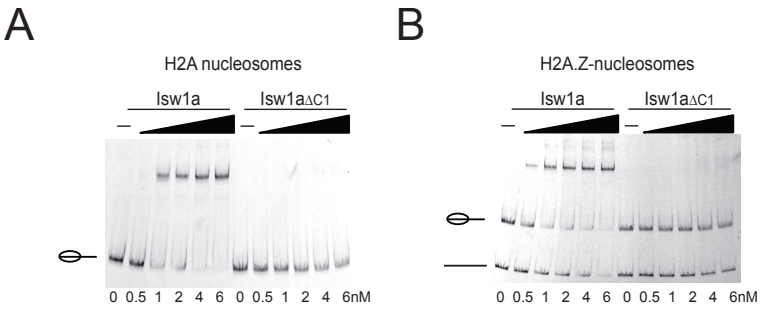

Figure 2.3.14 $Isw1a_{\Delta C1}$ is nucleosome-binding deficient. (A) EMSA of wild type Isw1a and $Isw1a_{\Delta C1}$ with wild type nucleosomes. $Isw1a_{\Delta C1}$ is binding deficient. **(B)** EMSA of wild type Isw1a and $Isw1a_{\Delta C1}$ with H2A.Z nucleosomes. $Isw1a_{\Delta C1}$ is binding deficient. The number of replicates is at least three for all independent experiments.

Nevertheless, it leaves the question open, whether this construct is at all functional. Functionality was tested using remodeling assays. Recombinant, full-length Isw1 monomer cannot mobilize nucleosomes (Supplementary Figure 5.8B). Instead, Isw1 needs its associated Ioc subunits (either Ioc3 or Ioc2-Ioc4) to 'activate' its sliding abilities. Presumably this is associated with concurrent structural changes.

Remarkably, Isw1a$_{\Delta C1}$ can slide wild type nucleosomes as efficiently as native Isw1a (Figure 2.3.15). H2A.Z-containing nucleosomes can be mobilized at the same rate, too, further emphasizing that Isw1a$_{\Delta C1}$ is indeed functional. It also reinforces the hypothesis that the C-terminus is not H2A.Z specific but rather a common 'nucleosome-binding' site.

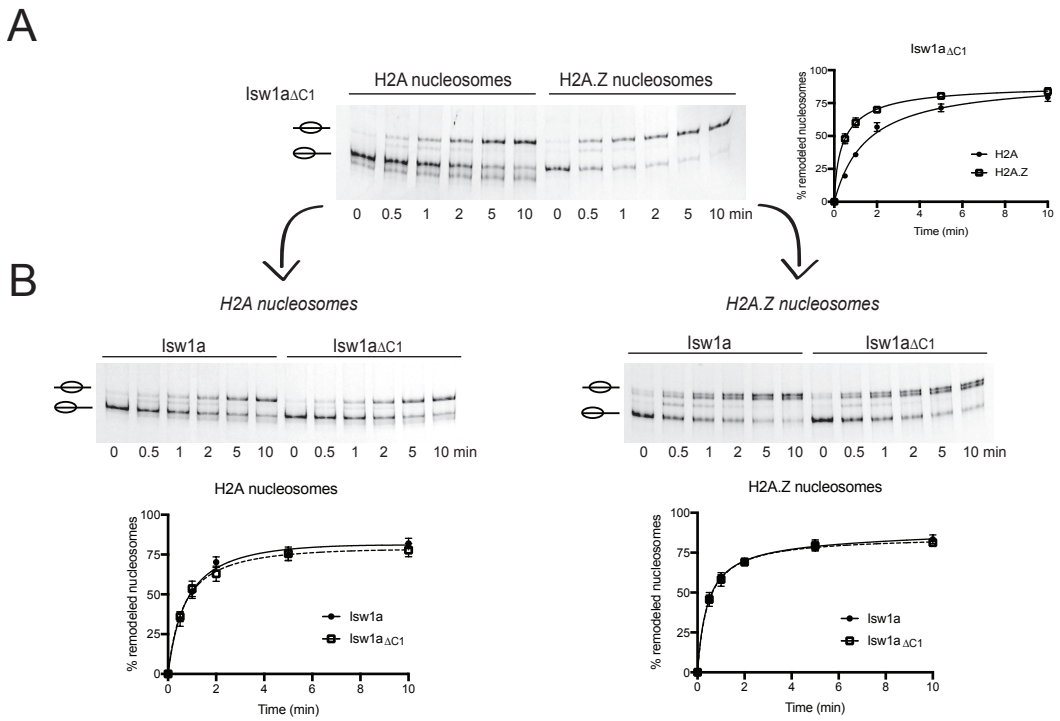

Figure 2.3.15 Isw1a$_{\Delta C1}$ slides H2A.Z-containing nucleosomes as efficiently as canonical nucleosomes. (A) Sliding assay of Isw1a$_{\Delta C1}$ with canonical and H2A.Z-containing nucleosomes. **(B)** Comparing analysis of sliding ability for H2A-containing nucleosomes (left panel) and H2A.Z-containing nucleosomes (right panel) between wild type Isw1a and Isw1a$_{\Delta C1}$. Sliding assays were quantitated and plotted as mean ± SEM. The number of replicates is at least three for all independent experiments.

Rethinking the sliding process in detail, the chromatin remodeler must get attached to the nucleosome through more or less stable interactions between remodeler and DNA and/or histones. Why then is the nucleosome-binding deficient Isw1a$_{\Delta C1}$ mutant capable of sliding nucleosomes at wild type levels? Seeing that Isw1 dramatically changes its conformation when bound to ADP or ATP[187] made me hypothesize that binding nucleotides can 'activate' the construct and allow binding and sliding actions. To answer this question, the idea was to capture the remodeler during its sliding process, when a stable remodeler-nucleosome interaction must be established. For this, an EMSA was set up. In a second step, nucleotides were added to activate the

ATPase, albeit no stop buffer was added (Figure 2.3.16A). The principle is that without the stop buffer the remodeler is not competed away as it is in a sliding assay, but stays bound to the nucleosome. Upon ATP addition, both Isw1a and Isw1a$_{\Delta C1}$ formed stable interactions with nucleosomes. To test dependency on hydrolysable ATP, the experiment was repeated, only that ADP (Figure 2.3.16C) and ATP-γ-S (Figure 2.3.16D) were added instead of ATP (Figure 2.3.16C). Nevertheless both constructs were capable of binding. This indicates that nucleotides in general lead to a conformational change in the Isw1a complex. Vary *et al.* found that Isw1 alone is not capable of binding to nucleosomes in an ATP-independent manner[170]. Also, binding of Isw1a to nucleosomes was not enhanced upon addition of ATP. My suggestion is, that Isw1 changes its conformation when binding to its subunit Ioc3. The Ioc3 C-terminus mediates remodeler-nucleosome contacts. When missing, nucleotide binding can change the conformation of Isw1 and still allows Isw1a$_{\Delta C1}$ to bind to nucleosomes. Taken together, Isw1a$_{\Delta C1}$ is functional and Ioc3 seems to play a role in nucleosome targeting. Without nucleotides, Isw1a$_{\Delta C1}$ cannot guide the remodeler complex onto nucleosomes. This may conclude that binding of the Ioc3 C-terminus to nucleosomes is an important step in recruiting Isw1a onto chromatin before remodeling is taking place.

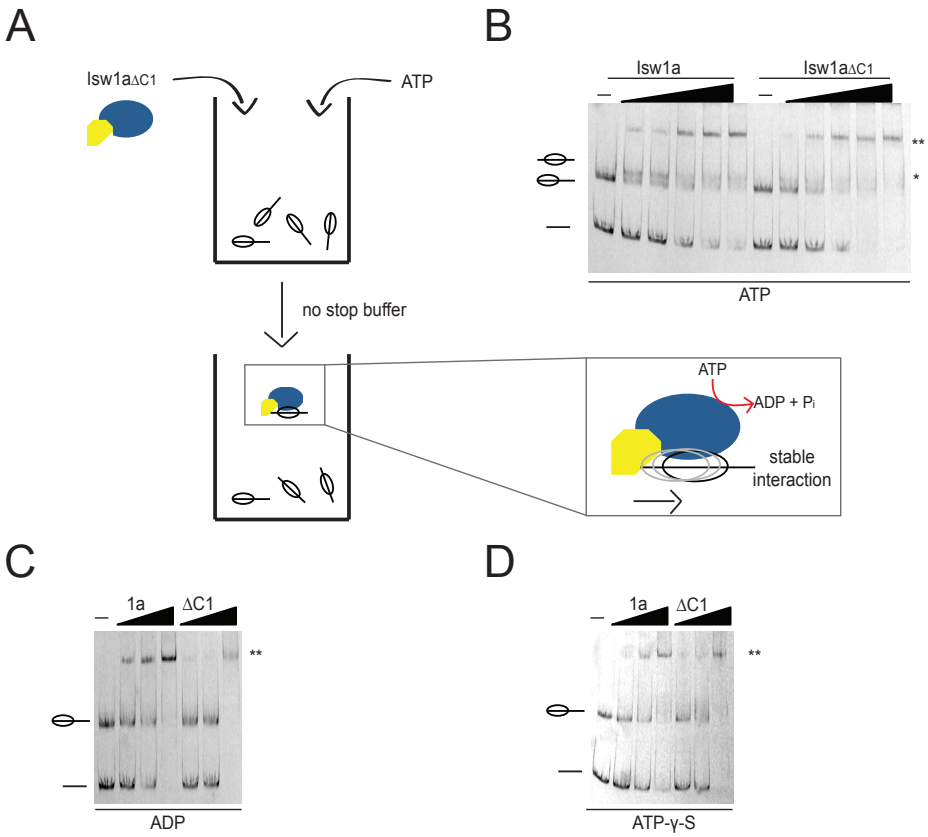

Figure 2.3.16 Isw1a$_{\Delta C1}$ can form short, stable interactions with nucleosomes. (A) Schematic overview of a sliding EMSA **(B)** ATP-dependent binding assays of Isw1a and Isw1a$_{\Delta C1}$ to wild type nucleosomes. The star (*) marks middle-positioned nucleosomes (endpoint of the sliding reaction). Two stars (**) mark stable nucleosome-protein interactions. **(C)** ADP-dependent binding assays of Isw1a and Isw1a$_{\Delta C1}$ to wild type nucleosomes. Two stars (**) mark stable nucleosome-protein interactions. **(D)** ATP-γ-S dependent binding assays of Isw1a and Isw1a$_{\Delta C1}$ to wild type nucleosomes. Two stars (**) mark stable nucleosome-protein interactions. The number of replicates is at least three for all independent experiments.

2.3.2.2 The Ioc3 N-terminus regulates H2A.Z recognition and remodeling activity of Isw1a

The crystal structure leaves a large part of the N-terminus unresolved. While structural information is missing, the aim was to investigate its contributions to Isw1a functions. A stable, truncated complex could be purified from yeast, Isw1a$_{\Delta N1}$, consisting of Isw1 and Ioc3$_{\Delta N1}$ (see Figure 2.3.13). Truncation was chosen to mimic the same N-terminal truncation, which was used to obtain the crystal structure

(deletion of aa 1-137). The truncation is 15 kDa in size. Isw1a$_{\Delta N1}$ was able to bind to nucleosomes (Figure 2.3.18A). However, it was not able to fully distinguish between wild type and H2A.Z-containing nucleosomes (Figure 2.3.18A). While Isw1a preferentially bound to H2A.Z-containing nucleosomes, this effect was reduced in the N-terminal deletion mutant. Direct comparison with the binding behavior of Isw1a to H2A.Z nucleosomes draws attention to another interesting feature. While Isw1a formed only one stable complex with nucleosomes at any given concentration, Isw1a$_{\Delta N1}$ formed apparently two stable complexes with nucleosomes at higher concentrations (Figure 2.3.18B). The additional, second shift is likely consisting of either one nucleosome bound by two Isw1a$_{\Delta N1}$ protein complexes, or one Isw1a$_{\Delta N1}$ coordinates binding of two mononucleosomes. Either option leads to an increased molecular weight of the remodeler-mononucleosome complex. The Ioc3 N-terminus must thus be a repressive domain, which allows multiple binding events in its absence. Further, the H2A.Z recognition site is presumably inside the N-terminus since its absence abrogates preferential binding of Isw1a$_{\Delta N1}$ to H2A.Z-containing nucleosomes. To extend this effect, cEMSAs were conducted. Here, most of the H2A.Z preference is lost and validates the previous EMSA (Figure 2.1.18C).

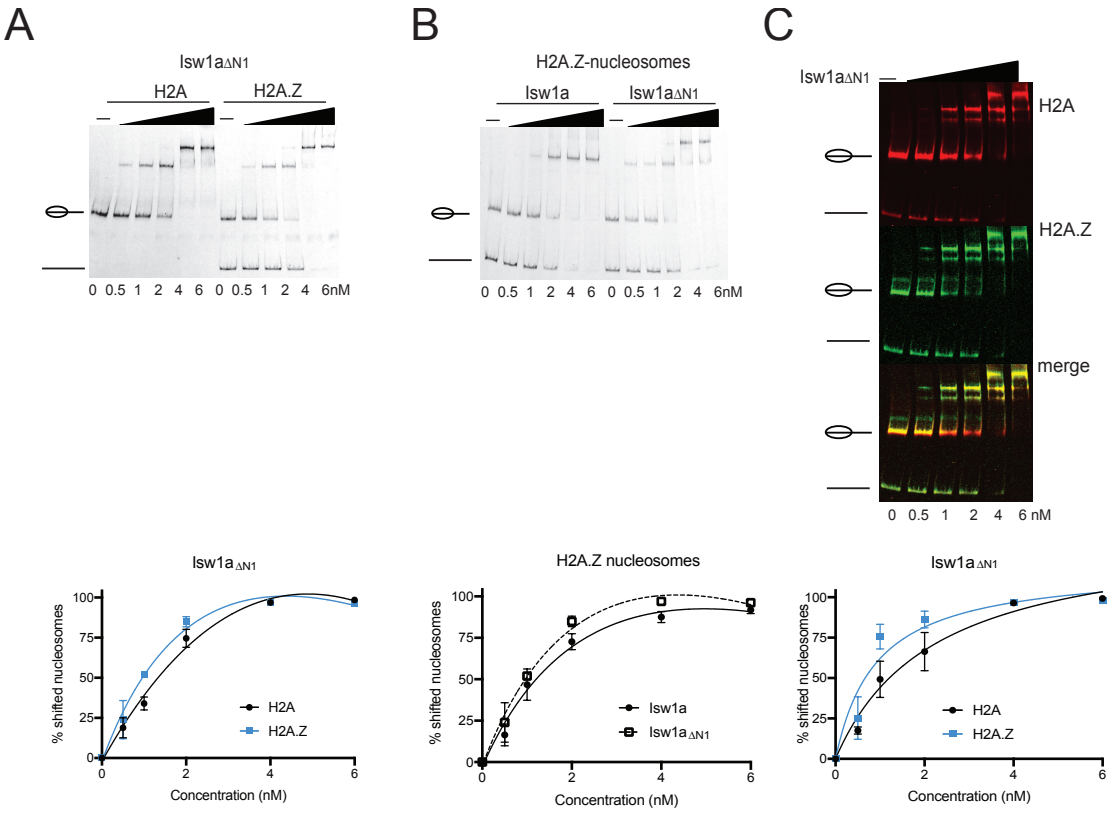

Figure 2.3.18 Isw1a$_{\Delta N1}$ does not distinguish between canonical H2A- and H2A.Z-containing nucleosomes. **(A)** EMSA of Isw1a$_{\Delta N1}$ with wild type H2A and H2A.Z-containing

nucleosomes. **(B)** Comparison of Isw1a and Isw1a$_{\Delta N1}$ with H2A.Z-containing nucleosomes. Note the second, upcoming shift in Isw1a$_{\Delta N1}$. **(C)** Competitive EMSA of Isw1a and H2A.Z-containing nucleosomes. EMSAs and cEMSAs were quantitated and plotted as mean ± SEM. The number of replicates is at least three for all independent experiments.

The outcome of the binding assays suggests that the Ioc3 N-terminus contributes to H2A.Z recognition. Hence, sliding activity was monitored for this truncation mutant. Interestingly, a large difference in remodeling activity can be observed between canonical H2A and H2A.Z-containing nucleosomes (Figure 2.3.19A). Therefore, Isw1a$_{\Delta N1}$ can indeed distinguish between both substrates, suggesting that a second H2A.Z recognition site may be present in the complex. In direct comparison to wild type Isw1a, sliding activity of Isw1a$_{\Delta N1}$ for H2A-containing nucleosomes is diminished, while its sliding activity for H2A.Z-containing nucleosomes is greatly enhanced (Figure 2.3.19B). In conclusion, these findings support the notion that the Ioc3 N-terminus partially regulates H2A.Z recognition. Apparent discrepancies may be due to a second, not yet identified H2A.Z recognition site.

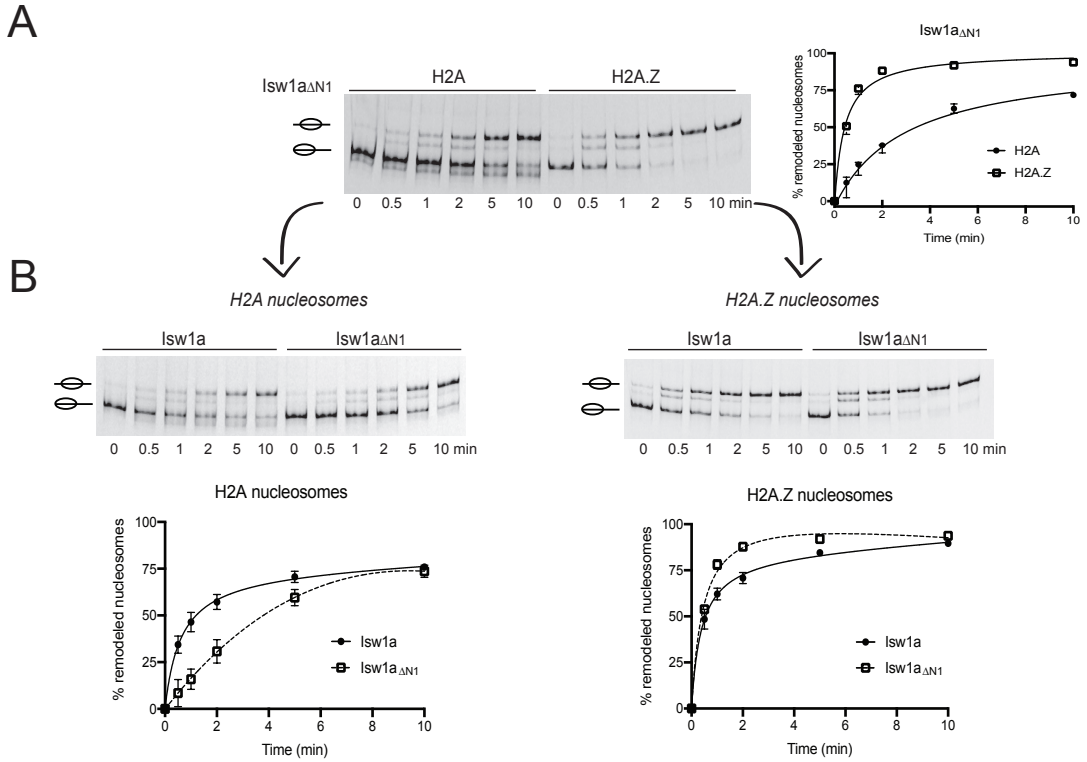

Figure 2.3.19 Isw1a$_{\Delta N1}$ slides H2A.Z-containing nucleosomes more efficiently than canonical H2A-containing nucleosomes. (A) Sliding assay of Isw1a$_{\Delta N1}$ with canonical and H2A.Z-containing nucleosomes. **(B)** Comparing sliding ability for H2A-containing nucleosomes (left panel) and H2A.Z-containing nucleosomes (right panel) for wild type Isw1a and Isw1a$_{\Delta N1}$. Sliding assays were quantitated and plotted as mean ± SEM. The number of replicates is at least three for all independent experiments.

2.3.2.3 The Ioc3 N-terminus and C-terminus have distinct contributions to Isw1a functions

In 2011 the Richmond lab proposed a model how Isw1a binds to nucleosomes[167]. The Ioc3 construct used included both N- and C-terminal deletions (see section 1.3.3.1 and Figure 2.3.13). Both termini have distinct functions in Isw1a binding and sliding activity (see sections 2.3.4 and 2.3.5). Therefore, I was interested to investigate an Isw1a remodeler with both truncations ($Ioc3_{\Delta N1C1}$). Thus, I purified the mutant $Isw1a_{\Delta N1C1}$ from yeast (see chapter 2.1). EMSAs were performed to evaluate the impact of the double truncation on Isw1a. Surprisingly, lacking binding ability in the $Isw1a_{\Delta C1}$ construct can be rescued by the additional deletion of the N-terminus in the $Isw1a_{\Delta N1C1}$ complex. While $Isw1a_{\Delta C1}$ was binding deficient, $Isw1a_{\Delta N1C1}$ was able to form a stable complex with mononucleosomes (Figure 2.3.21A). The mutual absence of the C- and the N-terminus allows $Isw1a_{\Delta N1C1}$ to bind to wild type nucleosomes. It seems, as if both termini influence each other. Additionally, $Isw1a_{\Delta N1C1}$ also shows no distinction between canonical H2A- and H2A.Z-containing nucleosomes, being in line with the functional consequences displayed by $Isw1a_{\Delta N1}$. (Figure 2.3.21A). The competitive EMSA confirms the outcome and shows the same affinity of $Isw1a_{\Delta N1C1}$ for canonical H2A- and H2A.Z-containing nucleosomes, comparable to $Isw1a_{\Delta N1}$ (Figure 2.3.21B).

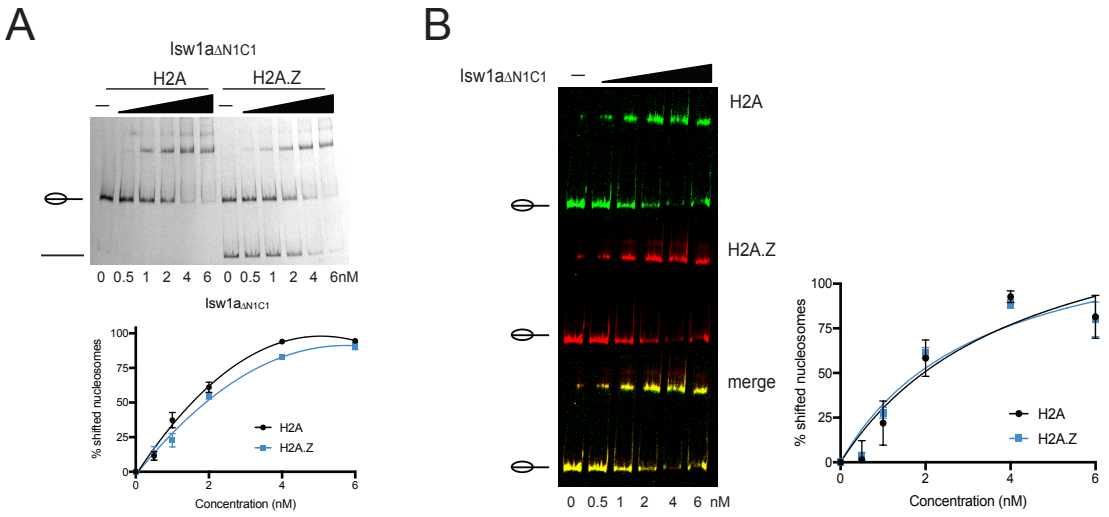

Figure 2.3.21 The H2A.Z-recognition site lies within the Ioc3 N-terminus. (A) EMSA of $Isw1a_{\Delta N1C1}$ with canonical H2A- and H2A.Z-containing nucleosomes displays a loss of preference for H2A.Z-containing nucleosomes. **(B)** Competitive EMSA of $Isw1a_{\Delta N1C1}$ with

canonical H2A- and H2A.Z-containing nucleosomes displays a loss of preference for H2A.Z-containing nucleosomes. EMSAs and cEMSAs were quantitated and plotted as mean ± SEM. The number of replicates is at least three for all independent experiments.

Deletion of the C-terminus severely affects nucleosome-binding abilities, yet leaves nucleosome sliding activity unaffected. Thus, deleting both, the N- and the C-terminus, should give comparable outcomes for sliding activity compared with the N-terminal deletion only. Indeed, Isw1a$_{\Delta N1C1}$ greatly preferred sliding of H2A.Z-containing nucleosomes (Figure 2.3.22A). Direct comparison with wild type Isw1a shows that sliding of wild type nucleosomes is diminished. However, sliding of H2A.Z-containing nucleosomes is not altered. These results for Isw1a$_{\Delta N1C1}$ mimic the sliding behavior of Isw1a$_{\Delta N1}$.

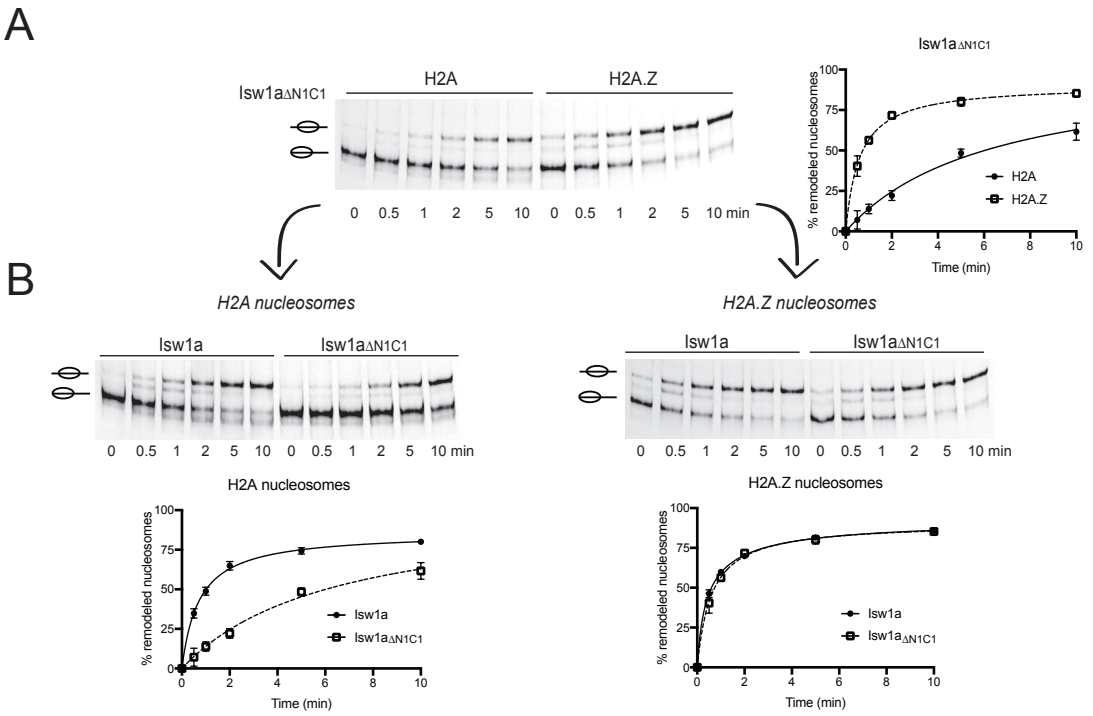

Figure 2.3.22 Isw1a$_{\Delta N1C1}$ preferentially slides H2A.Z-containing nucleosomes. (A) Sliding assay of Isw1a$_{\Delta N1C1}$ with canonical H2A- and H2A.Z-containing nucleosomes **(B)** Comparing sliding ability for H2A-containing nucleosomes (left panel) and H2A.Z-containing nucleosomes (right panel) for wild type Isw1a and Isw1a$_{\Delta N1C1}$. Sliding assays were quantitated and plotted as mean ± SEM. The number of replicates is at least three for all independent experiments.

Accordingly, competitive sliding assays were conducted. In both cases, Isw1a$_{\Delta N1C1}$ and Isw1a$_{\Delta N1}$ display a great preference for H2A.Z-containing nucleosomes (Figure 2.3.23A). The Ioc3 C-terminus does not affect sliding activity. Despite not being able

to preferentially recognize H2A.Z-containing nucleosomes in binding assays, sliding activity of both, Isw1a$_{\Delta N1}$ and Isw1a$_{\Delta N1C1}$ is stimulated to the same extent as wild type Isw1a when using H2A.Z-containing nucleosomes as a substrate (Figure 2.3.23C). This may indicate that (i) binding and activity are uncoupled or (ii) there must be a second, unknown H2A.Z recognition site buried inside the complex that acts specifically on sliding activity. It is known, that the human ISWI complexes are stimulated by histone H2A.Z [248]. Nevertheless, it seems that preferred binding and sliding is Isw1a specific, since the Isw1b complex did not display increased sliding activity for H2A.Z-containing nucleosomes (Supplementary Figure 5.8A)

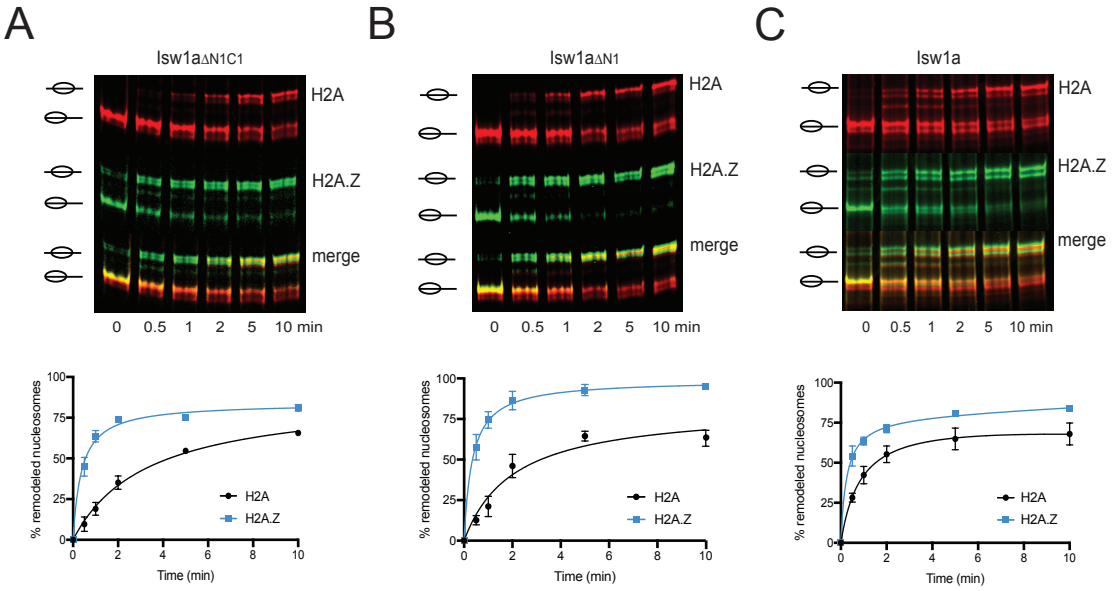

Figure 2.3.23 The Ioc3 C-terminus does not affect sliding activity of Isw1a. (A) Competitive sliding assay of Isw1a$_{\Delta N1C1}$ with canonical H2A- and H2A.Z-containing nucleosomes. **(B)** Competitive sliding assay of Isw1a$_{\Delta N1}$ with canonical H2A- and H2A.Z-containing nucleosomes. **(C)** Competitive sliding assay of wild type Isw1a with canonical and H2A.Z-containing nucleosomes. Data adapted from Figure 2.3.12B. Competitive sliding assays were quantitated and plotted as mean ± SEM. The number of replicates is at least three for all independent experiments.

I suggest that specifically the Ioc3 subunit is responsible for Isw1a binding to H2A.Z-containing nucleosomes *in vitro*. The uninterrupted acidic patch of H2A.Z may then lead to increased ATP hydrolysis in Isw1, thus increasing sliding activity as was already seen for all human ISWI members in Goldman *et al.*[248]. Nevertheless, Isw1 stimulation is unique to the Isw1a complex. Ioc4 and Ioc2 in Isw1b seem either to slow down H2A.Z-induced ATPase activity or binding of Ioc3 leads to a conformational change and stimulation. To summarize, the Ioc3 termini control Isw1a

functions. While the Ioc3 C-terminus highly promotes binding to nucleosomes, it does not affect sliding activity. The lacking binding ability can be rescued by additional deletion of the Ioc3 N-terminus. This part acts as a repressive element, since without it, multiple binding events are possible. Further, the Ioc3 N-terminus seems to carry at least one H2A.Z recognition motif, since in its absence H2A.Z recognition does not take place. The additional deletion of the Ioc3 C-terminus did not change the results. The ambivalent outcome of the sliding assays for Isw1a$_{\Delta N1C1}$ and Isw1a$_{\Delta N1}$ hints towards a more complicated role for the N-terminus and needs further truncations to elucidate its molecular mechanism.

2.4 Working Model

In my thesis I analyzed the molecular mechanism for the recruitment of Isw1a and Isw1b to target sites. Here, I propose a three step model of target recognition and chromatin remodeler activation.

In the first step the remodeler gets recruited onto chromatin. Besides Isw1, in Isw1a the Ioc3 C-terminus is responsible for doing so. In Isw1b the DNA-binding sites in the Ioc4$_{PWWP}$ domain help mediating those contacts.

In the second step, specific recognition takes place. The Ioc3 N-terminus recognizes the histone variant H2A.Z and guides the Isw1a complex to the +1 nucleosome. The aromatic cage of the PWWP domain preferentially binds Set2-mediated H3K36me3 and therefore recruits the Isw1b complex onto gene bodies.

In the third step, upon the addition of ATP, the catalytic subunit Isw1 becomes activated and allows the remodeler complexes to move nucleosomes in their specific modes, according to their associated Ioc subunits.

However, it is unclear whether those three steps happen simultaneously or consecutive. Yet all three steps must be executed to ensure proper remodeler activities and an organized chromatin structure. Particularly, Isw1b recycles methylated histones and prevents the incorporation of acetylated histones. Isw1a prevents increased histone turnover, as well. Further, RNA polymerase II only gets access to the canonical promoter located in the TSS. Thanks to the concerted action of Isw1a and Isw1b, cryptic promoter sites stay hidden and thus the production of cryptic transcripts (ncRNAs) is hindered.

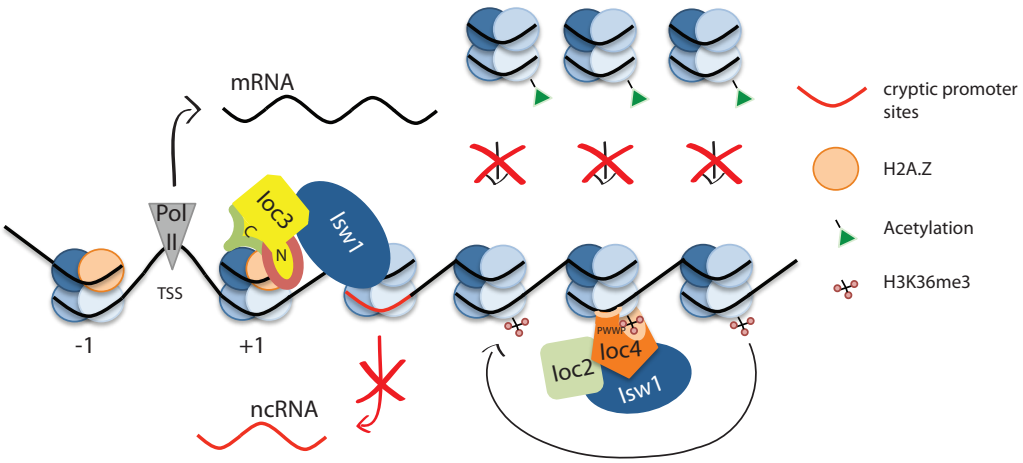

3. Discussion

3.1 Isw1a and Isw1b are similar, yet distinct complexes

The separate Isw1a and Isw1b chromatin remodeler complexes were first described by Vary and colleagues[170]. They recognized Isw1 as a shared subunit for both complexes. The highly regulatory elements AutoN and NegC control ATPase activity in Isw1 and the HSS domain association with chromatin[151,249]. Being the subunit of both complexes, similar functions were anticipated. Isw1a consist of Isw1 and Ioc3, Isw1b consist of Isw1, Ioc4 and Ioc2. The Ioc subunits mainly characterize the functions of the complex. *In vivo*, both reside at different genomic locations. Isw1a is found at promoter sites, supporting a role for transcriptional repression[168]. Isw1b is found on gene bodies, being recruited by H3K36me3 recognition of its PWWP domain during actively transcribed genes[158,202]. The PWWP domain is the only known domain in Ioc4 and Isw1b. Although Ioc2 harbors a PHD-like domain and shares C-terminal homology with the human androgen receptor, its contribution to complex function is unknown. Ioc3 has few annotated domains, however, I could show highly regulatory elements in its termini. Both, Isw1a and Isw1b contribute to a properly organized chromatin structure and suppress cryptic transcription. Isw1b does so by preventing trans histone exchange and recycling old, methylated histones. Newly, acetylated histones can thus not be incorporated. Since acetylation would open up chromatin structure and give access to cryptic promoter-like elements, access to RNA Polymerase II is thus denied[158]. Isw1a is acting on the 5'-ends of genes. By precisely positioning the +1 nucleosome and organizing evenly spaced nucleosome patterns, it aids to establish a properly organized chromatin structure[164,192]. Its recruitment also suppresses initiation of cryptic transcription (preliminary data, unpublished). A detailed mechanism is still elusive. Here, I examined the contribution of the different Ioc subunits Ioc3 and Ioc4 for their respective complex. I could give insights into a novel recruitment mechanism for Isw1a and point out the importance and characteristics of the PWWP domain for Isw1b.

3.1.1 The Ioc3 termini control activity and recruitment of Isw1a to H2A.Z

Concurrently, the role of Ioc3 in Isw1a is not fully understood. We and others have hypothesized that Ioc3 guides Isw1a on its correct position, given the fact that Isw1 is also a subunit in Isw1b complex. In this study, I propose a detailed analysis of the functions of Ioc3 for Isw1a recruitment to nucleosomes.

The localization of Ioc3 and thus Isw1a was subject of several previous studies. Using ChIP-on-chip, our own lab found Ioc3 localization at the ends of genes[158]. Higher resolution MNase ChIP-seq experiments resolved Ioc3 recruitment to the +1 and -1 nucleosome[192]. Comparing its localization with the most common PTMs found at this position, we hypothesized that H3K4me3 or histone acetylation could potentially recruit the complex. Also, the histone variant H2A.Z gets incorporated into nucleosomes flanking the TSS[132]. Those three preferred targets were examined carefully.

The histone mark H3K4me3 is found at promoter sites and co-localizes with Isw1a. Nevertheless, no preferential binding or increased sliding activity could be noticed compared to unmethylated nucleosomes.

Testing a variety of acetylation marks on H3, H4 or in combination did not lead to an effect that could explain preferred Isw1a recruitment. Also a doubly modified nucleosome carrying both H3K4 methylation and acetylation was not preferentially bound *in vitro* by Isw1a. Admittedly, not all combinations of all possible acetylations were tested. The H3 and H4 poly acetylated nucleosomes (H3K4,9,14,18-H4K5,8,12,16ac) did reconstitute badly leaving the interpretation of the assays performed open to debate, but hint towards no preferred recruitment. Nevertheless, all experiments performed suggest that neither H3K4 methylation nor acetylation is likely to be involved in Isw1a recruitment. The competitive assays (cEMSA and cSliding assay) serve as a validation control since the outcome of those sensitive techniques was in agreement with the previously conducted regular EMSAs and sliding assays.

Supporting this finding is the fact that neither Isw1 nor Ioc3 harbor a suitable domain that could explain recognition of lysine methylation (e.g. PWWP domain,

PHD finger) or acetylation (e.g. bromodomain). Santos-Rosa *et al.* saw Isw1 binding to H3K4me3[209]. The co-Immunoprecipitation (co-IP) experiments only shed light on the *in vivo* situation. Purified Isw1 alone did not recognize H3K4me3-containing nucleosomes as a preferred substrate in their experiments, hinting towards an indirect contact mediated through other factors present in the whole cell extract[209].

Seeing as acetylation and H3K4 methylation do not preferentially recruit Isw1a and the lack of a specific domain to do so, I hypothesized that the histone variant H2A.Z can recruit Isw1a. Indeed, H2A.Z containing nucleosomes were preferentially recognized in *in vitro* binding and sliding assays. The more sensitive competitive alternatives enhanced the differences between canonical and H2A.Z-containing nucleosomes. Additionally, the yeast variant Htz1 displays a similar preference in separate experiments to exclude the possibility that human H2A.Z recognition is a mere artifact. An earlier study suggested that Htz1-containing nucleosomes decrease nucleosome sliding ability of Isw1. Indeed, they used a mixture of Isw1a and Isw1b remodeler that in general slide in different directions[166].

In contrast, co-IPs using whole cell extract could not validate H2A.Z preference for *in vivo* settings. Such an interaction between ioc4 and Hzt1 was once observed in mass spectrometry experiments using a *chz1*Δ*nap1*Δ background[115]. It is possible that the interaction between Isw1a and Htz1 is unstable during the Co-IP and therefore cannot be detected. This problem could be circumvented by crosslinking samples *in vivo*. Another explanation is the composition of the buffer. Varying salt concentrations can change protein-protein interactions and stability. Though histone octamers prefer high salt conditions, this can disrupt protein-protein interactions. Thus, finding a balance that suits both needs is somewhat challenging and needs further experiments.

Since the absence of a known domain for methylation or acetylation recognition, I speculated that binding between Htz1 and Isw1a is rather mediated through a broader surface. Crystallizing Ioc3-HSS was a pioneer step in elucidating the roles of Ioc3 and Isw1 separately. Thanks to the high resolution, four hydrogen bonds from each protein stabilizing complex-DNA interactions could be observed[167]. Nevertheless, the HAND-SANT-SLIDE domain is just a short part of Isw1, leaving for instance the orientation of the ATPase unanswered. Taking a closer look at the crystallized amino acids in Ioc3, I discovered N- and C-terminal truncations, a common strategy to aid crystallization by removing flexible, unstructured regions.

Yet, those ends of Ioc3 raised my particular interest, since although the crystal structure provided much information, it failed to answer how Isw1a gets recruited onto chromatin (or now it may bind to Htz1). Inspecting the cut termini of Ioc3 in the crystal structure carefully, acidic and basic stretches could be noticed that may serve as H2A.Z recognition site. Generating separate N- and C-terminal mutants allowed me to understand the functions of the ends of Ioc3 even further. Surprisingly, both mutants displayed different binding outcomes.

Isw1a$_{\Delta C1}$ was the only stable construct among the C-terminal truncations (see section 2.1.2.2). The small 5 kDa truncation displays many positively charged amino acids, which seemingly target Isw1a onto chromatin. Intact Isw1 cannot compensate for the lacking Ioc3 C-terminus, designating it a key role in chromatin targeting. Surprisingly, upon the addition of ATP, Isw1a$_{\Delta C1}$ seems to become "activated" since remodeling is taking place. To capture the remodeler "in action" a sliding assay was conducted, that was not stopped using the usual stop buffer, but immediately loaded on a native-PAGE gel. The resulting gel analysis revealed that some nucleosome fractions are indeed bound by Isw1a$_{\Delta C1}$ hinting towards an Isw1 involvement in chromatin targeting, however at later stages. The cryo-EM structure of Isw1 monomer comes to a similar conclusion, in which Isw1 changes it conformation depending on whether nucleotides are bound or not[187]. Notably, this structure uses a C-terminally truncated Isw1. Keeping in mind the adjacent AutoN region that inhibits Isw1 activity, the truncation could hint towards a longer, unnotated AutoN region. This is likely since my purification of recombinant Isw1, as well as the endogenous purification of yeast Isw1 monomer performed by Vary *et al.* come to the same conclusion that full-length Isw1 monomer is unable to bind DNA or nucleosomes in an ATP-independent manner[170]. Nevertheless a conformational change in Isw1 is likely to favor chromatin association. This enforces the position of Ioc3 in Isw1a. While full-length, wild type Isw1 may be inactive, binding to the Ioc3 subunit may lead to a conformational change bringing Isw1 in a "ready-to-go" state. Upon nucleotide binding its ATPase gets activated in another changing step. This hypothesis is speculative and needs further experiments for validation, however, could explain the sliding activity of the Isw1a$_{\Delta C1}$ construct.

Besides the small C-terminally truncated mutant, the 15 kDa N-terminal truncation mutant Isw1a$_{\Delta N1}$ was the only stable complex among the N-terminal truncation mutants (see section 2.1.2.2). Seeing both, a stretch of basic and acidic amino acids in the N-terminus, I hypothesized that they may be responsible for H2A.Z recognition. Indeed, Isw1a$_{\Delta N1}$ could not distinguish between H2A- and H2A.Z-containing nucleosomes, however, displayed multiple binding events. Competitive EMSAs supported the outcome of the EMSA and suggest that the Ioc3 N-terminus is responsible for H2A.Z recognition. Interestingly, remodeling assays displayed an ambivalent outcome. While Isw1a$_{\Delta N1}$ showed reduced activity for canonical nucleosomes, activity was enhanced for H2A.Z-containing nucleosomes. Since the results for binding and sliding did not match, I hypothesized the existence of a second, H2A.Z binding site within the Isw1a complex. Besides, these outcomes prove the Ioc3 N-terminus as a regulating module for the Isw1a complex.

Seeing the multiple outcomes of the Isw1a$_{\Delta N1}$ construct, one have to bear in mind the size of the truncation. The 15 kDa large N-terminus could in principle harbor more than one binding site. It would be worth examining the N-terminus even further and to generate at least two more, smaller truncation mutants. The above-mentioned acidic amino acids and adjacent basic amino acids could have opposing roles for Ioc3 and Isw1a, however, deleting both may lead to ambivalent *in vitro* results.

Finally, I was interested, whether a deletion of both Ioc3 termini impacts Isw1a. Notably, Isw1a$_{\Delta N1C1}$, unlike Isw1a$_{\Delta C1}$, showed recovered nucleosome-binding ability, bringing up the hypothesis whether both termini may influence each other. Further, H2A.Z recognition was still absent, supporting the notion that the H2A.Z recognition motif lies within the Ioc3 N-terminus. As for sliding activity, the C1-truncation alone had no effect on Isw1a sliding activity. In line with that is the outcome of the Isw1a$_{\Delta N1C1}$ sliding assays, which mimicked remodeling ability of the Isw1a$_{\Delta N1}$ construct. Interestingly, a recent paper discovered that Isw1a displays specificity towards dinucleosomes. This preference of Isw1a derives from the Ioc3-HLB domain[191]. The crystal structure does not give information about the shape of the Ioc3 N-terminus, however, it is located in close proximity to the Ioc3 HLB domain. Is it thus interesting to evaluate whether the Ioc3 N-terminus may affect functions of the HLB domain or impacts dinucleosome specificity per se.

In summary, Isw1a is a novel H2A.Z interactor. Since Isw1b did not display such a preference, Ioc3 must be the subunit responsible for generating substrate specificity. The crystal structure already provides insights into DNA-binding of Ioc3-HSS, yet works with an Ioc3 truncation mutant that I chose to examine even further. I could demonstrate that the C-terminus is crucial for chromatin association, whereas the N-terminus is partially but not exclusively responsible for H2A.Z recognition. It is a further complex regulating element. Besides Isw1, no other remodeler protein is known to harbor self-regulating domains within its own sequence[151]. With my studies I could shed light on the structural functions of Ioc3 that the crystal structure missed to display. Further I elucidated the molecular mechanism of how Isw1a gets intrinsically regulated and recruited to the ends of genes.

3.1.2 The relevance of the Ioc4$_{PWWP}$ domain

Despite the plethora of known PWWP-domain containing proteins, mechanistic functions are still elusive for most of them. In this study, I propose a novel, detailed analysis of the Ioc4$_{PWWP}$ domain, its impact on Ioc4 and finally on Isw1b.

The only known domain in Ioc4 and Isw1b is the PWWP domain, which plays a vital role in Isw1b functions. The PWWP domain does not exist by itself, but is rather embedded in Ioc4, which is one subunit of the Isw1b complex. Like most of the PWWP domains, it can bind to DNA with μM affinity. Compared with published DNA-binding preferences, the Ioc4$_{PWWP}$ domain seems to be ordinary – it does not distinguish between AT-rich or GC-rich sequences. Unlike HDGF, which preferentially recognizes a GC-rich promoter element[226], although this claim is disputed[224]. Ioc4$_{PWWP}$ seems to interact through electrostatic interactions with the sugar-phosphate backbone. Surprisingly, the PWWP domain bound better to ssRNA than to ssDNA, although overall affinity was higher for double stranded nucleic acids. DNA-binding is thought to be mediated through a positively charged surface, which was found in all PWWP crystal structures published so far. In 2020, the Cramer Lab suggested PWWP binding across DNA gyres[239]. Using this structure for a homology model, the Ioc4$_{PWWP}$ domain seems to bind similarly (Li and Bergmann *et al.*,

BioRxiv). To evaluate the impact of DNA-binding, $PWWP_{2KE}$ was generated, agreeing with the homology model in which those two point mutations play a key role in DNA-binding and make the $PWWP_{2KE}$ mutant DNA-binding deficient. Residual DNA-binding was observed in $Ioc4_{2KE}$ and even $Ioc4_{\Delta PWWP}$, hinting towards other, nonspecific binding sites in the protein. Similar observations were made for the PWWP domains in LEDGF[227,250,251].

A second common feature of all PWWP domains is methyl lysine recognition. Despite some exceptions (Pdp1[237], HDGF2 and HDGF[219]) a high-throughput mass spectrometry screen supported the hypothesis that PWWP domains are a H3K36me3 specific substrate[228], which could be confirmed for our $Ioc4_{PWWP}$ domain[158,202] and many others (e.g. BRPF1, BRPF2, HDGF2, WHSC1[218,219]). Maltby *et al.* annotated the three residues critical for forming the aromatic cage necessary for H3K36me3 recognition in the $Ioc4_{PWWP}$ domain, yet leaving a detailed recruitment mechanism still to be elucidated[202].

Here, I could unravel the impact of the $Ioc4_{PWWP}$ domain for Ioc4 and subsequently for the Isw1b complex. Next to wild type Isw1b, I purified $Isw1b_{\Delta PWWP}$ and $Isw1b_{2KE}$. The strongest effects could be observed for $Isw1b_{\Delta PWWP}$, which demonstrated not just impaired sliding activity *in vitro*, but also mislocalized *in vivo*, allowing the rise of cryptic transcription, probably because trans-histone exchange is taking place. $Isw1b_{2KE}$ showed a similar, yet diminished phenotype. Also, full-length LEDGF dramatically reduced chromatin association when the DNA-binding interface was interrupted[227,252]. In the case of PSIP1 this leads to reduced HIV-infectivity in cells[227].

A further feature observed is the long insertion motif that leads to the extraordinary length of the $Ioc4_{PWWP}$ domain. Usually ranging between 100-130 amino acids, $Ioc4_{PWWP}$ counts 178 amino acids. The 83 amino acids long insertion was carefully examined. The insertion motif alone ($PWWP_{INS}$) enables histone H3/H4 tetramer binding, while $PWWP_{\Delta INS}$ does not bind histone octamers at all. The PWWP domain alone has a preference of binding histone H3/H4 tetramers, whereas full-length Ioc4 binds all four histone octamers. This indicates a particular specificity, since the insertion motif is located between β2 and β3 – the secondary structure that harbors

the aromatic cage. It is possible, that the insertion motif attracts particular histone H3/H4 tetramers to bring the H3 tail in close proximity, facilitating H3K36me3 recognition by the adjacent aromatic cage, however, this hypothesis is speculative. Residual acidic patches in $Ioc4_{\Delta INS}$ might enable binding of all histone octamers, pointing towards an auxillary function to stabilize nucleosome attachment. Although allowing histone-binding for PWWP, the insertion motif seems not to affect Ioc4 or Isw1b as an $Ioc4_{\Delta INS}$ or $Isw1b_{\Delta INS}$ mutant in terms of nucleosome attachment, respectively. Nevertheless, the homology model suggests additional binding to DNA from the insertion motif. This may be true to some degree, since $PWWP_{\Delta INS}$ was indeed unable to form a stable protein-DNA complex. This effect was not seen in $Ioc4_{\Delta INS}$, though, which can be explained by the numerous lysines and arginines that provide a binding surface for the DNA backbone. The existence of other, but much shorter insertion motifs was confirmed in other PWWP domains as well (e.g. BRPF1). PWWP domains harboring an insertion motif may fulfill additional tasks, but until now their functions remain elusive.

The general question, whether DNA-binding or histone-binding (particular methyl lysine recognition) predominantly decides about functionally, is still unclear. My DNA- and histone-binding assays suggest a more decisive role for DNA-binding, since a DNA-binding deficient PWWP (the $PWWP_{2KE}$ mutant) could still bind to histones. On a functional level, the DNA-binding impaired $Ioc4_{2KE}$ failed to correctly target Isw1b (as $Isw1b_{2KE}$) onto chromatin. The histone-binding deficient $PWWP_{\Delta INS}$ domain still correctly localizes $Isw1b_{\Delta INS}$ on genes. This may suggest, that DNA-binding is more critical than histone recognition, and to speculate even further, that the first contact is maintained between the protein and DNA and in a second step only, lysine recognition is taking place. A concerted binding event considering nucleosomal DNA and histone tails was proposed already by van Nuland *et al.*[227]. To give reliable information about sequence of events, though, it requires further experiments.

Further, RNA binding was investigated. In fact, Isw1 and Ioc2 were identified to interact with RNA in *in vivo* cross-linking experiments[175]. My *in vitro* studies demonstrate a preference for ssRNA compared to dsRNA, however a stable complex was only achieved with dsRNA. The tested DNA:RNA hybrid showed a similar

affinity to dsDNA. *In vivo* studies were not conducted, leaving only the speculation of a possible relevance of Ioc4 interacting with the elongating RNA transcript.

To summarize, I provide a detailed analysis of the $Ioc4_{PWWP}$ domain. Its *in vitro* functions do not differ extremely from other known PWWP-domain containing proteins, but could be validated. Interestingly, a long insertion motif was identified, that had no phenotypic outcomes in the experiments conducted. Yet the relevance of the PWWP domain becomes clear when looking at *in vivo* data. Without its PWWP domain, Isw1b remodeler complex fails to correctly target to mid to 3'-ends of genes. Despite being a trimeric complex, Isw1 and Ioc2 can only partially rescue the functions of the complex, leading to the generation of noncoding RNAs. Thus, the presence of Set2-mediated H3K36me3 is as important as the presence of a mere domain in Isw1b, giving the PWWP domain a pivotal role in recruiting and regulating a whole complex.

3.1.3 Ioc2 – the forgotten subunit?

The Isw1b complex consists of Isw1, Ioc2 and Ioc4. The Isw1b complex requires binding of both, Ioc2 and Ioc4 subunits to Isw1 to be stable[170]. Ioc2 interacts with the SANT and the SLIDE domain of Isw1, so does Ioc4[168].

While Isw1 and Ioc4 are well studied, very little is known about Ioc2. Up to now it is not known whether Ioc2 acts merely as a scaffold for Isw1 and Ioc4 or has a specific role. During my PhD, I tried to purify recombinant Ioc2. Unfortunately, it proved to be aggregated in nanoDSF measurements (data not shown), thus I could not study the *in vitro* characteristics of Ioc2. In my own sliding experiments I noticed that the $Isw1b_{\Delta PWWP}$ mutant still exhibited residual sliding ability. This must be due to Isw1 and Ioc2, since the functional domain of Ioc4 was deleted. Ioc2 bears a PHD-like domain, that could potentially recruit Isw1b specifically onto chromatin. It is not explored yet, whether Ioc2 contributes to histone recognition and thus sliding activity in Isw1b.

The role of Ioc2 presumably has been underestimated. When talking about Isw1b, many studies neglect Ioc2 completely, while only few take its existence into

account. Vary *et al.* noticed that *ioc2*Δ in an additional *isw2*Δ*chd1*Δ background leads to a temperature sensitive mutant[170]. However, *ioc4*Δ in the same background showed no effect. This suggests that Ioc2 has a role independent from Isw1b functions. Besides, they noticed that purified Ioc2-Myc elutes in two different peaks, where the authors hypothesize that one peak could represent Ioc2 in a yet unidentified complex. Similar observations were observed by Lafon *et al.*, pointing into the direction that Ioc2 must have additional roles independent of Isw1b[196]. Notably, *ioc2*Δ in a *gcn5*Δ*sas3*Δ background exacerbated loss of viability, while *ioc4*Δ had not such an effect. Contrarily, *ioc3*Δ could even rescue the phenotype. The authors conclude that only Isw1a and not Isw1b appears to antagonize the activities of those acetyltransferases. Unfortunately no comprehensive working model could be established from the few information.

3.2 Future directions

During my PhD I was able to elucidate the molecular mechanisms of Isw1a and Isw1b recruitment *in vitro*. Nevertheless, there are many factors that were not taken into account yet.

For instance, as discussed in the previous chapter, the role of Ioc2 per se and in Isw1b remains largely unresolved. It would be of advantage to invest into a working protein purification to study the *in vitro* functions of recombinant Ioc2 more closely. Besides, *in vivo* functions also need a closer look. It would be interesting to see whether Isw1b$_{\Delta PHD}$ localizes differently in a genome wide analysis when compared to wild type Isw1b or whether the missing PHD-like domain impairs sliding activity.

Remarkably, I marked the H2A.Z binding site in Ioc3, which is responsible in targeting Isw1a to H2A.Z-containing nucleosomes *in vitro*. Nevertheless, the truncated Ioc3 N-terminus is large. Inspecting its amino acid sequence more closely it reveals an acidic patch and many basic residues. Since specific recognition of H2A.Z requires a basic patch, I hypothesize that the basic residues embedded in the N-terminus are responsible for this effect. More and smaller truncations mutants of Ioc3 could answer this question. Further, it would be interesting to investigate whether the *in vitro* findings correlate with the *in vivo* situation by analyzing a genome-wide distribution of the two mutants Isw1a$_{\Delta N1}$ and Isw1a$_{\Delta C1}$.

Generally, the exact recruitment mechanism is still awaits confirmation *in vivo.* Also, it may require interactions with other proteins on top of H2A.Z. Together with the core facility for Protein Analytics I performed mass spectrometry (data not shown) and found several potential candidates to interact with Isw1a. Among them, the most interesting is Reb1. It was already shown that only with the addition of a barrier factor like Reb1 or Abf1, Isw1a is able to generate correctly spaced nucleosomal arrays *in vitro*[164]. A direct interaction between the remodeler and the barrier factors could not be validated so far.

The *in vivo* and *in vitro* functions of Ioc4 have widely studied by myself and others. What is still to be elucidated is the concrete function of the insertion motif inside the PWWP domain. I found that PWWP$_{\Delta INS}$ abrogated interaction with histones, yet the effect does not get carried through to Isw1b levels. Isw1b$_{\Delta INS}$ had

presumably no problem in correct localization genome-wide. The acidic surface noticed in the insertion motif is responsible for histone-binding, however, I hypothesize that it may as well act as a recruitment platform for other proteins. Mass spectrometry experiments and yeast-two-hybrid screens could shed light on that. Chances are, that it is just an evolutionary artifact that was not yet abrogated, nevertheless there are many insertion-motif-containing PWWP domains, which speaks for an outstanding role.

Next to the acidic stretch inside the insertion motif, Ioc4 reveals two more acidic stretches. Similar arrangements can be observed in other chromatin remodelers, too, for example Chd1 or the Ioc3 C-terminus. I hypothesize that these acidic stretches share a common feature that allows them to work as chromatin remodeler. Mutating those amino acids in neutral alanines or negatively charged glutamic acids could answer this question when conducting *in vitro* and *in vivo* assays.

Obtaining the cryoEM structure of Isw1b would be outstanding for the future understanding of Isw1b functions. It could answer the question, for instance, how Ioc4 and Ioc2 connect to the SANT and SLIDE domain of Isw1. My preliminary data suggests that the Ioc4 C-terminus binds to the complex in a pilot experiment (data not shown). Further I hypothesize that the Ioc4 C-terminus connects to the SLIDE domain of Isw1 in particular. My initial idea of truncating those amino acids is based on a sequence similarity with the HSSB domain in Ioc3. Nevertheless, performing cryoEM on Isw1b is somewhat challenging and requires sophisticated equipment and understanding.

To finally summarize, just to study the field of Isw1 chromatin remodelers requires a plethora of experiments. Despite many efforts that had already been undertaken, the full and detailed mechanism is still to be elucidated. My proposal for future experiments restricts to experiments immediately connected to my work. It will probably take decades and dozens of PhD students to gain the full understandings.

4. Materials and Methods

4.1 Materials

4.1.1 Technical devices

Description	Supplier
-20 °C Freezer	Liebherr
-80 °C Freezer	Thermo Scientific
4 °C Fridge	Liebherr
37 °C Incubator (*E. coli*)	Binder
30 °C Incubator (*S. cerevisiae*)	Memmert
Äkta pure	GE Healthcare
Autoclave	Systec
Bead beater	Precellys
Cell Density Meter Ultraspec 10	Amersham Biosciences
Centrifuges	Beckman, Eppendorf
ChemiDoc System	BioRad
Freezer mill	SPEX SamplePrep
Incubation shaker	New Brunswick Scientific
Licor	Odyssey
Microwave	Panasonic
Magnetic stirrer	Heidolph
MilliQ-Water system	Millipore
Nanodrop 2000c	Thermo Scientific
PCR cycler	Biorad, Eppendorf
pH-meter	Mettler Toledo
Pipetboy Accu-Jet® pro	Brand
Pipettes	Eppendorf
Rotating Wheel	New Brunswick Scientific
Scales	Epson
Scanner	Epson
Shaker	New Brunswick Scientific
Sonifier	Heinemann
Tube Roller	Star lab
Typhoon FLA9500	GE Healthcare
Thermomixer	Eppendorf
UV Spectrophotometer	Thermo Scientific

4.1.2 Consumables

Description	Supplier
1.5 ml and 2 ml Reaction tubes	Greiner, Sarstedt
0.2 ml Thin-walled Tube with Flat Cap	peqlab

Amicon 5 ml, 15 ml	Millipore
Amylose-Sepharose beads	BioLabs
Calmodulin-Sepharose beads 4B	GE Healthcare
Combi Tips Plus	Eppendorf
Filter paper	Whatman
Filter tips	Biozym, Gilson
Glass Pipettes 5 ml, 10 ml, 25 ml	Hirschmann
Glassware	Schott
HiTrap Heparin column 1 ml	GE Healthcare
IgG-Sepharose beads	GE Healthcare
Membrane filter 0.2 µm	Millipore
Mini Protean TGX Stain-free Gels	Biorad
N_2, liquid	Cryotherm
Ni-NTA beads	Qiagen
Parafilm M	Parafilm®
PCR reaction tubes	Greiner
pH Indicator stripes	Merck
Pipette tips	Biozym, Greiner, Sarstedt
Protein Gel Cassettes	Biorad
Protein SDS Gels (Precast)	Biorad
Protan Nitrocellulose Transfer Membran	Whatman
ResourceQ Anion Exchange column	GE Healthcare
Sterican needles	Braun
Superdex200 Increase 10/30GL	GE Healthcare
Syringes 1 ml, 3 ml, 5 ml, 10 ml	Braun
Water, RNAse free	Ambion
Water	VWR
Zellutrans Dialysierschlauch 12-14 kDa	Roth

4.1.3 Chemicals

Description	**Supplier**
Acetic Acid	Sigma
Acrylamide 37.5:1, 29:1	Serva
Arginine	Roth, Sigma
Agar (LB)	Serva
Agarose	Sigma
Ammonium-Bicarbonate	Sigma
Ampicillin	Serva
Ammonium persulfate	AppliChem
ATP	Roche
Bacto Agar	BD
Beta-Mercaptoethanol	Sigma
Benzamidine	Sigma
Benzonase	Sigma
Bovine serum albumin	Sigma
Calcium Chloride	Merck, Stricker
Complete Protease Inhibitor Cocktail tablets	Roche
Coomassie Brilliant Blue	Sigma
Disodium-Hydrogen-Phosphate	Sigma
DMSO	Sigma
DNAse I	Roche
dNTP Mix	NEB

DTT	Roth
EDTA	Sigma
EGTA	Sigma
Ethanol. absolute	Kost Alkohole
Ethidiumbromide Solution	Sigma, Thermo
Formaldehyde, 37 % (v/v)	Roth
Glacial Acetic Acid	Applichem
Glucose	Roth, Merck
Glutamic Acid	Serva
Glycerol	VWR
Glycine	Sigma
Heparin	Serva
HEPES	Serva
IPTG	Calbiochem
Imidazole	Merck
Leupeptin	Roth
Lysozyme	Serva
Magnesium Acetate	Sigma
Magnesium Chloride	VWR
Maltose	Sigma
MES	Sigma
Methanol	Normapur
Milkpowder	Serva
Monopotassium Phosphate	Sigma
MOPS	Sigma
NP-40 (Ipegal)	Sigma
Orange G	Eurobio
Pepstatin A	Fluka
PIPES	Sigma
PMSF	Sigma
Ponceau S	Serva
Potassium Chloride	Merck
SDS	Serva
Silver Nitrate	Sigma
Sodium Acetate	Merck
Sodium Azide	Fluka
Sodium Chloride	Serva
Sodium Carbonate	Merck
Sodium Hydroxide	Sigma
Sodium Phosphate	Sigma
Sodium Thiosulfate Pentahydrate	Merck
TEMED	Sigma
Tricine	Sigma
Tris (Trizma ® Base)	Sigma
Triton-X-100	Sigma
Tween 20	Sigma

4.1.4 Kits, enzymes and markers

Description	**Supplier**
100 bp DNA marker	NEB
1 kb DNA marker	NEB
3C-Protease HRV	Thermo Scientific

Dpn1	NEB
Mini-, Midiprep kit	Qiagen
PCR purification kit	Metabion
Page Ruler plus Prestained Protein Marker	Thermo Scientific
Phusion DNA Polymerase	Biolabs
Polymerase, hot start	Biolabs
TEV protease	Selfmade

4.1.5 Antibodies

Table 4.1 Antibodies used in this study

Name	**Supplier**	**Host**	**Application**	**Dilution**
α-Flag	Sigma	mouse	Western blot	1:5000
α-TAP	Sigma	mouse	Western blot	1:1660
α-Htz1	Active Motif	rabbit	Western blot	1:3000
α-H3	Abcam	mouse	Western blot	1:3000
α-mouse HRP	VWR	goat	Western blot	1:10000
α-rabbit HRP	VWR	goat	Western blot	1:10000

4.1.6 Plasmids

Table 4.2 Plasmids used in this study

Name	**Insert**	**Antibiotic Resistance**	**Organism**	**Parent plasmid**
pRSF_IOC4[1-178]	6xHis-PWWP	Kan	*S. cerevisiae*	pRSF-Duet1
pRSF_IOC4$_{1\text{-}178}$ K149E K150E	6xHis-PWWP 2KE	Kan	*S. cerevisiae*	pRSF-Duet1
pGEX_IOC4[1-178]Δ43-105	GST-PWWPΔINS	Amp	*S. cerevisiae*	pGEX6P-1
pCoofy4-HIS-MBP-3C + Ioc4 FL	6xHis-MBP-Ioc4	Kan	*S. cerevisiae*	pCoofy4
pCoofy4-HIS-MBP-3C + Ioc4 dINS	6xHis-MBP-Ioc4ΔINS	Kan	*S. cerevisiae*	pCoofy4
pCoofy4-HIS-MBP-3C + Ioc4 K149E K150E	6xHis-MBP-Ioc4 2KE	Kan	*S. cerevisiae*	pCoofy4
pCoofy4-HIS-MBP-3C + Ioc4 dPWWP	6xHis-MBP-Ioc4ΔPWWP	Kan	*S. cerevisiae*	pCoofy4

pCoofy4-His-MBP-3C + Isw1FL clone 1	6xHis-MBP-Isw1	Kan	*S. cerevisiae*	pCoofy4
pCoofy35_MBP-Ioc3FL-His13 clone 3	MBP-Ioc3-13xHis	Kan	*S. cerevisiae*	pCoofy35

4.1.7 Oligonucleotides and Primers

Table 4.3 Oligonucleotides and Primers used in this study

Name	**Description**	**Sequence 5'-3'**
ΔIoc4_seqF	Forward primer of genomic deletion of Ioc4	AAAATATCGTGGCTCCCCG
ΔIoc4_seqR	Reverse primer of genomic deletion of Ioc4	TTGGACTATCAAAGACTGCG
IOC3_3xFlag-F	Genomic 3x Flag tag - pBS-3xFlag [KanMX]	TTCTTCTTTTGATGATGGTAGAGTTAAAAGGCAGCGCACTAGGGAACAAAAGCTGGAG
IOC3_3xFlag-R	Genomic 3x Flag tag - pBS-3xFlag [KanMX]	AGGAGTTTCACAATCTTCACGTTCGTTGAAAGCTAGTTGTCTATAGGGCGAATTGGGT
mid 601-F (Cy5)	601 sequence for mid-positioned Nucl	GGGTCTAGAGGCAAGGTCGCTGTTCAATA
IOC4-TAPa	Genomic C-term TAP-tag - pBS1539	TAGTGAAGACGTAAAGGAAGAAGAAAGCAAAGTAGGAGCATCCATGGAAAAGAGAAG
IOC4-TAPb	Genomic C-term TAP-tag - pBS1539	TTGTTCAAAAGCAGAGTACATCAACTGCAATAGCAACAGGTACGACTCACTATAGGG
IOC4b-rev	IOC4 PWWP; NotI & Stop	TTTGCGGCCGCTCAAGCCTC TGA TTC CAT GTC TGC
EMSA_For30bp-Cy5	Cy5 labeled for DNA EMSA	GGC AAG GTC GCT GTT CAA TAC ATG CAC AGG
EMSA_Rev_30bp	Reverse Primer for DNA EMSA	CCTGTGCATGTATTGAACAGCGAC CTTGCC
IOC4_Δpwwp-for	Ioc4Δpwwp ; amino acid 179 for genomic deletion	GTTAACTACATTTTTCAGAACGGCGTGTCATTCTCCGATAATGCCAGATGAAGAGGAATATGTAGAGG
EMSA_For_RNA_AT rich Cy5	Cy5 labeled for DNA EMSA (AT rich)	GGC AAG GUC GCU GUU CAA UAC AUG CAC AGG
EMSA_Rev_RNA_AT rich	Reverse Primer for RNA EMSA (AT rich)	CCU GUG CAU GUA UUG AAC AGC GAC CUU GCC
MBP_seq_F	Forward seq primer MBP	CTATGGAAAACGCCCAG

	(pCoofy4)	
pCoofy4_Ioc4FL_F	Forw PCR primer cloning Ioc4FL (pCoofy4)	AAGTTCTGTTCCAGGGGCCCA TGTCTGAAGCGATATTCC
pCoofy4_Ioc4FL_R	Rev PCR primer cloning Ioc4FL (pCoofy4)	AGAACATCAGGTTAATGGCGTCA TGCTCCTACTTTGCTTTC
pCoofy4_ΔPWWP_F	For PCR primer cloning ΔPWWP (pCoofy4)	AAGTTCTGTTCCAGGGGCCCCCA GATGAAGAGGAATATGTAG
pCoofy4_Ioc3_F	For PCR primer cloning Ioc3FL (pCoofy4)	AAGTTCTGTTCCAGGGGCCCATGGATTCTCCAT CCAATTC
pCoofy4_Ioc3_R	Rev PCR primer cloning Ioc3FL (pCoofy4)	AGAACATCAGGTTAATGGCGCTAAGTGCGCTGC CTTTTAAC
pCoofy4_Ioc3_seq1F	Forw seq primer for Ioc3 No.1	TTGATGGTAAAAGTGCC
pCoofy4_Ioc3_seq2F	Forww seq primer for Ioc3 No.2	ATGATGGACAATCGATGAG
pCoofy4_Ioc3_seq3F	Forw seq primer for Ioc3 No.3	CTTTTGTTCTCACTGTACG
pCoofy4_Isw1_F	For PCR primer cloning Isw1FL (pCoofy4)	AAGTTCTGTTCCAGGGGCCCATGGCCTATATGT TAGCTATTG
pCoofy4_Isw1_R	Rev PCR primer cloning Isw1FL (pCoofy4)	AGAACATCAGGTTAATGGCGTTAATGAGTGGTT TCGTTTTC
pCoofy4_Isw1_seq1F	For seq primer for Isw1	ATAAATAGATGGACGCCAG
pCoofy4_Isw1_seq2F	For seq primer for Isw1	TGTCGTTGTCTTGTATG
pCoofy4_Isw1_seq3F	For seq primer for Isw1	AAACACTAGAGGAAGTTCG
pCoofy4_Isw1_seq4F	For seq primer for Isw1	ATTGTCGGTTAACAACTCG
IOC4-TAPa_ΔC_F	TAP-tagging fwd for Ioc4	TAGGATATTATTTAACTTAAGAAAAAGGGAACT GAACAAATCCATGGAAAAGAGAAG
IOC3-TAPa	Fwd primer TAP-tag for Ioc3	TTCTTCTTTTGATGATGGTAGAGTTAAAAGGCA GCGCACTTCCATGGAAAAGAGAAG
IOC3-TAPb	Rev primer TAP-tag for Ioc3	AGGAGTTTCACAATCTTCACGTTCGTTGAAAGC TAGTTGTTACGACTCACTATAGGG
EMSA_Forw_RNA_G Crich	25 bp Forward primer for EMSA annealing GC rich	CCC GGU GCC GAG GCC GCU CAA UUG G
EMSA_Rev_RNA_G Crich	25 bp Forward primer for EMSA annealing GC rich	CCA AUU GAG CGG CCU CGG CAC CGG G
Ioc3_DNAbind_F_LB	Forward primer for Ioc3 binding, Cy5 labeled at 3' end	CTAGGCTTATATACGGGTTCATGCGC
Ioc3_DNAbind_R_LB	Reverse primer for Ioc3	GCGCATGAACCCGTATATAAGCCTAG

	binding	
Ioc3_ΔN_F _phospho5'	Fwd primer cloning Ioc3ΔN (starting at 5' end of HSSB loop)	CGAGAATGGCGTCAACAAC
Ioc3_ΔN_R _phospho5'	Rev primer cloning Ioc3ΔN (starting at HRV 3C site)	GGGCCCCTGGAACAGAAC
Ioc3_ΔC_F _phospho5'	Fwd primer cloning Ioc3ΔC (starting at TEV cleavage site)	TTGATTGAGAATTTATACTTCCAAG
Ioc3_ΔC_R _phospho5'	Rev primer cloning Ioc3ΔC (starting at 3' end of HSSB loop)	TGGGAGTGGTTCATTAGC
Ioc3_ΔN_pYG_R_phospho5'	Rev primer cloning Ioc3ΔN in pYG038 (including start codon)	CATTTTGTAGCCTGCTTTTTTGTACA
Ioc3_Δ1-137_pYG_F_phospho 5'	Fwd primer cloning Ioc3ΔN in pYG038	GTAGAACCCGCTTTGATCCC
Ioc3_Δ138-312_pYG_R_phospho 5'	Rev primer cloning Ioc3Δ138-312 in pYG038	TTGTTCATGGGCTGGTTTAG
Ioc3_ΔC_pYG_F_phospho5'	Fwd primer cloning Ioc3ΔC in pYG038	AACCCAGCTTTCTTGTACA
Ioc3_Δ365-746_pYG_F_phospho 5'	Fwd primer cloning Ioc3Δ365-746 in pYG038	TATAATACGGAATATGATAGCGAGG
Ioc3_Δ747-787_pYG_R_phospho 5'	Rev primer cloning Ioc3Δ747-787 in pYG038	GTTTACAGTCTGTCGCTG
pBS1539_bb_fwd_1	Fwd primer for Gibson Assembly Ioc3 truncations	AAAAGGCAGCGCACTTCCATGGAAAAGAGAAGATGG
pBS1539_bb_rev_1	Rev primer for Gibson Assembly Ioc3 truncations (backbone)	ACGCCATTCTCGCATTCCTCCAGCTTTTGTTCC
Ioc3ΔN_fwd	Fwd primer for Gibson Assembly Ioc3 truncations	ACAAAAGCTGGAGGAATGCGAGAATGGCGTCAAC
Ioc3ΔN_rev	Rev primer for Gibson Assembly Ioc3 truncations	TCTCTTTTCCATGGAAGTGCGCTGCCTTTTAAC

pBS1539_bb_rev_2	Rev primer for Gibson Assembly Ioc3 truncations	AGCGGGTTCTACCATTCCTCCAGCTTTTGTTCC
Ioc3Δ1-137_fwd	Fwd primer for Gibson Assembly Ioc3 truncations	ACAAAAGCTGGAGGAATGGTAGAACCCGCTTTG
pBS1539_bb_rev_3	Rev primer for Gibson Assembly Ioc3 truncations in pBS1539 (backbone)	GGATGGAGAATCCATTCCTCCAGCTTTTGTTCC
Ioc3Δ138-312_fwd	Fwd primer for Gibson Assembly Ioc3 truncations	ACAAAAGCTGGAGGAATGGATTCTCCATCCAATTCTATC
pBS1539_bb_fwd_2	Fwd primer for Gibson Assembly Ioc3 truncations in pBS1539	AATGAACCACTCCCATCCATGGAAAAGAGAAGATGG
Ioc3Δ365-787_rev	Rev primer for Gibson Assembly Ioc3 truncations	TCTCTTTTCCATGGATGGGAGTGGTTCATTAGC
pBS1539_bb_fwd_3	Fwd primer for Gibson Assembly Ioc3 truncations in pBS1539	CGACAGACTGTAAACTCCATGGAAAAGAGAAGATGG
Ioc3Δ747-787_rev	Rev primer for Gibson Assembly Ioc3 truncations	TCTCTTTTCCATGGAGTTTACAGTCTGTCGCTGTATC
Ioc3ΔN-TAPa	Fwd primer for yeast transformation	ACCAAGTACTTCAAGCAAAGTTTGCAATCCCCTATTGTTTATGCGAGAATGGCGTCAAC
Ioc3Δ1-137-TAPa	Fwd primer for yeast transformation	ACCAAGTACTTCAAGCAAAGTTTGCAATCCCCTATTGTTTATGGTAGAACCCGCTTTG
Ioc3Δ138-312-TAPa	Fwd primer for yeast transformation	ACCAAGTACTTCAAGCAAAGTTTGCAATCCCCTATTGTTTATGGATTCTCCATCC
Ioc3ΔN-TAPa_2	Fwd primer for yeast transformation - 60 bp overhangs	GGCCAACAAAACTATCACTTACCAAGTACTTCAAGCAAAGTTTGCAATCCCCTATTGTTTATGCGAGAATGGCGTCAAC
IOC3-TAPb_2	Rev primer for yeast transformation - 60 bp overhangs	TAATCGAAATGCAGCCTGTAAGGAGTTTCACAATCTTCACGTTCGTTGAAAGCTAGTTGTTACGACTCACTATAGGG
Ioc3_Δ1-137_pBS_R_phospho5	Rev primer cloning Ioc3Δ1-137 in pBS1539	CATTCCTCCAGCTTTTGTTC
Ioc3ΔC1-TAP_F_phospho5'	Fwd primer cloning Ioc3ΔC1 in pBS1539	TCCATGGAAAAGAGAAGA

4.1.8 Bacterial strains and yeast cell lines

4.1.8.1 *E. coli* strains

Table 4.4 *E. coli* strains used in this study

Strain	Genotype	Selection marker
BL21 (DE3) RIL Aachen	E. coli B F^- ompT hsdS(r_B^- m_B^-) dcm^+ Tet^r gal λ(DE3) endA Hte [argU ileY leuW Cam^r]	Cam
BL21 (DE3)	E. coli B F^- ompT $hsdS_B$(r_B^- m_B^-) gal dcm^+ (DE3)	-
DH5α	Fφ80*lac*ZΔM15Δ(*lac*ZYA*arg*F)U169 *rec*A1 *end*A1 *hsd*R17(r_K^-, m_K^+) *pho*A *sup*E44 λ^- *thi*-1 *gyr*A96*rel*A1	-

4.1.8.2 Yeast strains

Table 4.5 Yeast strains used in this study

Strain	Parental strain	*Genotype*	Made by
BY4741	-	*MATa his3Δ1 leu2Δ0 met15Δ0 ura3Δ0*	Open Biosystems
YLS019	BY4741	*MATa his3Δ1 leu2Δ0 met15Δ0 ura3Δ0 Δhtz1::HIS*	Lisa Schuster
YMS034	BY4741	*MATa his3Δ1 leu2Δ0 met15Δ0 ura3Δ0 chd1Δ::KanMX*	Open Biosystems
YMS060	S228C	*MATa his3Δ1 leu2Δ0 met15Δ0 ura3Δ0 ioc3Δ:: IOC3-TAP-HIS3*	Open Biosystems
YMS061	S288C	*MATa his3Δ1 leu2Δ0 met15Δ0 ura3Δ0 ioc4Δ:: IOC4-TAP-HIS3*	Open Biosystems
YMS099	BY4741	*MATa his3Δ1 leu2Δ0 met15Δ0 ura3Δ0 ioc3Δ::IOC3-3xFlag-KanMX*	Michaela Smolle
YMS205	YMS034	*MATa his3Δ1 leu2Δ0 met15Δ0 ura3Δ0 chd1Δ::KanMX ioc4Δ::HIS3*	Michaela Smolle
YMS254	BY4741	*MATa his3Δ1 leu2Δ0 met15Δ0 ura3Δ0 ioc4Δ::IOC4-3xFLAG-HIS3*	Michaela Smolle
YMS255	BY4741	*MATa his3Δ1 leu2Δ0*	Michaela Smolle

		met15Δ0 ura3Δ0 ioc4Δ::IOC4Δ43-105-3xFLAG-HIS3	
YMS263	YMS255	*MATa his3Δ1 leu2Δ0 met15Δ0 ura3Δ0 ioc4Δ::IOC4Δ43-105-3xFLAG-HIS3 chd1Δ::HYG*	Michaela Smolle
YMS264	BY4741	*MATa his3Δ1 leu2Δ0 met15Δ0 ura3Δ0 ioc4::IOC4Δ1-178-3xFLAG-HIS3*	Michaela Smolle
YMS265	BY4741	*MATa his3Δ1 leu2Δ0 met15Δ0 ura3Δ0 ioc4::IOC4K149E K150E-3xFLAG-HIS3*	Michaela Smolle
YMS266	YMS034	*MATa his3Δ1 leu2Δ0 met15Δ0 ura3Δ0 chd1Δ::KanMX ioc4Δ::IOC4Δ1-178-3xFLAG-HIS3*	Michaela Smolle
YMS267	YMS265	*MATa his3Δ1 leu2Δ0 met15Δ0 ura3Δ0 chd1Δ::KanMX ioc4Δ::IOC4 K149E K150E-3xFLAG-HIS3*	Michaela Smolle
YMS333	YMS255	*MATa his3Δ1 leu2Δ0 met15Δ0 ura3Δ0 3xFLAGΔ::IOC4Δ43-105-TAP-URA3*	Julia Schluckebier
YMS334	YMS264	*MATa his3Δ1 leu2Δ0 met15Δ0 ura3Δ0 3xFLAGΔ::IOC4Δ1-178-TAP-URA3*	Julia Schluckebier
YMS335	YMS265	*MATa his3Δ1 leu2Δ0 met15Δ0 ura3Δ0 3xFLAGΔ::IOC4 K149E K150E-TAP-URA3*	Julia Schluckebier
YMS348	BY4741	*MATa his3Δ1 leu2Δ0 met15Δ0 ura3Δ0 ioc3Δ::IOC3Δ365-787_(ΔC)-TAP-URA3*	Julia Schluckebier
YMS349	BY4741	*MATa his3Δ1 leu2Δ0 met15Δ0 ura3Δ0 ioc3Δ::IOC3Δ365-746-TAP-URA3*	Julia Schluckebier
YMS350	BY4741	*MATa his3Δ1 leu2Δ0 met15Δ0 ura3Δ0 ioc3Δ::IOC3Δ1-137-TAP-URA3*	Julia Schluckebier
YMS351	BY4741	*MATa his3Δ1 leu2Δ0 met15Δ0 ura3Δ0 ioc3Δ:: IOC3Δ747-787-TAP-URA3*	Julia Schluckebier
YMS352	BY4741	*MATa his3Δ1 leu2Δ0 met15Δ0 ura3Δ0*	Julia Schluckebier

		ioc3Δ::IOC3Δ138-312-TAP-URA3	
YMS353	BY4741	*MATa his3Δ1 leu2Δ0 met15Δ0 ura3Δ0 Δioc3:: IOC3Δ1-312-TAP-URA3*	Julia Schluckebier
YMS355	YMS038	*MATa his3Δ1 leu2Δ0 met15Δ0 ura3Δ0 Δioc3::IOC3Δ1-137(ΔN1)_747-787(ΔC1)-TAP-URA3*	Julia Schluckebier

4.1.9 Software

Application	**Software**
Image analysis	Image Quant TL 5.0
Image processing	Adobe Photoshop Adobe Illustrator
Graphing and Statistics	Graphpad Prism 8.0
Sequence alignment	Clustal Omega, Protein Blast (web browser based)
Computation of physical and chemical parameters for a given protein	ProtParam. Expasy (web browser based)

4.1.10 Buffers and solutions

Ingredients in *italics* were freshly added before use.

Name	**Ingredients**
Ampicillin stock solution (1000x)	10 mg/ ml Ampicillin
Blocking Buffer	1x TBS 5 % (w/v) Milk powder
Bodengel	25 % (v/v) Acrylamide (37.5:1) 35 % (v/v) Tris pH 8.8 40 % Water

	APS TEMED
Calmodulin Binding Buffer (CBB)	10 mM Tris pH 8.0 10 % (v/v) Glycerol 150 mM KCl 1 mM Magnesium Acetate 1 mM Imidazole 2 mM CaCl2 0.1 % (v/v) NP-40 1 mM DTT
Calmodulin Elution Buffer (CEB)	10 mM Tris pH 8.0 10 % (v/v) Glycerol 150 mM KCl 1 mM Magnesium Acetate 1 mM Imidazole 10 mM EGTA pH 8.0 0.1 % (v/v) NP-40 0.5 mM DTT *1 mM PMSF*
Coomassie Staining solution	10 % (v/v) Acetic acid 40 % (v/v) Ethanol 2 g/l Coomassie Brilliant Blue R-250 50 % Water
Coomassie Destaining solution	40 % (v/v) Methanol 10 % (v/v) Acetic Acid 50 % Water
Dialysis Buffer 1	20 mM PO_4^{3-} pH 8.0 250 mM NaCl 50 mM Arg/Glu 1 mM DTT
Dialysis Buffer 2	20 mM PO_4^{3-} pH 8.0 250 mM NaCl 1 mM DTT

Elution Buffer 1	50 mM Tris pH 7.5 500 mM NaCl 1,7g/50 ml Imidazole 50 mM Arg/Glu 1 mM DTT
Elution Buffer 2	50 mM Tris pH 7.5 500 mM NaCl 1.7 g/50 ml Imidazole 1 mM DTT
EMSA Buffer D	50 mM Tris pH 7.5 100 mM NaCl 20 % (v/v) Glycerol 1 mM DTT
GST Purification Buffer A	10 mM Tris pH 7.5 20 mM PO_4^{3-} pH 6.8 2M NaCl 0.01 % (v/v) NP-40 1 mM DTT *1 µg/ ml Benzamidin* *1 µg/ ml Pepstatin A* *2 µg/ ml Leupeptin* *1 mM PMSF*
GST Purification Buffer B	10 mM Tris pH 7.5 20 mM PO_4^{3-} pH 6.8 1M NaCl 0.01 % (v/v) NP-40
GST Purification Buffer C	10 mM Tris pH 7.5 20 mM PO_4^{3-} pH 6.8 100 mM NaCl 0.01 % (v/v) NP-40
Huang IP Buffer	50 mM Hepes pH 7.4 150 mM NaCl 10 % (v/v) Glycerol

	0.5 % (v/v) NP-40 1 mM EDTA 100 mM PMSF
Huang IP Wash Buffer	50 mM Hepes pH 7.4 150 mM NaCl 1 mM EDTA
Kanamycin stock solution (1000x)	10 mg/ ml Kanamycin
Lysis Buffer	50 mM Tris pH 7.5 500 mM NaCl 20 mM Imidazole 1 mM DTT *1 µg/ ml Benzamidin* *1 µg/ ml Pepstatin A* *2 µg/ ml Leupeptin* *1 mM PMSF*
Maltose Elution buffer	10 mM Tris pH 7.5 20 mM PO_4^{3-} pH 6.8 100 mM NaCl 0.01 % (v/v) NP-40 25 mM Maltose
Native PAGE	5 % or 7 % (v/v) Acrylamide (37.5:1) 0.5x TBE 0.375 % TEMED (v/v) 0.075 % APS (v/v)
Nucleosome Sliding Assay Buffer A	50 mM Tris pH 8.0 10 mM MgCl2 1 mM DTT
PBS	140 mM NaCl 2.7 mM KCl 10 mM Na_2HPO_4 1.8 mM KH_2PO_4
Pull Down Buffer PD2A	10 mM Tris pH 7.5 20 mM PO_4^{3-} pH 6.8

	250 mM NaCl 0.1 % (v/v) NP-40 1 mM DTT
Pull Down Buffer PD3	20 mM PO_4^{3-} pH 8.0 250 mM NaCl 25 mM Imidazole 10 % (v/v) Glycerol 1 mM DTT
Running Buffer	0.4x TBE 2 % (v/v) Glycerol
Stop Buffer	700 ng competitor plasmid DNA 1.5 M KCl
SDS PAGE Resolving Buffer	1.5 M Tris pH 8.8 0.4 % (v/v) SDS
SDS-PAGE Stacking Buffer	0.5 M Tris pH 6.8 0.4 % (v/v) SDS
TAP Extraction buffer	40 mM HEPES-KOH pH 7.5 10 % (v/v) Glycerol 350 mM NaCl 0.1 % (v/v) Tween 20 1 µg/ ml Pepstatin A 2 µg/ ml Leupeptin 1 mM PMSF
TBE	45 mM Tris pH 7.6 45 mM Boric acid 1 mM EDTA
TBS, 10x	500 mM Tris pH 7.5 1.5M NaCl
TBST	50 mM Tris pH 7.5 150 mM NaCl 0.1 % (v/v) Tween 20
TE	10 mM Tris-HCl pH 8.0 0.1 mM EDTA

TEV Cleavage buffer	10 mM Tris pH 8.0 10 % (v/v) Glycerol 150 mM NaCl 0.1 % (v/v) NP-40 0.5 mM EDTA 1 mM DTT
Transfer Buffer	25 mM Tris pH 8.3 192 mM Glycine 20 % (v/v) Methanol

4.2 Methods

4.2.1 Molecular Biology Methods

4.2.1.1 Agarose gel electrophoresis

DNA fragments of PCR based DNA preparations were analyzed on agarose gels containing ethidium bromide for DNA visualisation. Gels were run in 1x TAE buffer for 15 min at 300 V.

4.2.1.2 Oligo annealing

Cy5-labeled, single-stranded, forward oligos were annealed with its unlabeled, complementary reverse, single-stranded oligo. The 26 bp RNA stock solutions were diluted to 50 µM and added in stoichiometric amounts to 50 µl TE buffer, containing 50 mM NaCl. The mixture was heated to 95 °C for 5 min. After that temperature dropped by 0.2 °C/ min until 20 °C to ensure a clean oligo anneal. The 30 bp DNA stock solutions were diluted to 50 µM and added in stoichiometric amounts to 50 µl TE buffer, containing 50 mM NaCl. The mixture was heated to 95 °C for 5 min. After that temperature dropped by 1 °C/ min until 20 °C to ensure a clean oligo anneal.

4.2.1.3 Polymerase Chain Reaction (PCR)

Amplification of widom 601-sequence (147 bp – Cy5-/IRD700-/IRD800- labeled)

2 min	94 °C	
30 s	94 °C (Denaturation)	30x
1 min	56 °C (Annealing)	
30 s	68 °C (Amplification)	
5 min	68 °C	
∞	8 °C	

Amplification of widom 601-sequence (203 bp/215 bp – Cy5-/IRD700-/IRD800-labeled)

2 min	94 °C	
30 s	94 °C (Denaturation)	5x
1 min	48 °C (Annealing)	
30 s	68 °C (Amplification)	
30 s	94 °C (Denaturation)	25x
1 min	58 °C (Annealing)	
30 s	68 °C (Amplification)	
5 min	68 °C (Final Extension)	
∞	8 °C	

4.2.2 Biochemical methods

4.2.2.1 SDS polyacrylamide gel electrophoresis and stainings

Lämmli loading buffer was added to each protein sample and heated to 95 °C for 5 min. The mixture and a protein marker were loaded on home made gels. The percentage of polyacrylamide in each gel varied between 8 % (v/v) and 20 % (v/v), depending on the size of the proteins that were to be separated. For further analysis via Western Blot see 4.2.2.2. For pull down assays 4-20 % gradient gels (for wildtype and mutant Ioc3, Ioc4, and Isw1) and 12 % (v/v) SDS-PAGE gels (for wild type and mutant PWWP) were used. Gels were run at 120 V and 13 W in Running buffer until visible separation of the marker (20-40 min) and subsequently stained with Coomassie Blue or silver nitrate. Gels were scanned using an Epson scanner and Lab Scan software.

Coomassie Stainings:

SDS-PAGE gels were separated from the glass chamber and put into Coomassie Staining solution for 30 min. After that, the gels was put for 3 h into Coomassie Destaining solution until protein bands were visible.

Silver Stainings:

SDS-PAGE gels were separated from the glass chambers and fixated for 60 min in 50 % (v/v) methanol, 12 % (v/v) glacial acetic acid and 50 µl 37 % (v/v) formaldehyde (added before use). After Fixation the gel was washed two times with 50 % (v/v) ethanol before a 1 min-incubation in 0.02 % (w/v) sodium thiosulfate pentahydrate. The gel was washed two times in MilliQ water and the incubated for 15 min in 0.2 % (w/v) silver nitrate and 75 µl 37 % (v/v) formaldehyde. The gels was washed two times in MilliQ water and further developed in 6 % (w/v) sodium carbonate, 2 ml of the 0.02 % (w/v) sodium thiosulfate pentahydrate solution and 50 µl 37 % (v/v) formalehyde until protein bands became visible. The developing reaction was stopped by washing in 50 mM EDTA for 15 min.

4.2.2.2 Western Blots

SDS-PAGE gels were run as described previously. After protein separation a semi-dry blotting device was used to blot the separated proteins onto a nitrocellulose membrane. The membrane was soaked in Transfer buffer, the blotting device was assembled and run at 125 mA for 40 min. To check for successful transfer the nitrocellulose membrane was stained with 15 ml Ponceau S for 5 min. Then the membrane was washed with water and put in a 50 ml falcon tube together with the blocking solution. The membrane and blocking solution were incubated rolling for 1 h at RT. Then the membrane was washed three times 5 min with 10 ml TBST. After that the membrane was incubated with the primary antibody for 2 h at RT before it got rinsed with TBST three times for 5 min. The membrane was incubated with the secondary antibody in TBST for 1 h at RT. The membrane was developed by adding 2 ml of chemiluminescent HRP substrate, incubating 5 min at RT before measuring chemoluminesence by evaluating the HRP signal using the Fusion FX Vilber Lourmat.

4.2.2.3 Nucleosome Reconstitutions

Histone octamers were reconstituted with Cy5-, IRD700- or IRD800-labeled 147 bp, 215 bp or 203 bp DNA fragments by serial dilution. For this, 1 µg DNA and 1 µg histone octamers were mixed in a master mix containing 2 M NaCl and Initial Dilution Buffer in a final volume of 10 µl and incubated for 15 min at 37 °C. Then the reaction was transferred to 30 °C. The reaction was serially diluted with 3.3 µl, 6.7 µl, 5.0 µl, 3.6 µl, 4.7 µl, 6.7 µl, 10 µl, 30 µl, 20 µl for 15 min incubations at 30 °C with each dilution. Finally, the reaction was diluted with 100 µl Final Dilution Buffer and incubated for 15 min at 30 °C. The reconstituted nucleosomes were run on a 5 % (v/v) native PAGE gels together with 5 µg, 10 µg and 15 µg of the corresponding DNA to ensure the quality of the reconstitution and to measure the concentrations of the reconstituted nucleosomes by using a standard curve. Detection of the DNA wrapped around the nucleosome bands was obtained with the Typhoon FLA 9500 for Cy5-labeled substrates or with the Licor for IRD700/IRD800-labeled substrates. Mononucleosomes were stored at 4 °C. Note that all nucleosomes listed in Table 4.6 were reconstituted with Cy5-labeled DNA, IRD700-labeled DNA and IRD800-labeled DNA, which leads to a plethora of 75 different kinds of nucleosomes.

Table 4.6 Nucleosomes used in this study

	NCP 147 bp	end-position 203 bp	middle-position 215 bp	Species	Source
Wild type $CAR4_{T45C}$	✓	✓	✓	*Homo sapiens*	Philipp Voigt
H3K36me0	✓	✓	✓		
H3K36me3	✓	✓	✓		
Wild $type_{T32C}$	✓	✓	✓	*Homo sapiens*	Till Bartke
H3K4me0		✓			
H3K4me3		✓			
H3K4me3-H2A.Z		✓			
H3K9,14ac		✓			
H4K5,8,12ac		✓			
H3K4me3 - H3K9,14,18,23,27ac		✓			
H2A.Z	✓	✓	✓		
Wild type H2A		✓		*Saccharomyces cerevisiae*	www.histonesource.com
Htz1		✓			
Wild typeE		✓		*Homo sapiens*	Epicypher
polyAc		✓			

4.2.2.4 Nucleosome Sliding Assays

To analyze the nucleosome sliding ability of wild type and mutant, native Isw1a and Isw1b remodeler complexes, nucleosome sliding assays were carried out. Mononucleosomes were reconstituted as described in 4.2.2.3. Each reaction contained 10 fmol remodeler, 1 mM ATP, 0.1 % (w/v) BSA and 44 mM KCl in nucleosome sliding buffer A., It was incubated for 0 min, 0.5 min, 1 min, 2 min, 5 min and 10 min before quenching the reaction with ice-cold Stop Buffer. Aliquots were electrophoresed through 0.4x TBE and 2 % (v/v) glycerol in 7 % (v/v) acrylamide

gels for 3 h at 300 V, 4 °C, followed by fluorophore detection using the Typhoon FLA 9500 (Cy5) or the Licor (IRD700, IRD800).

4.2.2.5 Competitive nucleosome Sliding Assays (cSliding Assays)

Competitive sliding assays were conducted the same way as regular sliding assays. Nucleosomes labeled with either IRD700 or IRD800 were mixed at a 1:1 ratio. This mixture contained 30 fmol of each nucleosome. For cSliding Assays with Isw1a end-positioned substrates and for Isw1b middle-positioned substrated were used. Reactions were set up and analyzedas described in 4.2.2.4.

4.2.2.6 Electrophoretic mobility shift assays (EMSAs)

EMSAs were used to investigate binding ability of proteins to DNA, RNA or nucleosomes. Proteins were titrated into a mix containing 15 fmol of Cy5-labeled DNA, RNA or nucleosomes, 6.8 µg BSA and 7.5 mM $MgCl_2$ in a total volume of 15 µl in EMSA Buffer D and incubated 5 min on ice. DNA and RNA sequences used for this experiment are listed in Table 4.3. Resolving of the unbound DNA or RNA to protein-bound fraction was conducted in 0.4x TBE and 2 % (v/v) glycerol through 7 % (v/v) native-PAGE gels at 4 °C, 150 V for 2 h. Resolving of the unbound nucleosomes was conducted accordingly in 5 % (v/v) native-PAGE gels at 4 °C, 150V for 2h. Visualization of flourecent Cy5-labeled substrates was enabled with the Typhoon FLA 9500.

4.2.2.7 Competitive electrophoretic mobility shift assays (cEMSAs)

The proceduce of cEMSAs is as described above, but instead of 15 fmol Cy5-labeled nucleosomes, 7.5 fmol IRD700 and 7.5 fmol IRD800-labeled nucleosomes (e.g. IRD700-labeled H3K36me0 and IRD800-labeled H3K36me3) were pipetted together and used for binding reactions. Visualization of IRD700/800 dyes was done by the Licor.

4.3.3.8 Co-Immunoprecipitations (Co-IPs)

Co-IPs were conducted to validate previously found interaction partners of Isw1a or Isw1b containing Flag-tagged Ioc3 or Flag-tagged Ioc4, respectively. Yeast cells were first grown in 5 ml overnight cultures before inocculating 200 ml of YPD. Cells were harvested at an OD_{600}=1.0, aliquoted in 200 OD fractions and washed twice with ice cold PBS. 800 µl of Huang IP buffer was added to the pellet and resuspended. 800 µl of zirconia beads were added and cells were lysed in the Precellys bead beater 3 times 30 s at 5600 rpm with 5 min breaks on ice between each cycle. 15 µl of whole cell extract was kept for input control. The remaining whole cell extract was incubated with 15 µl of previously washed Flag agarose beads at 4°C 1 h on a rotating wheel. After that the beads were centrifuges, supernatant discarded and the remaining beads were washed three times with Huang IP wash buffer. The Flag-tagged proteins were eluted with Lämmli Loading buffer,s run on SDS-PAGE gel before further analysis by Western Blot.

4.2.2.9 Pull down assays

Pull down assays were performed to validate direct interaction between proteins and histone octamers. 3 µg of recombinant yeast octamers and 2 µg of recombinant protein were incubated with respective beads (see Table 4.7). The beads were prewashed three times with Pull Down Buffer PD3 when Ni-NTA was used. Amylose-Sepharose beads were prewashed three times with Pull Down Buffer PD2A. The mock reaction contained yeast octamers and beads. 2 µg of purified 6xHis-MBP was added to the mock reaction of all protein conctructs that contained MBP (see Table 4.7). The Pull down reaction and mock reaction were incubated in 200 µl of their respective Pull down buffer for 2 h at 4 °C rolling. After that, beads were washed three times with their respective Pull down wash buffer. Protein elution was done with Lämmli Loading buffer. The Pull down and mock elutions (80 % each) were loaded next to a 20 % input of each component on an SDS-PAGE gel and run until a clear separation of the marker was visible. A Coomassie staining was performed to visualize the bands (see 4.2.2.1)

4.2.2.10 Thermal Shift Assay (TSA)

To optimize buffer contitions for a recombinant protein a Thermal Shift Assay was performed. The protein was pipetted in different buffers in a 96 well plate containing SYBR Orange and 8 μM of recombinant protein. Reactions were heated to 95 °C in a qPCR machine with at a rate of 0.5 °C per minute. The principle of a TSA is that hydrophobic regions inside a protein are hidden under native conditions. Denaturing a protein by heat exposes those regions, SYBR Orange starts binding and autoflouresence is rising. The fluorescence curves were normalized and plotted against time. Taking 0.5 fluorescence allows reading the meltin temperature (T_m) from the y-axis. The higher the T_m the more stabilizing is the buffer for the protein.

4.3 General procedure for purification of recombinant proteins

Transformed *E. coli* were grown at 37 °C in 0.5 l – 1 l of LB media with appropriate antibiotics (see Table 4.1) until OD_{600} = 0.6-0.9, put into the coldroom for 45 min and then induced via 0.25 mM IPTG at 16 °C over night. The next day cells were harvested and washed twice with ice cold PBS. The pellet was resuspended with an equal volume of **Cell lysis buffer** (Table 4.7), containing 250 µl DNAse (2.5 mg/ ml) I, 250 µl Lysozyme (100 mg/ ml) and one tablet of cOmplete EDTAse free Inhibitor per 50 ml cell suspension. This mixture was sonicated for 3x45 s and 2x30 s with a Heinemann sonicator in the cold room, using a setting of 5 at 40 %. The lyzed cells were centrifuged at 45000 rpm for 45 min at 4 °C to remove cell debris. The supernatant was incubated with **Beads,** pre-washed with **Cell lysis buffer,** for 2-3 h at 4 °C on a rolling incubator. After incubation the beads were washed three times with **Wash buffer**. GST-$PWWP_{\Delta INS}$ bound to glutathione sepharose was incubated with 3C-HRV Protease to remove the GST-tag over. The beads were washed two times with GST purification buffer B and once with GST purification buffer C. The supernatant was collected and directly dialysed into Dialysis buffer 2. All other proteins were eluted from their respective beads with **Elution buffer** (table 4.7).

Table 4.7 Purification buffers

Protein construct	**Cell lysis buffer**	**Beads**	**Wash buffer**	**Elution buffer**	**Dialysis buffer**
6xHis-PWWP	Lysis buffer	Ni-NTA	Lysis buffer	Elution buffer 2	Dialysis buffer 2
6xHis-PWWP 2KE	Lysis buffer	Ni-NTA	Lysis buffer	Elution buffer 2	Dialysis buffer 2
GST-PWWPΔINS	GST purification buffer A	Glutathione -Sepharose	GST purification buffer B and C	-	Dialysis buffer 2
6xHis-MBP-Ioc4	Lysis buffer	Ni-NTA	Lysis buffer	Elution buffer 1	Dialysis buffer 1
6xHis-MBP-Ioc4 2KE	Lysis buffer	Ni-NTA	Lysis buffer	Elution buffer 1	Dialysis buffer 1
6xHis-MBP-Ioc4ΔINS	Lysis buffer	Ni-NTA	Lysis buffer	Elution buffer 1	Dialysis buffer 1
6xHis-MBP-Ioc4ΔPWWP	Lysis buffer	Ni-NTA	Lysis buffer	Elution buffer 1	Dialysis buffer 1
MBP-Ioc3-13xHis	GST purification buffer A	Amylose-Sepharose	GST purification buffer C	Maltose Elution buffer	-
6xHis-MBP-Isw1	Lysis buffer	Ni-NTA	Lysis buffer	Elution buffer 1	Dialysis buffer 1

After elution from the beads, most proteins were further purified using the ÄKTA Pure system. Details can be found in Result section 2.1. Table 4.8 summarizes the details for each purification step. As a final step proteins were dialyzed over night into **Dialysis buffer** 1 or 2 (Table 4.7). For further details of the purification, folding and stability testing of individual proteins, see Result section 2.1.

Table 4.8 Äkta columns and parameters

Column	**Chromatography**	**Elution**
HiTrap Heparin	Affinity chromatography	20 mM PO_4^{3-} pH 8.0 50 mM Arg/Glu NaCl gradient from 50 mM – 2 M over 30 column volumes
ResourceQ	Anion Exchange	50 mM Tris pH 7.5 NaCl gradient from 10 mM – 1M over 10 column volumes
Superdex200 Increase 10/300GL	Size exclusion chromatography	20 mM PO_4^{3-} pH 8.0 500 mM NaCl 50 mM Arg/Glu 10 % (v/v) Glycerol

4.4 Purification of endogenous protein complexes from yeast

Genomically TAP-tagged wild type and mutant Ioc3 and Ioc4 (wild type and mutant Isw1a and Isw1b complexes, respectively) yeast strains (see Table 4.5) were grown over night in 5 ml YPD media and used to inocculate 50 ml cultures to grow to an OD_{600} of 1.0. 12 l YPD media were inocculated with 1 ml of the 50 ml culture and grown to an OD_{600} of 3.0-5.0. The cells were harvested by centrifuging at 4 °C and 4000 rpm for 20 min. After that cells were washed twice with ice cold PBS. Pellets were resuspended with an equal volume of TAP Extraction buffer and snap frozen as "popcorn". Cell lysis was performed with a freezer mill using 6 cycles. Each cycle contained 2 min pre-cooling before milling at a rate of 15 cps with an additional 1 min cooling time. The resulting powder was defrosted on ice and briefly centrifuged at 4000 rpm for 10 min at 4 °C. The supernatant was centrifuged in the ultracentrifuge at 45000 rpm at 4 °C for 1 h. After ultracentrifugation the supenatant divided into a small pellet at the bottom, followed by a clear, soluble phase and on top a white layer. The clear phase was carefully removed without disturbing either the bottom pellet or the white layer on top and incubated with 300 µl of IgG-sepharose beads at 4 °C for 3 h. The beads were pre-washed with TAP Extraction buffer. After incubation the beads were washed once with TAP Extraction buffer and twice with TEV cleavage buffer. Beads were resuspended with 1 ml of TEV cleavage buffer and 30 µl of home-made TEV protease and left rotating at 4 °C over night. The next day beads were briefly centrifuged and the flow-through collected containing cleaved protein complexes. The beads were washed 5 times with 1 ml of CBB and the supertantant was each time collected to get a final volume of 6 ml. 3 µl of 1 M $CaCl_2$ was added before incubation with 150 µl of pre-washed calmodulin sepharose beads for 2 h at 4 °C rolling on an incubator. The beads were pre-washed with Calmodulin Binding Buffer. Elution of the bound complexes was performed by washing two times with 0.5 ml of CEB. Elution fractions were pooled in fresh tubes and analyzed by silver stain.

5. Supplementary

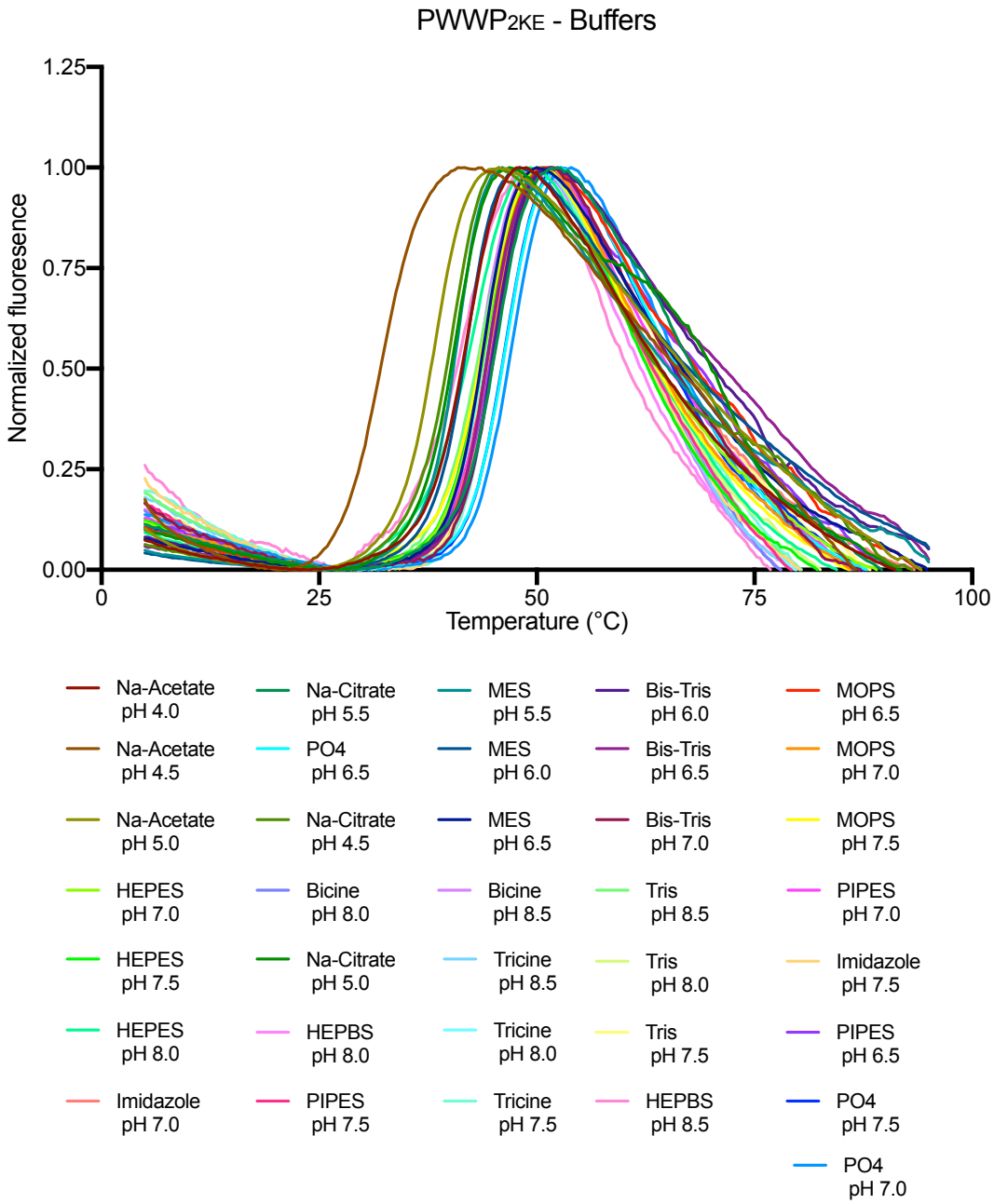

Supplementary Figure 5.1 Thermal Shift Assay (TSA) screens for optimal buffer conditions for $PWWP_{2KE}$. Stability test for purifed $PWWP_{2KE}$ with several, color coded buffers reveal different melting curves. High melting temperatures indicate a stable buffer condition. In this case, phosphate buffers lead to higher melting temperatures. The most unsuitable buffers are Na-Acetate pH 4.0 and pH 4.5.

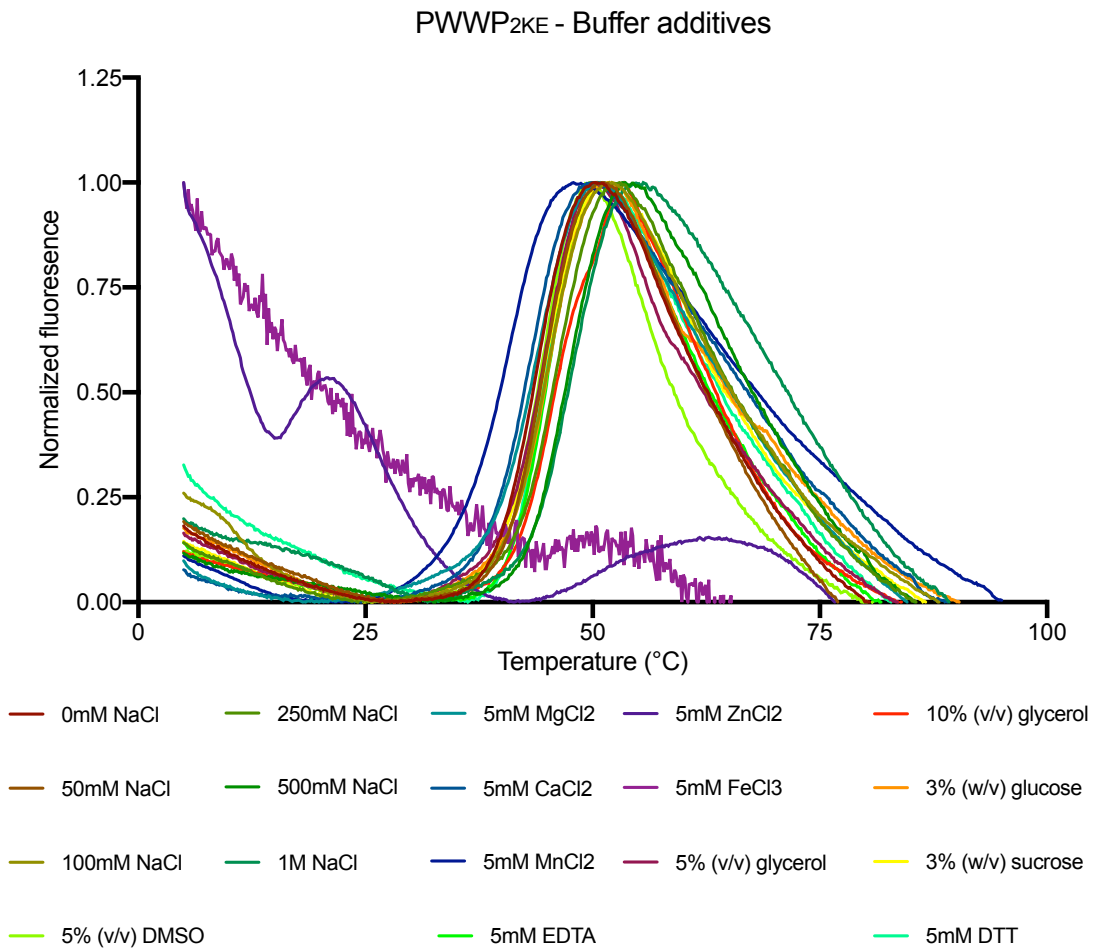

Supplementary Figure 5.2 TSA screens for optimal buffer additives for $PWWP_{2KE}$. Stability tests with $PWWP_{2KE}$ show that high salt concentrations (500 mM and 1 M) are suitable buffer ingredients, whereas $ZnCl_2$ and $FeCl_3$ immediately leads to protein aggregation.

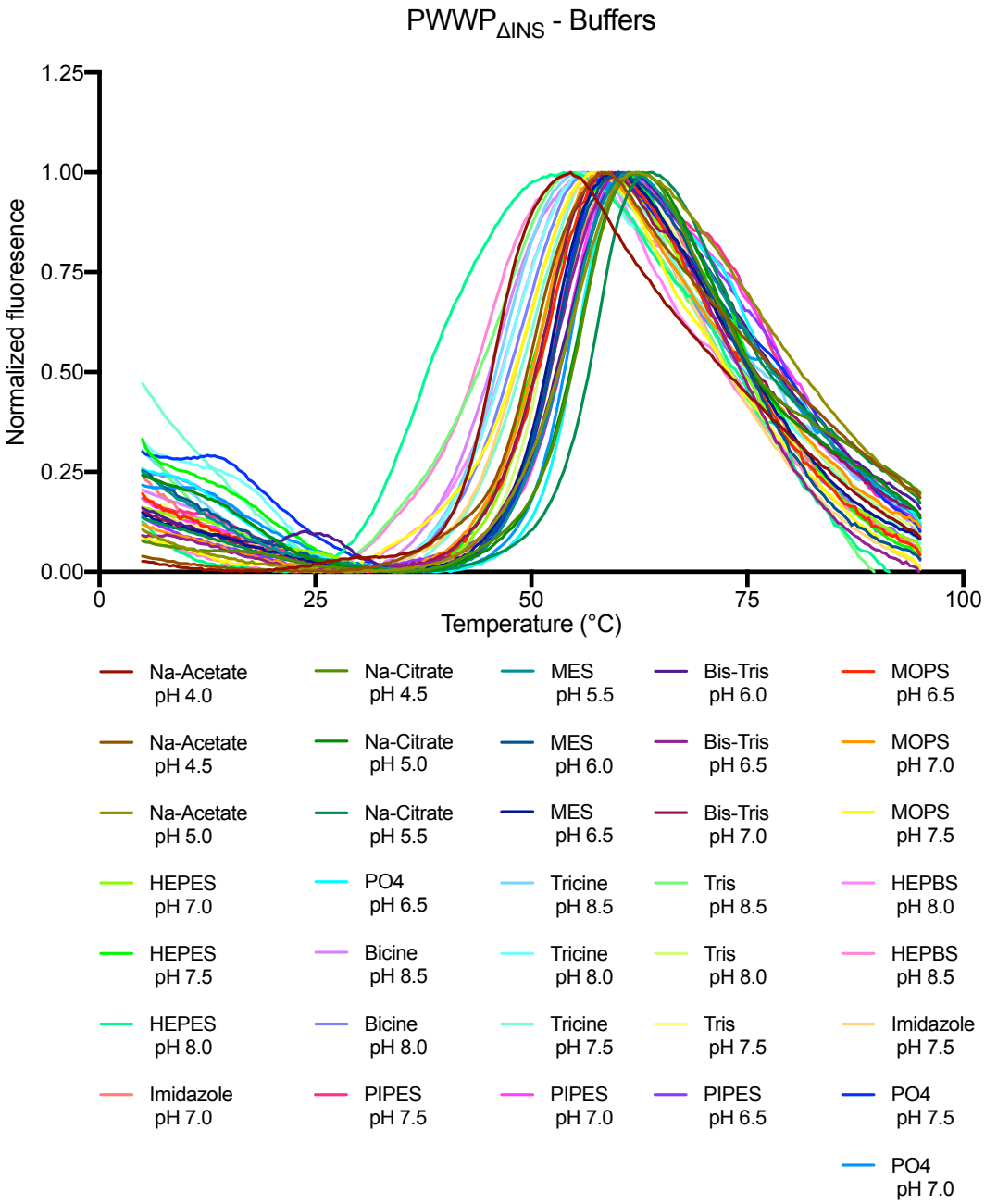

Supplementary Figure 5.3 TSA screens for optimal buffer conditions for PWWP$_{\Delta INS}$. Stability test for purifed PWWP$_{\Delta INS}$ with several, color coded buffers reveal different melting curves. High melting temperatures indicate a stable buffer condition. In this case, Na-citrate leads to higher melting temperatures. The most unsuitable buffers are HEPES pH 7.0 or HEPBS pH 8.0. The chosen PO_4^{3-} pH 7.0 is evidently not the best buffer, however, still reveals stabilizing effects for the protein.

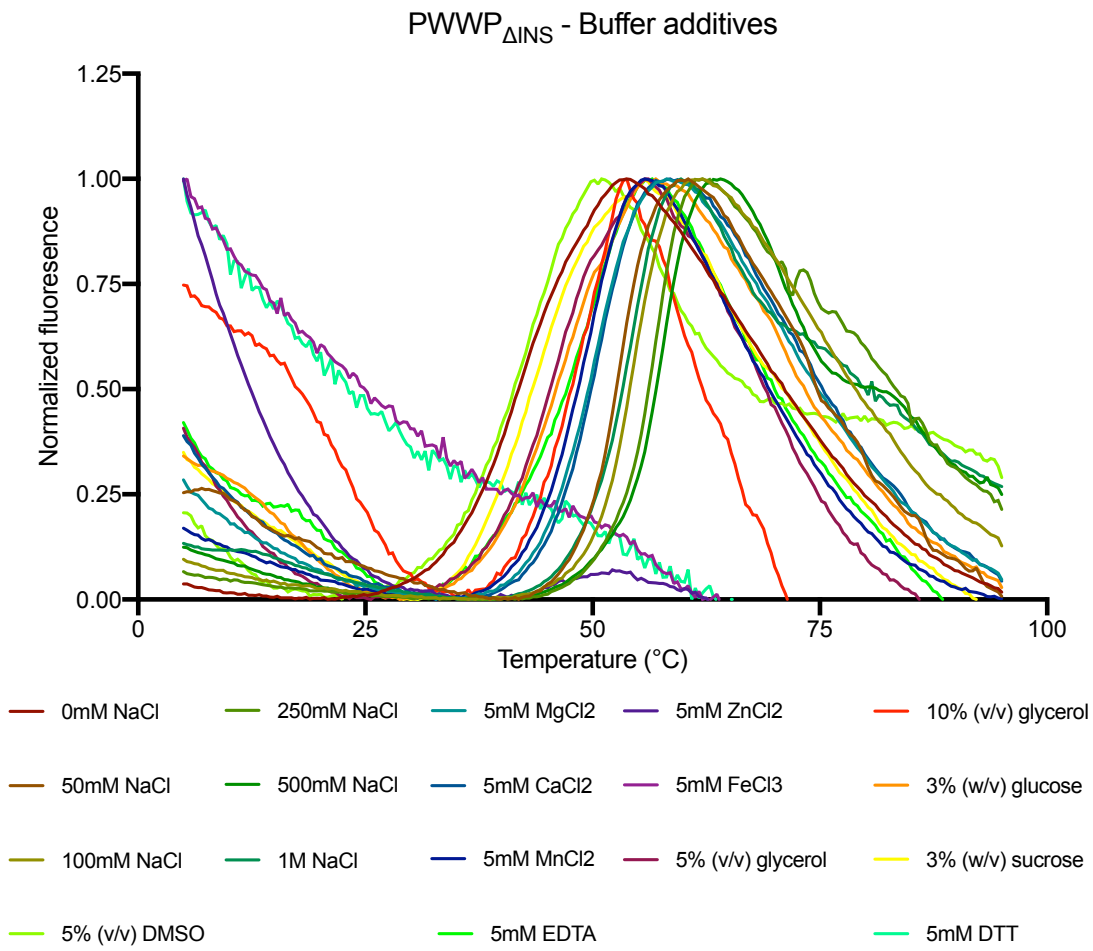

Supplementary Figure 5.4 TSA screens for optimal buffer additives for for PWWP$_{\Delta INS}$. Stability tests with PWWP$_{\Delta INS}$ show that high salt concentrations (500 mM and 1 M) are suitable buffer ingredients, whereas $ZnCl_2$ and $FeCl_3$ lead to protein aggregation.

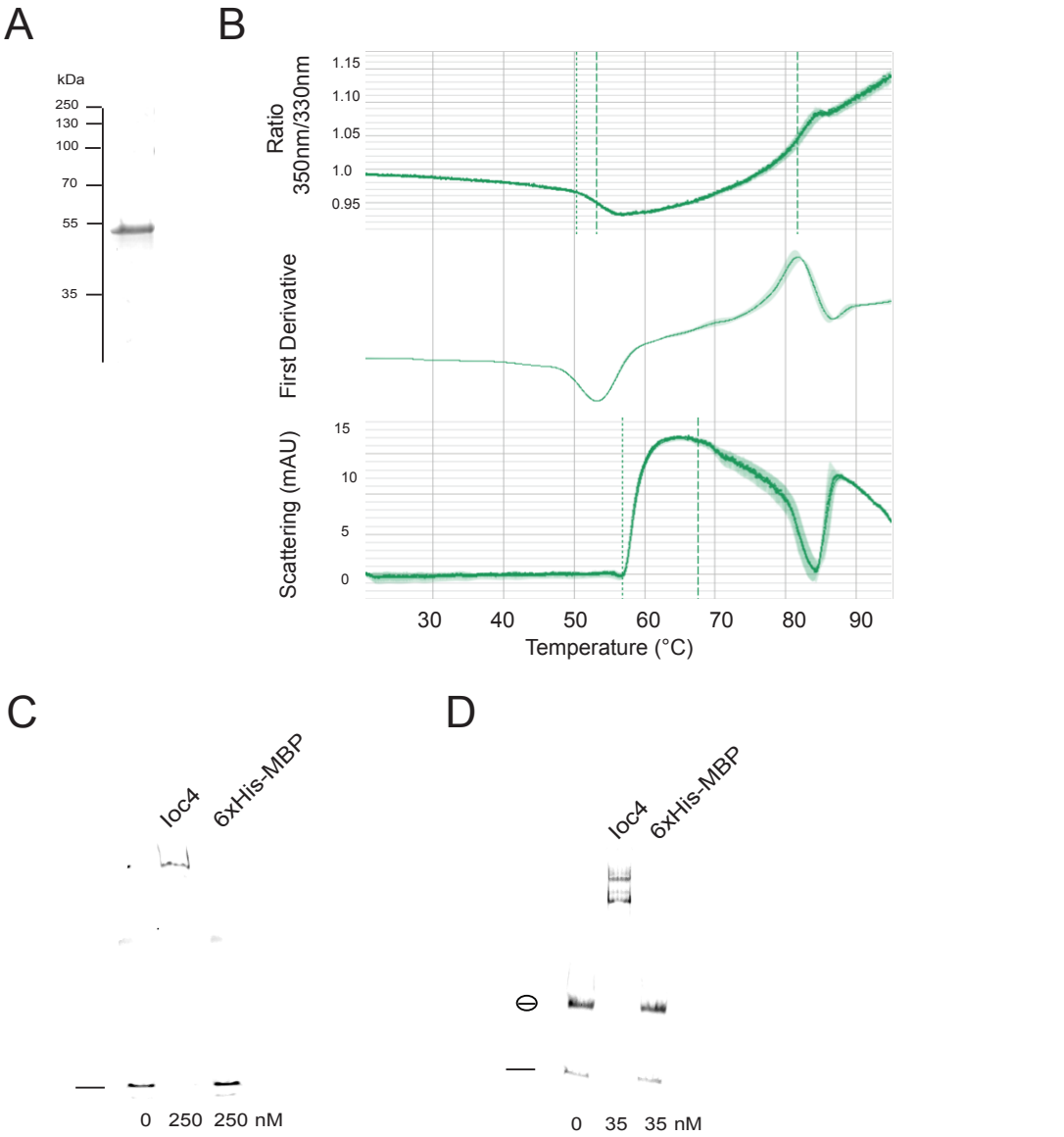

Supplementary Figure 5.5 Quality and binding control of 6xHis-MBP. (A) SDS-PAGE gel with purified 6xHis-MBP. The purified protein is a kind gift from Umut Günsel. **(B)** nanoDSF spectrum of 6x-His-MBP differs from wild type and mutant Ioc4, Ioc3 and Isw1 spectra. **(C)** EMSA with dsDNA showing that 6xHis-MBP cannot bind to DNA at the highest, used concentration. Ioc4 serves as a control. **(D)** EMSA with NCPs showing that 6xHis-MBP cannot bind to nucleosomes at the highest, used concentration. Ioc4 serves as a positive control.

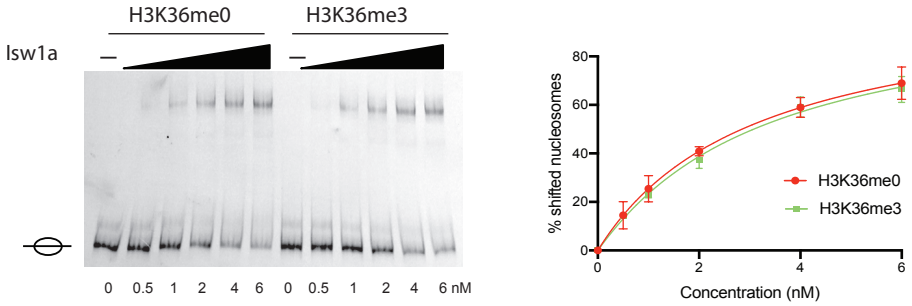

Supplementary Figure 5.6 Isw1a does not distinguish between middle-positioned H3K36me0- and H3K36me3-containing nucleosomes in EMSAs. EMSAs were quantitated and plotted as mean ± SEM. The number of replicates is three.

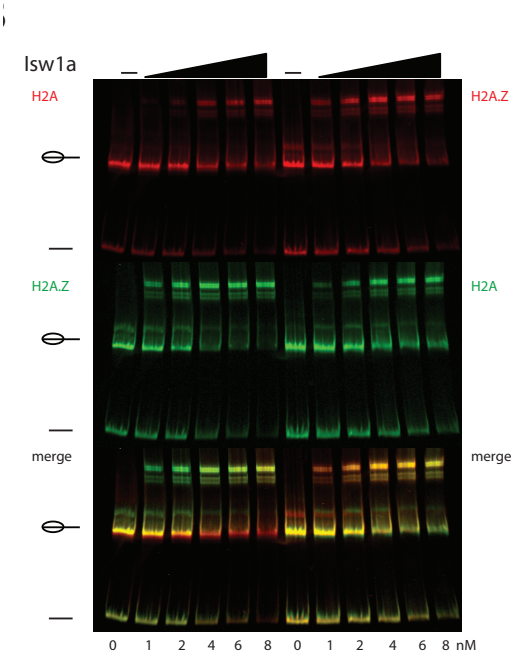

Supplementary Figure 5.7 Isw1a specifically recognizes H2A.Z-containing nucleosomes. Dye switch experiment demonstration the equality of both used dyes, IRD700 (red) and IRD800 (green). The left side of the gel displays cEMSAs with wild type H2A nucleosomes in red (IRD700-labeled DNA) and H2A.Z-containing nucleosomes in green (IRD800-labeled DNA). On the right side of the gel a dye switch was performed. Wild type H2A was displayed as green (IRD800-labeled DNA) and H2A.Z was displayed as red (IRD700-labeled DNA).

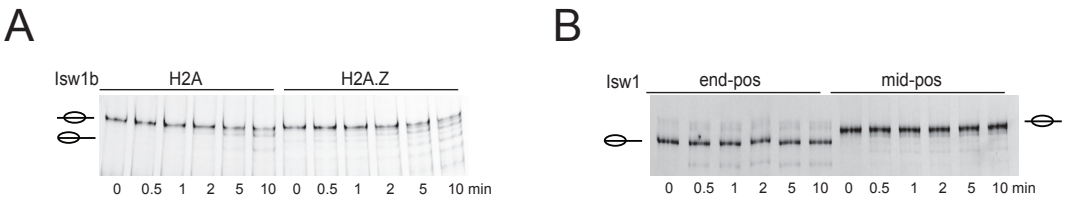

Supplementary Figure 5.8 Isw1b and Isw1 monomer controls. (A) Sliding assay with Isw1b comparing wild type H2A and H2A.Z-containing nucleosomes. Although different remodeling stages can be observed, affinity for the initial, mid-positioned nucleosome is the same for both substrates. **(B)** Sliding assay of Isw1 monomer reveals that it can neither mobilize end-positioned nor mid-positioned nucleosomes in addition of ATP in a time dependent manner.

Abbreviations

%	percent
(v/v)	(volume/volume)
(w/v)	(weight/volume)
°C	degree Celcius
µg	mircogram
µl	microliter
A	Ampere
aa	amino acid
ACT	actin
ADP	adenosine diphosphate
Amp	ampicillin
APS	ammonium persulfate
ATP	adenosine triphosphate
bp	base pairs
BSA	bovine serum albumine
Cam	chloramphenicole
CBP	calmodulin binding protein
ChIP	chromatin immunoprecipitation
CLB	coil-linker-DNA-binding motif
Co-IP	co-immunoprecipitation
Cys	cysteine
DMSO	dimethylsulfoxide
DNA	desoxyribonucleic acid
DNMT	DNA methyltransferase
dNTP	desoxynucleotide
DTT	dithiothreitol
E. coli	*Escherichia coli*
EDTA	ethylenediaminetetraacetic acid
EGTA	ethylene glycol-bis(β-aminoethyl ether)-N,N,N,N-tetraacetic acid
fmol	femtomol
forw, fwd, fw	forward
Gcn	general control nonrepressible
H3K36me3	trimethylated lysine 36 on histone 3

H3K4me3	trimethylated lysine 4 on histone 3
H3K*N*ac	Histone H3 acetylated on lysine number *N*
HCl	hydrochloric acid
HDAC	histone deacetylase
HEPES	2-[4-(2-hydroxyethyl)piperazin-1-yl]ethanesulfonic acid
His	histidine
HLB	helical-linker-DNA-binding domain
HSS	Hand-Sant-Slide domain
INO	iositol requiring
Ioc	ISWI one complex
Itc	ISWI two complex
ISWI	Imitation switch
IP	immunoprecipitation
IPTG	isopropyl β-D-1-thiogalactopyranoside
Kan	kanamycine
kb	kilobase
l	liter
L1	loop1
LB	lysogeny broth
M	molar
mA	milliampere
mg	milligram
min	minute
ml	milliliter
mM	millimolar
MWCO	molecular weight cut off
NaCl	sodium chloride
NCP	nucleosome core particle
NDR, NFR	nucleosome depleted region, nucleosome free region
ng	nanogram
nM	nanomolar
NP-40	nonyl phenoxypolyethoxylethanol
OD	optical density
ORF	open reading frame
PAGE	polyacrylamide gelelectrophoresis
PCR	polymerase chain reaction

PEG	polyethylenglycol
pH	potentia hydrogenii
PHD	plant homeodomain
pI	isoelectric point
PMSF	phenylmethylsulfonyl fluoride
PolII	RNA polymerase II
PTM	posttranslational modification
PWWP	proline-tryptophane-tryptophane-proline
rev, rw	reverse
RNA	ribonucleic acid
rpm	rounds per minute
RT	room temperature
S. cerevisiae, S.c.	*Saccharomyces cerevisiae*
S. pombe	*Schizosaccharomyces pombe*
SANT	Swi3, Ada2, N-Cor and TFIIB
SDS	sodium dodecyl sulfate
SDS-PAGE	sodium dodecyl sulfate polyacrylamide gel electrophoresis
sec, s	seconds
SLIDE	SANT-like ISWI domain
SWI/SNF	Switch/sucrose non-fermentable
TAE	Tris-acetate EDTA
TAP	tandem affinity purification
TBS	Tris-buffered saline
TE	Tris-EDTA
TEMED	tetramethylethylenediamine
T_m	melting temperature
tRNA	transfer RNA
TES	transcription end site
TEV	Tobacco Etch Virus
TSS	transcription start site
V	volt
wt	wild type
YPD	yeast extract peptone dextrose

Bibliography

1. Kornberg RD. Chromatin Structure : A Repeating Unit of Histones and DNA Chromatin structure is based on a repeating unit of eight. *Science*. 1974;184:868-871.
2. Richmond TJ, Finch JT, Rushton B, Rhodes D, Klug A. Structure of nucleosome core particle at 7 Å resolution. *Nature*. 1984;311:532-537.
3. Luger K, Mäder AW, Richmond RK, Sargent DF, Richmond TJ. Crystal structure of the nucleosome core particle at 2.8 Å resolution. *Nature*. 1997;389(6648):251-260. doi:10.1038/38444
4. Tolstorukov I, Cregg JM. Classical genetics. *Methods Mol Biol*. 2007;389:189-201. doi:10.1385/1-59745-456-7:189
5. Tolstorukov MY, Colasanti A V., McCandlish DM, Olson WK, Zhurkin VB. A Novel Roll-and-Slide Mechanism of DNA Folding in Chromatin: Implications for Nucleosome Positioning. *J Mol Biol*. 2007;371(3):725-738. doi:10.1016/j.jmb.2007.05.048
6. Thoma F, Koller T, Klug A. Involvement of histone H1 in the organization of the nucleosome and of the salt-dependent superstructures of chromatin. *J Cell Biol*. 1979;83(2 I):403-427. doi:10.1083/jcb.83.2.403
7. Olins AL, Olins DE. Spheroid chromatin units (v bodies). *Science*. 1974;183(4122):330-332. doi:10.1126/science.183.4122.330
8. Schalch T, Duda S, Sargent DF, Richmond TJ. X-ray structure of a tetranucleosome and its implications for the chromatin fibre. *Nature*. 2005;436(7047):138-141. doi:10.1038/nature03686
9. Robinson PJJ, Fairall L, Huynh VAT, Rhodes D. EM measurements define the dimensions of the "30-nm" chromatin fiber: Evidence for a compact, interdigitated structure. *Proc Natl Acad Sci U S A*. 2006;103(17):6506-6511. doi:10.1073/pnas.0601212103
10. Robinson PJ, Rhodes D. Structure of the "30 nm" chromatin fibre: A key role for the linker histone. *Curr Opin Struct Biol*. 2006;16(3):336-343. doi:10.1016/j.sbi.2006.05.007
11. Tremethick DJ. Higher-Order Structures of Chromatin: The Elusive 30 nm Fiber. *Cell*. 2007;128(4):651-654. doi:10.1016/j.cell.2007.02.008
12. Li G, Reinberg D. Chromatin higher-order structures and gene regulation. *Curr Opin Genet Dev*. 2011;21(2):175-186. doi:10.1016/j.gde.2011.01.022
13. Maeshima K, Imai R, Tamura S, Nozaki T. Chromatin as dynamic 10-nm fibers. *Chromosoma*. 2014;123(3):225-237. doi:10.1007/s00412-014-0460-2
14. Clark DJ, Kimura T. Electrostatic mechanism of chromatin folding. *J Mol Biol*. 1990;211(4):883-896. doi:10.1016/0022-2836(90)90081-V
15. Smith CD, Shu S, Mungall CJ, Karpen GH. The Release 5.1 Annotation of Drosophila melanogaster Heterochromatin. *Science*. 2007;316(4):527-534. http://www.globalbuddhism.org/jgb/index.php/jgb/article/view/88/100
16. Hergeth SP, Schneider R. The H1 linker histones: multifunctional proteins beyond the nucleosomal core particle. *EMBO Rep*. 2015;16(11):1439-1453. doi:10.15252/embr.201540749
17. David L, Huber W, Granovskaia M, Toedling J, Palm CJ, Bofkin L, Jones T, Davis RW, Steinmetz LM. A high-resolution map of transcription in the yeast genome. *Proc Natl Acad Sci U S A*. 2006;103(14):5320-5325. doi:10.1073/pnas.0601091103

18. Grunstein M. Molecular model for telomeric heterochromatin in yeast. *Curr Opin Cell Biol*. 1997;9(3):383-387. doi:10.1016/S0955-0674(97)80011-7
19. Wright RHG, Le Dily F, Beato M. ATP, Mg2+, Nuclear Phase Separation, and Genome Accessibility. *Trends Biochem Sci*. 2019;44(7):565-574. doi:10.1016/j.tibs.2019.03.001
20. Shin Y, Chang YC, Lee DSW, Berry J, Sanders DW, Ronceray P, Wingreen NS, Haataja M, Brangwynne CP. Liquid Nuclear Condensates Mechanically Sense and Restructure the Genome. *Cell*. 2018;175(6):1481-1491.e13. doi:10.1016/j.cell.2018.10.057
21. Heyn P, Salmonowicz H, Rodenfels J, Neugebauer KM. Activation of transcription enforces the formation of distinct nuclear bodies in zebrafish embryos. *RNA Biol*. 2017;14(6):752-760. doi:10.1080/15476286.2016.1255397
22. Hnisz D, Shrinivas K, Young RA, Chakraborty AK, Sharp PA. A Phase Separation Model for Transcriptional Control. *Cell*. 2017;169(1):13-23. doi:10.1016/j.cell.2017.02.007
23. Yamamoto T, Schiessel H. Transcription Driven Phase Separation in Chromatin Brush. *Langmuir*. 2016;32(12):3036-3044. doi:10.1021/acs.langmuir.6b00442
24. Erdel F, Rippe K. Formation of Chromatin Subcompartments by Phase Separation. *Biophys J*. 2018;114(10):2262-2270. doi:10.1016/j.bpj.2018.03.011
25. Buchan JR, Muhlrad D, Parker R. P bodies promote stress granule assembly in Saccharomyces cerevisiae. *J Cell Biol*. 2008;183(3):441-455. doi:10.1083/jcb.200807043
26. Jiang C, Pugh BF. Nucleosome positioning and gene regulation: Advances through genomics. *Nat Rev Genet*. 2009;10(3):161-172. doi:10.1038/nrg2522
27. Struhl K, Segal E. Determinants of nucleosome positioning. *Nat Struct Mol Biol*. 2013;20(3):267-273. doi:10.1038/nsmb.2506
28. Lieleg C, Krietenstein N, Walker M, Korber P. Nucleosome positioning in yeasts: methods, maps, and mechanisms. *Chromosoma*. 2014;124(2):131-151. doi:10.1007/s00412-014-0501-x
29. Zhang Z, Wippo CJ, Wal M, Ward E, Korber P, Pugh BF. A packing mechanism for nucleosome organization reconstituted across a eukaryotic genome. *Science*. 2011;332(6032):977-980. doi:10.1126/science.1200508
30. Lee W, Tillo D, Bray N, Morse RH, Davis RW, Hughes TR, Nislow C. A high-resolution atlas of nucleosome occupancy in yeast. *Nat Genet*. 2007;39(10):1235-1244. doi:10.1038/ng2117
31. Hughes AL, Rando OJ. Mechanisms underlying nucleosome positioning in vivo. *Annu Rev Biophys*. 2014;43(1):41-63. doi:10.1146/annurev-biophys-051013-023114
32. Thomas JO, Furber V. Yeast Chromatin Structure. *FEBS Lett*. 1976;66(2).
33. Jiang C, Pugh BF. A compiled and systematic reference map of nucleosome positions across the Saccharomyces cerevisiae genome. *Genome Biol*. 2009;10(10):1-11. doi:10.1186/gb-2009-10-10-r109
34. Schones DE, Cui K, Cuddapah S, Roh TY, Barski A, Wang Z, Wei G, Zhao K. Dynamic Regulation of Nucleosome Positioning in the Human Genome. *Cell*. 2008;132(5):887-898. doi:10.1016/j.cell.2008.02.022
35. Tirosh I, Barkai N. Two strategies for gene regulation by promoter nucleosomes. *Genome Res*. 2008;18(7):1084-1091. doi:10.1101/gr.076059.108
36. Mavrich TN, Ioshikhes IP, Venters BJ, Jiang C, Tomsho LP, Qi J, Schuster SC, Albert I, Pugh BF. A barrier nucleosome model for statistical positioning of

nucleosomes throughout the yeast genome. *Genome Res*. 2008;18(7):1073-1083. doi:10.1101/gr.078261.108
37. Lohr D. Nucleosome transactions on the promoters of the yeast GAL and PHO genes. *J Biol Chem*. 1997;272(43):26796-26798. doi:10.1074/jbc.272.43.26795
38. Kaplan CD, Laprade L, Winston F. Transcription elongation factors repress transcription initiation from cryptic sites. *Science*. 2003;301(5636):1096-1099. doi:10.1126/science.1087374
39. Thompson DM, Parker R. Cytoplasmic Decay of Intergenic Transcripts in Saccharomyces cerevisiae. *Mol Cell Biol*. 2007;27(1):92-101. doi:10.1128/mcb.01023-06
40. Goodman AJ, Daugharthy ER, Kim J. Pervasive antisense transcription is evolutionary conserved in budding yeast. *Mol Biol Evol*. 2013;30(2):409-421. doi:10.1093/molbev/mss240
41. Frías-Lasserre D, Villagra CA. The importance of ncRNAs as epigenetic mechanisms in phenotypic variation and organic evolution. *Front Microbiol*. 2017;8(DEC):1-13. doi:10.3389/fmicb.2017.02483
42. Hennig BP, Fischer T. The great repression: Chromatin and cryptic transcription. *Transcription*. 2013;4(3):37-41. doi:10.4161/trns.24884
43. Camblong J, Iglesias N, Fickentscher C, Dieppois G, Stutz F. Antisense RNA Stabilization Induces Transcriptional Gene Silencing via Histone Deacetylation in S. cerevisiae. *Cell*. 2007;131(4):706-717. doi:10.1016/j.cell.2007.09.014
44. Waddington CH. Towards a theoretical biology. *Nature*. 1968;218(5141):525-527. doi:10.1038/218525a0
45. Dupont C, Armant DR, Brenner CA. Epigenetics: Definition, mechanisms and clinical perspective. *Semin Reprod Med*. 2009;27(5):351-357. doi:10.1055/s-0029-1237423
46. Kouzarides T. Chromatin Modifications and Their Function. *Cell*. 2007;128(4):693-705. doi:10.1016/j.cell.2007.02.005
47. Jenuwein T, Allis CD. Translating the histone code. *Science*. 2001;293(5532):1074-1080. doi:10.1126/science.1063127
48. Santisteban MS, Kalashnikova T, Smith MM. Histone H2A.Z regulates transcription and is partially redundant with nucleosome remodeling complexes. *Cell*. 2000;103(3):411-422. doi:10.1016/S0092-8674(00)00133-1
49. McKinley KL, Cheeseman IM. The molecular basis for centromere identity and function. *Nat Rev Mol Cell Biol*. 2016;17(1):16-29. doi:10.1038/nrm.2015.5
50. Meluh PB, Yang P, Glowczewski L, Koshland D, Smith MM. Cse4p is a component of the core centromere of Saccharomyces cerevisiae. *Cell*. 1998;94(5):607-613. doi:10.1016/S0092-8674(00)81602-5
51. Jack APM, Hake SB. Getting down to the core of histone modifications. *Chromosoma*. 2014;123(4):355-371. doi:10.1007/s00412-014-0465-x
52. Li G, Levitus M, Bustamante C, Widom J. Rapid spontaneous accessibility of nucleosomal DNA. *Nat Struct Mol Biol*. 2005;12(1):46-53. doi:10.1038/nsmb869
53. Workman JL, Abmayr SM. *Fundamentals of Chromatin*.; 2014. doi:10.1007/978-1-4614-8624-4
54. Clarke S. Protein methylation. *Curr Opin Cell Biol*. 1993;5(6):977-983. doi:10.1016/0955-0674(93)90080-A
55. Voigt P, LeRoy G, Drury WJ, Zee BM, Son J, Beck DB, Young NL, Garcia BA, Reinberg D. Asymmetrically modified nucleosomes. *Cell*.

2012;151(1):181-193. doi:10.1016/j.cell.2012.09.002
56. Paik WK, Kim S. Protein methylation. *Science*. 1971;174(6):114-119. doi:10.1016/0955-0674(93)90080-A
57. Shi X, Hong T, Walter KL, Ewalt M, Michishita E, Hung T, Carney D, Peña P, Lan F, Kaadige MR, Lacoste N, Cayrou C, Davrazou F, Saha A, Cairns BR, Ayer DE, Kutateladze TG, Shi Y, Côté J, et al. ING2 PHD domain links histone H3 lysine 4 methylation to active gene repression. *Nature*. 2006;442(7098):96-99. doi:10.1038/nature04835
58. Carrozza MJ, Li B, Florens L, Suganuma T, Swanson SK, Lee KK, Shia WJ, Anderson S, Yates J, Washburn MP, Workman JL. Histone H3 methylation by Set2 directs deacetylation of coding regions by Rpd3S to suppress spurious intragenic transcription. *Cell*. 2005;123(4):581-592. doi:10.1016/j.cell.2005.10.023
59. Chu Y, Sutton A, Sternglanz R, Prelich G. The Bur1 Cyclin-Dependent Protein Kinase Is Required for the Normal Pattern of Histone Methylation bySet2. *Mol Cell Biol*. 2006;26(8):3029-3038. doi:10.1128/mcb.26.8.3029-3038.2006
60. Youdell ML, Kizer KO, Kisseleva-Romanova E, Fuchs SM, Duro E, Strahl BD, Mellor J. Roles for Ctk1 and Spt6 in Regulating the Different Methylation States of Histone H3 Lysine 36. *Mol Cell Biol*. 2008;28(16):4915-4926. doi:10.1128/mcb.00001-08
61. Strahl BD, Grant PA, Briggs SD, Sun Z-W, Bone JR, Caldwell JA, Mollah S, Cook RG, Shabanowitz J, Hunt DF, Allis CD. Set2 Is a Nucleosomal Histone H3-Selective Methyltransferase That Mediates Transcriptional Repression. *Mol Cell Biol*. 2002;22(5):1298-1306. doi:10.1128/mcb.22.5.1298-1306.2002
62. Yoh SM, Cho H, Pickle L, Evans RM, Jones KA. The Spt6 SH2 domain binds Ser2-P RNAPII to direct Iws1-dependent mRNA splicing and export. *Genes Dev*. 2007;21(2):160-174. doi:10.1101/gad.1503107
63. Liu J, Zhang J, Gong Q, Xiong P, Huang H, Wu B, Lu G, Wu J, Shi Y. Solution structure of tandem SH2 domains from Spt6 protein and their binding to the phosphorylated rna polymerase II C-terminal domain. *J Biol Chem*. 2011;286(33):29218-29226. doi:10.1074/jbc.M111.252130
64. Sun M, Larivière L, Dengl S, Mayer A, Cramer P. A tandem SH2 domain in transcription elongation factor Spt6 binds the phosphorylated RNA polymerase II C-terminal repeat domain (CTD). *J Biol Chem*. 2010;285(53):41597-41603. doi:10.1074/jbc.M110.144568
65. Close D, Johnson SJ, Sdano MA, McDonald SM, Robinson H, Formosa T, Hill CP. Crystal structures of the S. cerevisiae Spt6 core and C-terminal tandem SH2 domain. *J Mol Biol*. 2011;408(4):697-713. doi:10.1016/j.jmb.2011.03.002
66. Diebold ML, Loeliger E, Koch M, Winston F, Cavarelli J, Romier C. Noncanonical tandem SH2 enables interaction of elongation factor Spt6 with RNA polymerase II. *J Biol Chem*. 2010;285(49):38389-38398. doi:10.1074/jbc.M110.146696
67. Li J, Moazed D, Gygi SP. Association of the histone methyltransferase Set2 with RNA polymerase II plays a role in transcription elongation. *J Biol Chem*. 2002;277(51):49383-49388. doi:10.1074/jbc.M209294200
68. Krogan NJ, Baetz K, Keogh MC, Datta N, Sawa C, Kwok TCY, Thompson NJ, Davey MG, Pootoolal J, Hughes TR, Emili A, Buratowski S, Hieter P, Greenblatt JF. Regulation of chromosome stability by the histone H2A variant Htz1, the Swr1 chromatin remodeling complex, and the histone acetyltransferase NuA4. *Proc Natl Acad Sci U S A*. 2004;101(37):13513-

13518. doi:10.1073/pnas.0405753101
69. Drouin S, Laramée L, Jacques PÉ, Forest A, Bergeron M, Robert F. DSIF and RNA polymerase II CTD phosphorylation coordinate the recruitment of Rpd3S to actively transcribed genes. *PLoS Genet*. 2010;6(10):1-12. doi:10.1371/journal.pgen.1001173
70. Joshi AA, Struhl K. Eaf3 chromodomain interaction with methylated H3-K36 links histone deacetylation to pol II elongation. *Mol Cell*. 2005;20(6):971-978. doi:10.1016/j.molcel.2005.11.021
71. Keogh MC, Kurdistani SK, Morris SA, Ahn SH, Podolny V, Collins SR, Schuldiner M, Chin K, Punna T, Thompson NJ, Boone C, Emili A, Weissman JS, Hughes TR, Strahl BD, Grunstein M, Greenblatt JF, Buratowski S, Krogan NJ. Cotranscriptional set2 methylation of histone H3 lysine 36 recruits a repressive Rpd3 complex. *Cell*. 2005;123(4):593-605. doi:10.1016/j.cell.2005.10.025
72. Govind CK, Qiu H, Ginsburg DS, Ruan C, Hofmeyer K, Hu C, Swaminathan V, Workman JL, Li B, Hinnebusch AG. Phosphorylated Pol II CTD recruits multiple HDACs, including Rpd3C(S), for methylation-dependent deacetylation of ORF nucleosomes. *Mol Cell*. 2010;39(2):234-246. doi:10.1016/j.molcel.2010.07.003
73. Li B, Gogol M, Carey M, Pattenden SG, Seidel C, Workman JL. Infrequently transcribed long genes depend on the Set2/Rpd3S pathway for accurate transcription. *Genes Dev*. 2007;21(11):1422-1430. doi:10.1101/gad.1539307
74. Lee KY, Chen Z, Jiang R, Meneghini MD. H3K4 methylation dependent and independent chromatin regulation by JHD2 and SET1 in budding yeast. *G3 Genes, Genomes, Genet*. 2018;8(5):1829-1839. doi:10.1534/g3.118.200151
75. Li B, Gogol M, Carey M, Lee D, Seidel C, Workman JL. Combined action of PHD and chromo domains directs the Rpd3S HDAC to transcribed chromatin. *Science*. 2007;316(5827):1050-1054. doi:10.1126/science.1139004
76. Kim TS, Buratowski S. Dimethylation of H3K4 by Set1 Recruits the Set3 Histone Deacetylase Complex to 5′ Transcribed Regions. *Cell*. 2009;137(2):259-272. doi:10.1016/j.cell.2009.02.045
77. Briggs SD, Bryk M, Strahl BD, Cheung WL, Davie JK, Dent SYR, Winston F, David Allis C. Histone H3 lysine 4 methylation is mediated by Set1 and required for cell growth and rDNA silencing in Saccharomyces cerevisiae. *Genes Dev*. 2001;15(24):3286-3295. doi:10.1101/gad.940201
78. Noma K ichi, Grewal SIS. Histone H3 lysine 4 methylation is mediated by Set1 and promotes maintenance of active chromatin states in fission yeast. *Proc Natl Acad Sci U S A*. 2002;99(SUPPL. 4):16438-16445. doi:10.1073/pnas.182436399
79. Roguev A, Schaft D, Shevchenko A, Pijnappel WWMP, Wilm M, Aasland R, Stewart AF. The Saccharomyces cerevisiae Set1 complex includes an Ash2 homologue and methylates histone 3 lysine 4. *EMBO J*. 2001;20(24):7137-7148. doi:10.1093/emboj/20.24.7137
80. Bae HJ, Dubarry M, Jeon J, Soares LM, Dargemont C, Kim J, Geli V, Buratowski S. The Set1 N-terminal domain and Swd2 interact with RNA polymerase II CTD to recruit COMPASS. *Nat Commun*. 2020;11(1). doi:10.1038/s41467-020-16082-2
81. Li B, Carey M, Workman JL. The Role of Chromatin during Transcription. *Cell*. 2007;128(4):707-719. doi:10.1016/j.cell.2007.01.015
82. Miller T, Krogan NJ, Dover J, Tempst P, Johnston M, Greenblatt JF, Sherman

DR, Voskuil M, Schnappinger D, Harrell MI, Schoolnik GK, Muckelbauer JA, Voss ME, Liu R, Lorin A, Tebben AJ, Solomon KA, Lo C, Li Z, et al. COMPASS: A complex of proteins associated with a trithorax-related SET domain protein. *Proc Natl Acad Sci U S A*. 2001;98(26).

83. Dover J, Schneider J, Boateng MA, Wood A, Johnston KDM, Shilatifard A. Methylation of Histone H3 by COMPASS Requires Ubiquitination of Histone H2B by Rad6. *J Biol Chem*. 2002;16(10):609-613.
84. Sun ZW, Allis CD. Ubiquitination of histone H2B regulates H3 methylation and gene silencing in yeast. *Nature*. 2002;418(6893):104-108. doi:10.1038/nature00883
85. Kanno T, Kanno Y, Siegel RM, Jang MK, Lenardo MJ, Ozato K. Selective Recognition of Acetylated Histones by Bromodomain Proteins Visualized in Living Cells. *Mol Cell*. 2004;13(1):33-43. doi:10.1016/S1097-2765(03)00482-9
86. Dhalluin C, Carlson JE, Zeng L, He C, Aggarwal AK, Zhou MM. Structure and ligand of a histone acetyltransferase bromodomain. *Nature*. 1999;399(6735):491-496. doi:10.1038/20974
87. Jacobson RH, Ladurner AG, King DS, Tjian R. Structure and function of a human TAF(II)250 double bromodomain module. *Science*. 2000;288(5470):1422-1425. doi:10.1126/science.288.5470.1422
88. Kasten M, Szerlong H, Erdjument-Bromage H, Tempst P, Werner M, Cairns BR. Tandem bromodomains in the chromatin remodeler RSC recognize acetylated histone H3 Lys14. *EMBO J*. 2004;23(6):1348-1359. doi:10.1038/sj.emboj.7600143
89. Seto E, Yoshida M. Erasers of histone acetylation: The histone deacetylase enzymes. *Cold Spring Harb Perspect Biol*. 2014;6(4). doi:10.1101/cshperspect.a018713
90. Brownell JE, Allis CD. Special HATs for special occasions: Linking histone acetylation to chromatin assembly and gene activation. *Curr Opin Genet Dev*. 1996;6(2):176-184. doi:10.1016/S0959-437X(96)80048-7
91. Baker SP, Grant PA. The SAGA continues: Expanding the cellular role of a transcriptional co-activator complex. *Oncogene*. 2007;26(37):5329-5340. doi:10.1038/sj.onc.1210603
92. Spedale G, Timmers HTM, Pijnappel WWMP. ATAC-king the complexity of SAGA during evolution. *Genes Dev*. 2012;26(6):527-541. doi:10.1101/gad.184705.111
93. Koutelou E, Hirsch CL, Dent SYR. Multiple faces of the SAGA complex. *Curr Opin Cell Biol*. 2010;22(3):374-382. doi:10.1016/j.ceb.2010.03.005
94. Grant PA, Duggan L, Côté J, Roberts SM, Brownell JE, Candau R, Ohba R, Owen-Hughes T, Allis CD, Winston F, Berger SL, Workman JL. Yeast Gcn5 functions in two multisubunit complexes to acetylate nucleosomal histones: Characterization of an ada complex and the saga (spt/ada) complex. *Genes Dev*. 1997;11(13):1640-1650. doi:10.1101/gad.11.13.1640
95. Sun J, Paduch M, Kim SA, Kramer RM, Barrios AF, Lu V, Luke J, Usatyuk S, Kossiakoff AA, Tan S. Structural basis for activation of SAGA histone acetyltransferase Gcn5 by partner subunit Ada2. *Proc Natl Acad Sci U S A*. 2018;115(40):10010-10015. doi:10.1073/pnas.1805343115
96. Wang L, Dent SYR. Functions of SAGA in development and disease. *Epigenomics*. 2014;6(3):329-339. doi:10.2217/epi.14.22
97. Sterner DE, Grant PA, Roberts SM, Duggan LJ, Belotserkovskaya R, Pacella

LA, Winston F, Workman JL, Berger SL. Functional Organization of the Yeast SAGA Complex: Distinct Components Involved in Structural Integrity, Nucleosome Acetylation, and TATA-Binding Protein Interaction. *Mol Cell Biol*. 1999;19(1):86-98. doi:10.1128/mcb.19.1.86

98. Pokholok DK, Harbison CT, Levine S, Cole M, Hannett NM, Tong IL, Bell GW, Walker K, Rolfe PA, Herbolsheimer E, Zeitlinger J, Lewitter F, Gifford DK, Young RA. Genome-wide map of nucleosome acetylation and methylation in yeast. *Cell*. 2005;122(4):517-527. doi:10.1016/j.cell.2005.06.026
99. Schneider J, Bajwa P, Johnson FC, Bhaumik SR, Shilatifard A. Rtt109 is required for proper H3K56 acetylation: A chromatin mark associated with the elongating RNA polymerase II. *J Biol Chem*. 2006;281(49):37270-37274. doi:10.1074/jbc.C600265200
100. Driscoll R, Hudson A, Jackson SP. Yeast Rtt109 promotes genome stability by acetylating histone H3 on lysine 56. *Science*. 2007;315(5812):649-652. doi:10.1126/science.1135862
101. Han J, Zhou H, Horazdovsky B, Zhang K, Xu RM, Zhang Z. Rtt109 acetylates histone H3 lysine 56 and functions in DNA replication. *Science*. 2007;315(5812):653-655. doi:10.1126/science.1133234
102. Fillingham J, Recht J, Silva AC, Suter B, Emili A, Stagljar I, Krogan NJ, Allis CD, Keogh M-C, Greenblatt JF. Chaperone Control of the Activity and Specificity of the Histone H3 Acetyltransferase Rtt109. *Mol Cell Biol*. 2008;28(13):4342-4353. doi:10.1128/mcb.00182-08
103. Sutton A, Shia WJ, Band D, Kaufman PD, Osada S, Workman JL, Sternglanz R. Sas4 and Sas5 are required for the histone acetyltransferase activity of Sas2 in the SAS complex. *J Biol Chem*. 2003;278(19):16887-16892. doi:10.1074/jbc.M210709200
104. Allard S, Utley RT, Savard J, Clarke A, Grant P, Brandl CJ, Pillus L, Workman JL, Côté J. NuA4, an essential transcription adaptor/histone H4 acetyltransferase complex containing Esa1p and the ATM-related cofactor Tra1p. *EMBO J*. 1999;18(18):5108-5119. doi:10.1093/emboj/18.18.5108
105. Murr R, Loizou JI, Yang YG, Cuenin C, Li H, Wang ZQ, Herceg Z. Histone acetylation by Trrap-Tip60 modulates loading of repair proteins and repair of DNA double-strand breaks. *Nat Cell Biol*. 2006;8(1):91-99. doi:10.1038/ncb1343
106. Ikura T, Ogryzko V V., Grigoriev M, Groisman R, Wang J, Horikoshi M, Scully R, Qin J, Nakatani Y. Involvement of the TIP60 histone acetylase complex in DNA repair and apoptosis. *Cell*. 2000;102(4):463-473. doi:10.1016/S0092-8674(00)00051-9
107. Steger DJ, Eberharter A, John S, Grant PA, Workman JL. Purified histone acetyltransferase complexes stimulate HIV-1 transcription from preassembled nucleosomal arrays. *Proc Natl Acad Sci U S A*. 1998;95(22):12924-12929. doi:10.1073/pnas.95.22.12924
108. Shogren-Knaak M, Ishii H, Sun JM, Pazin MJ, Davie JR, Peterson CL. Histone H4-K16 acetylation controls chromatin structure and protein interactions. *Science*. 2006;311(5762):844-847. doi:10.1126/science.1124000
109. Wieland G, Orthaus S, Ohndorf S, Diekmann S, Hemmerich P. Functional Complementation of Human Centromere Protein A (CENP-A) by Cse4p from Saccharomyces cerevisiae. *Mol Cell Biol*. 2004;24(15):6620-6630. doi:10.1128/mcb.24.15.6620-6630.2004
110. West MHP, Bonner WM. Histone 2A, a Heteromorphous Family of Eight

Protein Species. *Biochemistry*. 1980;(1979):3238-3245.
111. Lindstrom KC, Vary JC, Parthun MR, Delrow J, Tsukiyama T. Isw1 Functions in Parallel with the NuA4 and Swr1 Complexes in Stress-Induced Gene Repression. *Mol Cell Biol*. 2006;26(16):6117-6129. doi:10.1128/mcb.00642-06
112. Van Daal A, Elgin SCR. Histone variant, H2AvD, is essential Drosophila melanogaster. *Mol Biol Cell*. 1992;3(6):593-602. doi:10.1091/mbc.3.6.593
113. Sopko R, Huang D, Preston N, Chua G, Papp B, Kafadar K, Snyder M, Oliver SG, Cyert M, Hughes TR, Boone C, Andrews B. Mapping pathways and phenotypes by systematic gene overexpression. *Mol Cell*. 2006;21(3):319-330. doi:10.1016/j.molcel.2005.12.011
114. Takahashi D, Orihara Y, Kitagawa S, Kusakabe M, Shintani T, Oma Y, Harata M. Quantitative regulation of histone variant H2A.Z during cell cycle by ubiquitin proteasome system and SUMO-targeted ubiquitin ligases. *Biosci Biotechnol Biochem*. 2017;81(8):1557-1560. doi:10.1080/09168451.2017.1326087
115. Luk E, Vu ND, Patteson K, Mizuguchi G, Wu WH, Ranjan A, Backus J, Sen S, Lewis M, Bai Y, Wu C. Chz1, a Nuclear Chaperone for Histone H2AZ. *Mol Cell*. 2007;25(3):357-368. doi:10.1016/j.molcel.2006.12.015
116. Mosammaparast N, Del Rosario BC, Pemberton LF. Modulation of Histone Deposition by the Karyopherin Kap114. *Mol Cell Biol*. 2005;25(5):1764-1778. doi:10.1128/mcb.25.5.1764-1778.2005
117. Andrews AJ, Chen X, Zevin A, Stargell LA, Luger K. The Histone Chaperone Nap1 Promotes Nucleosome Assembly by Eliminating Nonnucleosomal Histone DNA Interactions. *Mol Cell*. 2010;37(6):834-842. doi:10.1016/j.molcel.2010.01.037
118. Avvakumov N, Nourani A, Côté J. Histone Chaperones: Modulators of Chromatin Marks. *Mol Cell*. 2011;41(5):502-514. doi:10.1016/j.molcel.2011.02.013
119. Wu WH, Wu CH, Ladurner A, Mizuguchi G, Wei D, Xiao H, Luk E, Ranjant A, Wu C. N terminus of Swr1 binds to histone H2AZ and provides a platform for subunit assembly in the chromatin remodeling complex. *J Biol Chem*. 2009;284(10):6200-6207. doi:10.1074/jbc.M808830200
120. Mizuguchi G, Shen X, Landry J, Wu WH, Sen S, Wu C. ATP-Driven Exchange of Histone H2AZ Variant Catalyzed by SWR1 Chromatin Remodeling Complex. *Science*. 2004;303(5656):343-348. doi:10.1126/science.1090701
121. Morillo-Huesca M, Clemente-Ruiz M, Andújar E, Prado F. The SWR1 histone replacement complex causes genetic instability and genome-wide transcription misregulation in the absence of H2A.Z. *PLoS One*. 2010;5(8). doi:10.1371/journal.pone.0012143
122. Hua S, Kallen CB, Dhar R, Baquero MT, Mason CE, Russell BA, Shah PK, Liu J, Khramtsov A, Tretiakova MS, Krausz TN, Olopade OI, Rimm DL, White KP. Genomic analysis of estrogen cascade reveals histone variant H2A.Z associated with breast cancer progression. *Mol Syst Biol*. 2008;4(188):1-14. doi:10.1038/msb.2008.25
123. Svotelis A, Gévry N, Grondin G, Gaudreau L. H2A.Z overexpression promotes cellular proliferation of breast cancer cells. *Cell Cycle*. 2010;9(2):364-370. doi:10.4161/cc.9.2.10465
124. Suto RK, Clarkson MJ, Tremethick DJ, Luger K. Crystal structure of a nucleosome core particle containing the variant histone H2A.Z. *Nat Struct Biol*.

2000;7(12):1121-1124. doi:10.1038/81971
125. Horikoshi N, Arimura Y, Taguchi H, Kurumizaka H. Crystal structures of heterotypic nucleosomes containing histones H2A.Z and H2A. *Open Biol*. 2016;6(6). doi:10.1098/rsob.160127
126. Abbott DW, Ivanova VS, Wang X, Bonner WM, Ausió J. Characterization of the stability and folding of H2A.Z chromatin particles: Implications for transcriptional activation. *J Biol Chem*. 2001;276(45):41945-41949. doi:10.1074/jbc.M108217200
127. Park YJ, Dyer PN, Tremethick DJ, Luger K. A new fluorescence resonance energy transfer approach demonstrates that the histone variant H2AZ stabilizes the histone octamer within the nucleosome. *J Biol Chem*. 2004;279(23):24274-24282. doi:10.1074/jbc.M313152200
128. Thambirajah AA, Dryhurst D, Ishibashi T, Li A, Maffey AH, Ausió J. H2A.Z stabilizes chromatin in a way that is dependent on core histone acetylation. *J Biol Chem*. 2006;281(29):20036-20044. doi:10.1074/jbc.M601975200
129. Keogh MC, Mennella TA, Sawa C, Berthelet S, Krogan NJ, Wolek A, Podolny V, Carpenter LR, Greenblatt JF, Baetz K, Buratowski S. The Saccharomyces cerevisiae histone H2A variant Htz1 is acetylated by NuA4. *Genes Dev*. 2006;20(6):660-665. doi:10.1101/gad.1388106
130. Millar CB, Xu F, Zhang K, Grunstein M. Acetylation of H2AZ Lys 14 is associated with genome-wide gene activity in yeast. *Genes Dev*. 2006;20(6):711-722. doi:10.1101/gad.1395506
131. Kobor MS, Venkatasubrahmanyam S, Meneghini MD, Gin JW, Jennings JL, Link AJ, Madhani HD, Rine J. A protein complex containing the conserved Swi2/Snf2-related ATPase Swr1p deposits histone variant H2A.Z into euchromatin. *PLoS Biol*. 2004;2(5). doi:10.1371/journal.pbio.0020131
132. Raisner RM, Hartley PD, Meneghini MD, Bao MZ, Liu CL, Schreiber SL, Rando OJ, Madhani HD. Histone variant H2A.Z Marks the 5′ ends of both active and inactive genes in euchromatin. *Cell*. 2005;123(2):233-248. doi:10.1016/j.cell.2005.10.002
133. Weber CM, Ramachandran S, Henikoff S. Nucleosomes are context-specific, H2A.Z-Modulated barriers to RNA polymerase. *Mol Cell*. 2014;53(5):819-830. doi:10.1016/j.molcel.2014.02.014
134. Gu M, Naiyachit Y, Wood TJ, Millar CB. H2A.Z marks antisense promoters and has positive effects on antisense transcript levels in budding yeast. *BMC Genomics*. 2015;16(1):1-11. doi:10.1186/s12864-015-1247-4
135. Bagchi DN, Battenhouse AM, Park D, Iyer VR. The histone variant H2A.Z in yeast is almost exclusively incorporated into the +1 nucleosome in the direction of transcription. *Nucleic Acids Res*. 2020;48(1):157-170. doi:10.1093/nar/gkz1075
136. Sarcinella E, Zuzarte PC, Lau PNI, Draker R, Cheung P. Monoubiquitylation of H2A.Z Distinguishes Its Association with Euchromatin or Facultative Heterochromatin. *Mol Cell Biol*. 2007;27(18):6457-6468. doi:10.1128/mcb.00241-07
137. Hu G, Cui K, Northrup D, Liu C, Wang C, Tang Q, Ge K, Crane-Robinson C, Zhao K. H2A.Z Facilitates Access of Active and Repressive Complexes to Chromatin in Embryonic Stem Cell Self-renewal and Differentiation. *Cell Stem Cell*. 2014;12(2):180-192. doi:10.1016/j.stem.2012.11.003.H2A.Z
138. Fan JY, Gordon F, Luger K, Hansen JC, Tremethick DJ. The essential histone variant H2A.Z regulates the equilibrium between different chromatin

conformational states. *Nat Struct Biol*. 2002;9(3):172-176. doi:10.1038/nsb767
139. Jin C, Zang C, Wei G, Cui K, Peng W, Zhao K, Felsenfeld G. H3.3/H2A.Z double variant-containing nucleosomes mark "nucleosome-free regions" of active promoters and other regulatory regions. *Nat Genet*. 2009;41(8):941-945. doi:10.1038/ng.409
140. Bönisch C, Schneider K, Pünzeler S, Wiedemann SM, Bielmeier C, Bocola M, Eberl HC, Kuegel W, Neumann J, Kremmer E, Leonhardt H, Mann M, Michaelis J, Schermelleh L, Hake SB. H2A.Z.2.2 is an alternatively spliced histone H2A.Z variant that causes severe nucleosome destabilization. *Nucleic Acids Res*. 2012;40(13):5951-5964. doi:10.1093/nar/gks267
141. Dhillon N, Kamakaka RT. A histone variant, Htz1p, and a Sir1p-like protein, Esc2p, mediate silencing at HMR. *Mol Cell*. 2000;6(4):769-780. doi:10.1016/S1097-2765(00)00076-9
142. Bork P, Koonin E V. An expanding family of helicases within the "DEAD/H" superfamily. *Nucleic Acids Res*. 1993;21(3):751-752. doi:10.1093/nar/21.3.751
143. Clapier CR, Cairns BR. The biology of chromatin remodeling complexes. *Annu Rev Biochem*. 2009;78:273-304. doi:10.1146/annurev.biochem.77.062706.153223
144. Narlikar GJ, Sundaramoorthy R, Owen-Hughes T. Mechanisms and functions of ATP-dependent chromatin-remodeling enzymes. *Cell*. 2013;154(3):490-503. doi:10.1016/j.cell.2013.07.011
145. Flaus A, Martin DMA, Barton GJ, Owen-Hughes T. Identification of multiple distinct Snf2 subfamilies with conserved structural motifs. *Nucleic Acids Res*. 2006;34(10):2887-2905. doi:10.1093/nar/gkl295
146. Carlson M, Osmond BC, Botstein D. Mutants of Yeast Defective in Sucrose Utilization. *Genetics*. 1981;98:25-40.
147. Neigeborn L, Carlson M. Genes Affecting the Regulation of SUC2 Gene Expression By Glucose Repression in Saccharomyces cerevisiae. *Genetics*. 1984;108:845-858.
148. Abrams E, Neigeborn L, Carlson M. Molecular analysis of SNF2 and SNF5, genes required for expression of glucose-repressible genes in Saccharomyces cerevisiae. *Mol Cell Biol*. 1986;6(11):3643-3651. doi:10.1128/mcb.6.11.3643
149. Yang X, Zaurin R, Beato M, Peterson CL. Swi3p controls SWI/SNF assembly and ATP-dependent H2A-H2B displacement. *Nat Struct Mol Biol*. 2007;14(6):540-547. doi:10.1038/nsmb1238
150. Dechassa ML, Zhang B, Horowitz-Scherer R, Persinger J, Woodcock CL, Peterson CL, Bartholomew B. Architecture of the SWI/SNF-Nucleosome Complex. *Mol Cell Biol*. 2008;28(19):6010-6021. doi:10.1128/mcb.00693-08
151. Ludwigsen J, Pfennig S, Singh AK, Schindler C, Harrer N, Forné I, Zacharias M, Mueller-Planitz F. Concerted regulation of ISWI by an autoinhibitory domain and the H4 N-terminal tail. *Elife*. 2017;6:1-24. doi:10.7554/eLife.21477
152. Woodage T, Basrai MA, Baxevanis AD, Hieter P, Collins FS. Characterization of the CHD family of proteins. *Proc Natl Acad Sci U S A*. 1997;94(21):11472-11477. doi:10.1073/pnas.94.21.11472
153. Yoshikawa K, Tanaka T, Ida Y, Furusawa C, Hirasawa T, Shimizu H. Comprehensive phenotypic analysis of single-gene deletion and overexpression strains of Saccharomyces cerevisiae. *Yeast*. 2011;10(February). doi:10.1002/yea
154. Laschober GT, Ruli D, Hofer E, Muck C, Carmona-Gutierrez D, Ring J, Hutter

E, Ruckenstuhl C, Micutkova L, Brunauer R, Jamnig A, Trimmel D, Herndler-Brandstetter D, Brunner S, Zenzmaier C, Sampson N, Breitenbach M, Fröhlich KU, Grubeck-Loebenstein B, et al. Identification of evolutionarily conserved genetic regulators of cellular aging. *Aging Cell*. 2010;9(6):1084-1097. doi:10.1111/j.1474-9726.2010.00637.x

155. Garay E, Campos SE, González de la Cruz J, Gaspar AP, Jinich A, DeLuna A. High-Resolution Profiling of Stationary-Phase Survival Reveals Yeast Longevity Factors and Their Genetic Interactions. *PLoS Genet*. 2014;10(2). doi:10.1371/journal.pgen.1004168
156. Qian W, Ma D, Xiao C, Wang Z, Zhang J. The Genomic Landscape and Evolutionary Resolution of Antagonistic Pleiotropy in Yeast. *Cell Rep*. 2012;2(5):1399-1410. doi:10.1016/j.celrep.2012.09.017
157. Tsukiyama T, Palmer J, Landel CC, Shiloach J, Wu C. Characterization of the imitation switch subfamily of ATP-dependent chromatin-remodeling factors in Saccharomyces cerevisiae. *Genes Dev*. 1999;13(6):686-697. doi:10.1101/gad.13.6.686
158. Smolle M, Venkatesh S, Gogol MM, Li H, Zhang Y, Florens L, Washburn MP, Workman JL. Chromatin remodelers Isw1 and Chd1 maintain chromatin structure during transcription by preventing histone exchange. *Nat Struct Mol Biol*. 2012;19(9):884-892. doi:10.1038/nsmb.2312
159. Radman-Livaja M, Quan TK, Valenzuela L, Armstrong JA, van Welsem T, Kim TS, Lee LJ, Buratowski S, van Leeuwen F, Rando OJ, Hartzog GA. A key role for Chd1 in histone H3 dynamics at the 3′ ends of long genes in yeast. *PLoS Genet*. 2012;8(7). doi:10.1371/journal.pgen.1002811
160. Luk E, Ranjan A, FitzGerald PC, Mizuguchi G, Huang Y, Wei D, Wu C. Stepwise histone replacement by SWR1 requires dual activation with histone H2A.Z and canonical nucleosome. *Cell*. 2010;143(5):725-736. doi:10.1016/j.cell.2010.10.019
161. Kawashima S, Ogiwara H, Tada S, Harata M, Wintersberger U, Enomoto T, Seki M. The INO80 complex is required for damage-induced recombination. *Biochem Biophys Res Commun*. 2007;355(3):835-841. doi:10.1016/j.bbrc.2007.02.036
162. Morrison AJ, Highland J, Krogan NJ, Arbel-Eden A, Greenblatt JF, Haber JE, Shen X. INO80 and γ-H2AX interaction links ATP-dependent chromatin remodeling to DNA damage repair. *Cell*. 2004;119(6):767-775. doi:10.1016/j.cell.2004.11.037
163. Udugama M, Sabri A, Bartholomew B. The INO80 ATP-Dependent Chromatin Remodeling Complex Is a Nucleosome Spacing Factor. *Mol Cell Biol*. 2011;31(4):662-673. doi:10.1128/mcb.01035-10
164. Krietenstein N, Wal M, Watanabe S, Park B, Peterson CL, Pugh BF, Korber P. Genomic Nucleosome Organization Reconstituted with Pure Proteins. *Cell*. 2016;167(3):709-721.e12. doi:10.1016/j.cell.2016.09.045
165. Brahma S, Udugama MI, Kim J, Hada A, Bhardwaj SK, Hailu SG, Lee TH, Bartholomew B. INO80 exchanges H2A.Z for H2A by translocating on DNA proximal to histone dimers. *Nat Commun*. 2017;8. doi:10.1038/ncomms15616
166. Li B, Pattenden SG, Lee D, Gutiérrez J, Chen J, Seidel C, Gerton J, Workman JL. Preferential occupancy of histone variant H2AZ at inactive promoters influences local histone modifications and chromatin remodeling. *Proc Natl Acad Sci U S A*. 2005;102(51):18385-18390. doi:10.1073/pnas.0507975102
167. Yamada K, Frouws TD, Angst B, Fitzgerald DJ, Deluca C, Schimmele K,

Sargent DF, Richmond TJ. Structure and mechanism of the chromatin remodelling factor ISW1a. *Nature*. 2011;472(7344):448-453. doi:10.1038/nature09947

168. Pinskaya M, Nair A, Clynes D, Morillon A, Mellor J. Nucleosome Remodeling and Transcriptional Repression Are Distinct Functions of Isw1 in Saccharomyces cerevisiae. *Mol Cell Biol*. 2009;29(9):2419-2430. doi:10.1128/mcb.01050-08
169. Clapier CR, Cairns BR. Regulation of ISWI involves inhibitory modules antagonized by nucleosomal epitopes. *Nature*. 2012;492(7428):280-284. doi:10.1038/nature11625
170. Vary JC, Gangaraju VK, Qin J, Landel CC, Kooperberg C, Bartholomew B, Tsukiyama T. Yeast Isw1p Forms Two Separable Complexes In Vivo. *Mol Cell Biol*. 2003;23(1):80-91. doi:10.1128/mcb.23.1.80-91.2003
171. Dziembowski A, Lorentzen E, Conti E, Séraphin B. A single subunit, Dis3, is essentially responsible for yeast exosome core activity. *Nat Struct Mol Biol*. 2007;14(1):15-22. doi:10.1038/nsmb1184
172. Torchet C, Hermann-Le Denmat S. High dosage of the small nucleolar RNA snR10 specifically suppresses defects of a yeast rrp5 mutant. *Mol Genet Genomics*. 2002;268(1):70-80. doi:10.1007/s00438-002-0724-z
173. Torchet C, Bousquet-Antonelli C, Milligan L, Thompson E, Kufel J, Tollervey D. Processing of 3′-extended read-through transcripts by the exosome can generate functional mRNAs. *Mol Cell*. 2002;9(6):1285-1296. doi:10.1016/S1097-2765(02)00544-0
174. Mitchell P, Petfalski E, Shevchenko A, Mann M, Tollervey D. The exosome: A conserved eukaryotic RNA processing complex containing multiple 3'→5' exoribonucleases. *Cell*. 1997;91(4):457-466. doi:10.1016/S0092-8674(00)80432-8
175. Babour A, Shen Q, Dos-Santos J, Murray S, Gay A, Challal D, Fasken M, Palancade B, Corbett A, Libri D, Mellor J, Dargemont C. The Chromatin Remodeler ISW1 Is a Quality Control Factor that Surveys Nuclear mRNP Biogenesis. *Cell*. 2016;167(5):1201-1214.e15. doi:10.1016/j.cell.2016.10.048
176. Mueller JE, Bryk M. Isw1 Acts Independently of the Isw1a and Isw1b Complexes in Regulating Transcriptional Silencing at the Ribosomal DNA Locus in Saccharomyces cerevisiae. *J Mol Biol*. 2007;371(1):1-10. doi:10.1016/j.jmb.2007.04.089
177. Stockdale C, Flaus A, Ferreira H, Owen-Hughes T. Analysis of nucleosome repositioning by yeast ISWI and Chd1 chromatin remodeling complexes. *J Biol Chem*. 2006;281(24):16279-16288. doi:10.1074/jbc.M600682200
178. Zentner GE, Tsukiyama T, Henikoff S. ISWI and CHD Chromatin Remodelers Bind Promoters but Act in Gene Bodies. *PLoS Genet*. 2013;9(2). doi:10.1371/journal.pgen.1003317
179. Liu X, Li M, Xia X, Li X, Chen Z. Mechanism of chromatin remodelling revealed by the Snf2-nucleosome structure. *Nature*. 2017;544(7651):440-445. doi:10.1038/nature22036
180. Zhou CY, Johnson SL, Lee LJ, Longhurst AD, Beckwith SL, Johnson MJ, Morrison AJ, Narlikar GJ. The Yeast INO80 Complex Operates as a Tunable DNA Length-Sensitive Switch to Regulate Nucleosome Sliding. *Mol Cell*. 2018;69(4):677-688.e9. doi:10.1016/j.molcel.2018.01.028
181. Eustermann S, Schall K, Kostrewa D, Lakomek K, Strauss M, Moldt M, Hopfner KP. *Structural Basis for Nucleosome Remodeling by the INO80*

Complex. Vol 556.; 2018. doi:10.1038/s41586-018-0029-y.Structural
182. Farnung L, Vos SM, Wigge C, Cramer P. Nucleosome-Chd1 structure and implications for chromatin remodelling. *Nature*. 2017;550(7677):539-542. doi:10.1038/nature24046
183. Qiu Y, Levendosky RF, Chakravarthy S, Patel A, Bowman GD, Myong S. The Chd1 Chromatin Remodeler Shifts Nucleosomal DNA Bidirectionally as a Monomer. *Mol Cell*. 2017;68(1):76-88.e6. doi:10.1016/j.molcel.2017.08.018
184. Tokuda JM, Ren R, Levendosky RF, Tay RJ, Yan M, Pollack L, Bowman GD. The ATPase motor of the Chd1 chromatin remodeler stimulates DNA unwrapping from the nucleosome. *Nucleic Acids Res*. 2018;46(10):4978-4990. doi:10.1093/nar/gky206
185. Lee Y, Park D, Iyer VR. The ATP-dependent chromatin remodeler Chd1 is recruited by transcription elongation factors and maintains H3K4me3/H3K36me3 domains at actively transcribed and spliced genes. *Nucleic Acids Res*. 2017;45(12):7180-7190. doi:10.1093/nar/gkx321
186. Nodelman IM, Bleichert F, Patel A, Ren R, Horvath KC, Berger JM, Bowman GD. Interdomain Communication of the Chd1 Chromatin Remodeler across the DNA Gyres of the Nucleosome. *Mol Cell*. 2017;65(3):447-459.e6. doi:10.1016/j.molcel.2016.12.011
187. Yan L, Wu H, Li X, Gao N, Chen Z. Structures of the ISWI–nucleosome complex reveal a conserved mechanism of chromatin remodeling. *Nat Struct Mol Biol*. 2019;26(4):258-266. doi:10.1038/s41594-019-0199-9
188. Clapier CR, Längst G, Corona DF V., Becker PB, Nightingale KP. Critical Role for the Histone H4 N Terminus in Nucleosome Remodeling by ISWI. *Mol Cell Biol*. 2001;21(3):875-883. doi:10.1128/mcb.21.3.875-883.2001
189. Clapier CR, Nightingale KP, Becker PB. A critical epitope for substrate recognition by the nucleosome remodeling ATPase ISWI. *Nucleic Acids Res*. 2002;30(3):649-655. doi:10.1093/nar/30.3.649
190. Shen Q, Beyrouthy N, Matabishi-Bibi L, Dargemont C. The chromatin remodeling Isw1a complex is regulated by SUMOylation. *Biochem J*. 2017;474(20):3455-3469. doi:10.1042/BCJ20170172
191. Bhardwaj SK, Hailu SG, Olufemi L, Brahma S, Kundu S, Hota SK, Persinger J, Bartholomew B. Dinucleosome specificity and allosteric switch of the ISW1a ATP-dependent chromatin remodeler in transcription regulation. *Nat Commun*. 2020;11(1). doi:10.1038/s41467-020-19700-1
192. Yen K, Vinayachandran V, Batta K, Koerber RT, Pugh BF. Genome-wide nucleosome specificity and directionality of chromatin remodelers. *Cell*. 2012;149(7):1461-1473. doi:10.1016/j.cell.2012.04.036
193. Parnell TJ, Schlichter A, Wilson BG, Cairns BR. The chromatin remodelers RSC and ISW1 display functional and chromatin-based promoter antagonism. *Elife*. 2014;4(4):e06073-e06073. doi:10.7554/eLife.06073
194. Mellor J, Morillon A. ISWI complexes in Saccharomyces cerevisiae. *Biochim Biophys Acta - Gene Struct Expr*. 2004;1677(1-3):100-112. doi:10.1016/j.bbaexp.2003.10.014
195. Morillon A, Karabetsou N, O'Sullivan J, Kent N, Proudfoot N, Mellor J. Isw1 Chromatin Remodeling ATPase Coordinates Transcription Elongation and Termination by RNA Polymerase II. *Cell*. 2003;115(4):425-435. doi:10.1016/S0092-8674(03)00880-8
196. Lafon A, Petty E, Pillus L. Functional Antagonism between Sas3 and Gcn5 Acetyltransferases and ISWI Chromatin Remodelers. *PLoS Genet*.

2012;8(10):1-13. doi:10.1371/journal.pgen.1002994
197. Gangaraju VK, Bartholomew B. Dependency of ISW1a Chromatin Remodeling on Extranucleosomal DNA. *Mol Cell Biol*. 2007;27(8):3217-3225. doi:10.1128/mcb.01731-06
198. Krajewski WA. Yeast Isw1a and Isw1b exhibit similar nucleosome mobilization capacities for mononucleosomes, but differently mobilize dinucleosome templates. *Arch Biochem Biophys*. 2014;546:72-80. doi:10.1016/j.abb.2014.02.003
199. Krajewski WA. Comparison of the Isw1a, Isw1b, and Isw2 nucleosome disrupting activities. *Biochemistry*. 2013;52(40):6940-6949. doi:10.1021/bi400634r
200. Eriksson PR, Clark DJ. The yeast ISW1b ATP-dependent chromatin remodeler is critical for nucleosome spacing and dinucleosome resolution. *Sci Rep*. 2021;11(1):1-14. doi:10.1038/s41598-021-82842-9
201. Kizer KO, Phatnani HP, Shibata Y, Hall H, Greenleaf AL, Strahl BD. A Novel Domain in Set2 Mediates RNA Polymerase II Interaction and Couples Histone H3K36 Methylation with Transcript Elongation. *Mol Cell Biol*. 2005;25(8):3305-3316. doi:10.1128/MCB.25.8.3305
202. Maltby VE, Martin BJE, Schulze JM, Johnson I, Hentrich T, Sharma A, Kobor MS, Howe L. Histone H3 Lysine 36 Methylation Targets the Isw1b Remodeling Complex to Chromatin. *Mol Cell Biol*. 2012;32(17):3479-3485. doi:10.1128/mcb.00389-12
203. Mito Y, Henikoff JG, Henikoff S. Genome-scale profiling of histone H3.3 replacement patterns. *Nat Genet*. 2005;37(10):1090-1097. doi:10.1038/ng1637
204. Tagami H, Ray-Gallet D, Almouzni G, Nakatani Y. Histone H3.1 and H3.3 Complexes Mediate Nucleosome Assembly Pathways Dependent or Independent of DNA Synthesis. *Cell*. 2004;116(1):51-61. doi:10.1016/S0092-8674(03)01064-X
205. Ahmad K, Henikoff S. The histone variant H3.3 marks active chromatin by replication-independent nucleosome assembly. *Mol Cell*. 2002;9(6):1191-1200. doi:10.1016/S1097-2765(02)00542-7
206. Katan-Khaykovich Y, Struhl K. Splitting of H3-H4 tetramers at transcriptionally active genes undergoing dynamic histone exchange. *Proc Natl Acad Sci U S A*. 2011;108(4):1296-1301. doi:10.1073/pnas.1018308108
207. Smolle M, Workman JL, Venkatesh S. reSETting chromatin during transcription elongation. *Epigenetics*. 2013;8(1):10-15.
208. Venkatesh S, Smolle M, Li H, Gogol MM, Saint M, Kumar S, Natarajan K, Workman JL. Set2 methylation of histone H3 lysine 36 suppresses histone exchange on transcribed genes. *Nature*. 2012;489(7416):452-455. doi:10.1038/nature11326
209. Santos-Rosa H, Schneider R, Bernstein BE, Karabetsou N, Morillon A, Weise C, Schreiber SL, Mellor J, Kouzarides T. Methylation of histone H3 K4 mediates association of the Isw1p ATPase with chromatin. *Mol Cell*. 2003;12(5):1325-1332. doi:10.1016/S1097-2765(03)00438-6
210. Stec I, Wright TJ, Van Ommen GJB, De Boer PAJ, Van Haeringen A, Moorman AFM, Altherr MR, Den Dunnen JT. WHSC1, a 90 kb SET domain-containing gene, expressed in early development and homologous to a Drosophila dysmorphy gene maps in the Wolf-Hirschhorn syndrome critical region and is fused to IgH in t(4;14) multiple myeloma. *Hum Mol Genet*. 1998;7(7):1071-1082. doi:10.1093/hmg/7.7.1071

211. Maurer-Stroh S, Dickens NJ, Hughes-Davies L, Kouzarides T, Eisenhaber F, Ponting CP. The Tudor domain 'Royal Family': Tudor, plant Agenet, Chromo, PWWP and MBT domains. *Trends Biochem Sci*. 2003;28(2):69-74.
212. Stec I, Nagl SB, Van Ommen GJB, Den Dunnen JT. The PWWP domain: A potential protein-protein interaction domain in nuclear proteins influencing differentiation? *FEBS Lett*. 2000;473(1):1-5. doi:10.1016/S0014-5793(00)01449-6
213. Dhayalan A, Rajavelu A, Rathert P, Tamas R, Jurkowska RZ, Ragozin S, Jeltsch A. The Dnmt3a PWWP domain reads histone 3 lysine 36 trimethylation and guides DNA methylation. *J Biol Chem*. 2010;285(34):26114-26120. doi:10.1074/jbc.M109.089433
214. Sue SC, Chen JY, Lee SC, Wu WG, Huang TH. Solution structure and heparin interaction of human hepatoma-derived growth factor. *J Mol Biol*. 2004;343(5):1365-1377. doi:10.1016/j.jmb.2004.09.014
215. Hung YL, Lee HJ, Jiang I, Lin SC, Lo WC, Lin YJ, Sue SC. The First Residue of the PWWP Motif Modulates HATH Domain Binding, Stability, and Protein-Protein Interaction. *Biochemistry*. 2015;54(26):4063-4074. doi:10.1021/acs.biochem.5b00454
216. Qiu C, Sawada K, Zhang X, Cheng X. The PWWP domain of mammalian DNA methyltransferase Dnmt3b defines a new family of DNA-binding folds. *Nat Struct Biol*. 2002;9(3):217-224. doi:10.1038/nsb759
217. Taverna SD, Li H, Ruthenburg AJ, Allis CD, Patel DJ. How chromatin-binding modules interpret histone modifications: Lessons from professional pocket pickers. *Nat Struct Mol Biol*. 2007;14(11):1025-1040. doi:10.1038/nsmb1338
218. Vezzoli A, Bonadies N, Allen MD, Freund SMV, Santiveri CM, Kvinlaug BT, Huntly BJP, Göttgens B, Bycroft M. Molecular basis of histone H3K36me3 recognition by the PWWP domain of Brpf1. *Nat Struct Mol Biol*. 2010;17(5):617-619. doi:10.1038/nsmb.1797
219. Wu H, Zeng H, Lam R, Tempel W, Amaya MF, Xu C, Dombrovski L, Qiu W, Wang Y, Min J. Structural and histone binding ability characterizations of human PWWP domains. *PLoS One*. 2011;6(6). doi:10.1371/journal.pone.0018919
220. Wen H, Li Y, Xi Y, Jiang S, Stratton S, Peng D, Tanaka K, Ren Y, Xia Z, Wu J, Li B, Barton MC, Li W, Li H, Shi X. ZMYND11 links histone H3.3K36me3 to transcription elongation and tumour suppression. *Nature*. 2014;508(7495):263-268. doi:10.1038/nature13045
221. Slater LM, Allen MD, Bycroft M. Structural variation in PWWP domains. *J Mol Biol*. 2003;330(3):571-576. doi:10.1016/S0022-2836(03)00470-4
222. Nameki N. Solution structure of the PWWP domain of the hepatoma-derived growth factor family. *Protein Sci*. 2005;14(3):756-764. doi:10.1110/ps.04975305
223. Qiu Y, Zhang W, Zhao C, Wang Y, Wang W, Zhang J, Zhang Z, Li G, Shi Y, Tu X, Wu J. Solution structure of the Pdp1 PWWP domain reveals its unique binding sites for methylated H4K20 and DNA. *Biochem J*. 2012;442(3):527-538. doi:10.1042/BJ20111885
224. Lukasik SM. High resolution structure of the HDGF PWWP domain: A potential DNA binding domain. *Protein Sci*. 2006;15(2):314-323. doi:10.1110/ps.051751706
225. Rona GB, Eleutherio ECA, Pinheiro AS. PWWP domains and their modes of sensing DNA and histone methylated lysines. *Biophys Rev*. 2016;8(1):63-74.

doi:10.1007/s12551-015-0190-6
226. Yang J, Everett AD. Hepatoma derived growth factor binds DNA through the N-terminal PWWP domain. *BMC Mol Biol*. 2007;8:1-9. doi:10.1186/1471-2199-8-101
227. Van Nuland R, Van Schaik FMA, Simonis M, Van Heesch S, Cuppen E, Boelens R, Timmers HTM, Van Ingen H. Nucleosomal DNA binding drives the recognition of H3K36-methylated nucleosomes by the PSIP1-PWWP domain. *Epigenetics and Chromatin*. 2013;6(1):1. doi:10.1186/1756-8935-6-12
228. Vermeulen M, Eberl HC, Matarese F, Marks H, Denissov S, Butter F, Lee KK, Olsen J V., Hyman AA, Stunnenberg HG, Mann M. Quantitative Interaction Proteomics and Genome-wide Profiling of Epigenetic Histone Marks and Their Readers. *Cell*. 2010;142(6):967-980. doi:10.1016/j.cell.2010.08.020
229. Laue K, Daujat S, Crump JG, Plaster N, Roehl HH, van Bebber F, Busch-Nentwich E, Dahm R, Frohnhöfer HG, Geiger H, Gilmour D, Holley S, Hooge J, Jülich D, Knaut H, Maderspacher F, Maischein HM, Neumann C, Nicolson T, et al. The multidomain protein Brpf1 binds histones and is required for hox gene expression and segmental identity. *Development*. 2008;135(11):1935-1946. doi:10.1242/dev.017160
230. Tian W, Yan P, Xu N, Chakravorty A, Liefke R, Xi Q, Wang Z. The HRP3 PWWP domain recognizes the minor groove of double-stranded DNA and recruits HRP3 to chromatin. *Nucleic Acids Res*. 2019;47(10):5436-5448. doi:10.1093/nar/gkz294
231. Qin S, Min J. Structure and function of the nucleosome-binding PWWP domain. *Trends Biochem Sci*. 2014;39(11):536-547. doi:10.1016/j.tibs.2014.09.001
232. Chen LY, Huang YC, Huang ST, Hsieh YC, Guan HH, Chen NC, Chuankhayan P, Yoshimura M, Tai MH, Chen CJ. Domain swapping and SMYD1 interactions with the PWWP domain of human hepatoma-derived growth factor. *Sci Rep*. 2018;8(1):1-15. doi:10.1038/s41598-017-18510-8
233. Dukatz M, Holzer K, Choudalakis M, Emperle M, Lungu C, Bashtrykov P, Jeltsch A. H3K36me2/3 Binding and DNA Binding of the DNA Methyltransferase DNMT3A PWWP Domain Both Contribute to its Chromatin Interaction. *J Mol Biol*. 2019;431(24):5063-5074. doi:10.1016/j.jmb.2019.09.006
234. Weaver TM, Morrison EA, Musselman CA. Reading more than Histones: The prevalence of nucleic acid binding among reader domains. *Molecules*. 2018;23(10):1-25. doi:10.3390/molecules23102614
235. Eidahl JO, Crowe BL, North JA, McKee CJ, Shkriabai N, Feng L, Plumb M, Graham RL, Gorelick RJ, Hess S, Poirier MG, Foster MP, Kvaratskhelia M. Structural basis for high-affinity binding of LEDGF PWWP to mononucleosomes. *Nucleic Acids Res*. 2013;41(6):3924-3936. doi:10.1093/nar/gkt074
236. Barski A, Cuddapah S, Cui K, Roh TY, Schones DE, Wang Z, Wei G, Chepelev I, Zhao K. High-Resolution Profiling of Histone Methylations in the Human Genome. *Cell*. 2007;129(4):823-837. doi:10.1016/j.cell.2007.05.009
237. Wang Y, Reddy B, Thompson J, Wang H, Noma K ichi, Yates JR, Jia S. Regulation of Set9-Mediated H4K20 Methylation by a PWWP Domain Protein. *Mol Cell*. 2009;33(4):428-437. doi:10.1016/j.molcel.2009.02.002
238. Hughes RM, Wiggins KR, Khorasanizadeh S, Waters ML. Recognition of trimethyllysine by a chromodomain is not driven by the hydrophobic effect.

Proc Natl Acad Sci U S A. 2007;104(27):11184-11188. doi:10.1073/pnas.0610850104

239. Wang H, Farnung L, Dienemann C, Cramer P. Structure of H3K36-methylated nucleosome–PWWP complex reveals multivalent cross-gyre binding. *Nat Struct Mol Biol*. 2020;27(1):8-13. doi:10.1038/s41594-019-0345-4
240. Shun M-C, Botbol Y, Li X, Di Nunzio F, Daigle JE, Yan N, Lieberman J, Lavigne M, Engelman A. Identification and Characterization of PWWP Domain Residues Critical for LEDGF/p75 Chromatin Binding and Human Immunodeficiency Virus Type 1 Infectivity. *J Virol*. 2008;82(23):11555-11567. doi:10.1128/jvi.01561-08
241. Kariola R, Raevaara TE, Lönnqvist KE, Nyström-Lahti M. Functional analysis of MSH6 mutations linked to kindreds with putative hereditary non-polyposis colorectal cancer syndrome. *Hum Mol Genet*. 2002;11(11):1303-1310. doi:10.1093/hmg/11.11.1303
242. Laguri C, Duband-Goulet I, Friedrich N, Axt M, Belin P, Callebaut I, Gilquin B, Zinn-Justin S, Couprie J. Human mismatch repair protein MSH6 contains a PWWP domain that targets double stranded DNA. *Biochemistry*. 2008;47(23):6199-6207. doi:10.1021/bi7024639
243. Hsu SS, Chen CH, Liu GS, Tai MH, Wang JS, Wu JC, Kung ML, Chan EC, Liu LF. Tumorigenesis and prognostic role of hepatoma-derived growth factor in human gliomas. *J Neurooncol*. 2011;107(1):101-109. doi:10.1007/s11060-011-0733-z
244. Mattioli F, Schaefer E, Magee A, Mark P, Mancini GM, Dieterich K, Von Allmen G, Alders M, Coutton C, van Slegtenhorst M, Vieville G, Engelen M, Cobben JM, Juusola J, Pujol A, Mandel JL, Piton A. Mutations in Histone Acetylase Modifier BRPF1 Cause an Autosomal-Dominant Form of Intellectual Disability with Associated Ptosis. *Am J Hum Genet*. 2017;100(1):105-116. doi:10.1016/j.ajhg.2016.11.010
245. You L, Zou J, Zhao H, Bertos NR, Park M, Wang E, Yang XJ. Deficiency of the chromatin regulator Brpf1 causes abnormal brain development. *J Biol Chem*. 2015;290(11):7114-7129. doi:10.1074/jbc.M114.635250
246. Sreerama N, Woody RW. Computation and Analysis of Protein Circular Dichroism Spectra. *Methods Enzymol*. 2004;383(1):318-351. doi:10.1016/S0076-6879(04)83013-1
247. Wei Y, Thyparambil AA, Latour RA. Protein helical structure determination using CD spectroscopy for solutions with strong background absorbance from 190 to 230nm. *Biochim Biophys Acta*. 2014;1844(12):2331-2337. doi:10.1016/j.bbapap.2014.10.001
248. Goldman JA, Garlick JD, Kingston RE. Chromatin remodeling by imitation switch (ISWI) class ATP-dependent remodelers is stimulated by histone variant H2A.Z. *J Biol Chem*. 2010;285(7):4645-4651. doi:10.1074/jbc.M109.072348
249. Mueller-Planitz F, Klinker H, Ludwigsen J, Becker PB. The ATPase domain of ISWI is an autonomous nucleosome remodeling machine. *Nat Struct Mol Biol*. 2013;20(1):82-89. doi:10.1038/nsmb.2457
250. Turlure F, Maertens G, Rahman S, Cherepanov P, Engelman A. A tripartite DNA-binding element, comprised of the nuclear localization signal and two AT-hook motifs, mediates the association of LEDGF/p75 with chromatin in vivo. *Nucleic Acids Res*. 2006;34(5):1653-1665. doi:10.1093/nar/gkl052
251. Tsutsui KM, Sano K, Hosoya O, Miyamoto T, Tsutsui K. Nuclear protein LEDGF/p75 recognizes supercoiled DNA by a novel DNA-binding domain.

Nucleic Acids Res. 2011;39(12):5067-5081. doi:10.1093/nar/gkr088

252. Hendrix J, Gijsbers R, De Rijck J, Voet A, Hotta JI, McNeely M, Hofkens J, Debyser Z, Engelborghs Y. The transcriptional co-activator LEDGF/p75 displays a dynamic scan-and-lock mechanism for chromatin tethering. *Nucleic Acids Res*. 2011;39(4):1310-1325. doi:10.1093/nar/gkq933